

Some pages of this thesis may have been removed for copyright restrictions.

If you have discovered material in AURA which is unlawful e.g. breaches copyright, (either yours or that of a third party) or any other law, including but not limited to those relating to patent, trademark, confidentiality, data protection, obscenity, defamation, libel, then please read our [Takedown Policy](#) and [contact the service](#) immediately

VELOCITY DISTRIBUTIONS IN A
PLATE HEAT EXCHANGER CHANNEL

A Thesis Submitted

by

ASHOK KUMAR

for

the Degree of .

DOCTOR OF PHILOSOPHY

NOVEMBER 1982

Department of Chemical Engineering
University of Aston in Birmingham.

DEDICATED TO

KATHLEEN, RAJ, RAV AND MY PARENTS

- SUMMARY

SUMMARY

The development of a Laser Doppler Anemometer technique to measure the velocity distribution in a commercial plate heat exchanger is described. Detailed velocity profiles are presented and a preliminary investigation is reported on flow behaviour through a single cell in the channel matrix.

The objective of the study was to extend previous investigations of plate heat exchanger flow patterns in the laminar range with the eventual aim of establishing the effect of flow patterns on heat transfer performance, thus leading to improved plate heat exchanger design and design methods.

Accurate point- velocities were obtained by Laser Anemometry in a perspex replica of the metal channel. Oil was used as a circulating liquid with a refractive index matched to that of the perspex so that the laser beams were not distorted.

Cell-by-cell velocity measurements over a range of Reynolds number up to ten showed significant liquid mal-distribution. Local cell velocities were found to be as high as twenty seven times average velocity, contrary to the previously held belief of four times. The degree of mal-distribution varied across the channel as well as in the vertical direction, and depended on the upward or downward direction of flow. At Reynolds numbers less than one, flow zig-zagged from one side of the channel to the other in wave form, but increases in Reynolds number improved liquid distribution.

A detailed examination of selected cells showed velocity variations in different directions, together with variation within individual cells.

Experimental results are also reported on the flow split when passing through a single cell in a section of a channel. These observations were used to explain mal-distribution in the perspex channel itself.

DEGREE OF DOCTOR OF PHILOSOPHY

ASHOK KUMAR
November 1982

KEY WORDS: PLATE HEAT EXCHANGERS
LASER DOPPLER ANEMOMETER
VELOCITY MEASUREMENT

ACKNOWLEDGEMENTS

I would like to take this opportunity to express my special thanks to my supervisor, Mr. A.F. Price, for his assistance, consistent encouragement, help with research and guidance and constructive criticism throughout this project.

I am also grateful to Mr. P. Murray and Mr. S. Cole of the Department Workshop for their help with the preparation of experimental equipment.

I would like to express my gratitude to the Science and Engineering Research Council for providing me with financial assistance, the Department of Chemical Engineering for providing the facilities for the research and acknowledge the assistance provided by APV Co. Ltd., concerning Plate Heat Exchangers.

My special thanks are due to my good friend Mike Jones for his initiation of the study on single cell and his advice and guidance throughout the work.

Presentation of point velocity measurements is due to my friend Miss Monir Hajimirzatayeb for her continuous and labouring effort in typing the numbers.

Finally, I am deeply indebted to Mrs. V. Rennison for typing the manuscript and all those numerous friends who provided moral support in the present study.

CONTENTS

		<u>Page</u>
CHAPTER 1	INTRODUCTION	1
1.1	Laser Doppler Anemometry (LDA)	1
1.2	Plate Heat Exchangers	1
1.2.1	Background	1
1.2.2	General Description	2
1.2.3	Plate Geometry	4
1.3	General Outline of Present Study	7
CHAPTER 2	THEORY AND DESCRIPTION OF LASER DOPPLER ANEMOMETRY	9
2.1.1	Introduction	9
2.1.2	Principles of Laser Doppler Anemometry	9
2.1.3	Advantages of Laser Anemometry	12
2.2	Classification of Laser Doppler Anemometry	12
2.2.1	Reference Beam Mode	12
2.2.2	Dual Scatter Mode	14
2.2.3	Dual Beam or Doppler Difference Mode	16
2.3	Doppler Difference Technique	19
2.3.1	The Doppler Shift Inter- pretation	19
2.3.2	Interpretation by Fringe Analysis	21

		<u>Page</u>
2.4	Signal Processing	24
2.4.1	Photon Correlation	24
2.5	The Auto-Correlation in Laminar Flow	31
2.6	Practical Applications of Laser Doppler Anemometry	36
CHAPTER 3	LITERATURE REVIEW ON PLATE HEAT EXCHANGERS	49
CHAPTER 4	EXPERIMENTAL WORK	65
4.1	Transparent Channel Models	65
4.1.1	Commercial Plates: SR1 (APV Ltd.)	65
4.1.2	Research Plates: Junior Paraflow (APV Ltd.)	70
4.2	Laser Anemometry Equipment	77
4.2.1	The Laser	77
4.2.2	Photomultiplier	77
4.2.3	Photon Correlator and Display Unit	78
4.2.4	Computing Data Processor	78
4.2.5	Setting up Procedure of Optical Configuration	79
4.3	Experimental	87
4.3.1	Initial Equipment Arrangement	87
4.3.2	Water as Working Fluid	90
4.3.3	Refractive Index Matching	106
4.3.4	Oil as Working Fluid	110
4.3.5	Modified Equipment Arrangement	120

		<u>Page</u>
4.4	Development of Experimental Technique	130
4.4.1	Introduction	130
4.4.2	Surface Conditions	132
4.4.3	Scattering Particles	133
CHAPTER 5	RESULTS	137
5.1	Junior Paraflow Single Cell	137
5.1.1	Single Input Flows	137
5.1.2	Simultaneous Inlets at Same Initial Pressure	137
5.1.3	Variation in Inlet Pressure	140
5.1.4	Double Initial Pressure in One Inlet	140
5.1.5	New Flow into Established Flow	141
5.2	Velocity Measurements in the SR1 perspex Channel	143
5.2.1	Low Flow Rates	145
5.2.2	High Flow Rates	159
5.2.3	Velocity Components	162
5.2.4	Variations Across Selected Single Cells	162
CHAPTER 6	DISCUSSION ON FLOW DISTRIBUTION	166
6.1	General	166
6.2	Analysis of Junior PHE Section	166
6.2.1	Flow Splitting at Cell Outlet	166
6.2.2	Performance Analysis	173
6.2.3	Practical Difficulties in Measurements	176

		<u>Page</u>
6.3	SR1 Analysis Using Water	177
6.3.1	Problems of Alignment	178
6.3.2	LDA Signals	180
6.3.3	Failure in Repeatability	183
6.4	Velocity Measurement Analysis of Low Flow Rates	189
6.4.1	Horizontal Component in Up-Flow	189
6.4.2	Angular Component in Up-Flow	194
6.4.3	Down-Flow	204
6.5	Velocity Measurements Analysis of High Flow Rates	211
6.5.1	Reynolds Number 5.291	211
6.5.2	Reynolds Number 7.078	211
6.6.	Relating Velocity Measurements and Performance Criteria	217
6.7	Analysis of Velocity Component Measurements	220
6.8	Velocity Measurement Velocity Across Selected Cells	222
CHAPTER 7	CONCLUSIONS	224
7.1	Junior PHE Single Cell	224
7.2	SR1 Velocity Measurements	225
CHAPTER 8	RECOMMENDATIONS FOR FURTHER WORK	232
8.1	Single Cell	232
8.2	Laser Doppler Measurements	233
8.3	General Development	235

APPENDICES

	<u>Page</u>	
A-1.0	General Description of the Computer System and Program for Anemometry	237
A-1.1	Background	237
A-1.2	Description of Application Program for Laser Anemometry	237
A-2.0	Calculation of Beam radius at Focus	244
A-3.0	Calculations of Reynolds Number	246
A-3.1	Calculation of Reynolds Number using Water	246
A-3.3	Calculation of Reynolds Number using Oil	247
A-3.4	Calculation of Higher Reynolds Number Using Oil	249
A-4.0	Calculation for Performance of Single Cell for the Junior PHE Section	253
A-5.0	Calculations of Standard Deviations	257
A-5.1	Low Flow Rate : Up-Flow	257
A-5.2	Low Flow Rate : Down-Flow	260
A-5.3	High Flow Rate : Up-Flow	262
	References	264

LIST OF FIGURES

<u>FIGURE</u>	<u>DESCRIPTION</u>	<u>PAGE</u>
Figure 1.1	Intermating Plate Cross-Section (2-dimensional)	5
Figure 1.2	Criss-Cross Plate Section (3-dimensional)	5
Figure 2.1	Diagram showing Doppler Shift on Scattering by a moving object 'P	11
Figure 2.2	Laser Doppler Arrangement for Reference Beam Mode	13
Figure 2.3	Optical Arrangement for the Dual Scatter Mode	15
Figure 2.4	Doppler Difference Arrangement	17
Figure 2.5	Scattering Geometry - Doppler Difference Effect	20
Figure 2.6	Fringe Pattern Produced in the Cross-Over Region due to Interference of Two Beams	20
Figure 2.7	Optical Geometry of Doppler Difference Arrangement	25
Figure 2.8	Photomultiplier Detector	26
Figure 2.9	Random Photon Arrival Pattern	26
Figure 2.10	Correlation Function of Photons	26
Figure 2.11	Simplified Schematic Representation of Photon Correlator	29
Figure 2.12	The Cosinusoidal Correlation Function	30
Figure 2.13	Analysis of Correlation Function	30
Figure 2.14	Parabolic Interpolation to Determine Turning Point Value	35

<u>FIGURE</u>	<u>DESCRIPTION</u>	<u>PAGE</u>
Figure 2.15	Cylindrical Container for the Study of Annular Gas Jets	42
Figure 4.1 (a)	Inlet/Outlet Port	69
Figure 4.1 (b)	Connection Between Channel and Inlet/Outlet Flanges	69
Figure 4.2	Line Diagram of Experimental Rig of Single Cell	74
Figure 4.3	Optional Configuration and Signal Processing Arrangement of Laser Doppler Anemometer	80
Figure 4.4	The Photomultiplier Assembly	81
Figure 4.5	Ray Diagram of Reflex Viewer - Plan view	83
Figure 4.6	Too Many Fringes in Beam Diameter	85
Figure 4.7	Few Fringes in Beam Diameter	85
Figure 4.8	Oscilloscope Display of Flow	85
Figure 4.9	Oscilloscope Display of Flow	86
Figure 4.10	Line Diagram of Initial Equipment Arrangement	88

<u>FIGURE</u>	<u>DESCRIPTION</u>	<u>PAGE</u>
Figure 4.11	Assembly of the Perspex Channel	89
Figure 4.12	Calibration Chart for Water	92
Figure 4.13	Calibration Curve for Oil	112
Figure 4.14	Representation of Channel Corrugations	114
Figure 4.15	Co-ordinate System for Channel Position	116
Figure 4.16	Plot of Viscosity <u>vs</u> Temperature of Oil	118
Figure 4.17	Line Diagram of Modified Experimental Equipment	121
Figure 5.1	Point Velocity Measurements	148
Figures 5.2 to 5.9	Point Velocity Measurements	150-158
Figures 5.10 to 5.11	Point Velocity Measurements	160-161
Figures 5.12 to 5.13	Point Velocity Measurements	164-165

<u>FIGURE</u>	<u>DESCRIPTION</u>	<u>PAGE</u>
Figure 6.1	Distribution Plot for Flow through Both Tubes at the same Initial Pressure	168
Figure 6.2	Distribution Plot for Flow through Both Tubes at Different Initial Inlet Pressure.	169
Figure 6.3	Distribution Plot for Flow Water Doubling one Inlet Pressure	170
Figure 6.4	Distribution Plot for Flow opened through Tubes at Different Intervals	172
Figure 6.5	Plot showing Performance Criteria <u>vs</u> Total Flow calculated at the Inputs for a Single Cell	174
Figure 6.6	Divergent Beams Crossing in the Channel	179
Figure 6.7 (a)	Signal from Particles crossing in the Central Region of Probe Volume	179
Figure 6.7 (b)	Signal from Particles crossing in the Probe Volume for Particle Size greater than Fringe Spacing	179
Figure 6.8	Particles crossing Path off Centre in the Fringe Pattern	182
Figure 6.9	Signal obtained from Particles crossing off centre of Fringe Pattern	182

<u>FIGURE</u>	<u>DESCRIPTION</u>	<u>PAGE</u>
Figure 6.10	Path of Particles crossing Fringe Pattern at Different Angles	182
Figure 6.11	Beams Intersecting in the Cell Volume	184
Figure 6.12	Beams not Intersecting in the Cell Volume	187
Figure 6.13	A Simple Development of Mal- Distribution in Cells	219
Figure A-1.1.	Structure of Experimental Execution Program	241
Figure A-1.2	General Structure of Malvern Application Programs	243
Figure A-3.1	Calibration Chart for Water	251

LIST OF TABLES

<u>TABLE</u>	<u>DESCRIPTION</u>	<u>PAGE</u>
2.1	Applications of Laser Doppler Anemometry	138
4.1	Refractive Indices of Oils	138
5.1	Flow through Tube "A" only	138
5.2	Flow through Tube "B" only	138
5.3	Flow through Both Tubes at Same Initial Pressure	139
5.4	Flow through Both Tubes at Different Initial Inlet Pressures	139
5.5	Flow after Doubling one Inlet Pressure	141
5.6	Flow through Tubes where Tube "B" opened first and then Tube "A"	142
5.7	Flow through Tubes where Tube "A" opened first and then Tube "B"	142
5.8	Parameters of the SR1 Plate	144
A-1.1	Questions Required by the Program	240
A-3.1	Reynolds Number Range of Low Flow Rate Measured	249
A-3.2	Reynolds Number Range of High Flow Rate Measured	252
A-4.1	Performance of Single Cell for Both Tubes at same Initial Pressure	255
A-4.2	Performance of Single Cell for Both Tubes at Different Inlet Initial Pressures	255
A-4.3	Performance of Single Cell for Double one Inlet Pressure	256
A-4.4	Performance of Single Cell for Tube "B" opened first and then Tube "A"	256

<u>TABLE</u>	<u>DESCRIPTION</u>	<u>PAGE</u>
A-4.5	Performance of Single Cell for Tube "A" opened first and then Tube "B"	256
A-5.1	Standard Deviations for Up-Flow Re = 0.0817	258
A-5.2	Standard Deviations for Up-Flow Re = 0.1028	258
A-5.3	Standard Deviations for Up-Flow Re = 0.1293	259
A-5.4	Standard Deviations for Up-Flow Re = 0.1616	259
A-5.5	Standard Deviations of Down-Flow Re = 0.0817	260
A-5.6	Standard Deviations of Down-Flow Re = 0.1028	261
A-5.7	Standard Deviations of Down-Flow Re = 0.1293	261
A-5.8	Standard Deviations of Down-Flow Re = 0.1616	262
A-5.9	Standard Deviations for Up-Flow Re = 5.291	262
A-5.10	Standard Deviations for Up-Flow Re = 7.078	263

LIST OF PLATES

<u>PLATE</u>	<u>DESCRIPTION</u>	<u>PAGE</u>
4.1	Stainless Steel Plate for SR1 Plate Heat Exchanger	66
4.2	Assembly of Single Cell	72
4.3	Experimental Equipment	123
4.4	Experimental Equipment	124
4.5	Assembly of Perspex Channel with the Experimental Rig	125
4.6	Perspex Channel of SR1 Plate Heat Exchanger	126
4.7	Optical Configuration of LDA System for Perspex Channel	127
4.8	Signal Processing and Output Units	128
4.9	Laser Beams passing through the Channel	129

NOMENCLATURE

NOMENCLATURE

The variables used in the present study are listed below, together with units and a brief description.

<u>Variable</u>	<u>Unit</u>	<u>Description</u>
A	m ²	Area of plate
A _t	cm ²	Area of tube
a _o	-	Experimental Constant
a b" c	-	Constants measured from cosinusiodal function
a ₁ b ₁	-	Distribution Constants
b	mm	Beam separation at arbitrary measurement point
b'	m	Mean plate gap
C _p	KJ/Kg°C	Specific Heat
D	m	Beam displacement produced by mirror and beam splitter combination
De	m	Equivalent diameter
d	cm	Distance from the arbitrary measurement point to the beams crossing
F	cm	Focal length of the lens
FP	-	Far point
G	Kg/s	Mass flow rate
g ₁ g ₂ g ₃	-	Amplitude for each turning point at delay times t ₁ t ₂ and t ₃

<u>Variable</u>	<u>Unit</u>	<u>Description</u>
$g_n g_z$	-	Amplitudes at times t_n and t_z on the correlation curve
$g(\tau)$	-	Correlation function for time τ
$g(p\delta t)$	-	Correlation function for number of photons counted for interval separated by time $p\delta t$
H	m	Height of intermingling troughs
$\Delta h_A \Delta h_B$	cm	Height changes in each tube "A" and "B"
$K_1 K_2$	-	Wave vectors
K_s	-	Scattered wave vector
$K_A K_B$	-	Performance criteria of cell based on tubes "A" and "B".
k	W/m ² °C	Overall heat transfer coefficient
m	-	Fringe visibility factor
N	-	Total number of terms in summations
Nu	-	Nusselt number
$n(t)$	-	Number of photons arrival events occurring with an interval of time δt at a time t
n_i	-	Number of photons counted in the i th interval
n	-	Number of fringes

<u>Variable</u>	<u>Unit</u>	<u>Description</u>
n'	-	Number of samples under investigation
n_s	-	Number of passes
P	-	Number of values of the function
Q	m^3/s	Volumetric flow rate
Q_M	cm^3	Total flow measured
Q_T	cm^3	Total volume leaving both tubes
$Q_{CA} \quad Q_{CB}$	cm^3	Calculated flow inputs from tubes "A" and "B"
$Q_{MA} \quad Q_{MB}$	cm^3	Flow measured at outlet of tubes "A" and "B"
R	-	Amplitude ratio
Re	-	Reynolds number
r	μm	Beam radius
r_f	μm	Beam radius at focus
S	m	Fringe spacing
T	$^{\circ}C$	Temperature
t	s	Time
t_{av}	s	Average of three turning points at delay times t_1 , t_2 and t_3
δt	s	Small interval of time
U	m/s	Average velocity of flow
V	m/s	Velocity of flow

<u>Variable</u>	<u>Unit</u>	<u>Description</u>
v'	m/s	Velocity of moving particle
V_o	m/s	Observed velocity
W	m	Plate width available for flow
x_i	-	Ratio of measured velocity to average velocity for sample i
\bar{x}	-	Mean average of velocities across the channel
Z	-	Experimental response
α	-	Angle of the scattering signal
β	-	Angle of component resolved
$\nu_1 \nu_2$	-	Doppler shifts
$\Delta \nu$	-	Change in frequency of light
θ	deg	Angle of beam separation
θ'	-	Number of heat transfer units (HTU)
η	-	Turbulence
λ	$^{\circ}A$	Wavelength of laser light
μ	Kg/ms	Viscosity of fluid
ρ	Kg/m ³	Density of fluid
σ	-	Standard deviation
τ	s	Sample time
\emptyset	-	Ratio of developed to projected area

CHAPTER 1

INTRODUCTION

1. INTRODUCTION

1.1 LASER DOPPLER ANEMOMETRY (LDA)

For many years two techniques were widely used to study flow patterns. One involved the use of mechanical probes to obtain information on fluid velocity, while the other used dye solutions injected into the flow to observe the streamlines produced as they are carried along by the current (applicable to low velocities).

In 1964 Yeh and Cummins (1) demonstrated the technique of using the Doppler shift of laser light to determine velocities. The basic principle is simple, small particles, either naturally or artificially introduced into the flow, act as light scattering centres. Particles having suitable characteristics will follow the flow faithfully without interference so that the light scattered in a given direction can be related to the particle velocity and hence to the flow.

1.2 PLATE HEAT EXCHANGERS

1.2.1 BACKGROUND

The earliest form of plate heat exchanger (PHE) appear to have been invented in Germany in the 1870's - the Alfa Laval's group hold patents dating back to 1878. Modern designs appeared in the 1920's and essentially similar plates exist today differing only in fine details of design. Manufacturers offer various plate sizes and spacings; mostly "tailor made" for specific duties.

These exchangers were originally used widely in the dairy, brewing and food industries, but their versatility is shown by the range of other industries in which they are now used. For instance, they have been used successfully for handling sulphite pulp, plastic emulsions, paints, organic solvents, chemicals and carbon-dioxide absorption liquors. In addition, they are now used in the nitrogen, electrolytic, phosphorous, sulphur, alumina, soap, plastic and detergent industries; and for heat recovery in ceramic, cement, glass and dyeing industries. Recently PHE's have been used in gas fields and offshore oil fields in the North Sea, as mentioned by Fuller (2) and Bond (3) and further developments are leading to the use of PHE's in nuclear power stations (2).

1.2.2 GENERAL DESCRIPTION

The Plate heat exchanger consists of a number of rectangular thin metal plates, clamped together in a pack and mounted between a top carrying bar and a bottom guide bar. The plates are clamped together tightly between a fixed head piece and a movable follower or tail piece. Although the plate thickness can be 0.6mm (4), the packs are capable of operating at working pressures up to 21 bar and temperatures of 260°C (3). Ports in the corner of each plate allow fluid to enter and leave each channel.

Each plate is stamped out of sheet metal in such a fashion that its surface has a corrugated or wavy appearance. When plates are clamped together, the corrugations on successive plates can interlock to form narrow, parallel

x flow channels with minimum points of contact. The patterns of the corrugation varies between manufacturers and the purpose of the wavy pattern is to produce turbulence (5) even at low velocities, thereby increasing the effectiveness of heat transfer. It is claimed that PHE's obtain heat transfer coefficient approximately 2½ times those in a shell and tube heat exchanger (9) for the same duty. The corrugations also increase the rigidity of the thin plates enabling it to better withstand the stresses to which it is subjected. A different arrangement of plates results in a three dimensional channel with multiple points of contact and a more rigid structure.

The heat transfer plates are arranged face to face (generally known as right-hand and left-hand plates) with the heating and cooling streams flowing on opposite sides of each plate. The distance between plates in the fluid channel is determined by the gasket which seals the outer edge of the plates and around the ports, and by pins pressed into the plate surface. The pack is compressed by tightening the mechanism which forces the plates together in a manner similar to a filter press. The gasket provides a good seal between the two fluids, making intermixing virtually impossible. Special gaskets are nowadays used into which vents are moulded to give immediate indication of leakage at any position without risk of liquid contamination (3).

A fluid enters at a corner of one end of the compressed pack of plates. It passes through alternate channels between plates in either series or parallel passages, the routing determined by whether or not the corner opening on each plate on to the channel is blocked off. Each channel containing a heat exchange fluid is sandwiched between two channels carrying the other heat exchange fluid except at the end of the unit.

A large number of potential flow arrangements exist in PHE's but they can be classified into three categories: series flow pattern, parallel flow pattern, and complex flow pattern. These have been discussed in detail by Fattah (7) and more recently Ito (8) has presented sixty-four possible flow arrangements with detailed diagrams, although descriptions are omitted.

1.2.3 PLATE GEOMETRY

Currently there are in excess of 150 individual plate channel designs which provide greater plate strength and promote turbulence in the fluid. At present there are two different type of configurations available:

- (i) The transverse intermating configurations pressed deeper than the plate spacing as shown in Figure 1.1 which are nested into the adjacent plate pack when assembled. There is a passage maintained between plates by embossed pips to provide interplate contacts

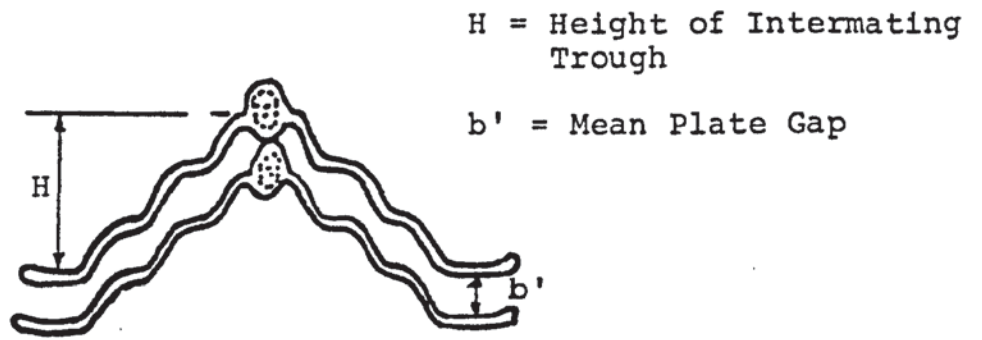


FIGURE 1.1 INTERMATING PLATE CROSS-SECTION
(2-dimensional channel)

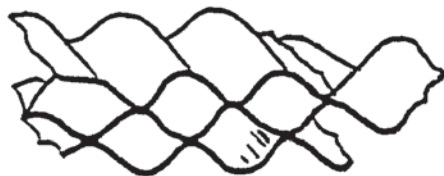


FIGURE 1.2 CRISS CROSS PLATE SECTION
(3-dimensional channel)

every 1300 to 1900mm² (3). The cross section provides a series of expansion and contracting zones which provides a two-dimensional passage variation, so giving a constant change of velocity and flow gap. Passage gaps in these types of corrugation vary between 1.5mm to 5mm and result in a considerable differential pressure to ensure fluid flow.

- (ii) The currently more popular plate used in industry has corrugations pressed to the depth of the gasket, and it is often called "chevron" or "herringbone" pattern. These plates form a criss-cross pattern of troughs as shown in Figure 1.2. The chevrons are reversed on the adjacent plates, so that when the plates are clamped together, a greater density of interplate contact point exists giving rise to one every 130mm² (3) and enables high pressures to be handled (5). This provides flow paths in three-dimensions which induce a constant change in flow direction and a high heat transfer coefficient at low rates.

These types of plates are the subject of this detailed investigation of hydrodynamic characteristics using advanced modern technology for velocity measurement.

Compared with all different types of compact heat exchangers (6) such as spiral, flat-plate, fin-plate and tube, PHE's have the most complex geometry. This causes great difficulty in applying analytical methods to predict

flow patterns and heat transfer coefficients. Therefore design methods for PHE's have been based on previous experience and experimental investigations carried out mainly by commercial manufacturers who are not yet prepared to divulge detailed design procedures.

The present study was carried out to investigate the flow characteristics in a commercial three-dimensional channel of a type widely used in industry, manufactured by APV Ltd., as type SR1. A single channel was fabricated from transparent polymethylmethacrylate, and the Laser-Doppler Anemometry technique was applied to measure point velocities in many positions.

1.3 GENERAL OUTLINE OF PRESENT STUDY

For over sixty years plate heat exchangers have been designed for industry with very little published knowledge of their thermal and hydraulic characteristics as Bond (3) pointed out very recently.

This present study is an extension of work initiated by Price and Fattah (10) in the early 1970's. They carried out a study of a single transparent replica of an APV Junior (research size) channel and visualised flow patterns by using aqueous dye. The current study is to provide clearer understanding of flow measurement in a commercial APV plate heat-exchanger channel named the SR1, by using the Laser-Doppler Anemometry technique.

A very close reproduction in plastic was made of the standard SRI metal plate, using the method outlined by Fattah (7) as a good representation of a single channel in a pack of plates.

Initially water was employed as a working fluid but due to extreme difficulties encountered in making experimental observations, this was abandoned and a more suitable liquid was searched for and found.

Point velocities were measured at selected positions in the channel, mainly near the inlet region, part way along the channel and near the outlet of channel. All measurements in this study were made in the laminar flow regime.

CHAPTER 2

THEORY AND DESCRIPTION OF LASER DOPPLER ANENOMETRY

2 THEORY AND DESCRIPTION OF LASER DOPPLER ANEMOMETRY

2.1.1 INTRODUCTION

Most conventional devices that are used for performing flow field diagnostics comprise physical types with probes such as pitot tubes and hot-wire anemometers. Although they are very successful and useful in many applications, they have substantial shortcomings: disturbance of the flow when measurements are being made means that correction factors have to be introduced to re-establish the unperturbed conditions; poor spatial resolution; poor directional sensitivity; they are usually non-linear and always require calibration. The streak and strobe photographic techniques are useful, but analysis of data is tedious. In spite of all these problems these conventional techniques are frequently used in many applications. However, there are many difficult applications (and plate heat exchanger channels are a good example) in which none of the previously available means of flow measurement is capable of obtaining the required measurements. The development of the LDA technique has opened many doors to previously inaccessible topics for practical study and revolutionised the field of experimental fluid mechanics.

2.1.2 PRINCIPLES OF LASER DOPPLER ANEMOMETRY

The LDA technique as its name implies, is based on the Doppler effect whereby the frequency of a wave phenomena

appears to change in direct proportion to the relative velocity between the observer and the source. An audible example of this phenomenon takes place when a train passes by an observer. A similar effect occurs when light (or sound) is scattered by an object that is moving with respect to a stationary source.

A stationary observer Q will detect a Doppler shift ν in the scattered radiation proportional to the relative velocity between the object P and source S, see Figure 2.1.

A vigorous derivation (11) of the equation of the Doppler shift in this case will yield:

$$\Delta\nu = \frac{2V}{\lambda} \cos \beta \sin \left(\frac{\alpha}{2} \right) \quad (2.1)$$

where $\Delta\nu$ = change in frequency of light

V = velocity of the object P moving

α = angle of the scattering signal

λ = Wavelength of laser light

β = angle of component resolved in the direction of the scattering vector.

The Doppler shift is typically a very small fraction of the base frequency of the laser (10^6 HZ out of a base frequency of about 5×10^{14} HZ) and these can be easily detected with a suitable photomultiplier.

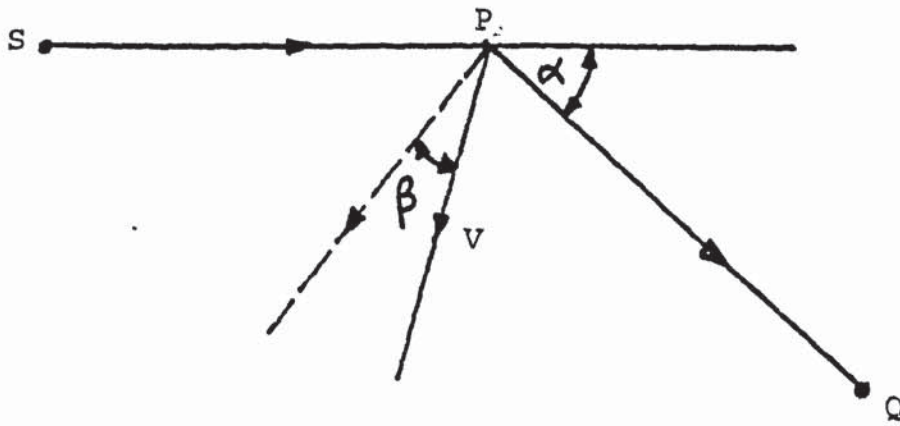


FIGURE 2.1 DIAGRAM SHOWING DOPPLER SHIFT ON
SCATTERING BY A MOVING OBJECT P

2.1.3 ADVANTAGES OF LASER ANEMOMETRY

The discussion in Section 2.1.1 provides good reasons to exploit the main characteristics of LDA system, in this study i.e.

- (i) all the information is carried via light beams, there is no disturbance of flow
- (ii) both magnitude and direction of the velocity can be measured simultaneously.
- (iii) fast response and no calibration required.
- (iv) the LDA is independent of fluid properties.

2.2 CLASSIFICATION OF LASER DOPPLER ANEMOMETRY SYSTEMS

All the LDA optical arrangements can be classified in three following categories:

- (1) Reference beam mode
- (2) Dual scatter mode
- (3) Dual beam or Doppler Difference mode.

These various classifications will be discussed in detail.

2.2.1 REFERENCE BEAM MODE

This arrangement was used by the pioneers of the LDA, Yeh and Cummins (1) in 1964. A simple arrangement is shown in Figure 2.2. Light from the laser is divided by the beam splitter, most of the light being focused by a lens to a point in a pipe where the velocity measurement is required. Light scattered by particles (artificially induced or already existing) moving with

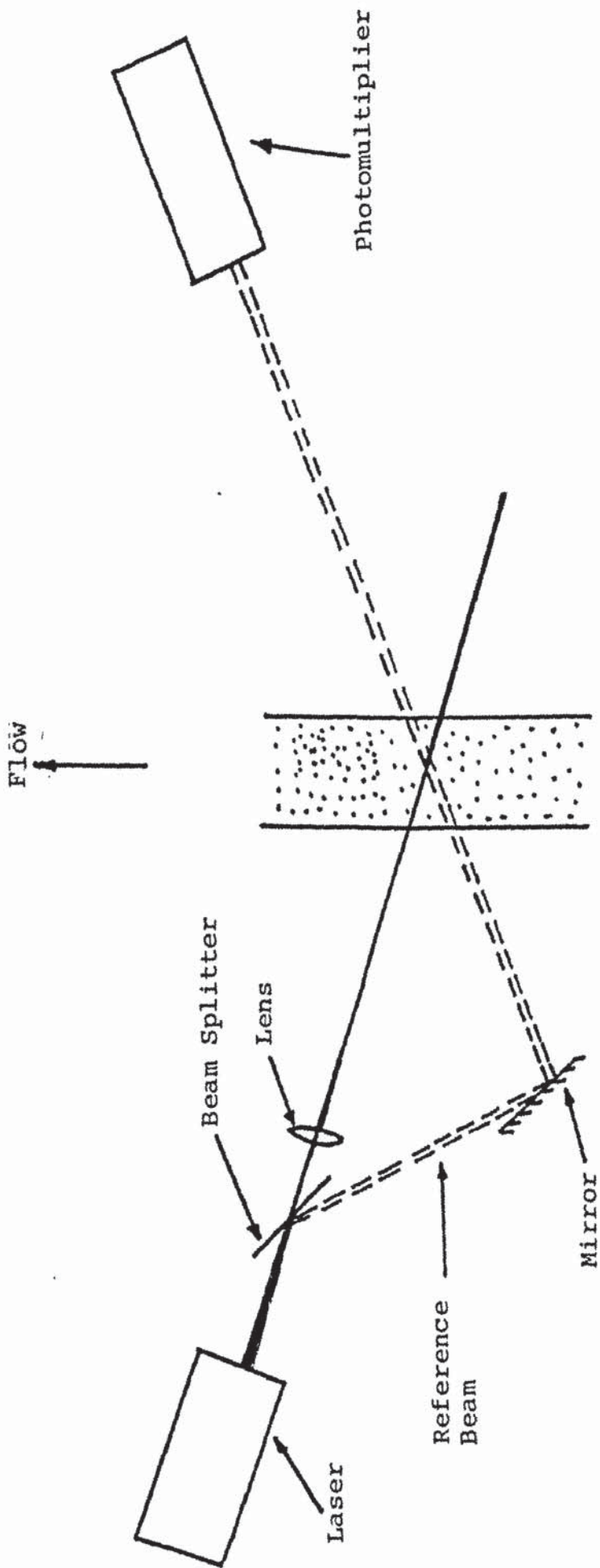


FIGURE 2.2 LASER DOPPLER ARRANGEMENT FOR REFERENCE BEAM MODE

fluid is received by the photomultiplier tube. The weaker beam from the beam splitter, the unshifted reference, is directed to the detector by the mirror. The output from the photomultiplier contains a signal of the difference frequency between the two beams which is of course the Doppler shift Δv which is given by the equation:

$$\Delta v = \frac{2V}{\lambda} \sin\left(\frac{\theta}{2}\right) \quad (2.2)$$

where V is the velocity of particles passing

λ is the wavelength of light

θ is the angle of beam separation

Yeh and Cummins (1) examined water flow in a circular tube and obtained the normal laminar velocity profile. Foreman et al. (12) measured flow velocities in gases and subsequently many other workers used this method. Further details can be found in Drain (11) or Durst et al. (13).

2.2.2 DUAL SCATTER MODE

This interesting variation of optical arrangement shown in Figure 2.3, developed by Durst and Whitelaw (14) in the early 70's. In this arrangement, an illuminating beam is scattered in two directions simultaneously. The light is made parallel by a lens and then follows a conventional optical path to the probe volume. Thereafter the scattered light is observed from two positions, the signals from which are combined to give a different

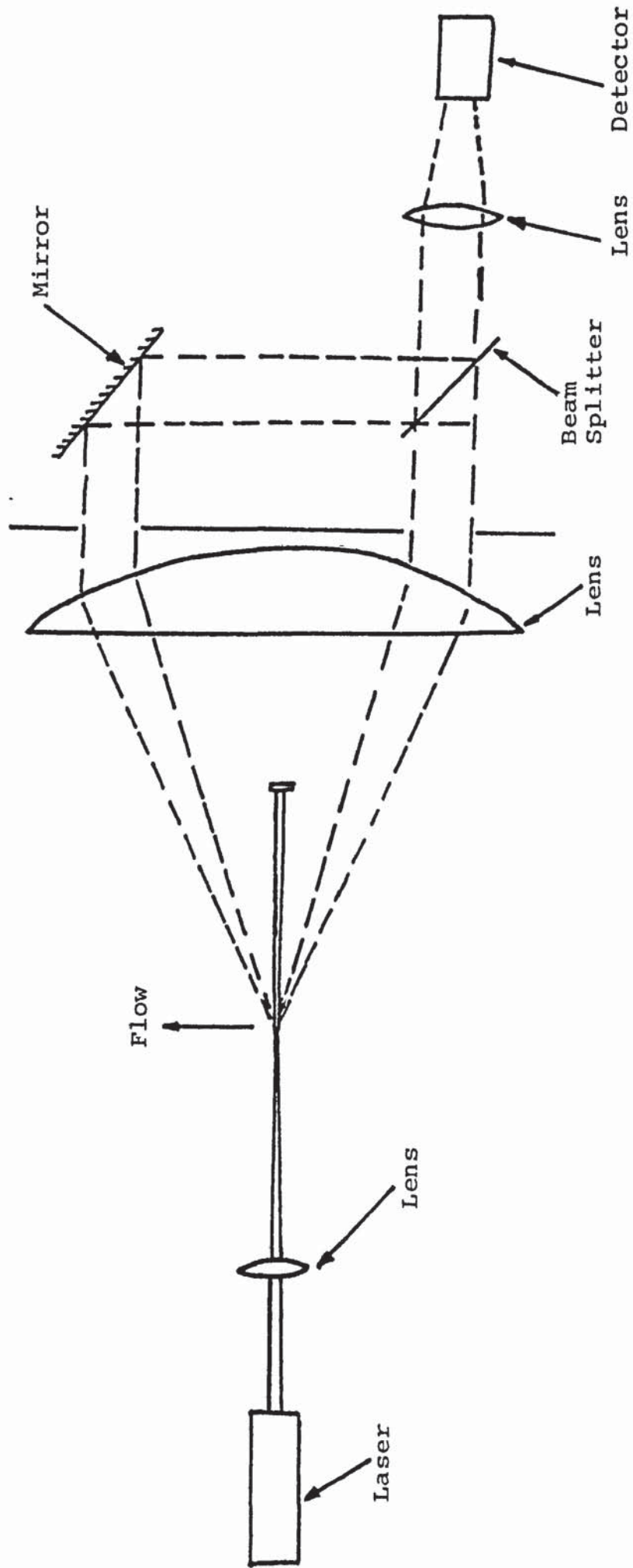


FIGURE 2.3 OPTICAL ARRANGEMENT FOR THE DUAL SCATTER MODE

Doppler shift known as a beat signal. The Doppler beat frequency is given by the equation:

$$\Delta \nu = \frac{DV}{F\lambda} \quad (2.3)$$

where D is the beam displacement produced by the mirror and beam splitter combination

V is the velocity of flow

F is the focal length of the lens

λ is the wavelength of light.

This arrangement provides more than one component of velocity simultaneously by receiving scattered light from a number of directions.

2.2.3 DUAL BEAM OR DOPPLER-DIFFERENCE MODE

This arrangement was developed by various workers. Drain (11) points out that the idea was conceived by a number of investigators at the same time (15-19). Although some authors such as Greated and Durrani (20), Watrasiewicz and Rudd (21), credit Rudd (22) for this work, ISL laboratories patented this technique in 1967, whereas Rudd described this phenomena in 1969.

This method is sometimes called "Doppler Difference" technique, "Dual beam" or Fringe method. A simple arrangement for a dual beam system is shown in Figure 2.4. The two illuminating beams derived from the laser are focused into a small region by a conventional lens. Scattered light from the particles in flow in

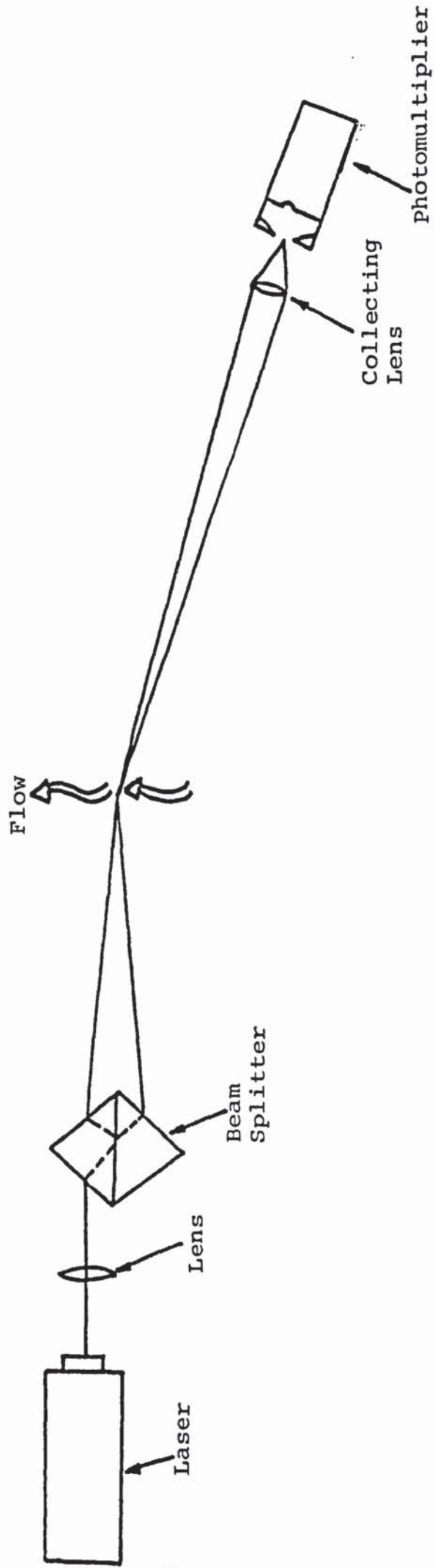


FIGURE 2.4 DOPPLER DIFFERENCE ARRANGEMENT

this region is focused onto the photodetector. Since light scattered from the beams reaches the detector simultaneously, a beat is obtained of frequency equal to the difference in Doppler shifts corresponding to the two angles of scattering. Then beat frequency $\Delta \nu$ is related by the following equation

$$\Delta \nu = \frac{2V}{\lambda} \sin\left(\frac{\theta}{2}\right) \quad (2.4)$$

where V is the velocity of particles passing through the active region

λ is the wavelength of light

θ is the angle of beam separation

This equation is the same as equation (2.2).

This particular system is the most popular and commonly used. Both the reference beam and dual scatter mode are difficult in practice to align when setting up the optical geometry and have a restricted accuracy of frequency measurement. Furthermore, frequency shifting devices can not be easily accommodated because they usually have a very restricted aperture (11)(23)(24). In order to minimise such practical difficulties, it was considered that the dual-beam scatter system was the most appropriate to use in this study.

2.3 DOPPLER DIFFERENCE TECHNIQUE

This technique has been briefly summarised in the previous section but will now be outlined in greater depth. Firstly the two different theoretical interpretations of this technique and then the optical arrangement will be outlined, and secondly how this technique is applied with the commercially available LDA system used in this work.

2.3.1 THE DOPPLER SHIFT INTERPRETATION

The scattering geometry of Doppler difference arrangement is as shown in Figure 2.5. Two focused beams of similar intensity with wave vectors K_1 and K_2 , inclined at angle θ scatter light in a third direction from the particle moving with velocity V' in the flow. The Doppler shifts for each beam are given by the equations (24)

$$v_1 = (K_S - K_1)V'$$

$$\text{and } v_2 = (K_S - K_2)V'$$

$$\text{where } v_1 \text{ and } v_2 = (K_2 - K_1)V' = K_O V'$$

$$\text{but } |K_1| = |K_2| = \frac{2\pi}{\lambda}$$

$$\text{so that } K_O = (K_2 - K_1) = 2 \sin\left(\frac{\theta}{2}\right) \frac{2\pi}{\lambda}$$

if V is the component of V' in the direction of K_O

$$\text{then } v_1 - v_2 = \frac{4\pi V'}{\lambda} \sin\left(\frac{\theta}{2}\right)$$

$$\text{or } v = \frac{2V}{\lambda} \sin\left(\frac{\theta}{2}\right) \quad (2.5)$$

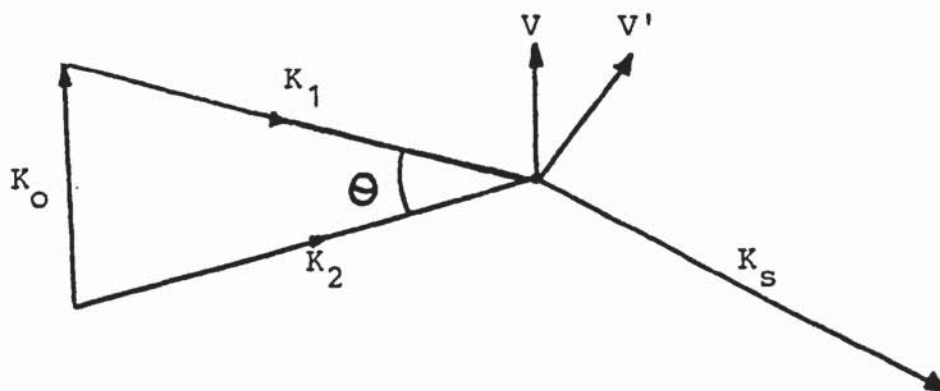


FIGURE 2.5 SCATTERING GEOMETRY-DOPPLER DIFFERENCE EFFECT

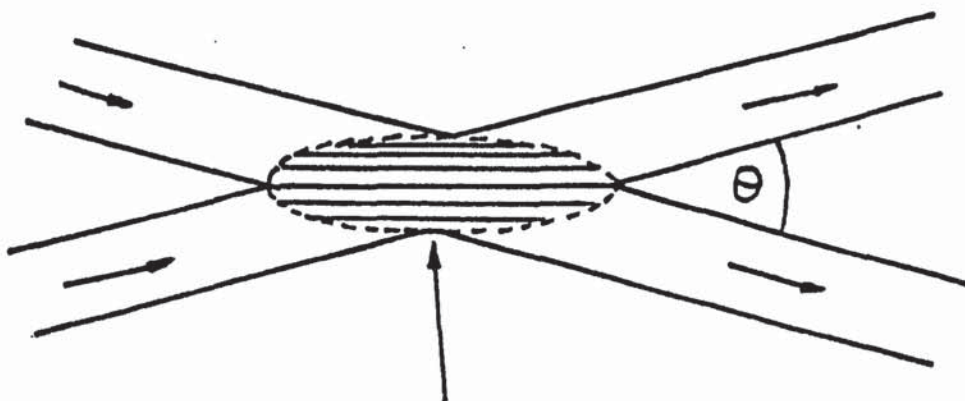


FIGURE 2.6 FRINGE PATTERN PRODUCED IN THE CROSS-OVER REGION DUE TO INTERFERENCE OF TWO BEAMS

Where V is the component of V' in the direction of K_0

θ is the angle between the two beams

K_S is the scattered wave vector

λ is the wavelength of the incident radiation

Thus the velocity of flow can be measured in a selected direction by adjusting the optical arrangement.

It is important to realise that equation (2.5) is independent of the direction of reception, thereby providing a greater flexibility in positioning the photodetector, thus allowing unwanted reflections to be minimised. This was another reason for using this technique in this study.

2.3.2 INTERPRETATION BY FRINGE ANALYSIS

There is another and simpler analysis of this technique which presents a much clearer phenomenological picture of the event that takes place when the particle is passing through the volume at the intersection of two beams.

As previously described in Section 2.3.1, the laser is split into two equal beams and focused on the position of interest in the flow. Because of the coherence of the source, the beams will interfere constructively and destructively with one another and therefore establish a set of closely spaced, planar, stationary interference fringes at the crossover region as shown in Figure 2.6.

The spacing S between these fringes will be given by the equation

$$S = \frac{\lambda}{2 \sin \theta/2} \quad (2.6)$$

where λ is the wavelength of incident light
 θ is the angle between the two beams

Consider a particle in the flow crossing these fringes. It will block off a great deal of light in a bright fringe and only a little light in a dark fringe. Therefore, the light which is transmitted can be collected and will fluctuate at the rate which the particle crosses the fringes. This will modulate the light at a frequency ν by the equation

$$\nu = \frac{V}{S} \quad (2.7)$$

Now substituting equation (2.6) into equation (2.7) we get

$$\nu = \frac{2V}{\lambda} \sin(\theta/2) \quad (2.8)$$

showing equations (2.8) and (2.5) are the same.

In the current study, the fringe spacing S needs to be calculated. In order to do this some assumptions have to

be made, i.e.

8

- (i) the nature of the beams is Gaussian
- (ii) when the beams cross at the measurement point, the fringe spacing is constant

Then from equation (2.6)

$$S = \frac{\lambda}{2 \sin(\theta/2)}$$

from Figure 2.7 for small angles $\sin(\theta/2) = \frac{b/2}{d}$

where b = beam separation at the arbitrary measurement point

d = distance from arbitrary measurement point to the beam crossing

λ = laser wavelength of beam

Hence eq. (2.6) becomes $S = \frac{\lambda d}{b}$ (2.9)

The arbitrary reference point is commonly taken as the exit from the beam splitter (but in this equipment used any point on the bisector of two beams can be taken).

As mentioned previously in Section 2.3 the interpretation of this method is given to Rudd (22) although wrongly. There are a number of leading workers in this field who refuse to accept the existence of fringes in the probe volume. Research workers at the Royal Signals and Radar Establishment, Pike (25,26) Abiss (27) argue strongly that fringe picture method has only a heuristic value

*I find a right
clear this
multiple
the
the*

and emphasise that 'no fringes exist really in the flow'. ^{why}

Even though the fringes can be projected on to a flat surface by using suitable lenses, they believe that the fringes exist only in the eye, because no damage can be done to the fringes. The writer feels that this controversy will continue for a considerably long period since there is no way of refuting this argument at the moment. The concept of the fringe pattern is useful in understanding what is happening because of its simplicity.

2.4 SIGNAL PROCESSING

In order to obtain maximum information and accuracy from LDA experiments, serious consideration must be given to signal processing to transform the raw signals from the detector into velocity information. There are various types of processing techniques available, spectrum analysers frequency tracking filters and simple counters. In this study, the simple counting technique was considered to be suitable and will be discussed below.

2.4.1 PHOTON CORRELATION

When scattered radiation is received at the detector or photomultiplier (PM) high intensity is converted to electrical signals. These photomultipliers as shown in Figure 2.8, are vacuum tubes in which electrons are released by light falling on a special photosensitive surface (or arrival of photons at photosensitive surface). The signal thus originates in digital form which can be easily processed by the photon correlator.

b = Beam separation at the arbitrary measurement point

d = Distance from arbitrary measurement point due to the beam crossing

θ = Angle between two beams

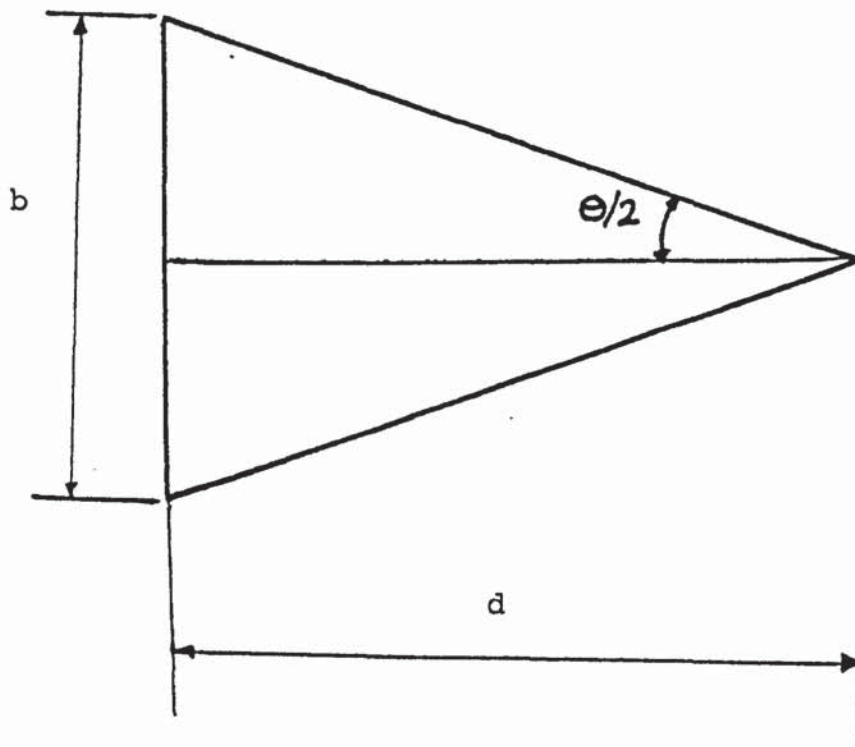


FIGURE 2.7 OPTICAL GEOMETRY OF DOPPLER-DIFFERENCE
ARRANGEMENT

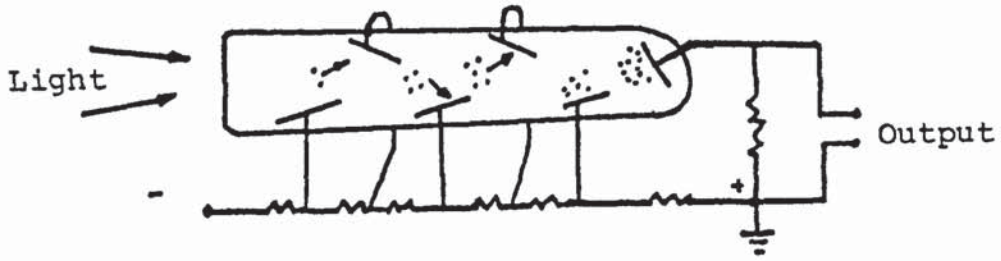


FIGURE 2.8 PHOTOMULTIPLIER DETECTOR

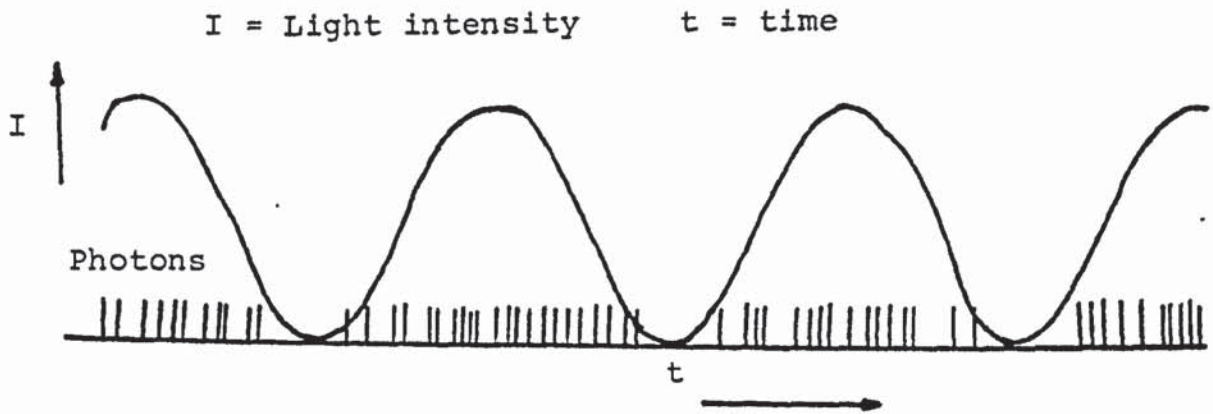


FIGURE 2.9 RANDOM PHOTON ARRIVAL PATTERN

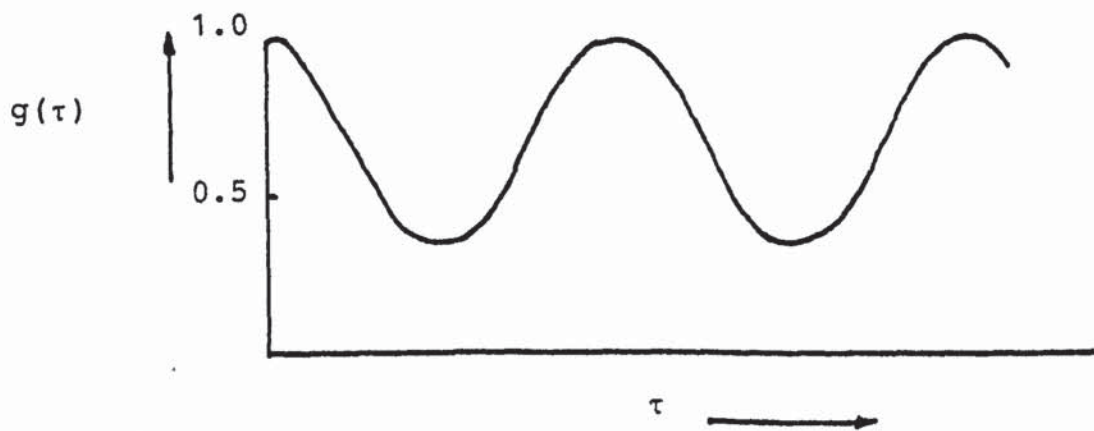


FIGURE 2.10 CORRELATION FUNCTION OF PHOTONS

Photon correlator measures the variation in light intensity as a result of fluctuations of the mean time intervals between photon arrivals. Usually sinusoidal variation in intensity as shown in Figure 2.9 would appear on the arrival of photons. The events occur at random but at any given time the probability of occurrence is proportional to the light intensity.

Assume that a correlation function $g(\tau)$ describes the probability of two events being separated by a time τ then the function can be defined by the expression

$$g(\tau) = n(t) n(t+\tau) \quad (2.10)$$

where $n(t)$ is the number of photons arrival events occurring with an interval of time δt at a time t

This produces a correlation function $g(\tau)$ which would have the behaviour of a sinusoidal function shown in Figure 2.10.

In order to implement the technique, photons are counted in successive small intervals of time δt (typically $1\mu s$). The number of photons counted in intervals separated by a time $p\delta t$ (where p is an integer) are correlated. The function computed is:

$$g(p\delta t) = \sum_{i=1}^{i=n} n_i (n_{i+p}) \quad (2.11)$$

where n_i is the number of photons counted in i th interval

N is the total number of terms in the summations. If P values of the function $g(\tau)$ are needed then P summations are necessary simultaneously. One of the methods for doing this is by the arrangement shown in Figure 2.11. Counts from the photomultiplier are directed to the main storage channel and are added or not depending on the setting of a gate which is controlled by the contents of the corresponding one bit shifting register, i.e. the gate is open if the number in the register is 1, closed if 0. Each sampled time clock pulse shifts the contents of this register one place to the right and enters the new clipped counts from the clip gate. To form the single clipped correlation function this delayed clipped data is then multiplied by the unclipped input. Thus a very simple form of multiplication is formed. And this results in a function in the storage channels approximately close to the true correlation function, (for further detailed discussions of the theory and design of a single-clipping correlator, see Cummins and Pike (28).

The correlation function generated in the correlator can be plotted to produce a cosinusoidal decay function. Such a function is shown in Figure 2.12. An equation computer fitted to this function would take the following form:

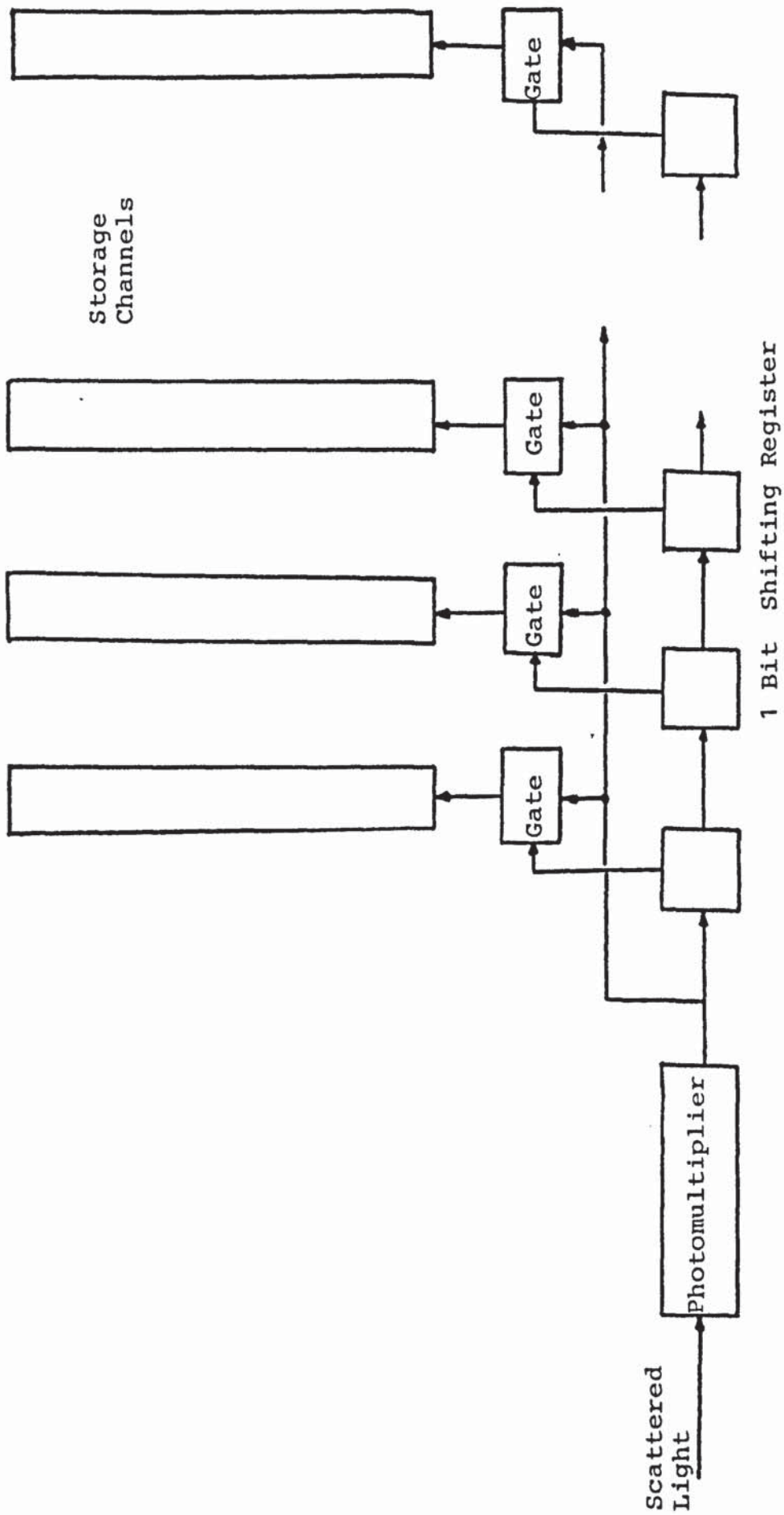


FIGURE 2.11 SIMPLIFIED SCHEMATIC REPRESENTATION OF PHOTON CORRELATOR

$g(\tau)$ = Correlation function

τ = Sample time

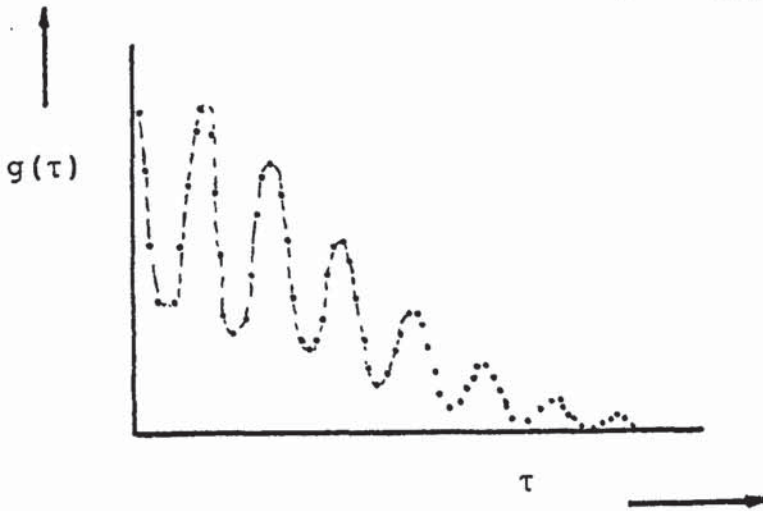


FIGURE 2.12 THE COSINUSOIDAL CORRELATION FUNCTION

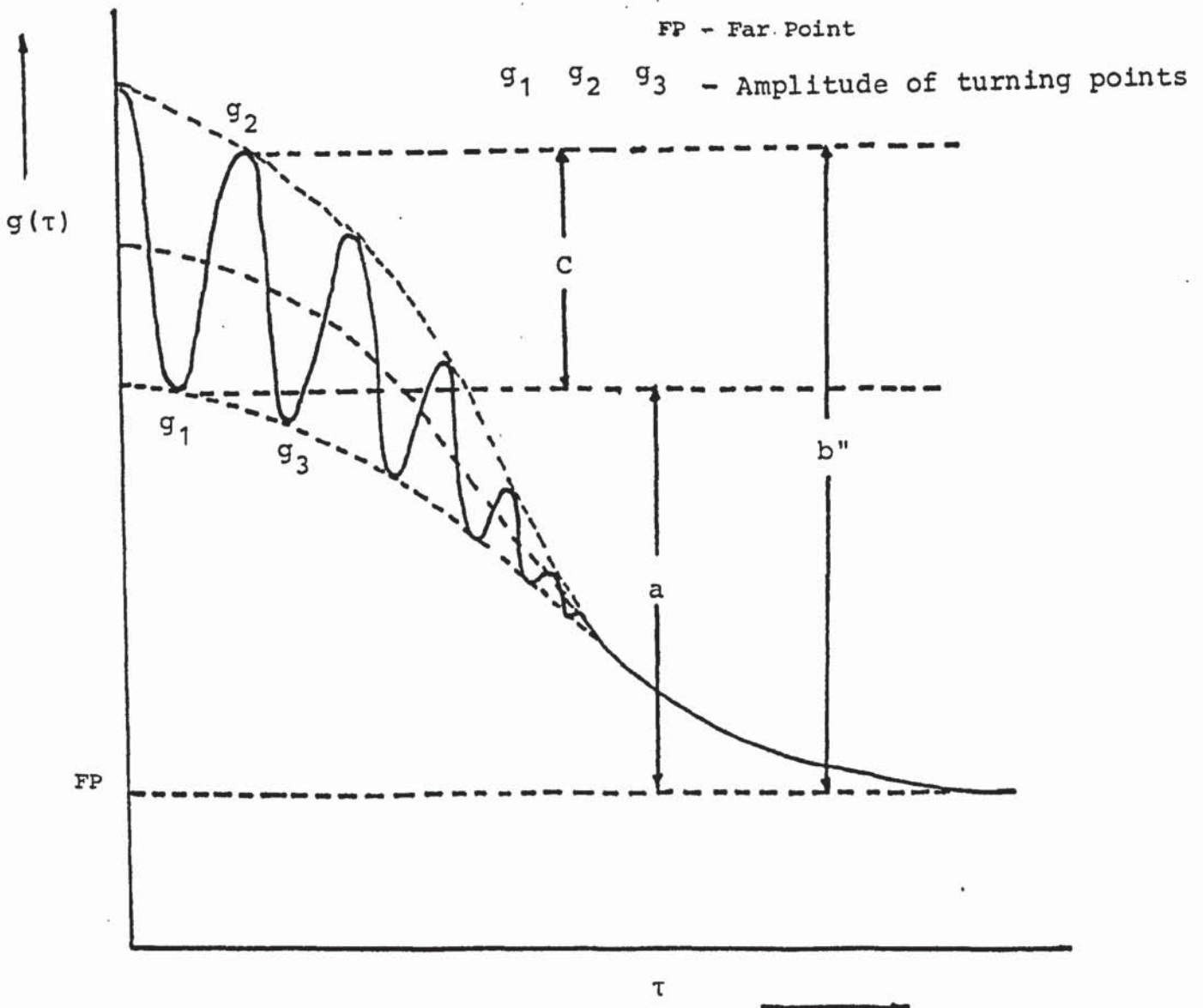


FIGURE 2.13 ANALYSIS OF CORRELATION FUNCTION

$$g(\tau) = \frac{a_0}{V} \exp\left(\frac{V^2 \tau^2}{r^2}\right) \left[1 + \frac{1}{2} m^2 \cos\left(\frac{2\pi V \tau}{S}\right) \right] \quad (2.12)$$

$g(\tau)$ is the correlation function

a_0 is experimental constant

V is the velocity of particle or flow

τ is the sample time

r is the beam radius

m is the fringe visibility factor ($0 < m < 1$)

S is the fringe spacing

A detailed analysis of signal processing and photon correlation has been presented by Pike (25) and Abiss et al. (24), and a theoretical development of the above equation is given by Abiss (27).

2.5 THE AUTO-CORRELATION IN LAMINAR FLOW

When the signal is treated as outlined in previous section a typical autocorrelation function of a process that meets the demands of the model (used in this study) is obtained as Figure 2.13.

The far point represents the amplitude of the coefficient that implies Uncorrelated data, this is measured directly from the correlator channels.

The Cosine term in eq. (2.12) arises from the intensity fluctuations caused by particles cutting the fringes and modulating scattered light.

The first three turning points on the Cosinusoidal of the correlation function are required, and can be achieved by adjusting sample time.

The amplitude for each of the turning points g_1 , g_2 and g_3 and the delay time at which they occur t_1 , t_2 and t_3 help to calculate velocity and turbulence estimates.

Hence the effective fringe visibility m is given by

$$m = \frac{c}{(a+b'')/2} \quad (2.13)$$

where $a = g_1 - \text{FP}$

$b'' = g_2 - \text{FP}$

$c = g_2 - g_1$

FP = Far Point

a , b'' and c are measured sections from Fig. 2.13.

Hence equation (2.13) becomes

$$m = \frac{2(g_2 - g_1)}{(g_2 + g_1 - 2\text{FP})} \quad (2.14)$$

The number of fringes n in the beam radius r are given by

$$n = \frac{2r}{S} \quad (2.15)$$

At this stage a 'simple rule of thumb' (25) formula is applied to the first few cycles of the correlation to give the value of turbulence η . We have

$$\eta = \frac{1}{\pi} \sqrt{\frac{1}{2} (R-1) + \frac{1}{8n^2}} \quad (2.16)$$

when R is the ratio

$$R = \frac{g_2 - g_1}{g_2 - g_3}$$

The 'observed' velocity, V_o is that obtained from the period of the Cosine, the best estimate is obtained by an averaging of the three turning points, t_{av}

$$t_{av} = \frac{1}{3} (t_1 + t_2 + t_3)$$

In order to make any calculations of velocity and turbulence estimates, the turning points g_1 , g_2 and g_3 and the delay times t_1 , t_2 and t_3 are required, as outlined below and also in the operating Manual (29).

These are calculated by differentiation of the correlation and the zero crossings of the resultant function. The differentiation is performed by subtraction of adjacent channel, for channels h and $h+1$, this gives an estimate for delay time $h + \frac{1}{2}$, providing location of each turning point to within one channel resolution of the correlator.

The exact turning point is located from the approximation using parabolic interpolation over the three points as shown in Figure 2.14.

The first estimate locates (g_n, t_n) , subsequently allowing g_z and t_z to be evaluated assuming a parabolic form

$$g = a(t-t_z)^2 + g_z \quad (2.17)$$

Differentiating eq. (2.13) and using measured $(\frac{dg}{dt})$ values allows the estimate to be obtained as

$$t_z = t_n - 0.5 - \frac{(\frac{dg}{dt})_H}{2a} \quad (2.18)$$

where $a = 1/2 \left[(\frac{dg}{db})_H - (\frac{dg}{dt})_L \right]$

and $g_z = g_n - a(t_n - t_z)^2$

hence $V_o = \frac{S}{\tau t_{av}} \quad (2.19)$

where τ is the correlator sample time.

This observed velocity V_o is then corrected for its systematic error (due to effects of both turbulence and finite beam width) to give true velocity V .

$$V = V_o \left[1 - \eta^2 - \frac{1}{m^2 n^2 \pi^2} \left(1 + \frac{m^2}{2} \right) \right] \quad (2.20)$$

$\left(\frac{dg}{dt}\right)_H$ = Differential at higher turning point

$\left(\frac{dg}{dt}\right)_L$ = Differential at lower turning point

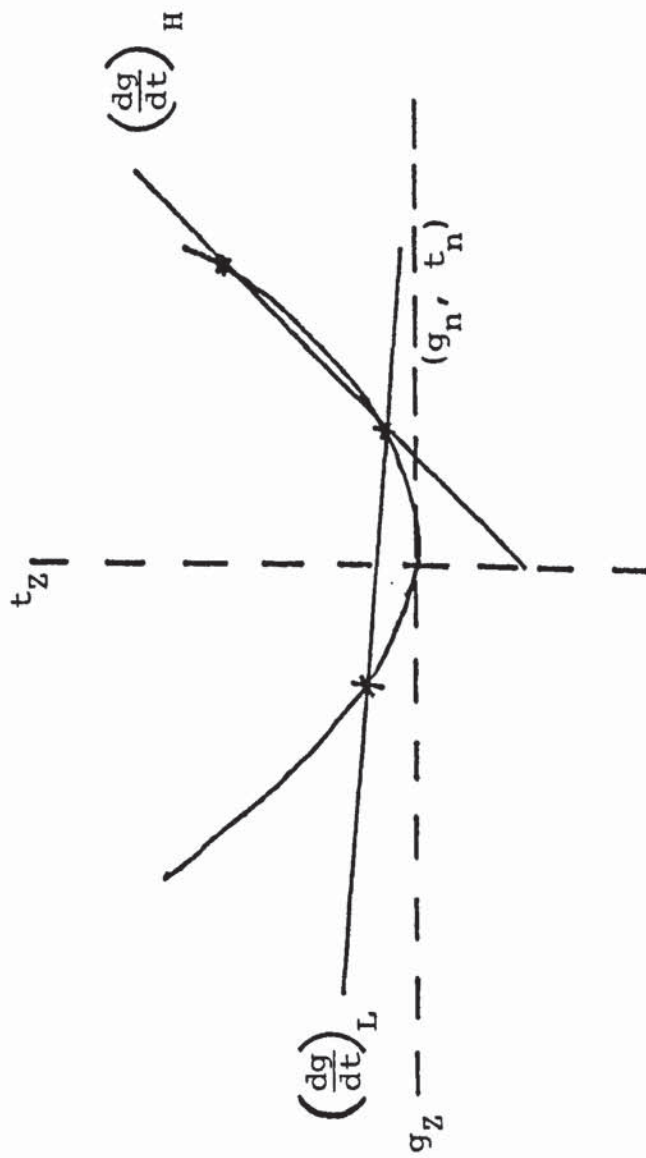


FIGURE 2.14 PARABOLIC INTERPOLATION OVER THE THREE POINTS TO DETERMINE TURNING POINT VALUE

In the present work, calculations were carried out by an algorithm that evaluated velocity and turbulence and was provided by the manufacturers (29). The procedure for using this algorithm is outlined in a summary form in Appendix A - 1.0.

2.6 APPLICATIONS OF LASER DOPPLER ANEMOMETRY

Since the present project is dependent on the application of Laser Doppler Anemometry for measurement of point velocities in PHE channels, it is considered useful to outline work already carried out in related fields.

THE LDA technique is now a powerful tool and has been widely used in various fluid flow systems in research and industry.

In the last few years several conference proceedings (31,32) and books (11, 13, 20, 21, 32) have been published on LDA. These will be reviewed in this section, together with more recent papers published in technical journals.

Watrasiewicz and Rudd (21) describe the use of LDA in wind tunnels for the measurement of wind velocities. But a much more detailed book (13) summarises specific applications in different flow situations, for example laminar, turbulent and complex flows such as those associated with shock waves, measurement in compressors and in a variety of combustion configurations. In each case the authors have paid great attention to optical

and electronic systems.

A very recent book by Drain (11) discusses applications of LDA to aerodynamics, combustion and measurement in microscopic and biological systems. Various areas in which LDA has been applied successfully are presented in Table 2.1 (34).

Several workers (36-38) have used the LDA in wind tunnels. Meyers (35) at NASA - Langely Research Centre made measurements in a 6.6 x 4.4 m high wind tunnel, and tunnel velocity of 51 m/s and a Reynolds number (Re) of 1×10^6 . A much smaller tunnel was used by Weinert (36) of size 150 mm.sq. but the flow rate was higher, Re range of $3-10 \times 10^7$, that is supersonic velocities, and made an attempt to measure flow in dead-air region. Boutier et al. (36) reported measurements in wind tunnel 1.75m long and 0.9m wide by using two-dimensional two colour fringes in back scatter mode. They do not report the size of their flow rate but the maximum velocity measured was 50 m/s. A comparison was made of LDA values with the pitot tube and a good agreement was achieved. Boutier recommended glass windows as a suitable material to allow passage of the beams and pointed out that perspex should be avoided because much of the light of beams scatter within it.

In the last few years interest has been developed in the investigation of flow in internal combustion engines (39-45). One of these references (39) describes measurement of mean velocity and characteristics of isothermal incompressible flow within a piston cylinder.

TABLE 2.1 APPLICATIONS OF LASER DOPPLER ANEMOMETRY

PHYSICAL-INDUSTRIAL	BIOLOGICAL
WIND TUNNELS	CELL MOTILITY
TURBINE DESIGN	PROTOPLASMIC STREAMING
LIQUID FLOW	SURFACE BLOOD FLOW
SOUND SPEED	RETINAL BLOOD FLOW
TURBULENCE	HEART VALVE EVALUATION
ENGINE EXHAUST	FLUID CIRCULATION IN FISH
SURFACE MOTION	AUDITORY STIMULUS AND RESPONSE
VIBRATION	ELECTROPHORESIS
FLAMES	
PARTICLE SIZING	
STACK EFFLUENCE	
NUCLEATION	
ELECTROPHORESIS	

A perspex piston was driven in simple harmonic motion, inside a perspex cylinder of 7.5 mm wall thickness, at a rotational speed of 200 rpm, ensuring highly turbulent flow within the cylinder.

It was shown that the entrance gave rise to a strong vortex near the piston, as the air was deflected radially along the piston face and cylinder wall. However there is some information missing since the authors fail to indicate the size of scattering particles used in the flow stream. They did state that fringe spacing was 4 μm at the intersection of two beams, hence it can be concluded that the particles were smaller than 4 μm . The authors do not also state whether the silicon-oil particles used were passed through any graded filters before they entered the chamber.

A major difficulty in this work was the signal quality obtained. Witze (42) used plastic windows and oil-droplet particle seeding, this gave rise to wetting of the windows surface and led to an unacceptable signal to noise ^{ratio (SNR)} when the engine operated. The plastic window was changed to quartz and the problem of seeding was overcome by changing oil-droplets to NaCl particles of 0.6 μm diameter. These were suitable but these soil the window after a short period. The Tio_2 of 0.2 μm diameter were tried and these did not soil the window but deteriorated the signal quality.

Witze found the paramount problem was the highly background light problem, which made measurement sometimes impossible. Measurements were made for 500-2500 rpm in the high swirl engine. The author compared results with the hot-wire Anemometer technique and found reasonable agreement between the two.

Similar experimental difficulties associated with the window were reported by Rask (43) who finally used the Quartz window but used a dried solution of salt/water as the seeding particles of $1\mu\text{m}$. But the windows became dirty after a short period and regular cleaning was necessary. Rask made measurements at 270 rpm and 200 rpm of engine speeds for various crank angles.

Recently Ramos et al. (40) carried out both theoretical and experimental studies of turbulence in the internal combustion engine. Their experimental work was similar to Morse et al. (39) but the rotational speed was much lower, at 31.25 rpm. The authors showed good agreement between theoretical and experimental results. The authors state that they used fringe spacing of $3\mu\text{m}$ and filtered the particles to less than $5\mu\text{m}$. However, this could give rise to a degradation of signal quality because the particle is large compared with the fringe spacing. Hence large particles span high and dark bands of a fringe pattern and therefore average out the variations of light intensity thus reducing the modulation of a signal from a moving particle. The authors have not

commented on the signal quality but other workers have been known to comment on this type of problem, see Ross (46).

Another type of flow geometry that has been investigated is the measurement of velocity characteristic in air jets (47, 48). Danielsson and Lundgren (47) tried to study instabilities in rotating flows. They constructed a rotating cylinder system of transparent plastic and investigated the size of throughput allowed before the general flow pattern collapsed and how this flow affected separation of gas mixtures. The arrangement is shown in Figure 2.15. Basically there are two cylinders, inner and outer. The outer cylinder rotates and is kept cooled by a water jacket to prevent heating of the plastic cylinder during rotation. In the inner cylinder the optical system was set up and measurements of velocity distribution and radial velocity profiles were obtained. The authors gave particular attention to the practical problems encountered during experimental work, e.g. reduction of light entering PM tube, seeding, type of scatter technique. It must be pointed out that the authors failed to obtain any result using gas mixtures of Freon 14 and Helium, but managed to obtain results with air. The authors do not point out the thickness of plastic walls or take account of this in their calculations.

about
effect of
thickness

In the last few years interest has developed in investigating air flow around rotating blades (49-57).

P = Pump

HE = Heat Exchanger

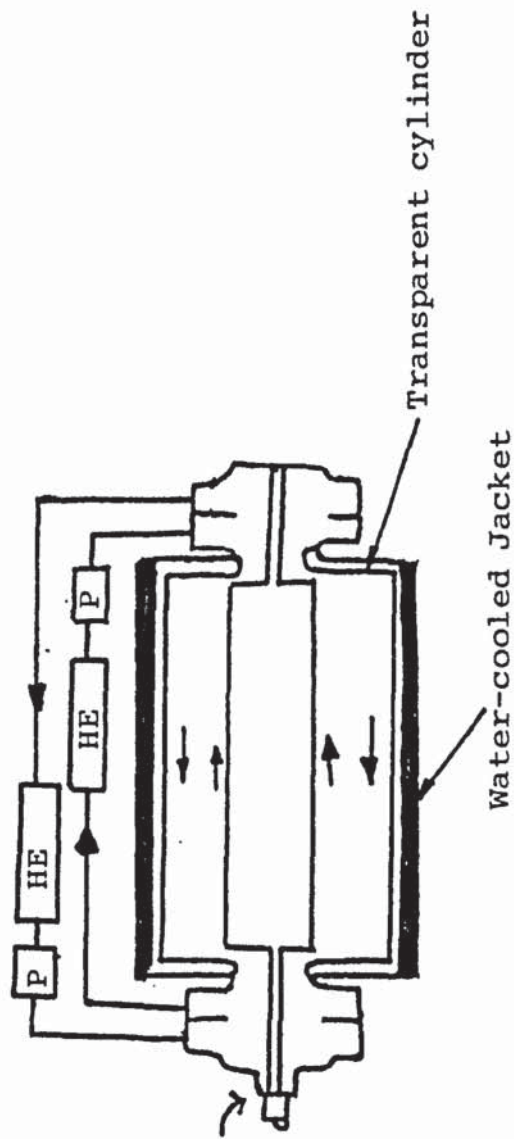


FIGURE 2.15 CYLINDRICAL CONTAINER FOR THE STUDY OF ANNULAR GAS JETS

Adrain et al. (49) made measurements at impeller speeds of 30 and 60 x 10³ rpm, Powell et al.(50) at 16 x 10⁶ rpm and Allos (51) at 63 x 10³ and 73 x 10³ rpm, while Miles (52) did not state the speed involved in his investigations.

Most of the workers (49, 50, 51, 54, 55, 56) reported contamination settling on the windows and this deteriorated the signal quality, therefore frequent cleaning was necessary at regular intervals, but in order to do this compressor had to be stopped. Schodl (55,56) developed a special device to clean windows while the compressor was still in operation. Most particles can be cleaned off the window but TiO₂ was impossible to remove. All these workers used various particles SiO₂, Al₂O₃, MgO and dust but the light flare at the windows caused difficulties in measurements. Allos made measurements approximately 7 mm from the wall while other workers (50, 56) reached much closer to the wall.

Although flare from the windows is a common problem, (49, 50) a method was developed to overcome this problem. Powell et al. and Schodl used fluorescent seed particles introduced into the flow to absorb laser light, subsequently emitting light at a different wavelength. An optical filter in the receiving optics filters out the unwanted light scattered from the surface near the probe volume. Powell et al. used seeding solution of rhodamine 66 in a 50-50 mixture (by volume) of ethylene glycol and benzylalcohol, which fluoresced orange when absorbing

green laser light. Thus when an average-pass filter was used in the receiving optics, the extraneous green scattered light was filtered out, also using these fluorescent particles Schodl measured flow about 0.5 mm from the wall.

Nearly all the workers mentioned practical problems except Miles who mentioned no such problems, in fact there was a significant amount of information missing, e.g. the type of optical system, fringe spacing, particle size used in seeding and beam angle separation.

In the last 2-3 years interest has developed in measurement of electrostatic precipitations (58, 59, 60, 46). Kawase et al. (58) used a model cell of an electrostatic precipitate made of glass plates and carried out measurements successfully. There is no mention of thickness of the glass plates and how account was taken of refraction through the glass. Ross (46) carried out similar measurements but found some problems in the signal quality. He acknowledged this may be due to large differences between size of seeding alumina particles (10 μ m) and fringe spacing (6 μ m), but he did not confirm this by either using smaller particles or larger fringe spacing.

Due to the unique ability of LDA to make measurements in a hostile environment, significant work has been carried out in combustion systems (61-71) from flames to industrial burners.

Owen (61) made measurements in spray flame burners of size 100 cm long and 12.23 cm diameter, of axial and tangential velocity profiles. Experimental difficulties were observed using Al_2O_3 and TiO_2 as seeding particles. The particles were deposited on windows and degraded the signal to the unacceptable level. Silicon oil droplets were tried and failed. They evaporated before reaching the combustion zone. Then microballoons (hollow spheres) of bakelite phenolic resin of 5 μm were used successfully. While, Caveney et al. (70) relied on particles naturally occurring in the flame, although gaseous flame was initially seeded with alumina or NaCl particles but stopped after a while, Cenker (71) used alumina, TiO_2 and latex spherical particles of 0.357 μm suspended in alcohol.

Similarly other workers (63, 64, 65) made measurements in different size of combustion chambers with or without reaction. Although they do not report experimental difficulties such as experienced by Owen, they have failed to supply comprehensive information, e.g. particle size.

The most recent industrial application of LDA system has been carried out in Poland by Grabek et al. (68). The authors studied two problems. One was measurement of gas motion in a cylinder for dust separation. The other was measurement of flow in industrial furnaces with the purpose of gaining control of the particle emission. The authors constructed a conical glass model of a cyclone of diameter 130 mm and 40 mm at top and bottom respectively with a height of 138mm. Seeding particles of a mixture of glycerine and water were used. The authors

attempted to measure three component at tangential, axial and radial velocity. They failed to obtain any measurement in radial direction because they found it extremely difficult to locate the precise position where measurements were carried out. However, the authors fail to point out how the precise position was determined in the other two cases. They also fail to point out the thickness of the glass used or make clear whether they accounted for refraction in determining cross-over positions. Furthermore some information is not given in the article, e.g. size of particle, fringe spacing.

In the case of a model furnace, the authors fail to provide size or description of the furnace but give all the velocity profiles (vertical and horizontal) in the furnace.

Another interesting application of LDA has been to measure velocity in a fluidized bed (72). The authors intended to fluidize a bed of spherical glass beads in a flow rate of a few cm/s to few hundred cm/s. by using a refractive index matched liquid (of ethyl and benzyl alcohol) as the fluidizing liquid. But no measurements were made due to incomplete installation of all the equipment. But the authors demonstrated that a signal can be obtained using this refractive matched liquid in a rotating flow system with glass beads. Tolerance of refractive index mismatch was reported to be 10^{-3} .

Investigations into jet engine noise patterns and velocity fields near the working propeller behind a model ship in a towing tank (73) have been attempted using LDA. Significant progress has not yet been made in this direction.

Because of the high resolution possible with LDA technique, this has been used most extensively in medicine and biology in flow of blood measurement (74,75,34), measurement of eye movement (76) and in skin friction drag measurements (77) much more recently.

Finally it must be pointed out that LDA is still widely used in the fundamental measurement of flow to compare results with existing theoretical knowledge and alternative experimental measurements. The continuing interest is worldwide for velocity measurements in turbulent pipes (78,79,80, 89-92) constricted and sudden expansion of tubes (81,82,83,84), flow measurement in bundles of tubes (85), flow around cylinders (86,87,88), resonant hydraulic circuits (93), polymer flow studies (94), oscillatory flows (95), secondary flows (96), three dimensional flow in a jet (97). Successful measurements have also been made in two phase flow (98-101), and a modified LDA technique has been used to provide particles size information (102-108).

All the previous work outlined above has been in flow systems where laser beams could easily be passed through the apparatus. Although the flows were complex

in various cases, there has been no work reported where measurements are made in a perspex channel of a plate heat exchanger. The present work is the first ever reported as the application of LDA in heat exchangers of a very complex geometry and will be discussed in the following chapters.

CHAPTER 3

LITERATURE REVIEW ON PLATE HEAT EXCHANGERS

3. LITERATURE REVIEW ON PLATE HEAT EXCHANGERS

The following literature survey is a comprehensive study of the available information on 3-dimensional trough form plate heat exchangers.

The latest such review was carried out by Fattah (7), so that the present review takes the development of the PHE's from 1975 to the present day. A brief background to each reported work is provided, together with suitable critical comments.

Fontaine and Lannoy (109) examined flow distribution in a plate heat exchanger channel using two plates clamped together from a PO1 Alfa-Laval exchanger. Mains water was used as the working fluid and this was mixed with distilled water as a tracer. The change of electrical conductivity in the exit stream was measured with time. This change with time was plotted and related to a residence-time distribution equation of the type:

$$Z = 1 - e^{-a_1 t^{b_1}} \quad (3.1)$$

where Z = experimental response

t = time

a_1 and b_1 are the distribution constants.

The authors used two different techniques for evaluating constants a_1 and b_1 . One was by direct modelling of a 'process reaction curve' and the other by

a regression method.

The 'process reaction curve' method is based on the sigmoidal shape of the curve of response vs time. This can be compared to the response caused by a unit step forcing function. From the model and the shape of the curve the value of ' a_1 ' and ' b_1 ' are evaluated.

The second method was by rearranging equation (3.1) and taking double logarithms, i.e.

$$(1-Z) = e^{-a_1 t^{b_1}} \text{ where } 0 < 1-Z < 1$$

and taking logarithms

$$-\ln(1-Z) = a_1 t^{b_1} \text{ then } \ln(1-Z) < 0$$

taking further logarithms

$$\ln[-\ln(1-Z)] = \ln a_1 + b_1 \ln t \quad (3.2)$$

The above equation represents a straight line and therefore both coefficients a_1 and b_1 can be evaluated.

Fontaine and Lannoy made measurements in the turbulent flow regime but the range of Reynolds number was not quoted, only 4 different flow rates at 72 l/hr, 85 l/hr, 112 l/hr and 114 l/hr.

They also do not comment to any extent on their results but merely point out that the direct method was better than the regression method because in the regression method, extrapolation may be necessary and may not be accurate.

At the beginning of the paper (109) the authors state their intention of learning of stagnant areas which decrease the efficiency of PHE's, but they do not at all comment on this in their conclusions. Essential information is not given and the mathematical development of the direct method model is confusing. The most interesting factor regarding this work is an attempt to examine a single channel, but there is no information about how the plates were clamped together or whether the arrangement of plates is 2-dimensional or 3-dimensional.

Although the authors do not state whether the flow was upwards or downwards, examination of the arrangement of flow diagram indicates clearly that the flow is upwards. It would have been useful if comparison had been made with downwards flow. They fail to point out whether the inlet and outlet ports were on the same or opposite sides of the plates.

Roig et al. (110) obtained data of Residence Time Distribution (RTD) for the holding section (presumably the channel) of a PHE (Alfa-Laval Model P20-HB). Two flow rates, 4 and 2 l/min were reported using water as the working fluid for the RTD data which were obtained

by imposing a step change in the concentration of red dye at the inlet and measuring the concentration of dye at the outlet. Samples of the outlet were collected at approximately two-second intervals.

The response to a step change (F curve) was plotted with time, for both rates. The data for both flow rates produced similar shapes. They found that average residence times were inversely proportional to the flow rates, and also showed that the RTD data followed closely the theoretical model of five tanks in series.

Considering this work, it is clear that there is no indication of the type of flow i.e. laminar or turbulent in the PHE channel. It is likely that the flow was turbulent but particular dimensions for calculating the Reynolds numbers are not quoted.

If the flow was not turbulent, effective sampling of the outlet stream would be extremely important in order to get representative results for analysis. Furthermore, there is no indication whether the flow was upward or downward.

Ito and Masubuchi (8) examined the dynamic analysis of PHE systems for various types of flows.

They classified the flow patterns as: series, parallel and complex. The authors prepared generally derived equations, with boundary conditions, based on a heat balance and the dynamics in the form of frequency responses to the change of either the inlet fluid temperature or the flow rate.

Although the authors suggest that the plate is a commercial type they provide no details. The diagram given in the publication appears to be the three-dimensional APV junior plate which is a rather small plate to be described as "commercial".

Ito and Masubuchi prepared equations for the heat transfer coefficients of plates, applying various assumptions which they claim have been justified in the past e.g.

- (i) The heat loss to the surroundings is negligible.
- (ii) There is no heat conduction in the direction of fluid flow in the plates and the fluids.
- (iii) The temperature and flow rates are uniform across the flow passage
- (iv) The film coefficient of heat transfer is greatly dependent on the fluid velocity and is proportional to an exponential function of the fluid velocity or the flow rate.

Ito and Masubuchi have based their equations on these assumptions, but Fattah (7) and Okada et al.(111)

showed that assumption (iii) is incorrect. Fattah found that at low Reynolds number the flow up the channel was mainly in the small recess adjacent to the gasket, on the same side of the channel as the ports splitting away to flow in a zig-zag manner up the channel as Re increases. Okada measured temperature profiles in a two-dimension PHE's for upwards and downwards flow, in the Reynolds number range from 100 to 21600. . Since the publication is only available in Japanese, a general impression of its contents have been obtained. It seems they found that for many different flow rates there was variation in temperatures across the channels. They presented their data as contour forms of temperature and found differences in different types of flow, i.e. diagonal and vertical flow in the channel. This certainly showing that neither is flow constant across the channel nor is temperature, hence showing clearly that assumptions by Ito and Masubuchi are not justified.

Again in the article by Ito and Masubuchi, it was not clear whether the flow was laminar or turbulent, but only reported flow rates of 2.4 l/min. on the hot side and 1.6 l/min on the cold side, using water as the working fluid. If the assumptions made by the authors are acceptable then their models prepared are justified.

The experimental investigation was carried out in two parts, firstly for the fluid temperature input and secondly for the input of a flow forcing signal.

The frequency responses for the temperature were obtained using sinusoidal changes in temperature of the inlet hot side fluid, and then measuring temperatures along the flow to calculate amplitude ratios and phase angles. The sinusoidal changes were made by mixing hot and cold water using a feedback temperature signal at the inlet of the heat exchanger. They obtained frequency responses of fluid temperature at five positions for parallel and complex flow for four and eight flow passages.

Also frequency responses were obtained for the input flow using sinusoidal changes of the flow rate of the hot side fluid, measuring temperatures and calculating amplitude ratios and phase angles. The sinusoidal changes were made by means of a control valve using the flow controller corresponding to sinusoidal signals. Frequency responses of the input forcing signal were obtained for four flow passages. There were no plots of eight flow passage and no reason was provided for this omission.

Although there was a good agreement between theoretical and experimental work, there are significant errors in the assumptions made. The authors emphasise in their conclusion that these experimental and theoretical results are based on the assumption of uniform flow and uniform temperature across the flow passage. This is a most unsatisfactory assumption. The results do not indicate

what is happening locally in individual channels, information which would be more useful to design engineers of PHE's.

In 1977 Marriott (112) published an interesting paper in which he discussed the importance of channels formed from plates of the Alfa-Flex systems (an arrangement of plates where the chevron angle differs on adjacent plates). It was claimed that energy savings of up to 25% can be made by this arrangement compared to a conventional PHE. Using the basic relationships of heat transfer without phase change he developed an equation to estimate θ' , the number of heat transfer units (HTU) as shown below:

$$\theta' = n_s k \cdot 2A / (G \cdot C_p) \quad (3.3)$$

where θ' = number of heat transfer units (HTU)

n_s = number of passes

k = overall heat transfer coefficient $w/m^2 \text{ } ^\circ\text{C}$

A = area of plate sq.m.

G = mass flow rate per channel kg/s

C_p = specific heat $\text{KJ/kg} \text{ } ^\circ\text{C}$

It is well known that the hydrodynamic characteristics of a channel bounded by plates having cross corrugations are very dependent upon the angle at which the corrugations cross each other. Marriott mentioned two chevron angles of plates, 65° and 130° and showed that with these angles

three quite different geometries can be obtained, as discussed below:

1. Two plates of small chevron angle (65°) - low θ' plates - are placed together, forming a channel which permits the passage of a relatively large fluid flow at a given pressure drop
2. Two plates of large included angle (135°) - high θ' - placed together, forming a channel that permits the passage of a small fluid flow at the same pressure drop when compared to low θ' channel.
3. One of each type of plate placed together forming a channel of intermediate characteristics - the medium θ' channel.

Then Marriott carried out calculations for the number of plates required for a single pass for both high and medium θ' channels by considering a practical situation. He estimated savings of up to 19% by using medium θ' channels as compared to the best available "pure" channels.

In this paper Marriott only considered relationship of θ' and channel arrangements and explained the advantages of mixed plates; no attempt was made to consider the flow behaviour in a channel; the arrangement was considered as a "black box". This approach is useful in estimating sizes of heat exchangers assembled from plates. Previous experience can be applied to predict whether or not a particular arrangement will be satisfactory.

Exactly how the performance of a given plate depends on what happens in the entrance and exit regions of a channel was not considered.

Cooper et al. (113) carried out an interesting study concerning the effect of fouling in PHE's by using water as a test fluid from a cooling tower.

The PHE tested was an APV model R405, 1.14m high and 0.45m wide made of stainless steel containing seven plates creating three countercurrent passes for the cooling water and heating medium. The test unit was installed on a petrochemical plant mounted with two small stainless steel shell and tube heat exchangers. The PHE was heated using hot steam condensate and the fouling was determined from the degradation of the overall heat transfer coefficient. Comparisons were made between two different types of heat exchangers.

Five tests were carried out for several velocities 0.2 to 1 m/s and surface temperatures of 321-334 K. The fluid velocity was calculated by the standard relationship:

$$U = \frac{G}{\rho A} \quad (3.4)$$

where G is the mass flow rate (Kg/s)

ρ is the density of fluid (Kg/m³)

A is the cross-sectional area of flow based on

two smooth plates as if there were no corrugation (m²)

Surface temperature was measured at the mid point of the plate. At the end of each test, deposits were photographed and sampled for chemical analysis. Then plates were cleaned and the unit reassembled for another test to be carried out. Each test produced primary elements of phosphorous, zinc and chrome from the water and silicon from suspended solids in the water and these deposits were on the upper third of the plates, the region near the hot water inlet and cold water outlet (a region of high temperature).

Cooper et al. found that the PHE fluid velocity of 0.45 m/s fouls about one-half as much as a tube side exchanger at 1.8 m/s, this was shown by the deposit analysis. Cooper et al. are the only group of workers who comment seriously on the flow velocity as a crucial parameter in PHE's. Although for convenience they have used the basic relationship of equation (3.4), they recognise that the definition of flow velocity in PHE's should be different and cannot be as straightforward as flow velocity in tubes. They recognise that in PHE's the flow velocity is characterised by constant fluctuations as the fluid passes over corrugations. They believe this induced turbulence which is superimposed on the flow velocity as a factor which must diminish fouling tendencies.

A detailed investigation on PHE's in recent years was carried out in the Soviet Union by Leginky et al. (114). The authors studied heat transfer in eight channels; seven kinds of PHE's enhanced by turbulence promoters in the form of hemispherical projections, and one with no turbulence promotor.

One of the interesting points to note about this work was that the authors used a single channel. For the first time beside Fattah (7) and Fontaine and Lannoy (108) this option was taken seriously. The authors passed heated air over the heat exchanger plate and discharged it to the atmosphere. The air flow rate ranged from 5 to 36 m³/hr. The heat exchanger surface temperatures corresponding to the temperature of condensing steam, ranged from 372 to 374K. The air temperature difference measured by three simultaneous acting differential thermocouples arranged uniformly over the channel height, ranged from 55 to 75K. This was carried out for each channel.

Leginky et al. tried to relate the data in the form of $Nu = f(Re)$

where Nu = Nusselt number

Re = Reynolds number in the range of 1240 to 8000.

In this study the experimental work was carried out in turbulent flow regime, no attention was paid to the laminar flow conditions.

Although a great deal of information was provided on the types of plates examined, it was not made clear whether these plates were commercial or not. None of the plates examined in this study have a corresponding geometry in the western world.

In the last few years many workers (115, 116, 117, 118) have stated that the flow distribution in a PHE channel is uniform and there are no dead or stagnant areas. This can be a misleading concept since in 1978 a publication by Price and Fattah (10) showed that there were stagnant zones in their qualitative study.

Price and Fattah had prepared a transparent channel of an APV junior paraflow and examined flow distribution using water and aqueous glycerol as working fluids. They injected aqueous dye and found that at low Reynolds number the flow up the channel was mainly in the small recess adjacent to the gasket on the same side of the channel as the ports. Small streams split away to flow in a zig-zag manner up the channel as Re increased. This certainly showed that parts of the channel were not being used effectively, hence stagnant zones. Also Price and Fattah provided pressure drop data for Reynolds number range from 3 to 5000 and found a significant effect on the friction factor and Reynolds number relationship caused by the ports and gap between plates. They also attempted to rationalise definitions of various terms normally encountered in flow situations.

Other work by Okada and Ohno (119) also supports the work of Price and Fattah. Okada had examined temperature

profiles in a 2-dimensional channel. He showed that there were various temperatures across the channel and vertically up the channel. Okada plotted these temperature profiles in contour form for Re range of 100 and 9000. Unfortunately this paper cannot be discussed in great depth because it is in Japanese and there is no English translation available, only a general impression can be made of this work.

Raju and Chand (120) have recently commented on the flow distribution in PHE's when making comparisons with shell and tube exchangers. They stated that "the distribution of flow through the plates in a pass is usually assumed to be uniform. This may not be the case when fluids are viscous, throughputs are high and plate packs are long. Calculating the actual flow distribution is not easy".

Rosenhow (121) recognised the problem of non-uniform flow and attempted to provide a theoretical approach to the problem and tried to explain the causes of poor distribution in the laminar flow regime. The author focused his attention by drawing the analogy of parallel tubes in shell and tube and parallel plates in PHE's. He showed that three main causes of non-uniformity of flow distributions were:

- (i) Superimposed gross natural convection in horizontal orientation.
- (ii) The effect of viscosity temperature relations permitting two different flowrates for the same pressure drop when liquids are cooled.
- (iii) Having non-uniform size passages resulting from large manufacturing errors and tolerance.

It must be pointed out that these recommendations are based on theoretical basis and applied to parallel plates.

Most of the previous work outlined above has been on the study of 3-dimensional PHE's. There has been an alternative approach to improve the performance of PHE's at Harwell (9) by leaving the plates plain and developing turbulence by including elements in the gasket material. The gasket would cover the whole surface between the plates and certain channels whose shape, depth and surface would provide a useful range of heat transfer, pressure drop properties. It is claimed that these exchangers cost between 30 and 50% of conventional PHE's. Only brief comments were provided on this new PHE. However, this technique would be extremely impractical in industry since PHE's plates are regularly stripped and cleaned. It would be very difficult to clean, and the gasket would easily break up in the cleaning process. In the long term these PHE's will not provide a good investment and hence are less attractive for commercial purposes.

Most recently in April 1981, an article by Bond (3) discussed the effective heat transfer of PHE's and pointed out that "there is little published data on the fundamentals of fluid flow and heat transfer in channels, which are used in plate heat exchangers".

It is apparent that most of the work reported in the literature has been on high Reynolds number and only Price and Fattah (10) examined low Reynolds number as a qualitative study using dye injections. There is a deep lack of understanding of fluid flow and heat transfer fundamentals in PHE's.

With this background of available literature and recalling the comments by Cooper et al. (113) on flow velocity, the present study was a serious attempt to examine hydrodynamic characteristics of a particular commercial PHE channel on a better understanding of heat transfer in PHE channels as a long term objective.

CHAPTER 4

EXPERIMENTAL WORK

4. EXPERIMENTAL WORK

4.1 TRANSPARENT CHANNEL MODELS

4.1.1 COMMERCIAL PLATES : SR1 (APV LTD)

In order to investigate the realistic hydrodynamic behaviour of a three dimensional APV SR1 PHE, a transparent plastic replica of the stainless steel plate surfaces shown in Plate 4.1 was prepared. The technique was similar to the one previously developed by Fattah (7), in conjunction with Stanley Plastics Ltd., Hambrook, Chichester. Although Boutier et al. (36) do not recommend perspex as a suitable material because of scattering of light beams; it was considered to be the only suitable material which would minimise difficulties in producing an acceptable replica of the actual channel. Furthermore the model channel prepared would have two other advantages in this work:

- (i) The identical shapes of the replicas compared to the metal plates would produce flow behaviour through the model channel of a very similar nature to that in an actual channel.
- (ii) The transparent plates allow correct positioning and assembly of both plates forming the channels, thus ensuring that the point to point contact normally maintained is achieved.

To obtain a channel "positive" and "negative" reproductions of a standard plate were produced by casting on the two opposite sides of a metal plate. The overall dimensions of the plastic plates were 59 x 22.4 cm with

PLATE 4.1 - STAINLESS STEEL PLATE FOR SR1 PLATE HEAT EXCHANGER

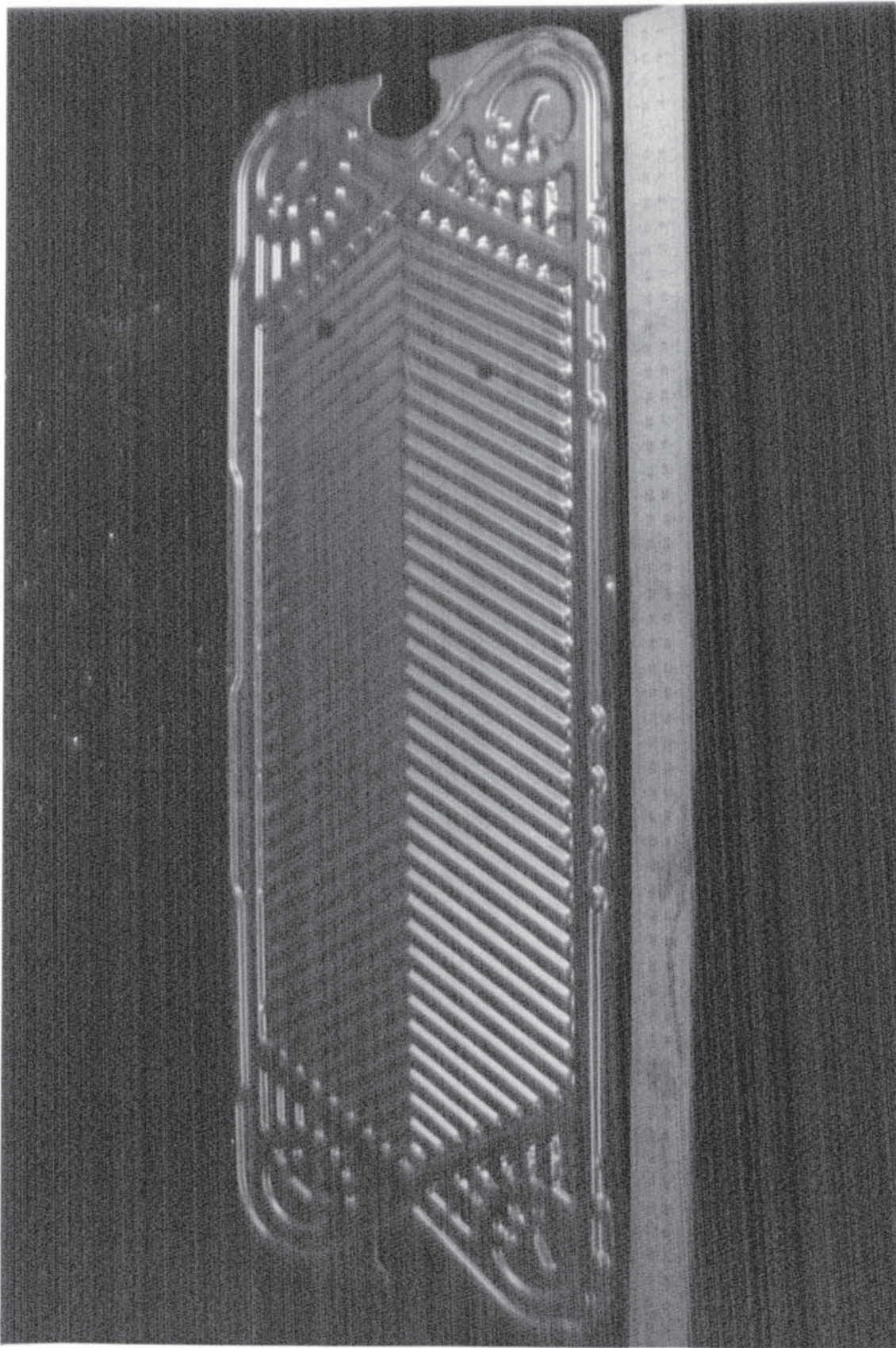


PLATE 4.1 - STAINLESS STEEL PLATE FOR SR1 PLATE HEAT EXCHANGER

a minimum thickness of 1.1 cm, while the metal plate measurements were 57.025 x 21 cm, with minimum thickness of 0.6 mm. Thus a 1 cm wide flange was provided around the edge of the perspex plates. The depth of the corrugations in chevron pattern was the same for the replica and metal plates. Previous work by the author (122) clearly showed that the plate surfaces must be protected from physical damage. This was achieved by covering the flat surfaces with transparent, adhesive sheet, while chevron surfaces were protected by a coating of wet plain flour covered with paper.

The flange was utilised by drilling 26 holes of 6.35 mm diameter for clamping bolts. Initially a steel flange of 6 mm thickness and 25 mm wide containing matching boltholes and overlapping the edge of the plates was used in conjunction with large diameter washers. These washers were used on both sides in order to spread the sealing load. However this method was found to be unsuccessful due to leakages, when flow was passed through the channel. Therefore, the steel flanges were replaced by specially prepared large rectangular washers of 25 x 20 mm. Six additional boltholes were drilled, three at the top and three at the bottom of the channel, parallel to the gasket strip isolating the unused ports. This provided a better seal, stopping any leakage of flow.



It was very important when assembling the channel, to take great care when tightening the bolts to similar stress. Overtightening or unbalanced stresses could cause one of the plates to crack and subsequently would have to be replaced, which consequently would delay the project. Furthermore, visual inspection of the assembled channel showed, when peaks of the corrugations were in contact.

The neoprene gasket provided by APV Ltd., normally used with metal plates was utilised in the plastic channel to establish a "standard channel" representing a channel of an actual pack of plates. The gasket was glued to the plastic channel using standard adhesive. A thin layer was applied to the gasket groove carefully, since adhesive contains chemicals which are likely to affect the perspex in varying degrees.

The inlet and outlet ports do not have a single radius but comprise a cross-section of two different radii inclined at an angle of 15° as shown in Figure 4.1(a). These semi-circular ports are 18 and 17 mm radius of the top and bottom section respectively. In order to establish flow distribution as close to the metal channel as possible, it was considered necessary to reproduce the geometry of these ports in the perspex. Therefore, the ports were carefully machined into the perspex plates. A feed pipe of 36 mm bore and 3 mm wall thickness was fabricated from perspex rod and secured to the channel and to connecting flanges with "Perspex cement No. 7" as shown in figure 4.1(b).

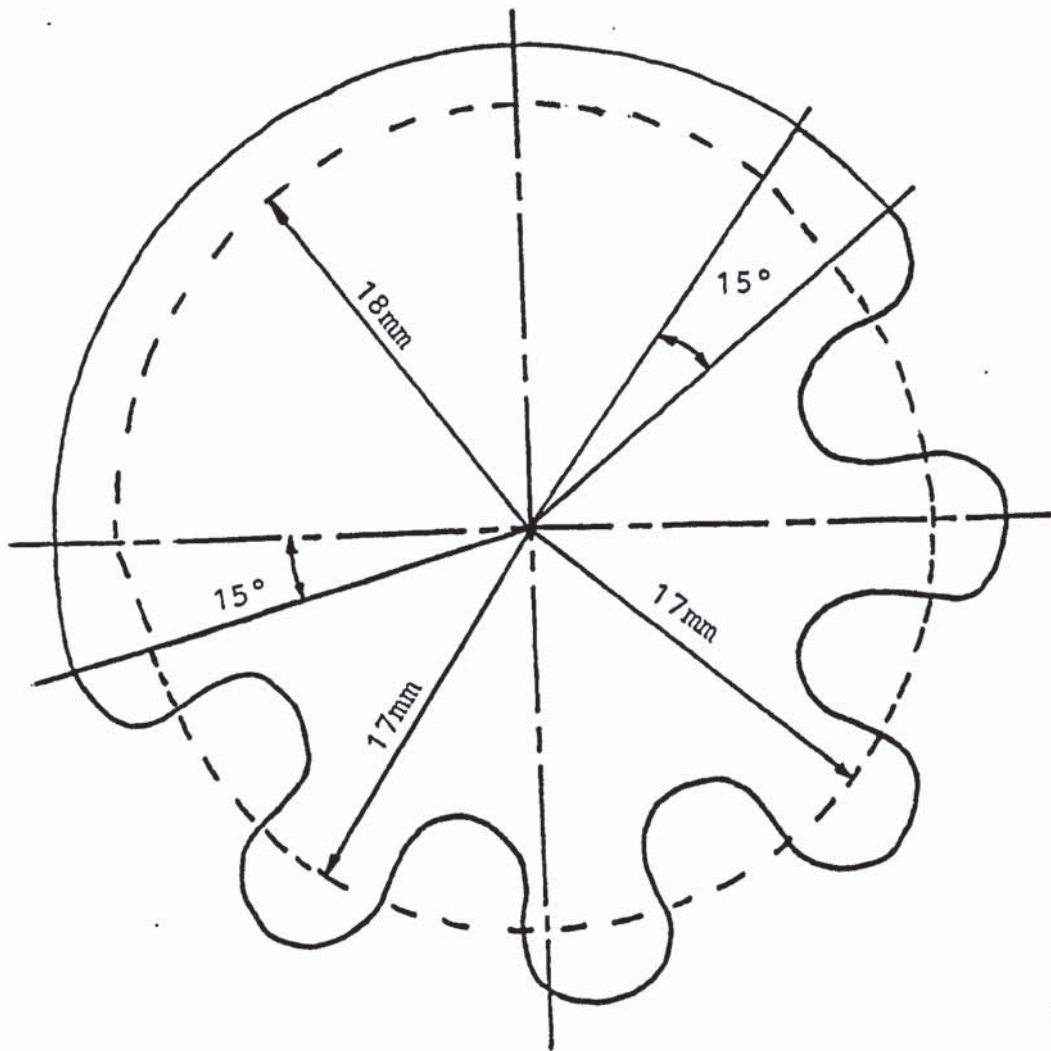


FIGURE 4.1 (a) INLET/OUTLET PORT

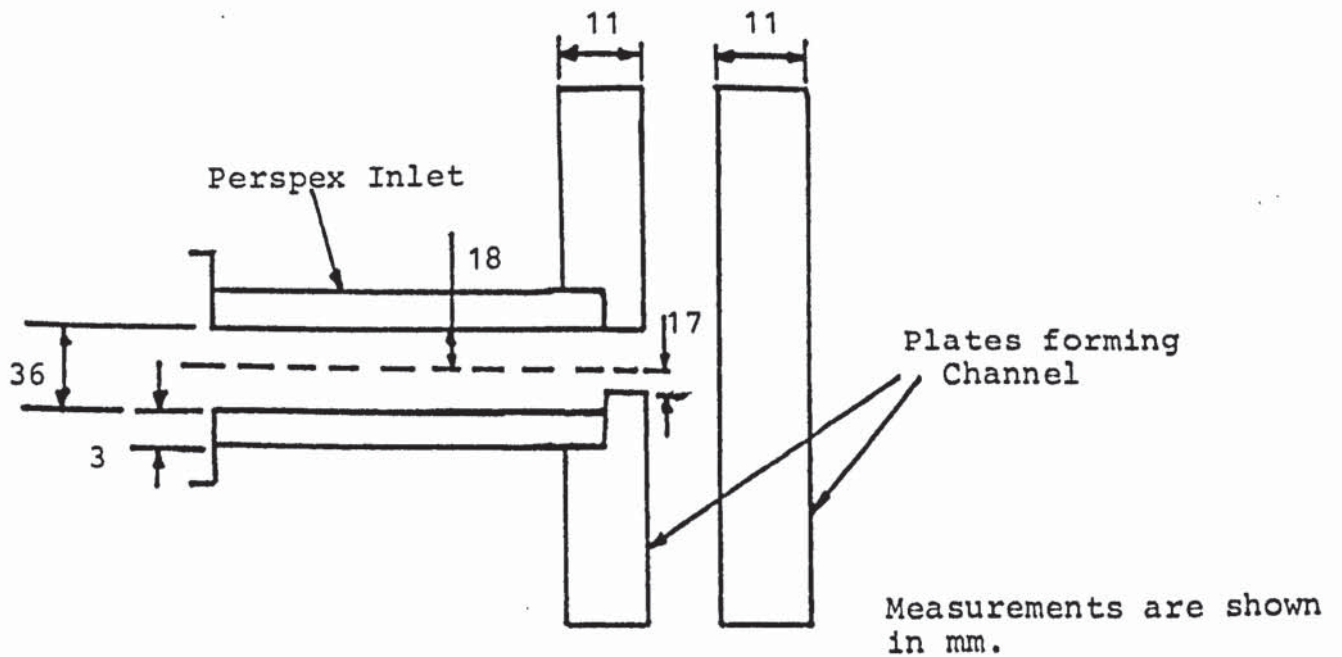


FIGURE 4.1 (b) CONNECTION BETWEEN CHANNEL AND INLET/OUTLET

This cement involves polymerization of the monomer (methylmethacrylate) by adding a catalyst then applying the polymer when it is still soft resulting in welds of high mechanical strength. This provided a good seal between the channel and the pipe sections.

4.1.2 RESEARCH PLATES : JUNIOR PARAFLOW (APV LTD.)

To provide a better understanding of the flow distribution in three-dimensional PHE's, another approach was also considered, in addition to point velocity measurements in the channel. It was strongly felt that an overall picture of the flow distribution in channel was important, particularly how elements of fluid pursued along the channel.

A consideration of the complex geometry of the flow channel highlights the difficulties of predicting the preferred path that a fluid element is likely to follow. In the general movement from inlet to outlet port, the fluid encounters a uniform grid structure containing many points of contact and consisting of the corrugated chevron pattern of peaks and valleys crossing one another. To be able to predict how the flow splits in different directions when approaching a point of contact would be helpful in the design of the future channels. Therefore, a study was undertaken of flow through a single "cell", defined as that volume in the channel bounded by four adjacent points of contact and the crossing valleys of the chevron pattern.

This understanding of flow in one cell would allow the preparation of a mathematical model describing flow in a channel, as a long-term objective. This mathematical description could be used to predict flow all over the channel, and could therefore eventually be used to explain the velocity measurement made in the channel. Such a model would also provide a useful understanding of the flow already reported in a previous work by Fattah (7). To prepare a mathematical model of a single cell, the Navier-Stokes equation used in the study of fluid mechanics for flow in three-dimensions were considered. This option was rejected since it is not possible to solve these equations for the complex boundary conditions associated with the geometry of the shape of a cell. Furthermore, such work would be beyond the scope of the present study. Another option was considered, by involving the preparation of a single cell and studying the flow behaviour through this cell. This option was found to be feasible.

In order to explain how the flow behaves in one cell the most appropriate method would be to define some form of performance criteria. These criteria would be assessed by measuring the flow entering the channel and then measuring the division of the outlet flows, thereafter calculating the ratio of outlet to total input flow through each outlet side would provide the performance criteria.

A small perspex section as shown in Plate 4.2 of the Junior Paraflow (prepared and used by Fattah (7) in

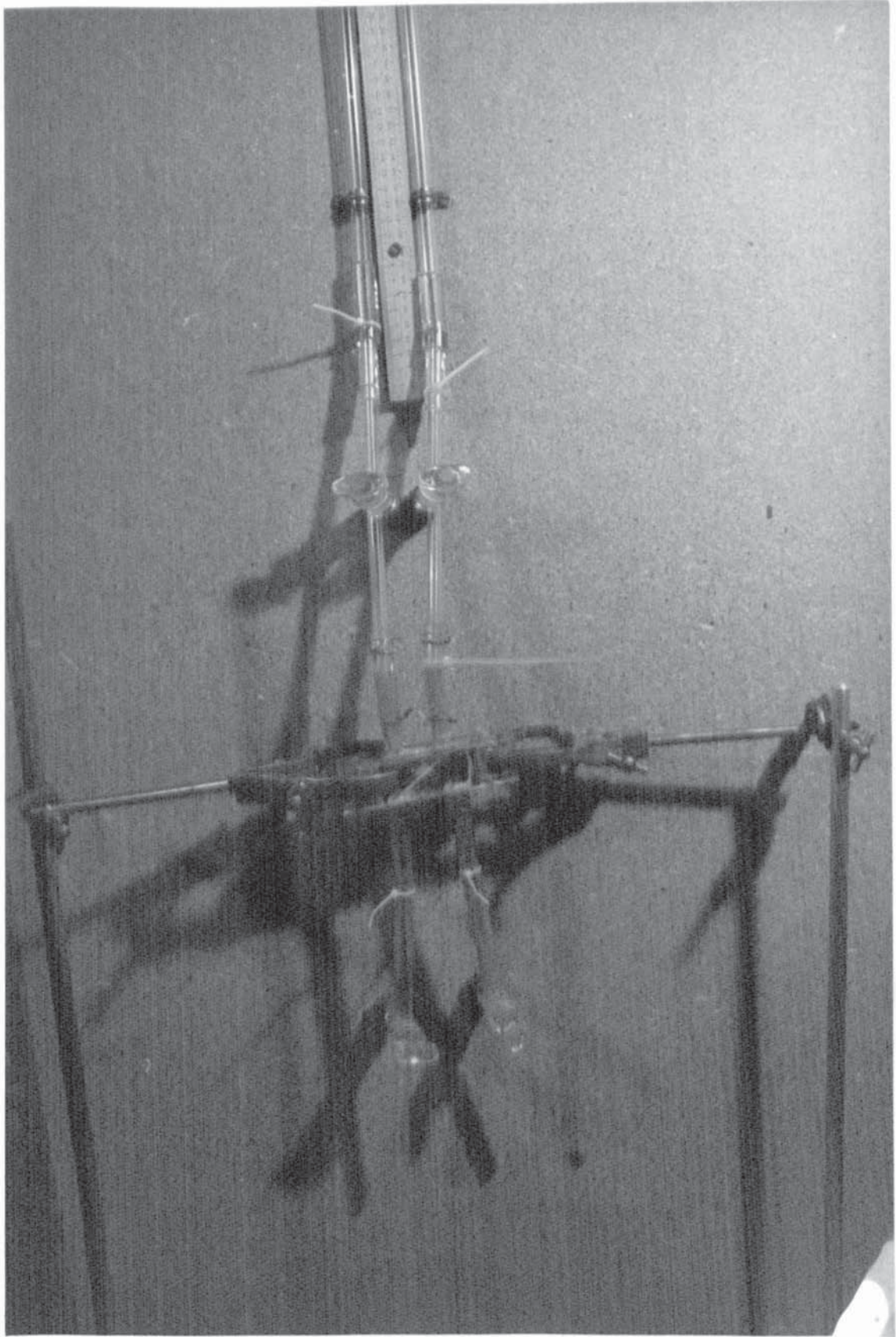


5- SMALL SECTION OF JUNIOR
PHE PERSPEX CHANNEL

1 2

5

3 4



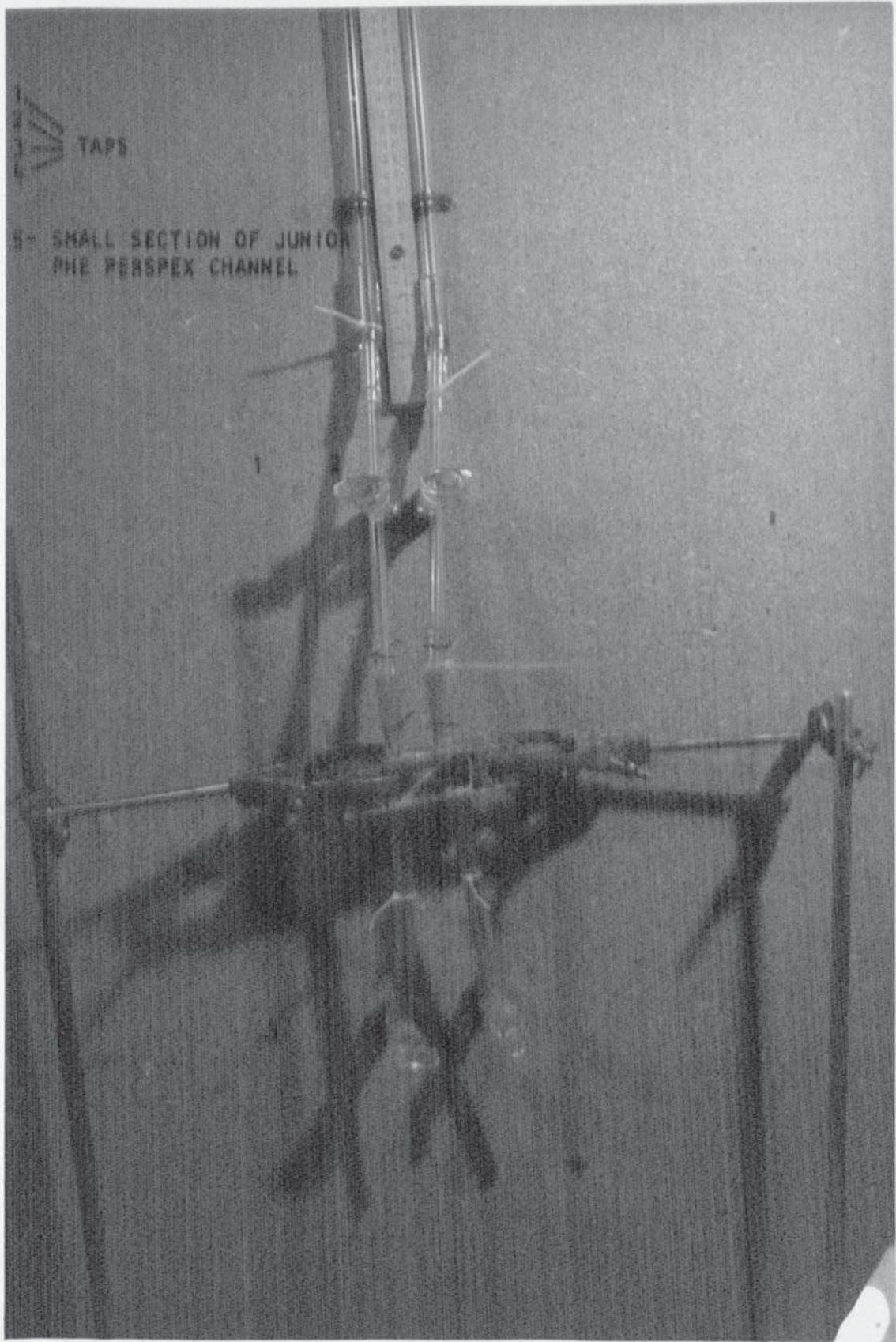


PLATE 4.2 - ASSEMBLY OF SINGLE CELL

his work) was used in the experimental work. This section was cleaned and polished carefully, using "Brasso" polish and then perspex polish without damaging any part of the surface of the channel section.

A line diagram of the experimental rig is shown in Figure 4.2. The channel section is blanked with candlewax leaving only one cell available for flow to take place. Araldite was tried initially to fill the valleys, but was found to be unsatisfactory in operation. Water was used as the working fluid to examine flow distribution. The inlet and outlet tubes of 9.525 mm diameter were connected to the channel section using Araldite. The inlet tubes were connected to very long (about 2m) tubes to provide suitable flow rates.

Initially trial experiments were carried out to determine the suitability of the experimental assembly. It was found that if taps 3 and 4 were open and taps 1 and 2 were closed, it was easier to make measurements. So throughout the experimental work, taps 3 and 4 remained open. Seven main experimental runs were carried out:

- (i) The first and second experiments were based on establishing flow splits through the valleys, A and B, in the cell.

In the first experiment for flow through valley A, tap 2 was closed and tap 1 was opened for a few seconds interval and then closed. The amount from each of the outlets was collected,

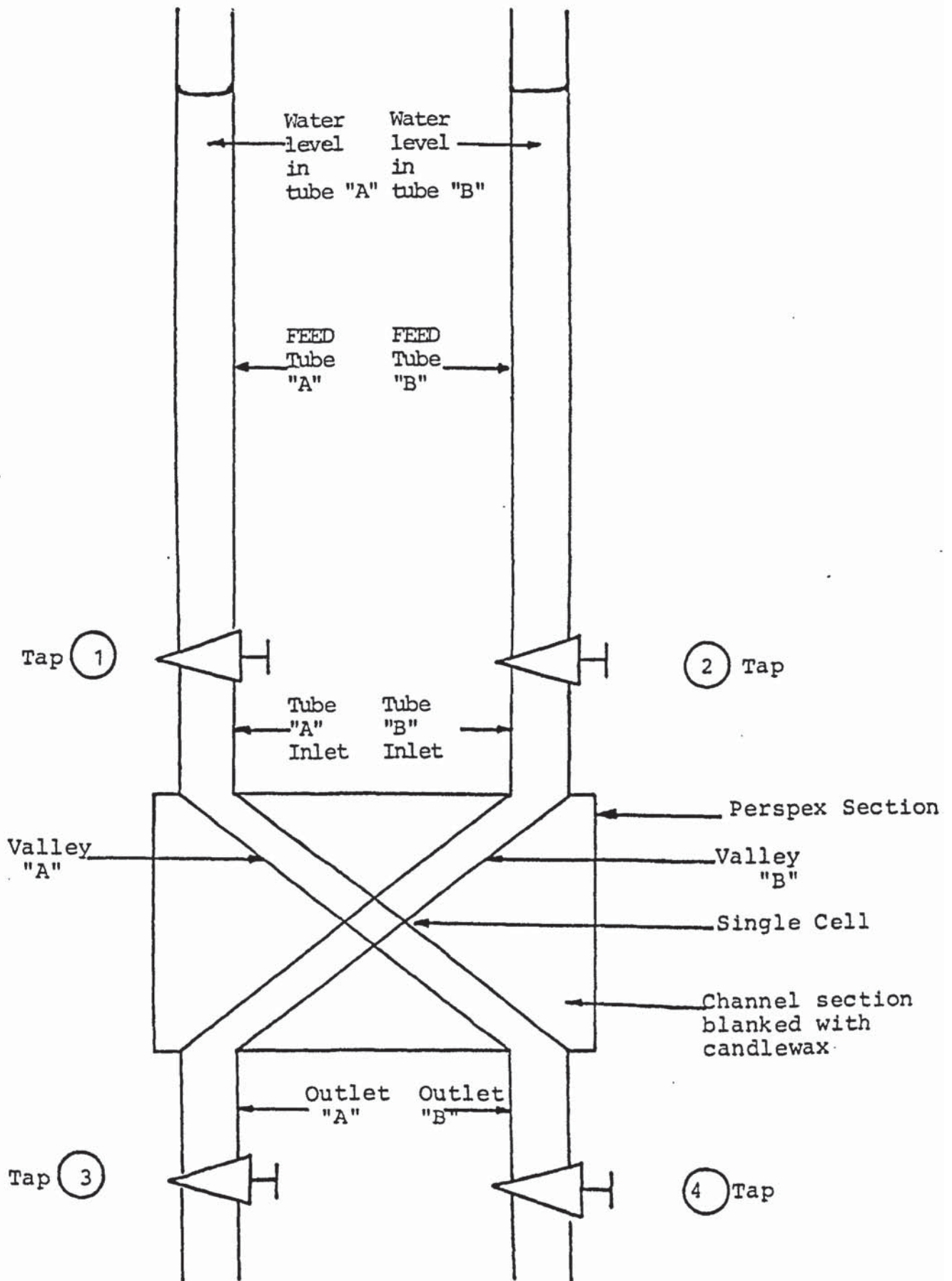


FIGURE 4.2 LINE DIAGRAM OF EXPERIMENTAL RIG OF SINGLE CELL

measured, and recorded.

In the second experiment for flow through valley B, tap 1 was closed and tap 2 was opened for a few seconds and then closed.

- (ii) To study the effect of equal pressure drops on each side of the cell the third experiment started with equal levels of water in the feed tubes. Taps 1 and 2 were opened simultaneously for a very short period of time and then both closed. The amount collected from each outlet was measured, and the level change of each inlet side was also recorded.
- (iii) The fourth experiment was intended to determine whether different levels of water in the feed tube affected the performance of the cell. The procedure was the same as in (ii) above, but the starting levels of water were different.
- (iv) In the fifth experiment the height level of one tube side was twice that of the other. The procedure followed was outlined in (ii) above.
- (v) In the sixth experiment, the influence of flow in one valley over the flow in the other valley was examined. This would show how much the flow in one valley is affected by the resistance of

flow in the other valley.

This was carried out by opening tap 1 and after a short interval tap 2, and then instantaneously both taps were closed. The amount collected from each outlet tube was measured.

- (vi) Finally in this experiment, the main objective was the same as in (v) above, to observe the influence of flow in one valley over the other valley. This time tap 2 was opened first and after a short interval tap 1, and then instantaneously both taps were closed. The amount collected from each outlet tube was measured.

For each experimental run, eight different measurements were made. In the experiments described in sections (ii) to (vi), no time interval was recorded, due to practical difficulty of trying to operate the taps and a stop watch simultaneously. Also the term "instantaneously" refers to manual operation of two taps by one person since the inlet levels dropped very rapidly. Furthermore, experimental difficulties were caused by air pockets being trapped near the outlets, so the volumetric flow rate collected at the outlets was not in agreement with change in levels at the inlets. Such results were rejected. Only the results which showed agreement of $\pm 4\text{cm}^3$ were reported.

4.2 LASER ANEMOMETRY EQUIPMENT

The significant components of the LDA system used as an integral part of the equipment in this study will be discussed in the following sections:

4.2.1 THE LASER

A 35mW Helium-Neon laser ($\lambda = 6328 \text{ \AA}$) provided the coherent light source. The laser operating in the transverse mode (TEM_{00}) had a beam radius of 550 microns. A lens of 14.4 cm focal length was used to provide sharper beam radius of 52.737119 microns at the focal length. This lens was placed between the laser and beam splitter as recommended by Abbiss et al. (24), to improve the performance of the beam splitter, but was not used in the early stages of the study. The calculations of beam radius using the lens are shown in the Appendix A-2.0.

The beam splitter RF 307 attached directly to the laser, is a bi-prism and can be adjusted to move the beams to intersect at the chosen point. Thus a perfect intersection can be obtained at the position of interest.

Further detailed information of laser and the beam splitter is available from supplier's manual (123).

4.2.2 PHOTOMULTIPLIER

The photomultiplier was a type RF 313, having a cathode voltage of 735 to 1000 V negative, and a maximum anode current of 100 mA. Attached to the photomultiplier were collecting lenses of adjustable

focal lengths variable between 75 mm and 205 mm. Three different size pinholes of 100, 200 and 400 μm were available to be fitted between the collecting lens system and the photomultiplier tube.

4.2.3 PHOTON CORRELATOR AND DISPLAY UNIT

To process the signal from the photomultiplier tube, a Malvern K7023 photon correlator was used which allows four operating modes, digital cross-correlation, signal enhancement, digital auto-correlation and probability analysis. The auto correlation mode was used and an oscilloscope type 0S255 was attached to the photon correlator to display the auto correlation function. A detailed description of the K7023 correlator is available in reference (124).

4.2.4 COMPUTING DATA PROCESSOR

The computing data processor used in this study is a Commodore PET desk top computer, interfacing the Malvern K7023 correlator.

More information is provided in the Appendix A-1.0, and the operating manual (30).

Results were also recorded on a hard copy using an IEEE488 peripheral device to redirect results to a Newbury 8300 R line printer.

4.2.5 SETTING UP PROCEDURE OF OPTICAL CONFIGURATION

The general arrangement of the optical configuration is shown in Figure 4.3. It was described in Chapter 2 as the Doppler Difference mode. Now the experimental operation of this arrangement will be discussed.

The laser was horizontally polarised by rotating a $\lambda/2$ plate fitted to the beam splitter to equalise the beam intensities. In practice this was done by adjusting the $\lambda/2$ plate lever and observing the refracted spot on the side of the inside wall of the beam splitter box. When the spot is at a minimum then the beam intensities are equal. A lens of 14.4 cm focal length was used to sharpen the beams. The beams could be adjusted with knobs to the point of interest. The front knob on the beam splitter, adjusts the distance of cross over from the front of the beam splitter, while the rear knob, separation of the beams, when leaving the beam splitter.

The next step involved aligning the PM tube. This is normally placed at an angle of $10^\circ - 14^\circ$ downwards from the main centre line of the beams in a forward scatter position. The eye-piece from PM assembly shown in Figure 4.4 was removed and the whole body adjusted until a bright circle of light could be seen in the barrel of the eye piece. The latter was replaced and the image of the intersection point focussed by the collecting lenses onto the pinhole.

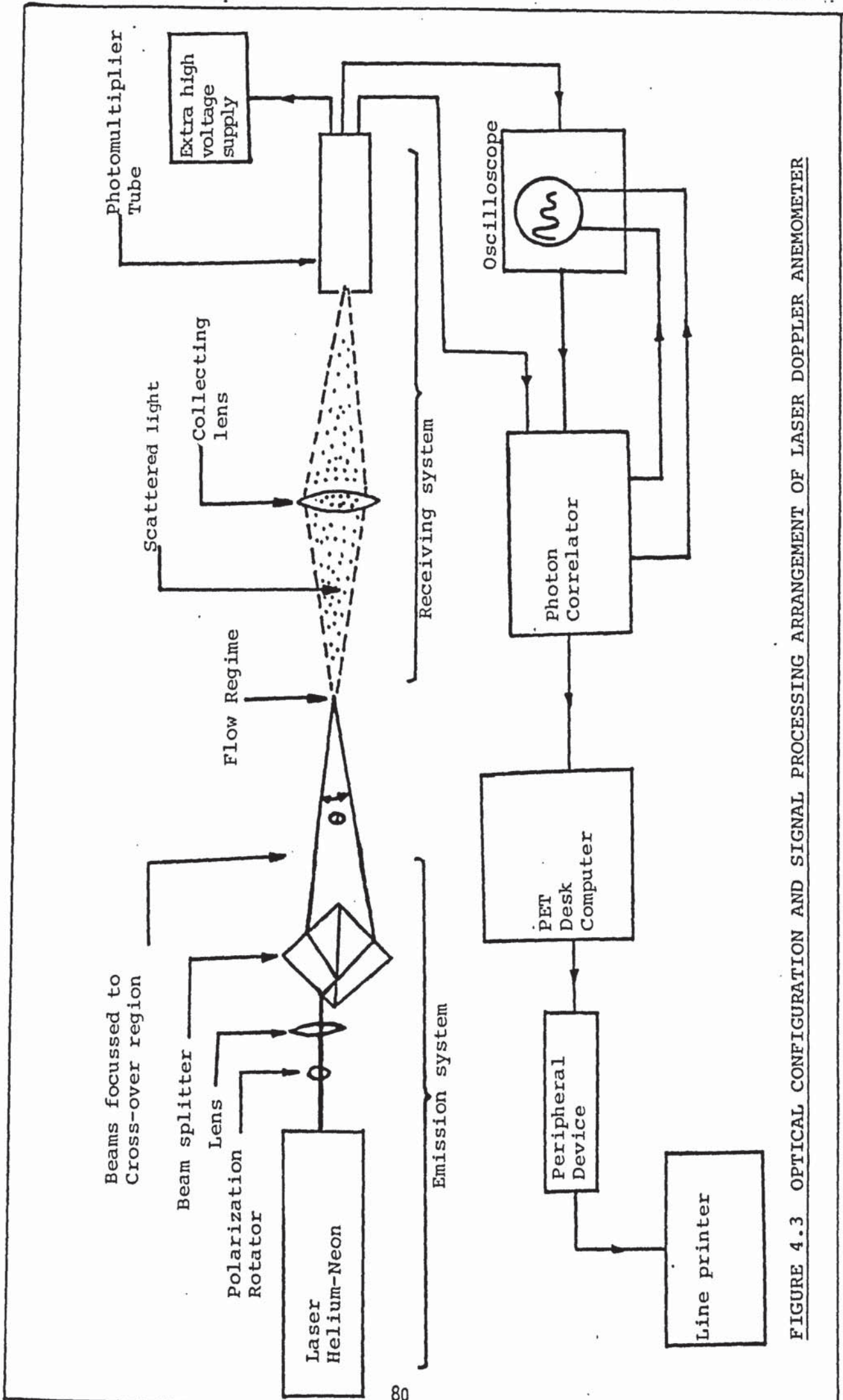


FIGURE 4.3 OPTICAL CONFIGURATION AND SIGNAL PROCESSING ARRANGEMENT OF LASER DOPPLER ANEMOMETER

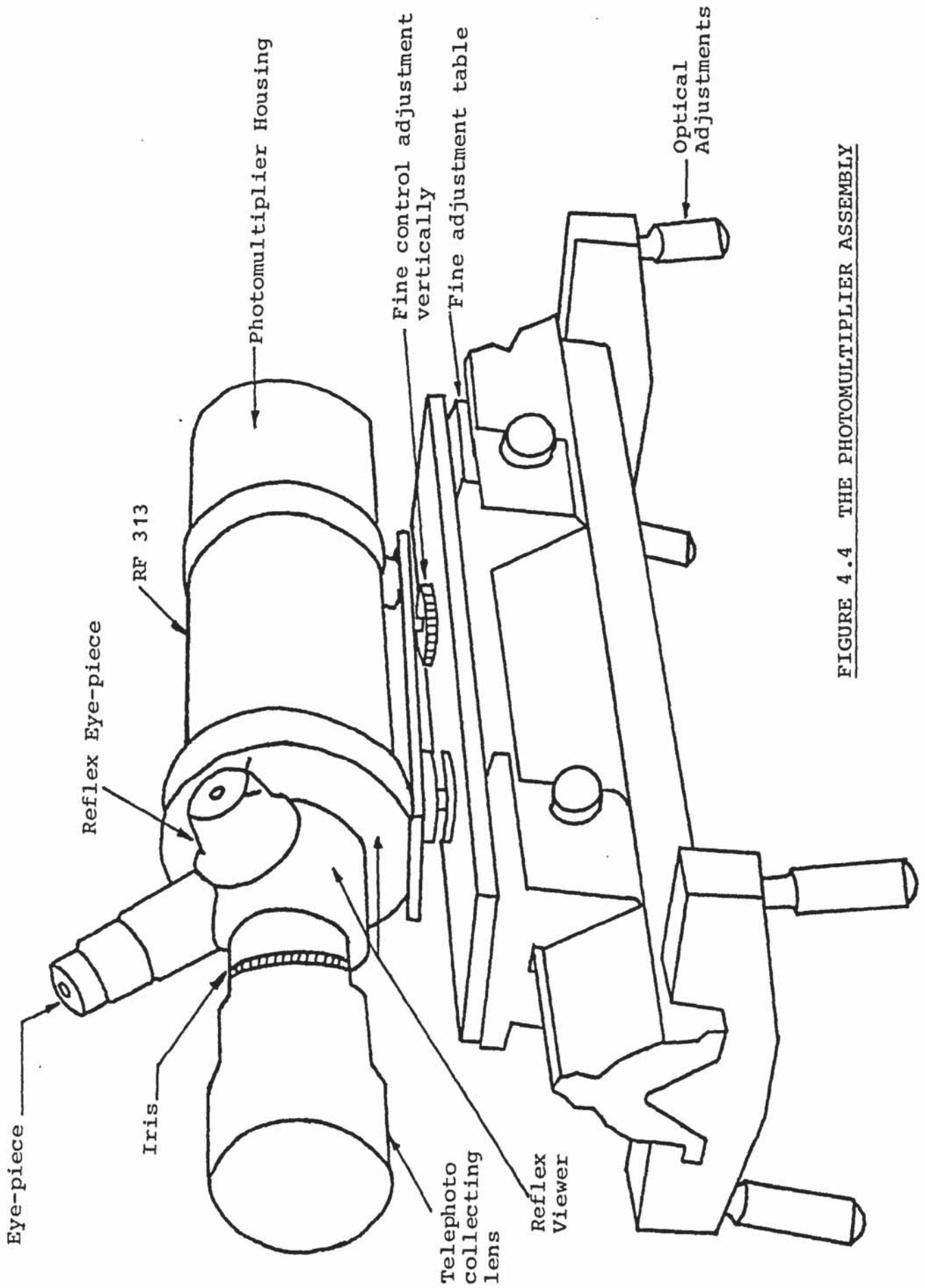


FIGURE 4.4 THE PHOTOMULTIPLIER ASSEMBLY

The pinhole is shown in Figure 4.5. When the crossover is difficult to focus, the optical bench of the PM assembly can be adjusted until a sharp image of the crossover is obtained. The PM tube is then moved slightly until the intersection point passes through the pinhole, leaving a small circle of red light around the hole. This alignment can be checked by observing through the reflex eye-piece, as shown in Figure 4.5, where a typical view of the intersection of beams and the cross-wires is given. If the cross-wires are not in line with the intersection of the beams, then fine adjustments can be made to line up the cross-wires with the pinhole. This is achieved with small allen screws fitted to the reflex system.

When alignment was complete the iris was closed and the PM assembly supply was switched on (± 15 V supply and Extra High Voltage (E.H.T.)). The signal lead from the photomultiplier was connected to the correlator and the "single clipped auto correlation" mode was chosen. The correlator was adjusted to a 1 micro-second sample time and 10^6 samples. The oscilloscope was switched on and the start button pressed on the correlator at which point the correlator stop lamp is lit. The plot on read out function switch was then selected and the first address 00 would display the counts in one second from the photomultiplier. For a good signal to correlate the count rate should be roughly always less than or equal to 250,000 and not greater than 10^6 . Sample time on the correlator was adjusted until a cosine curve with exponential decay as shown earlier in Figure 2.12 appeared on the oscilloscope display.

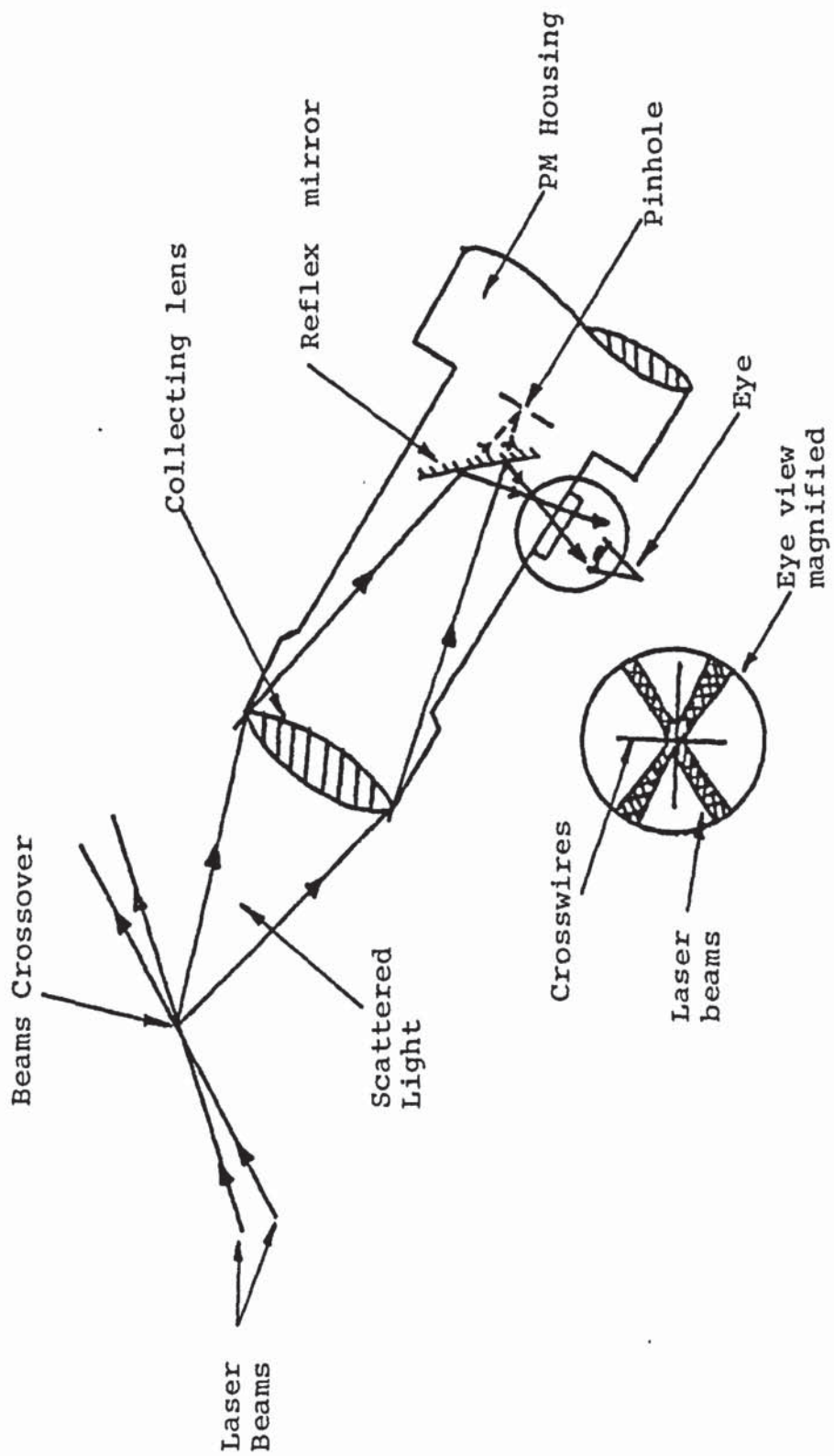


FIGURE 4.5 RAY DIAGRAM OF REFLEX VIEWER - PLAN VIEW

Sometimes this curve did not appear and some similar correlation appeared then the clip level (a facility on the correlator) can be adjusted to observe if better correlation curve can be obtained. If the clip number did not affect the correlation, then the following adjustment can be made to the correlation depending on the type of correlation curve:

- (1) If the correlation function was similar to Figure 4.6, then laser beams need adjustment. There are too many fringes in the probe volume. Therefore fringe spacing has to be increased, that is the ratio of (b/d) in equation 2.9, has to be increased. This would reduce the number of fringes according to equation 2.19.
- (2) If the correlation function was similar to Figure 4.7 then laser beam needs adjustment. This time there are not enough fringes in the probe volume, therefore the ratio of (b/d) has to be decreased.
- (3) When the correlation function was similar to Figure 4.8, the sample time and the clip number was reduced in proportion simultaneously.
- (4) When the correlation function similar to Figure 4.9 appeared, then the sample time and clip level was increased in proportion simultaneously.

When all the above methods failed to produce a correlation curve of the type Figure 2.2 then the flow is very turbulent or the PM tube is looking at one beam.

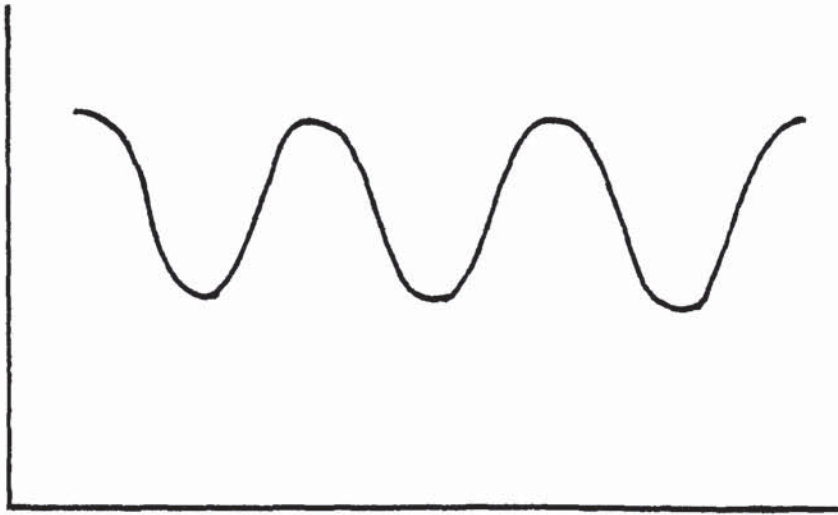


FIGURE 4.6 TOO MANY FRINGES IN BEAM DIAMATER

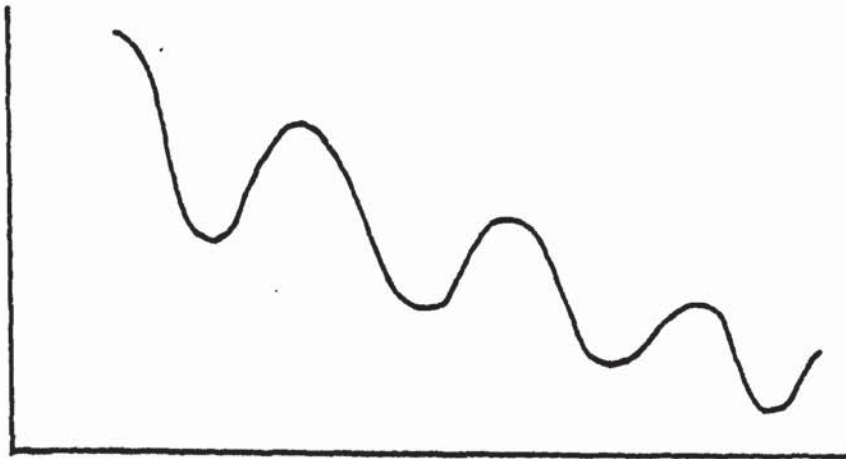


FIGURE 4.7 FEW FRINGES IN BEAM DIAMETER

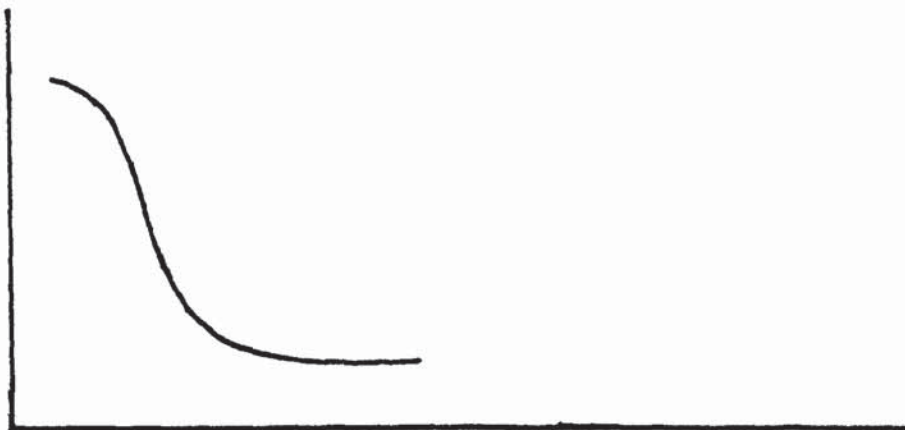


FIGURE 4.8 OSCILLOSCOPE DISPLAY OF FLOW

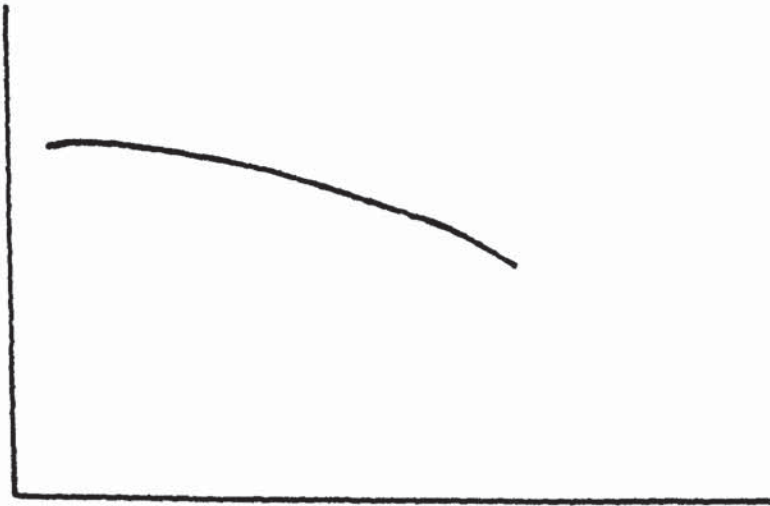


FIGURE 4.9 OSCILLOSCOPE DISPLAY OF FLOW

When satisfactory correlation curve was obtained, then the computer system was attached to the correlator and the results were evaluated. The programme that evaluated velocity and turbulence was provided by the manufacturers.

A more detailed operation of this LDA equipment is provided in the manufacturers operating manual (124).

4.3 EXPERIMENTAL

4.3.1 INITIAL EXPERIMENTAL ARRANGEMENT

The general arrangement of experimental equipment is shown in Figure 4.10. In this line diagram of the set up, only a brief outline of the optical arrangement is shown, since the detailed LDA arrangement has been shown earlier in Figure 4.3. The dotted section of Figure 4.10 has been expanded in Figure 4.11, to show how the perspex plate channel was assembled in conjunction with the rest of the rig. In this arrangement the perspex channel can be moved upwards, downwards and sideways conveniently, on a movable chassis. Thus the channel can be moved while the laser and the photo-multiplier tube remain fixed to make measurements at any chosen point.

In Figure 4.10, the set up is shown with Up-Flow in the channel; but Down Flow was also investigated. The delivery of Stuart Turner No. 12 centrifugal pumps

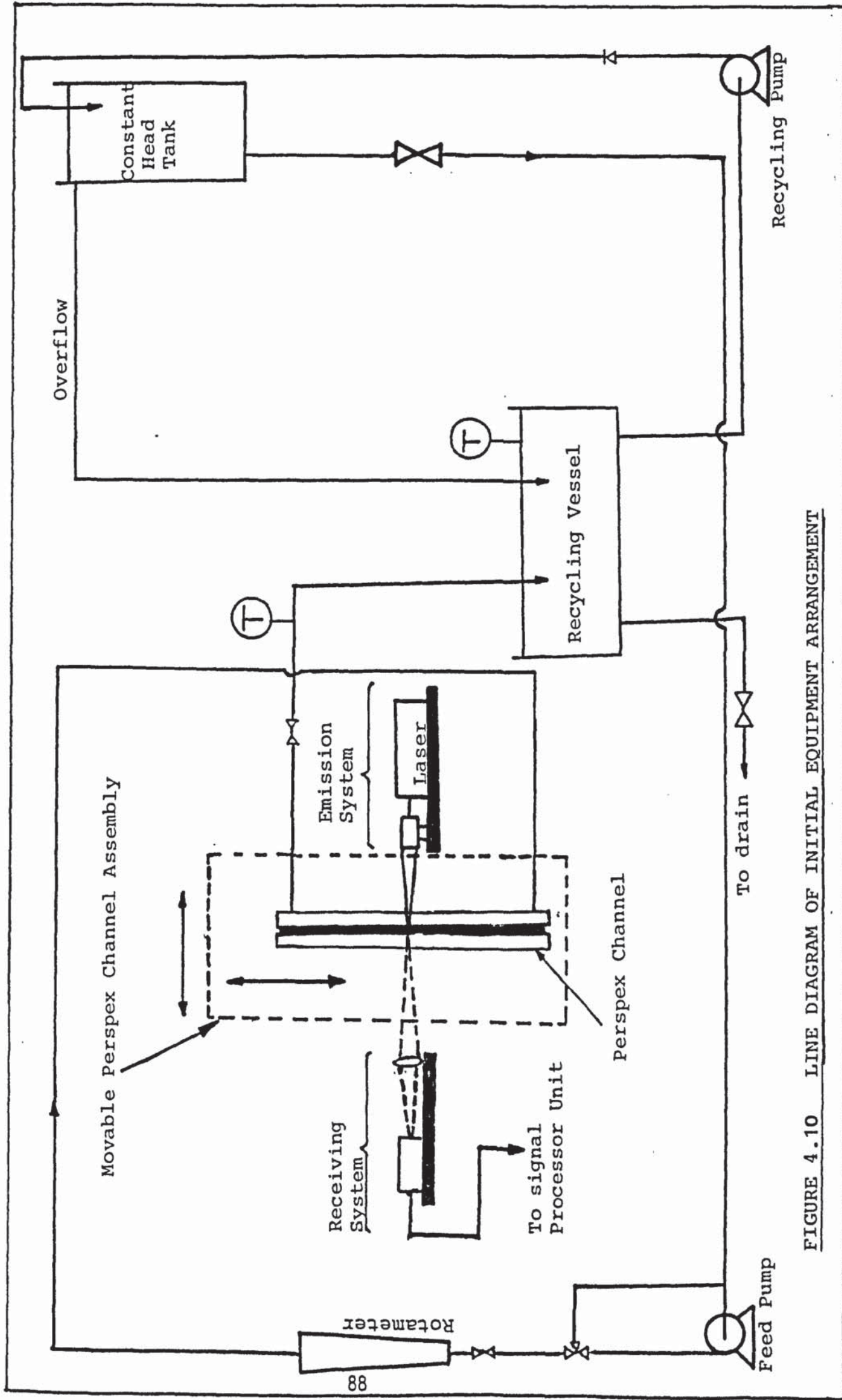


FIGURE 4.10 LINE DIAGRAM OF INITIAL EQUIPMENT ARRANGEMENT

- 1 - Perspex Channel
- 2 - Counter Weight to Channel
- 3 - Vertically Moving Carrier
- 4 - Moving Chassis

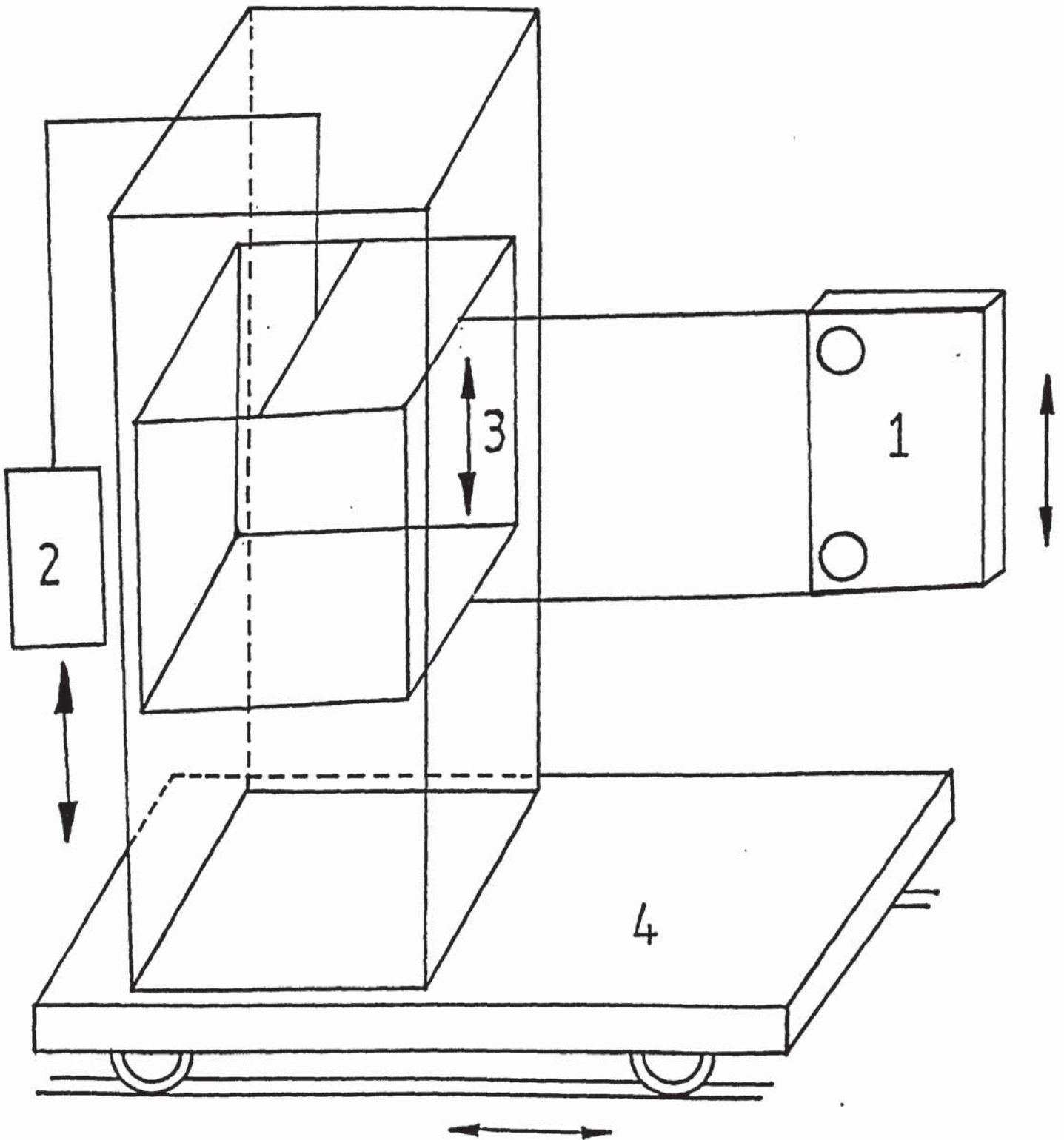


FIGURE 4.11 ASSEMBLY OF THE PERSPEX CHANNEL

was expected to fluctuate, so it was decided to rely on a constant-head tank to ensure constant flow. Nevertheless, the feed pump was used to drive air out of the system and to circulate the fluid when mixing was required. The physical limitations of the available head, e.g. the height, was determined by the size of the laboratory. A factor expected to influence the fluid flow profile in the channel was the entry conditions of flow at the inlet port. If the flow was fully developed at the inlet, a potential source of disturbance which would have a significant effect on the channel flow would be reduced or eliminated. Furthermore, the desirability of examining both Up and Down-Flow adds complexity to the pipework arrangement. Therefore to overcome this, substantial pipe lengths of diameter 15.875 mm "QVF" and fittings were used wherever possible in the arrangement. Flexible PVC tubes were introduced to connect the glass piping to the inlet and the outlet of the channel in order to provide smooth flow. The flexible PVC tubes used in their connections enabled quick and easy modifications whenever the direction of flow had to be reversed.

All the vessels, pipe sections, valves and reducers were assembled from standard "QVF".

4.3.2 WATER AS WORKING FLUID

The experimental arrangement used has already been described in section 4.3.1 and is shown in Figure 4.10.

In this set up, water was used as the working fluid because of its availability and non-dangerous nature.

Flow rates of water were measured using a "Fischer and Porter"FP- $\frac{1}{2}$ -17-G-10 flowrator with $\frac{1}{2}$ -GUSVT-410 stainless steel float. The calibration of the flowmeter was essential to allow the range of Reynolds number to be calculated, and was carried by direct weighing of effluent. Mass flow rates were measured for periods of one minute, the calibration was plotted, and a best straight line was drawn as shown in Figure 4.12. Unfortunately no manufacturers calibration was available to make a critical comparison.

Water became heated in the system during circulation around the arrangement, but this did not affect the flow significantly. The flow fluctuated a little, so a frequent check of temperature was made at the channel outlet and in the recycling vessel, using a mercury-in-glass thermometer with 0.1°C divisions.

The following description shows chronologically how the project work developed, showing possible deductions and hypotheses being generated and established or refuted.

The "positive" and "negative" plates were polished with perspex polish on all four sides, i.e. the inner working surfaces of the channel as well as the outer surfaces. Polishing proved to be a lengthy procedure where care had to be taken not to damage the channels by polishing very heavily. Polishing was an essential

Float: ½ GUSVT - 410

Rotameter: ½ FP-17G - 10

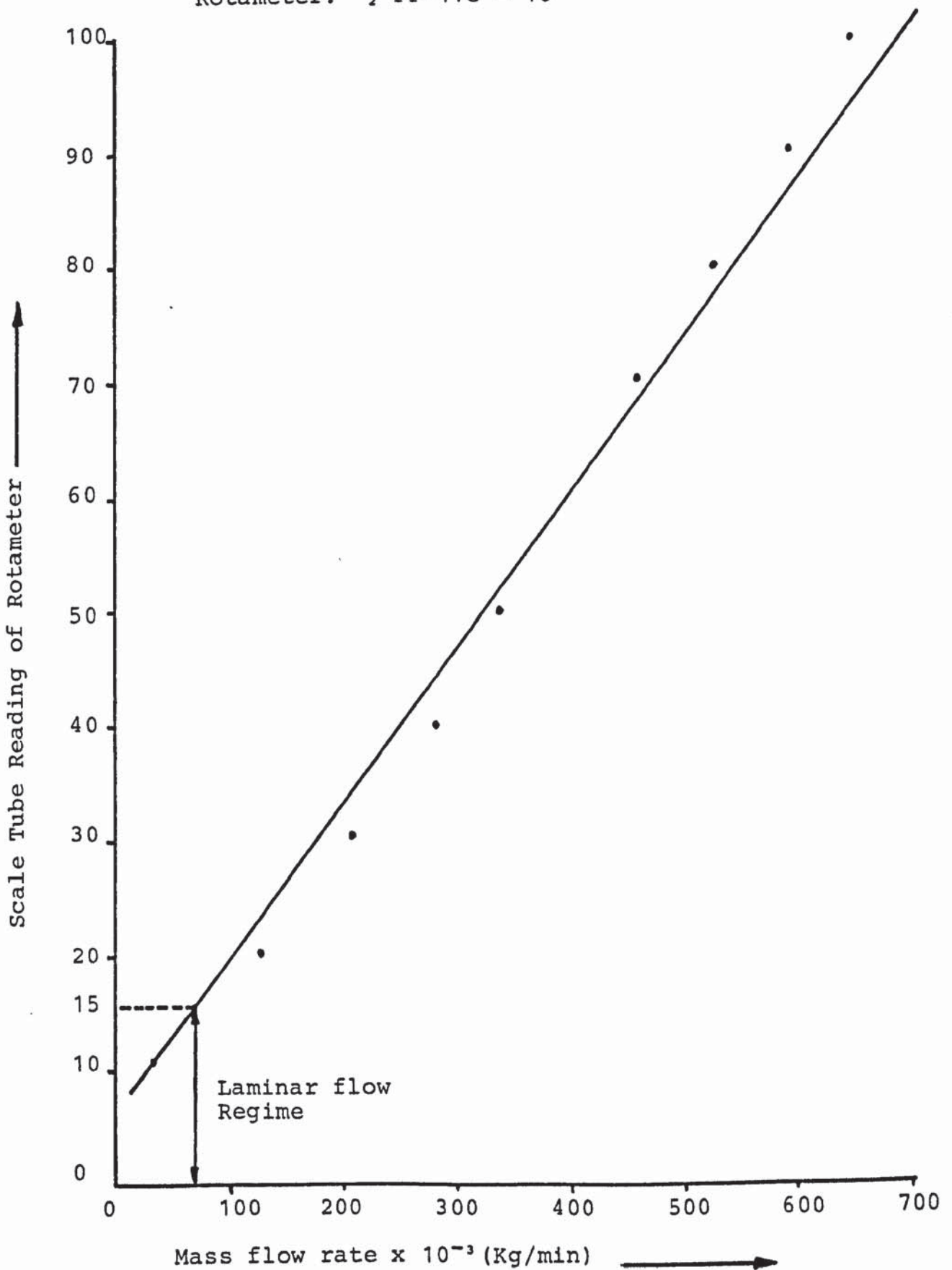


FIGURE 4.12 CALIBRATION CHART FOR WATER

part of this study to ensure that the beams passed through the thick perspex plates with minimum scatter as learned in the previous study by the author (122). The polish was applied on the surface by first pouring onto a suitable cloth, and gently applying to the channel. Then by using a smooth, clean cloth, the surface was polished several times using perspex polish over and again, until it was considered that no further improvement was taking place. The plates could then be clamped together and connected to the rest of the experimental set up.

From the flowmeter calibration, the range of laminar flow regime, $Re < 10$, in the channel can be calculated as shown in the Appendix A-3.0. It is shown that the laminar regime exists provided the float does not exceed a scale reading of about 15 on the flowrator. This would keep flow well within the laminar flow regime. The flow was maintained at this level throughout this experimental work, in Up-Flow direction.

When steady-laminar flow was obtained through the channel, the laser was switched on, and the beams were focussed onto the flow in the channel. As the beams passed through the channel, it was found that excessive distortions of the quality of the beams occurred, in spite of the extensive polishing. The distortions were clearly seen on a white background mounted beyond

the channel. Instead of the small circles of red light expected from sharp laser beams, large diffraction patterns were observed. This was attributed to several factors: distortions in the walls, refraction between the perspex wall and the water; reflection from the inner surfaces of the channel; the internal geometry of the channel acting as a form of lens causing deflection of the beams (also observed before (122)); and flare occurring at the solid/fluid boundaries. The beam splitter was rotated to find the position of minimum flare. This position was found to be when the plane of the beams leaving the splitter was parallel to the corrugations. As the channel was moved by adjusting the counterweight shown in Figure 4.11, there was also variation of the beams flare. This flare was greater near the gaskets than in the middle of the plates. Therefore a position of relatively small distortion of the beams was chosen to make measurements and was found to be in the middle of the cell volume.

The LDA equipment was arranged in the forward-scatter position as shown in Figure 4.3, but originally without the lens in the beam splitter. The beam splitter mounted parallel to the corrugations was adjusted for the beams to meet in the centre of the cell volume.

The water used in the experiments was not artificially seeded because an analysis of a sample showed that there were sufficient solid dust particles to provide scattering centres. To estimate a point

velocity, the procedure outlined in Section 4.2.5 was followed.

The first address 00 on the correlator measured a count rate of 2.5×10^6 in one second. Even at that stage of the project this figure was extremely high, a value of 10^6 being considered as more acceptable. Subsequent work and discussions with the supplier eventually established that a count rate of 250,000 (125) should be used, as indicated in section 4.2.5. Even though the initial count rate of 2.5×10^6 was very high, an attempt was made to correlate the flow, but no correlation could be obtained. Therefore the first main step was to reduce the count rate sufficiently, to obtain a correlation curve. Excessive flare from the perspex surface was thought to be affecting the count rate. The simplest method of reducing flare was to polish the surface even further. This was carried out with a great deal of time spent in polishing the four surfaces, until no further improvement could be made. A position of relatively minimum flare was chosen and another attempt made to correlate the flow, but the polishing had made hardly any difference to the large count rate.

Another method to reduce flare from the surfaces was made by cutting a small rectangular slit in black paper and attaching this to both outer surfaces of the channel. It was found by trial and error that this was

easier to align in the PM tube using slit on one side of the plate. With some careful positioning some of the flare was blanked off and the light entering the PM tube was reduced, but not sufficient to obtain good signals. A possible cause of poor signal quality was considered to be the particle size (11, 23, 46, 126) in the water. A sample was microscopically analysed showing that particle sizes varied between 5 - 40 μ m.

An approximate calculation showed that the fringe spacing was about 20 μ m. As Drain (11) points out in the Differential Doppler technique, an important factor in signal quality is particle size diameter. When this particle size diameter becomes large compared with the fringe spacing, the particles span light and dark bands of a fringe pattern, thus averaging out the variation of light intensity. Therefore the modulation of a signal from the passage of a particle deteriorates.

However, Pike (25) states that the particle size has no effect on signal quality, since he does not consider that fringes exist. The present author, having seen the fringes in the intersection volume by means of objective lenses from an optical microscope expected Drain's explanation to be plausible. It was deduced that the high count rate and poor signal quality stemmed from the size of scattering centres. Therefore, filtration was to be considered necessary to control particle size range.

Two filters (not shown) were added to the experimental arrangement in Figure 4.10. These filters to reduce particle sizes to less than $5\mu\text{m}$ were introduced just after the recycling pump, since the flow would pass through them on the way to the main constant head-tank. The flow was circulated through the rig and the particle sizes were analysed from the main recycling vessel. The analysis showed that these were in the range of $5\text{-}10\mu\text{m}$, mostly in $5\mu\text{m}$.

Further attempts were made to correlate the flow. Although the count rate had dropped slightly, no significant improvements were made to the signal quality. It was still felt that flare was the major obstacle in obtaining a good correlation.

Flare has caused great difficulty to other workers (42, 47) as mentioned in Chapter 2, additional literature on LDA was consulted, but most workers hardly commented on this problem, largely because the surfaces which beams passed were simple and thin. Therefore, a useful technique had to be developed to solve the present problem.

Since flare could not be reduced any further, the operating manual (124) was consulted in depth, and it provided the suggestion that if no correlation curve could be obtained, there would be two main

possibilities:

- (i) the flow may be turbulent (which was certainly not so in this case) or,
- (ii) the beams may not be crossing at the desired point, i.e. misalignment in the flow channel.

The latter was considered as a possibility, so in order to check this the procedure outlined in the operating manual was followed.

The count rate of each beam was measured separately by blocking each beam in turn, then the count rate of both beams was measured. If both beams were crossing at the point observed by the photomultiplier, then both beams separately would give the same count rate and each should be greater than the count rate of the combined beams. It was found that the count rate of each beam was greater than the combined beams but the individual count rates were not equal, showing that the beam intensities were not equal. This indicated that the beams were not crossing in the channel. One possible reason for this was that the beams were not entering the channel at the base of a valley in the corrugations, thus being deflected by refraction at the solid liquid interface and possibly being diffused by the lens effect of the curved surfaces. Very fine adjustment was needed to arrange for the beams to cross in the channel, as indicated by obtaining

an equal count rate from each beam. Then further correlation attempts were made, but still unsuccessful. This gave rise to suspicion that the equipment may not be working properly, so a simple test was made.

The LDA equipment was set up for measurement of flow using a fan and this produced satisfactory results. It was considered that the perspex thickness of the model plates may influence measurements, so tests were carried out by blowing air between two thick perspex sheets in order to see if measurements were possible in such an arrangement. Satisfactory results were obtained, indicating that the perspex thickness did not affect measurement.

Once again the LDA equipment was arranged in one chosen cell of the channel where there was minimum flare. Alignment was carefully tested and a correlation was carried out. An acceptable correlation curve was obtained. This was repeated for about fifty minutes during which time the signal quality deteriorated and then completely collapsed. The count rate check showed a drop from 700,000 to 200,000 during the fifty minutes without recovery. The equipment was switched off for a period of a few hours, and another attempt made, when satisfactory correlation curves were obtained. Again the signal collapsed after 30 minutes, and the count rate dropped from 500,000 to 200,000. At this point it was felt that the photomultiplier was becoming saturated,

causing the decay in signal quality. At this stage Malvern Instruments, the manufacturers of the equipment (125) were consulted for a possible solution; they advised that the count rate in one second should be about 250,000 which is not reported in the manual. It was found after another check that for one second the count rate was still 2×10^6 , showing that eight times greater than the acceptable light was entering the photomultiplier and causing saturation. The next step was to reduce the amount of light entering PM tube.

In order to do this, a neutral density filter was used which allowed passage of only 1/16 the incident light. This was placed in front of the beam splitter. This proved unsatisfactory, because the scattered light was also reduced drastically, and very poor signals were obtained, although the count rate dropped to 700,000 in one second.

A further attempt was made by drilling a small hole in the lens cap of the photomultiplier, and fitting a standard pinhole of 200 μ m diameter. This completely blocked most of the light giving no worthwhile results. The pinhole was replaced by a piece of paper containing a small, central hole and this was attached to the lens cap. This decreased the light entering significantly to a count of 500,000 and some correlations were obtained. Although the

correlations were obtained, the count rate still dropped from 500,000 to 200,000 in a span of sixteen minutes and did not recover. Therefore further light reduction was necessary. Another possibility considered was to work in back-scatter mode. This has been recommended by Drain (11), who points out that the amount of light is reduced, in order of two to three times as compared to forward scatter experiments, and this is most useful where the flow system is moving and the optical systems are fixed. This suggestion did not reduce the light further than already achieved on the forward scatter mode with paper on the lens cap. Some results were obtained, but the count rates dropped in 40 minutes, the correlation collapsed and failed to recover.

At this stage, the possibility of reducing the flare from surfaces by means of an anti-reflection coating was considered. It has been reported by Cole and Swords (127) in their study of measurements of an engine, that severe problems of flare can be controlled by a suitable coating. They used a magnesium fluoride film on the observation windows as the anti-reflection coating and minimised scattered light by painting all the internal surfaces of the cylinder, matt black. This possibility was considered in the present study, but for three main reasons was not carried out.

Firstly, if a coating was applied this may restrict the range of fluids that could be used in the channel and could conceivably react with or attack the perspex. Secondly, polishing the plate was regularly necessary and this would affect any coating applied. Thirdly, the plates were very expensive and the coating process caused an unacceptable risk of damaging the surfaces.

Again Malvern Instruments were consulted and a technician worked on the experimental rig to provide assistance in overcoming the problem. It was suggested that the curved perspex surface was distorting the beams, and it would be appropriate to sharpen the beam by means of a lens. This would not only reduce the flare at the surface where the beams entered, but would also reduce the volume of intersection and increase the power per unit area at the crossover point. The smaller the volume under inspection, the nearer would be the approach to measurement of a point velocity while the increased power should improve signal strength. Comments were also made on the lightness of the table supporting the optical equipment and on the lack of rigidity in the arrangement for moving the channel during runs. It was suggested that these factors could contribute to collapse of signal after an interval, possibly due to differential thermal expansion and affecting the optical paths out of alignment.

A much more rigid structure was constructed to hold the channel and better optical benches were obtained. A lens was placed in the position provided in the beam splitter holder to provide much sharper beams and improve the focussing in the back-scatter mode. To reduce some subsidiary reflections from the beam splitter onto the channel, a black tape drilled with two holes was used to cover this region; thus allowing the beams to pass through but absorbing all reflections. Further attempts were made to correlate the flow and although some results were obtained, the count rate still dropped and the signal collapsed after 30 minutes. Flare had been reduced significantly and it did not seem possible to reduce it further.

Again the equipment suppliers were consulted, and they suggested that the drop in count rate was caused by a lack of scattering particles as time proceeded.

This was a real possibility since at the beginning of a run the particles were settled at the bottom of the recycling vessel and at the bottom of the constant head tank. But as the flow circulated for a period, these particles circulated and were removed by the filters, thus the concentration of particles decreased as the run proceeded. Therefore the sample of water was drained from the system and a fresh sample was

tried together with a small quantity of methyl-soluble dye to encourage scattering properties. In fact no correlation curve was obtained using dye as scattering centres. A small quantity of milk as recommended by Drain (11) was tried, but no results were obtained. A small quantity of latex particles of 5 μ m were added, this also did not improve the correlations. A small quantity of chalk was tried, but this made no improvement to the correlation. Finally, the filters were removed and this did not increase the count rate nor produce continuous results. It was realised that saturation of the photomultiplier was a continuous and constant problem. Therefore it was decided to make measurements all over the channel, irrespective of the saturation problem.

The channel was adjusted to another position (another cell), the beams were crossed in the flow, aligned and the correlation procedure was followed. No correlation curve was obtained. All the possible considerations affecting the correlation were examined which only resulted in total failure to obtain any correlation, although the count rate was about 400,000.

Several attempts were made at different positions to correlate velocity measurements, only to result in total failure. Alignment was checked over and over again, but no significant measurements were made. Occasionally one measurement out of every

twenty readings was successful . Since the results were not repeatable it was decided to abandon using water as a suitable liquid to study flow distribution in PHE's channel.

It was learned after a detailed study of the failure of being able to make any further measurements that the fault was largely due to the beams being unable to cross effectively in the channel because of the internal geometry of the surfaces. The probability of the beams meeting properly in the channel was extremely low. The results obtained were situations where the beams fortuitously did cross in the channel. A much more detailed explanation for this failure to repeat the results in PHE channel will be discussed in Chapter 6.

Therefore it was decided that the only possible methods to overcome this problem of flare causing saturation of the photomultiplier was by refractive index matching. It might be possible to construct another channel using a material of the same refractive index as water (1.33), except that no such suitable material exists. The other possibility was to choose a suitable liquid of the same refractive index as perspex. This would obviously reduce the investigation to only one liquid but would overcome the problem of inadequate intersection of beams by completely overcoming the flare from the inside surfaces of the channel.

4.3.4 REFRACTIVE INDEX MATCHING

The earlier experimental work described in section 4.3.2 using water as the working fluid, was only marginally successful because of the path distortion suffered by the beams. To ensure that the beams would cross in the channel without distortion required that a transparent refractive-index matched liquid be identified and obtained for use as the working fluid. Although there might still be refraction in the walls of the perspex plates, at the solid/liquid interface, the beams should pass through the channel as a continuous system if the refractive index is matched well. This would also reduce or eliminate the problem of flare from the internal surfaces of the channel.

Initially a literature study was made to find if any previous researchers had used refractive index matching as a technique in flow problems.

From the literature of LDA work by Wang et al. (72) as reported in section 2.6 used this technique. They prepared a match of refractive indices of glass beads with a liquid mixture of ethyl and benzyl alcohols. But no previous workers have attempted to match refractive index of perspex with a suitable flowing liquid. Drain (11) recognises the difficulty in refractive index matching of suitable liquid with perspex since only organic liquids like toluene are available, such liquids tend to dissolve perspex.

Furthermore, many organic liquids are flammable and/or toxic. Since large quantities of liquid would be required for the present study, it was decided that such organic liquids would be unsuitable. Since there was no suitable liquid immediately available, a detailed literature survey was undertaken as an absolute necessity to overcome this problem.

Search showed (128) that the refractive index of perspex is 1.49, therefore a transparent liquid was required of similar refractive index.

The initial search (129) showed that the liquids with nearest refractive index to 1.49 were mostly organic, e.g. benzene, p-xylene and pyridine. A much more detailed review available from the University of Karlsruhe (130) of liquids for refractive index matching showed that from 124 different liquids only about twenty of these were potentially suitable. But all these liquids were organic type.

A further literature survey (129) was carried out to find if suitable inorganic liquid existed. There are inorganic complex solids which have refractive index of 1.49 but in solution their refractive index decreases considerably yielding colourful solutions and therefore unsuitable liquids. However sugar solutions were considered since aqueous solution of sucrose (cane sugar) of 80% w/w should provide a refractive index of 1.49. Experiments were carried

out, to prepare sugar solution of 80% by weight, but no satisfactory success was achieved. The sugar crystallised out as soon as the solution reached room temperature.

One other possibility was considered that if two liquids can be found of higher and lower refractive index than 1.49 then those could be mixed together to provide the appropriate refractive index. In a more detailed literature survey (129, 131) one possibility emerged of using mixture of oils. The table 4.1 shows the range of oils available for the refractive index matching for an acceptable temperature range.

TABLE 4.1 - REFRACTIVE INDICES OF OILS

TYPE OF OIL	REFRACTIVE INDEX
Mineral (Code 50)	1.458 ¹
Mineral (Code 40)	1.570 ¹
Tung	1.5174*
Cod-liver	1.481*
Perilla	1.481*

* Refractive index at 25°C

¹ Temperature not specified

Table 4.1 indicates that a mixture of Tung oil and one other oil would provide suitable refractive index of 1.49. It was decided to try a mixture of Tung and Cod-liver oils, because those were easy to obtain and safe to use in the large quantities required.

A sample of 500 Cm³ cod-liver was obtained from the suppliers, British Cod-liver Oil Ltd., Hull; and 500 Cm³ of tung oil were obtained from Lloyd W.S. Ltd., London. When received the sample of cod-liver oil was transparent but yellow in colour while the tung oil was a dark brown high viscosity liquid. Initially this caused concern for the transparency of a mixture. Since tung oil was not transparent and laser beams would not penetrate this oil by itself, but when these oils were combined, beams passed easily through the mixture. An 'ABBE 60' high accuracy refractometer was employed to measure the refractive index of each liquid. This instrument indicates the refractive index value to five figures after the decimal point whereas the literature quotes to four. The measured values were 1.4783 and 1.51779 for cod-liver oil and tung oil respectively at temperature of 20°C showing a slight difference between those reported (129) and the measured values. Various mixtures of these oils were prepared to find a suitable ratio which would provide a refractive index of 1.49. Two mixtures containing of 37.04% and 35.22% tung oil by volume

had refractive indices of 1.49135 and 1.48911 respectively. Both mixtures were used in the perspex plate channel and the laser beams passed through the channel without the deflection and distortions encountered when water was the working fluid. Visual inspection showed the 37.04% tung oil mixture, to the nearest match of refractive index, with only a pinpoint of light occurring at the point where the beams passed through the solid/liquid interface. Although this showed that the match was not perfect, it had the advantages that flare at the boundary had been eliminated and that the actual position of the boundary could be determined from the pinpoint of light.

4.3.4 OIL AS WORKING FLUID

The experimental rig used for this fluid was similar to the original arrangement described in section 4.3.2 and shown in Figures 4.10 and 4.11. However, the volume of the constant head-tank was much smaller, due to the amount of oil available. Since physical properties of the mixed oils were essential to calculate Reynolds number, and there was little information available in the literature, it was decided that the viscosity would be measured but that a weighted mean density would be acceptable since the densities of the separate oils were very similar.

The viscosity was measured using a 'TECHNICO 300 VISCOMETER' and gave a value of 0.0927 Kg/ms at 20°C temperature. Density of each oil reported in the literature (129) to be 925 kg/m³ at 25°C and 934 kg/m³ at 15°C for cod-liver and tung oil respectively. Hence an average density of the mixture was calculated to be 929.5 kg/m³ at 20°C.

Since the apparatus had previously contained water and it would be desirable to avoid forming an oil-water emulsion through the mixing action of the circulating centrifugal pumps, the equipment was carefully dried using hot air blowers. The flowrator described in section 4.3.2 was recalibrated with the oil mixture. The calibration was only possible for half the range of flowrator because at lower flows the calibration becomes discontinuous. Figure 4.13 shows the calibration curve for the oil mixture.

It was decided to make measurements at 20°C temperature since the physical properties of the fluid were measured and calculated at this temperature. A check of oil temperature was made at the outlet of channel and in the recycling vessel.

The perspex channel was polished with perspex polish as discussed previously in section 4.3.2 and assembled into the experimental arrangement.

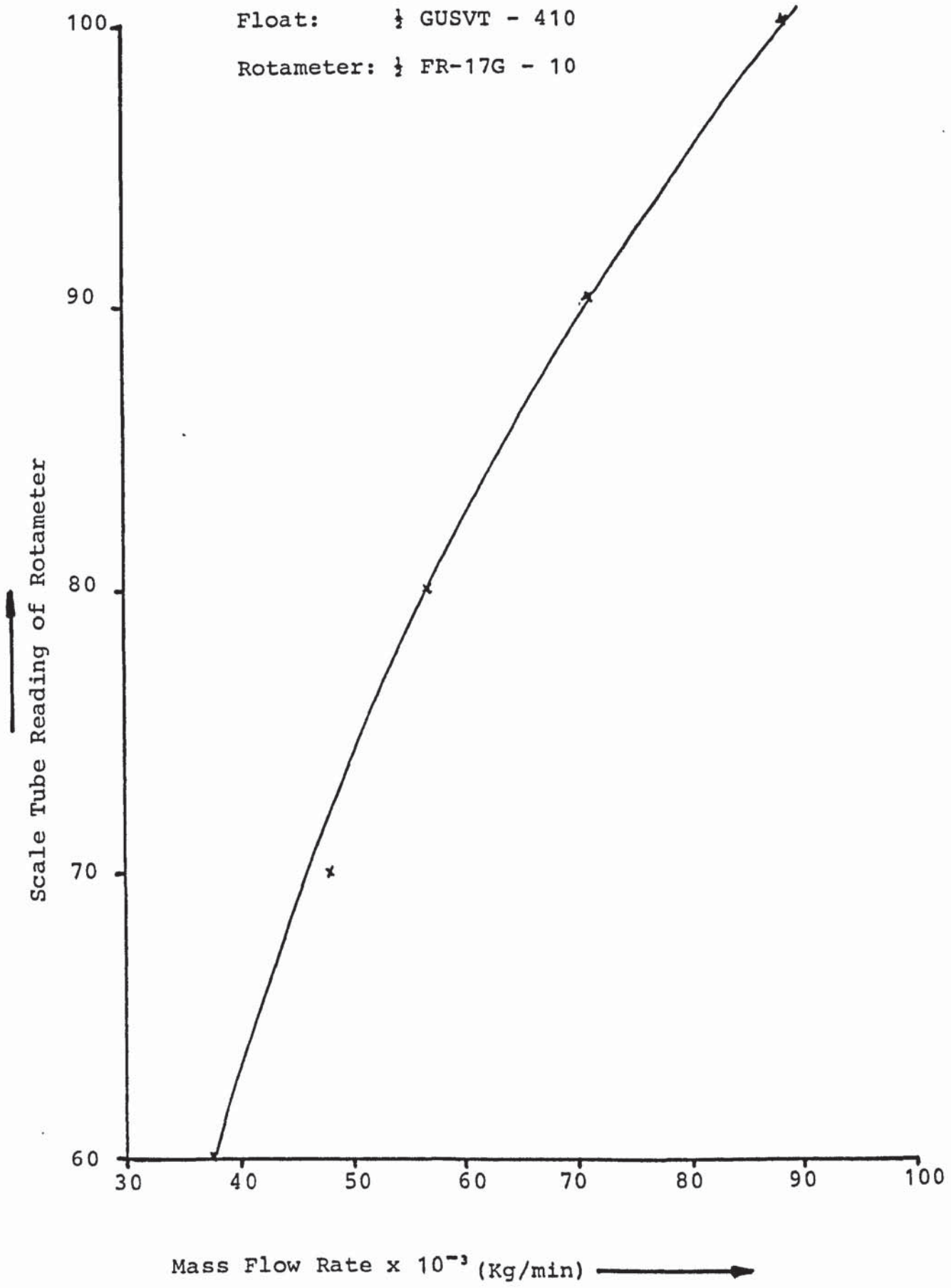


FIGURE 4.13 CALIBRATION CURVE FOR OIL

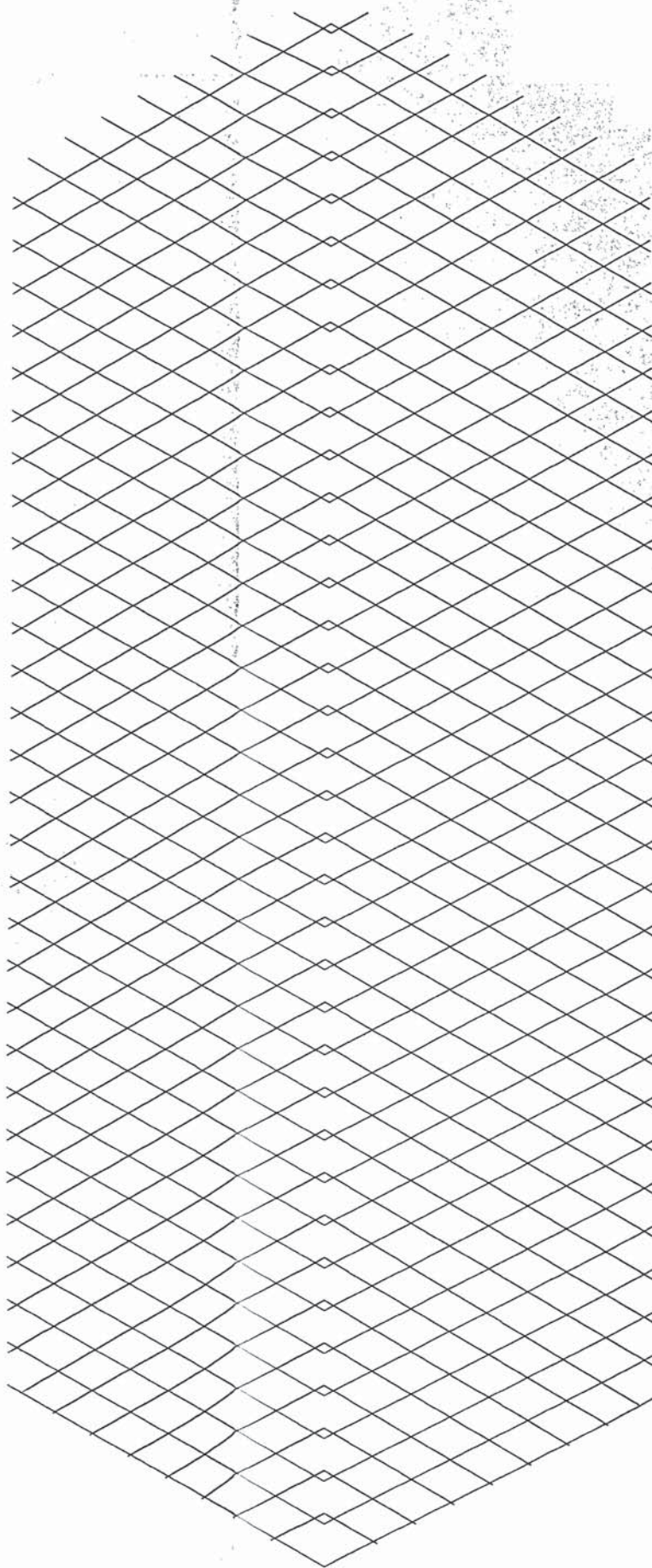
From the calibration curve and the calculation in Appendix A-3.3 laminar flow exists for all the flow rate range.

When steady flow was achieved through the channel, the laser was switched on and the beam splitter was adjusted to the horizontal plane. The beams were adjusted to cross in the centre of the cell volume. In order to determine the exact centre position of the cell volume, a special technique was developed.

From the drawings of the SR1 plate, the corrugation pattern was reproduced on transparent acetate cellulose sheet of the type used with overhead projectors. This provided an exact representation of the channel corrugations, as shown in Figure 4.14, where each point of intersection represents peak to peak contact. This sheet was attached to the perspex channel, on the same side as the photomultiplier tube and was used to assist identifying the particular cell. To accurately locate the centre of a particular cell, a graphical representation was generated with a defined co-ordinate system. Photocopies of graph paper of size A4 of 10 mm squares were reproduced on acetate sheets. These were attached in three sections to cover the channel.

FIGURE 4.14

FIGURE 4.14 - REPRESENTATION OF CHANNEL CORRUGATIONS



The middle section was A4 size acetate sheet, while top and bottom sections were cut to particular shapes to fit the channel. In each section, there were two sets of co-ordinate parameters, used as shown in Figure 4.15. The X and Y co-ordinates would help to identify a particular square on the acetate, while the co-ordinates X1 and Y1 would provide the exact position in the cell, to the nearest millimetre.

The position of the perspex channel was adjusted to locate the centre of a chosen cell, all the co-ordinates X, Y, X1 Y1 were recorded before measurements were carried out following the procedure in section 4.2.5. Although the count rate was initially high this was reduced and brought under control by using lens cap technique described in section 4.3.3.

The flow was not seeded, since an analysis of oil sample showed that sufficient natural particles already existed. Particle diameters ranged 5-20 μm but mostly were 10 μm in size.

Fringe spacing was calculated by projecting the beams onto a white surface positioned beyond the channel and the distance between the surface and the middle of the channel. These measurements were used in the computer program to calculate fringe spacing.

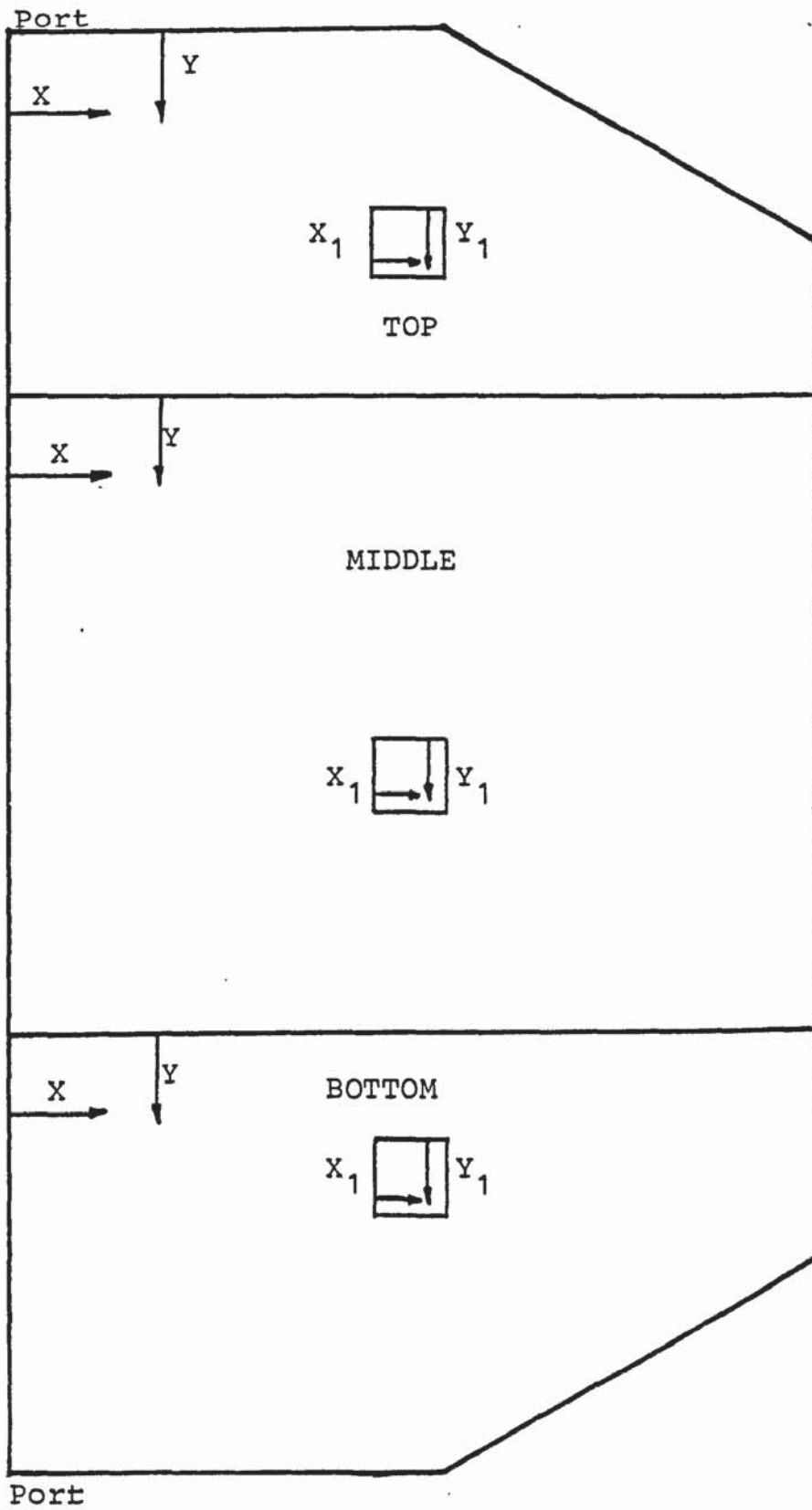


FIGURE 4.15 CO-ORDINATE SYSTEM FOR CHANNEL POSITION.

Fringe spacing remained fixed until adjustments were made to the channel or the beam splitter.

During the experiments it was observed that the temperature of oil was rising much higher than the chosen temperature of 20°C, although the float in the flowmeter remained in its initial position. The increase in temperature was caused by the mechanical work imparted by the recirculating pump to the oil being converted partially to heat energy. Therefore, a cooling heat exchanger was fitted between the recycling pump and the constant head tank to control the oil temperature. Experience showed that the operating temperature should be raised to 22°C since this was the optimum temperature achievable. A small immersion heater was sometimes used in the recycling vessel to boost the initial oil temperature until steady state temperature was achieved.

Since the operating conditions had been changed new physical properties were required. Accurate measurement was made of density, 931.98 kg/m³ at 22°C and viscosity over a range of temperatures using the 'TECHNICO 300 VISOMETER'. Literature (132) shows that there is a linear relationship between viscosity and temperature. Therefore best straight line was fitted as shown in Figure 4.16. The equation of the best straight line was:

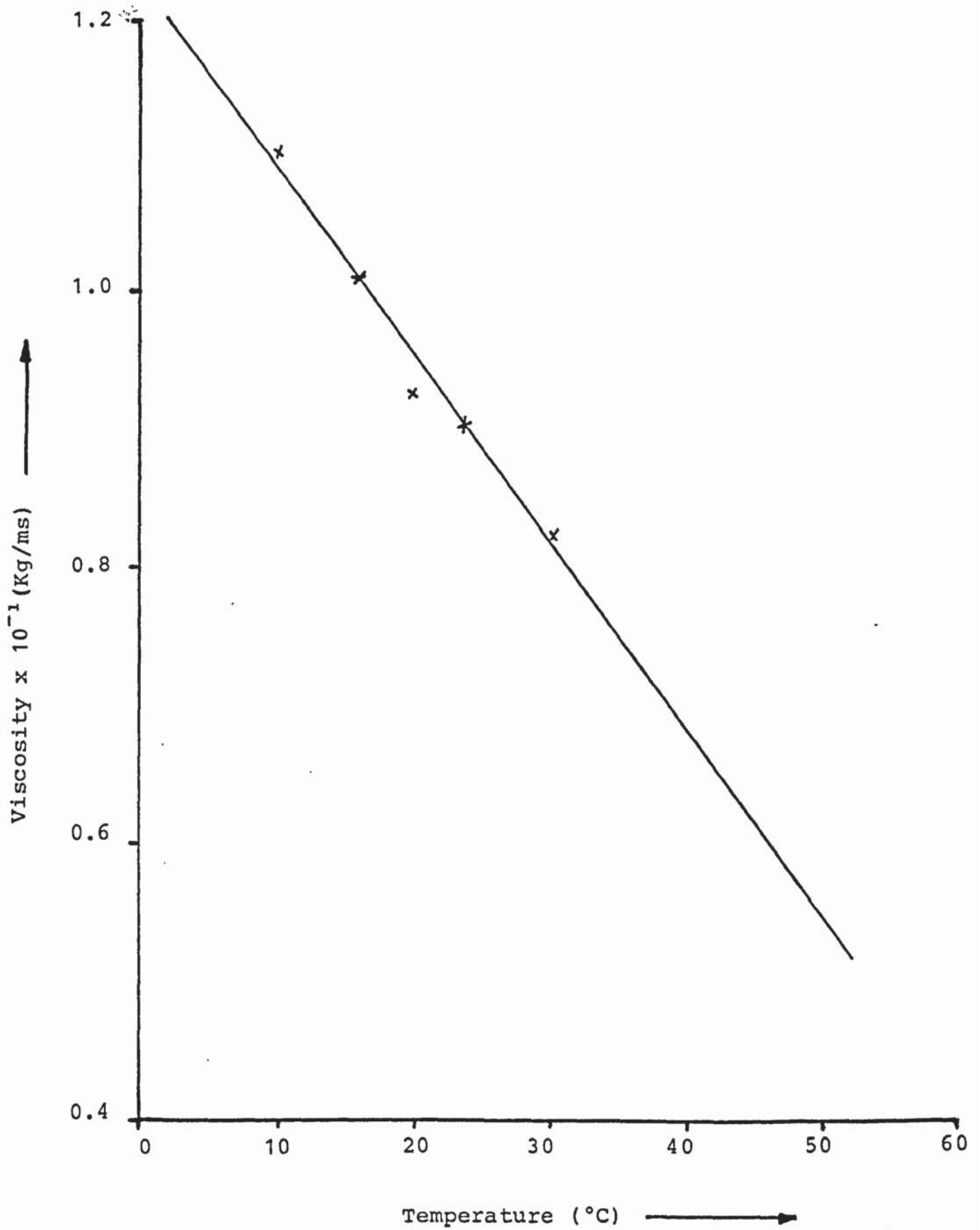


FIGURE 4.16 PLOT OF VISCOSITY VS TEMPERATURE OF OIL

$$\mu = (1.5052 - 0.02757T) \times 10^{-1} \quad (4.1)$$

where T = Temperature in (°C)

μ = Viscosity in (Kg/ms)

Therefore from the above equation, viscosity was calculated to be 0.08986 Kg/ms at 22°C oil temperature.

Initially velocity measurements were measured in the centre of the channel with the beam splitter in the horizontal plane for Up-flow.

Further velocity measurements were measured with the beam splitter plane arranged parallel to the corrugations, giving a velocity component at 60° to the vertical.

These measurements were mostly made at three zones in the channel.

- (i) inlet region - where flow just enters the channel and is distributed over the heat transfer surface,
- (ii) middle region - where flow could be fully developed (part-way along the channel),
- (iii) outlet region - where flow is collected ready to leave the channel.

The measurements were made in selected cells as detailed in Chapter 5.

4.3.5 MODIFIED EQUIPMENT ARRANGEMENT

In the early description of experimental work, low flow rates were achieved, at $Re < 1$, due largely to the high viscosity of the oil mixture. So to examine higher flow rates, a significant modification to the equipment was necessary.

Figure 4.17 shows the new experimental set up, with the LDA arrangement as shown in Figure 4.3. The dotted section in Figure 4.17 is connected to the arrangement shown in Figure 4.11. Since the height of the laboratory limited the available head it was decided to use a more powerful Stuart Turner No. 22 centrifugal pump, as the delivery pump. Although fluctuation in flowrate could be expected with this type of pump it was found that after a short period, the float stopped fluctating and remained at the set flow rate. Larger bore "QVF" pips and fittings of 35.1 mm diameter were used, as well as flexible PVC tubes and bellows wherever necessary. For the inlet a long PVC tube was used to allow the fluid flow profile to become fully developed before entering the channel.

A by-pass valve was introduced after the pump in order to balance the amount of flow required through the flowrator while avoiding cavitation in the pump. Two rotameters of metric tube size 47F with stainless steel floats type S were fitted.

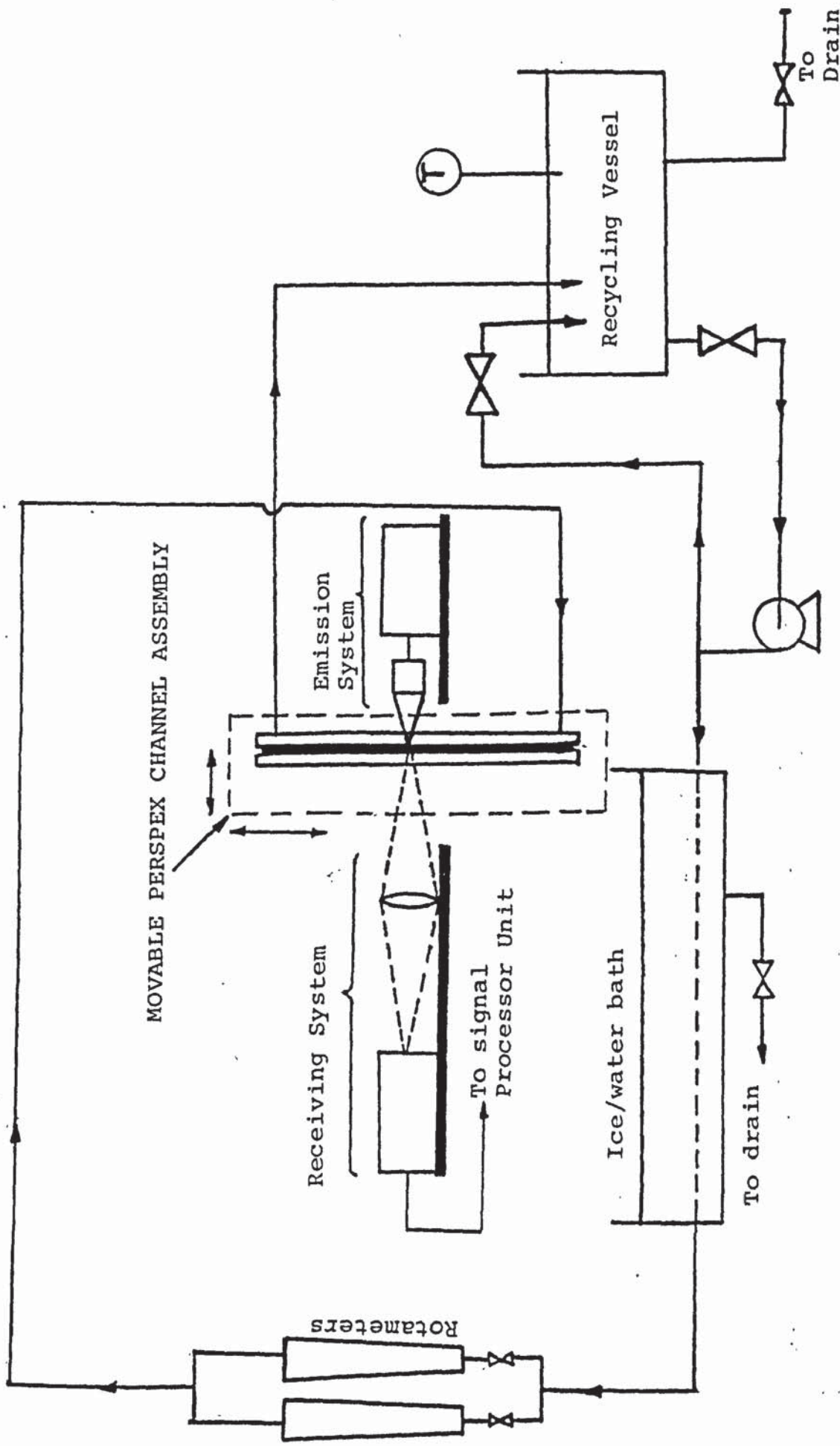


FIGURE 4.17 LINE DIAGRAM OF MODIFIED EXPERIMENTAL EQUIPMENT

During trial experiments it was found that the oil temperature increased with duration of run so an ice-water bath was arranged around a pipe to cool the oil to achieve good heat transfer. The optimum temperature of oil was found to be 34°C, measured in the recycling vessel. The fluid temperature leaving the channel was the same as the temperature in the recycling vessel.

The operating temperature was changed to 34°C and new physical properties of the fluid were obtained. The density was measured to be 933.98 kg/m³ and the viscosity was calculated from equation 4.1 to be 0.05678 Kg/ms.

It was extremely difficult to carry out any calibration of the rotameter due to the very high flow-rate. A calculation procedure outlined in Appendix A-3.4 was developed to estimate the flowrate, so that the Reynolds number could be calculated.

Photographs of the experimental rig can be seen in Plates 4.3 to 4.5, perspex channel in Plate 4.6, the Channel with LDA optical arrangement in Plate 4.7 and the signal processing equipment is shown in Plate 4.8. Furthermore, a close-up view of the laser beams passing through the channel is shown in photograph of Plate 4.9.

Steady laminar flow was arranged through the channel, the LDA equipment was aligned in a chosen spot and the procedure for making measurements was followed as out-

1 > ROTAMETERS

3 - WATER/ICE BATH

2

1

3

PLATE 4.3 - EXPERIMENTAL EQUIPMENT

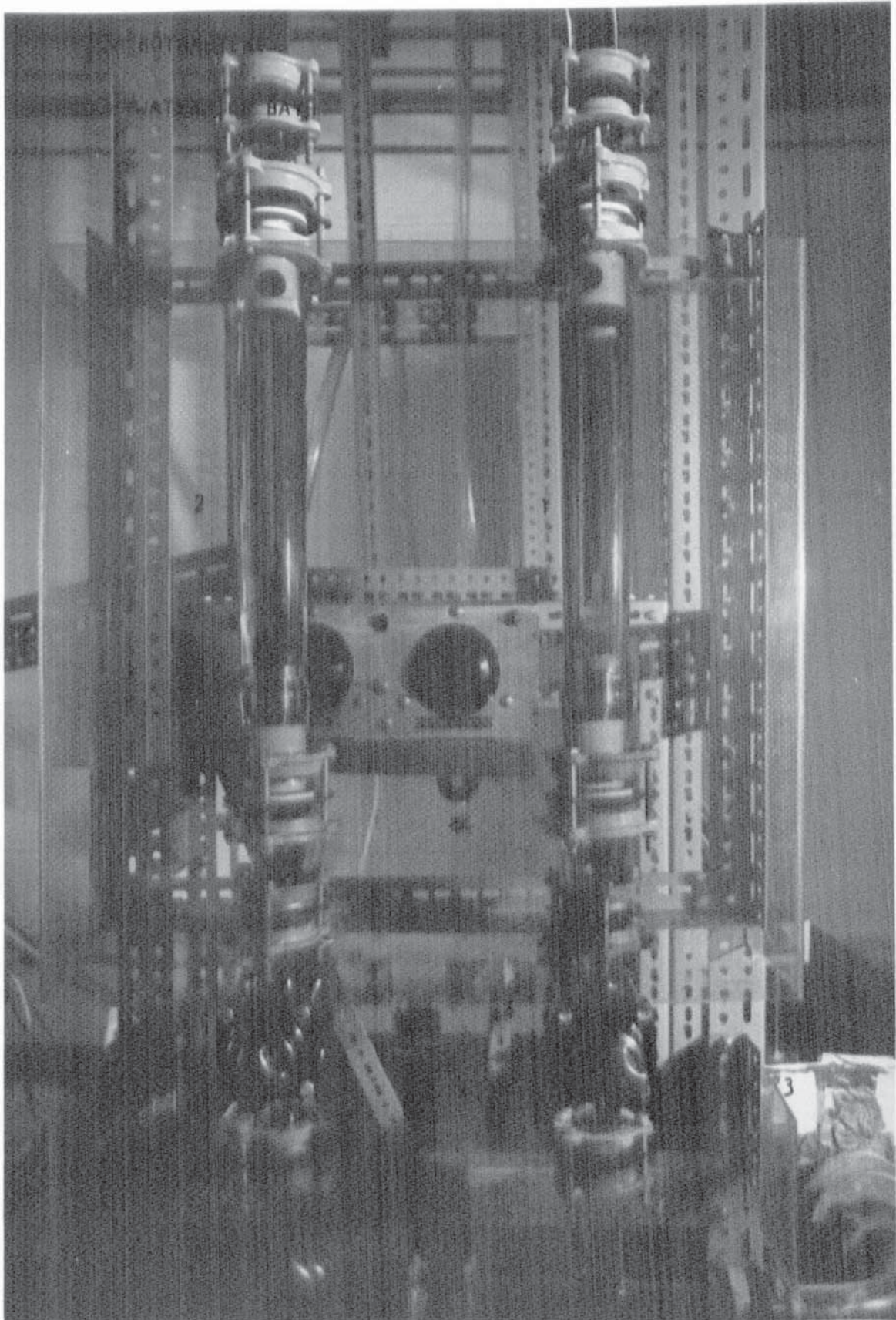


PLATE 4.3 - EXPERIMENTAL EQUIPMENT

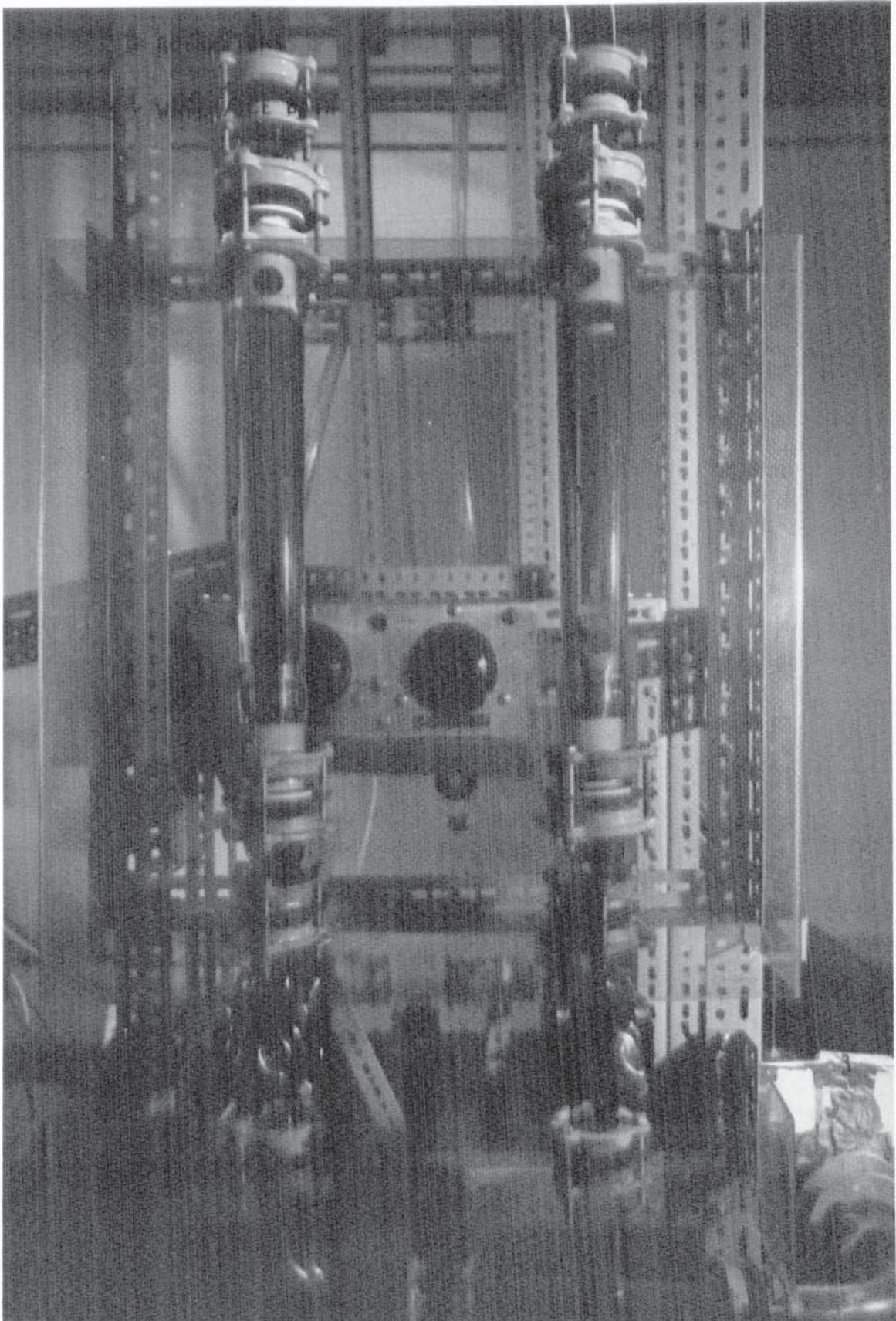


PLATE 4.3 - EXPERIMENTAL EQUIPMENT

- 1 - WATER/ICE BATH
- 2 - PUMP
- 3 - RECYCLING VESSEL

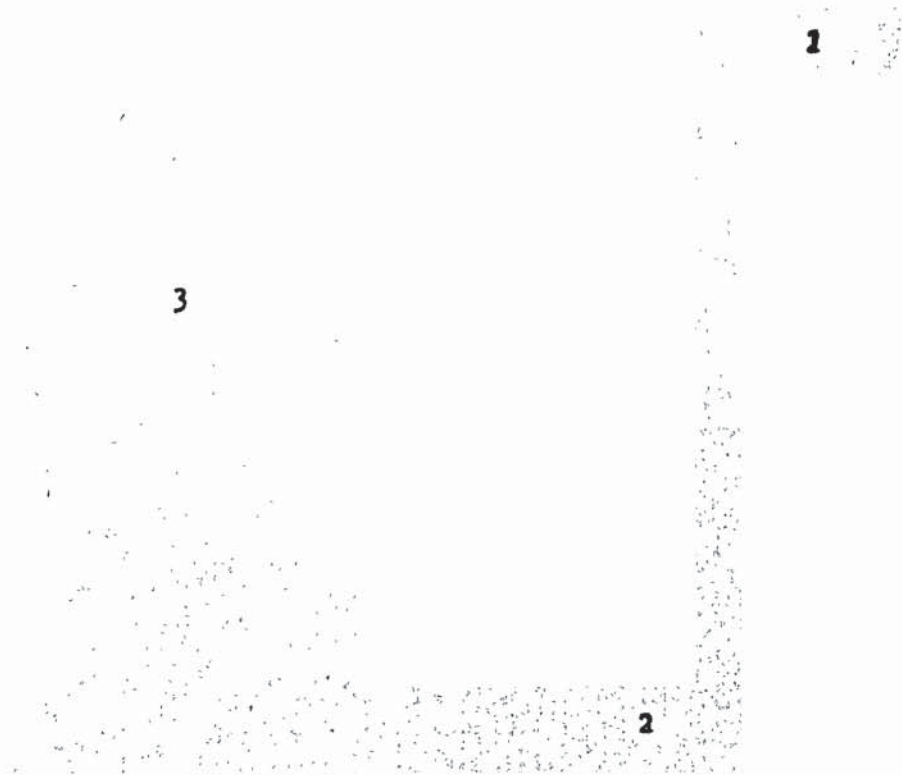


PLATE 4.4 - EXPERIMENTAL EQUIPMENT

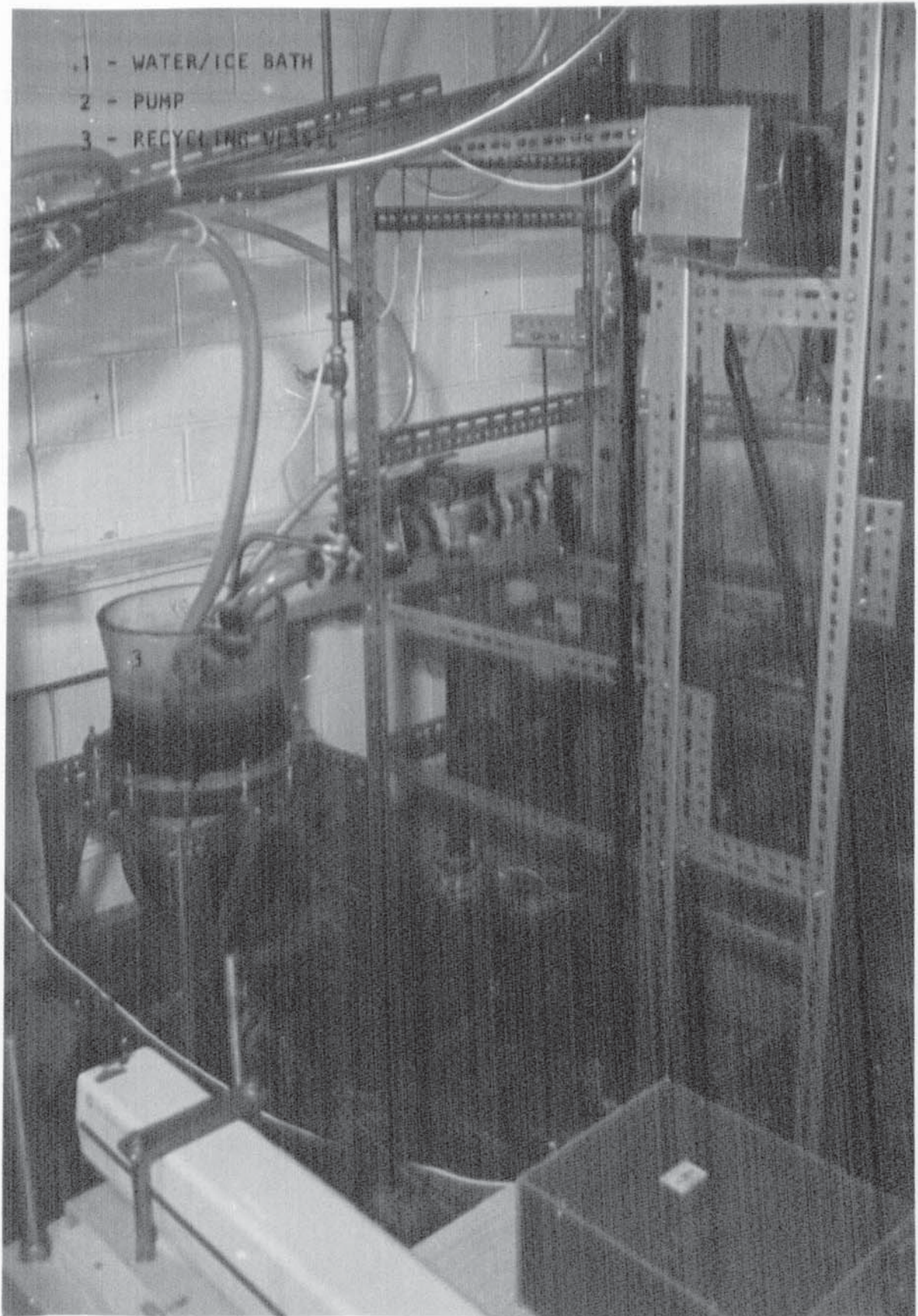


PLATE 4.4 - EXPERIMENTAL EQUIPMENT

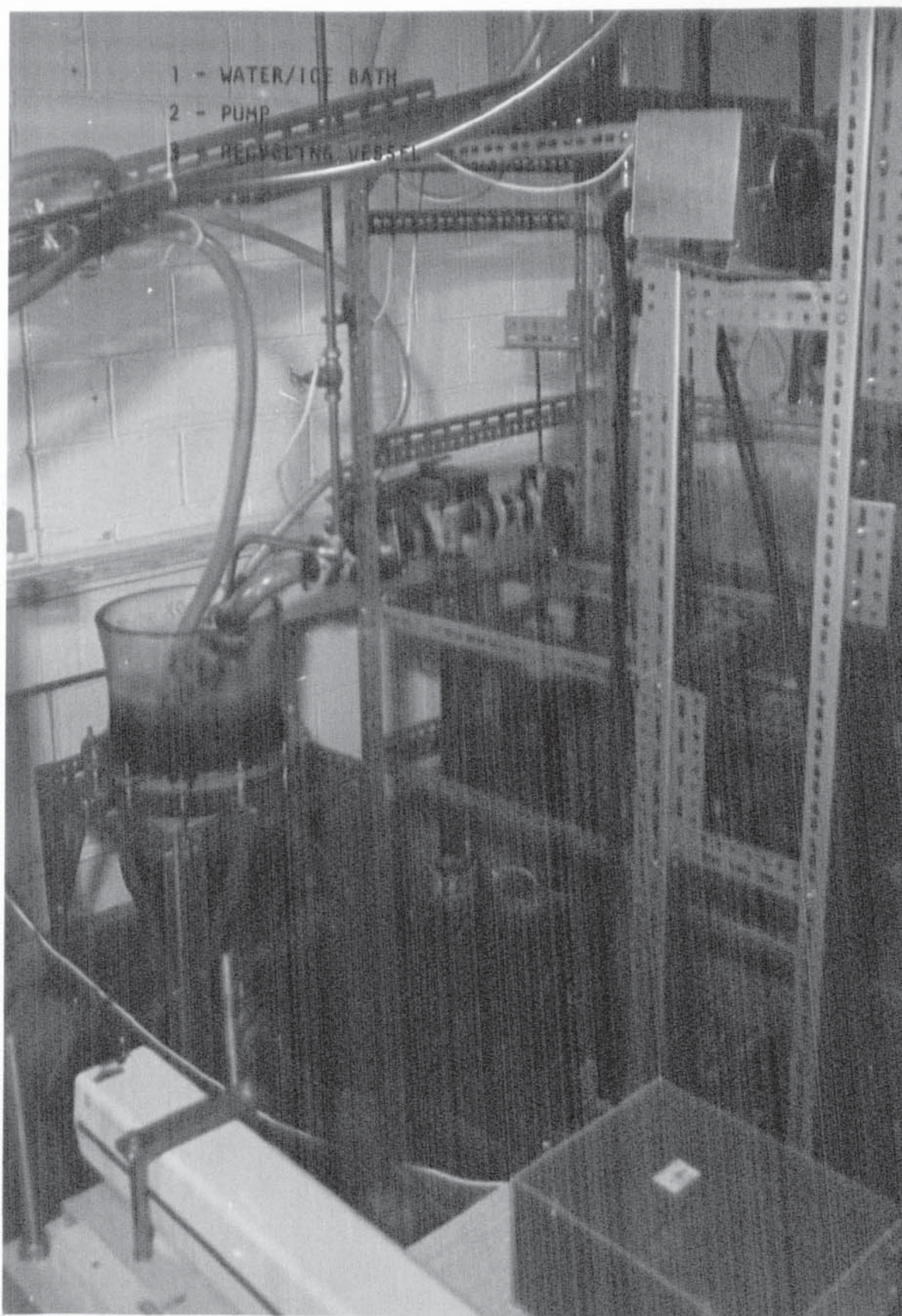


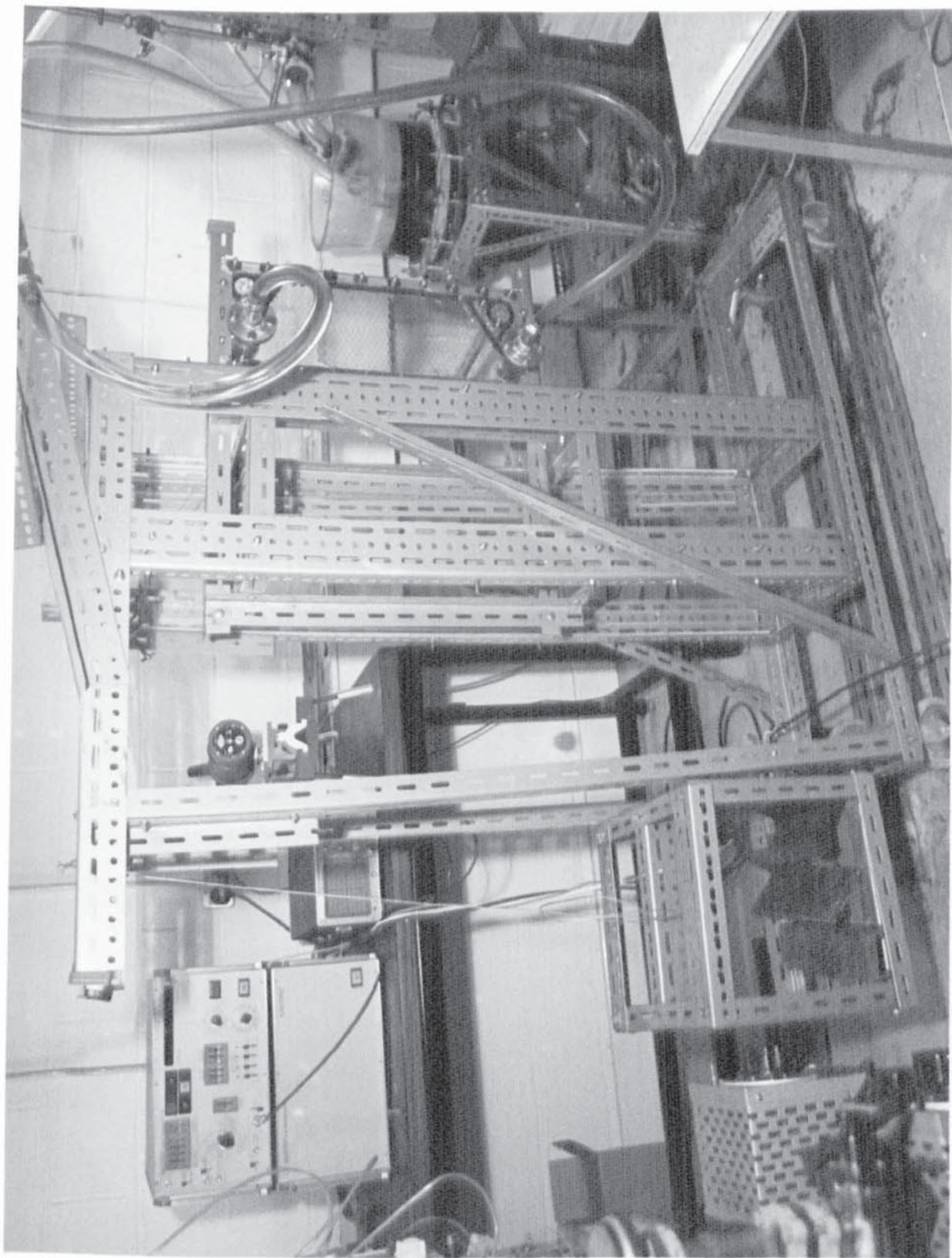
PLATE 4.4 - EXPERIMENTAL EQUIPMENT

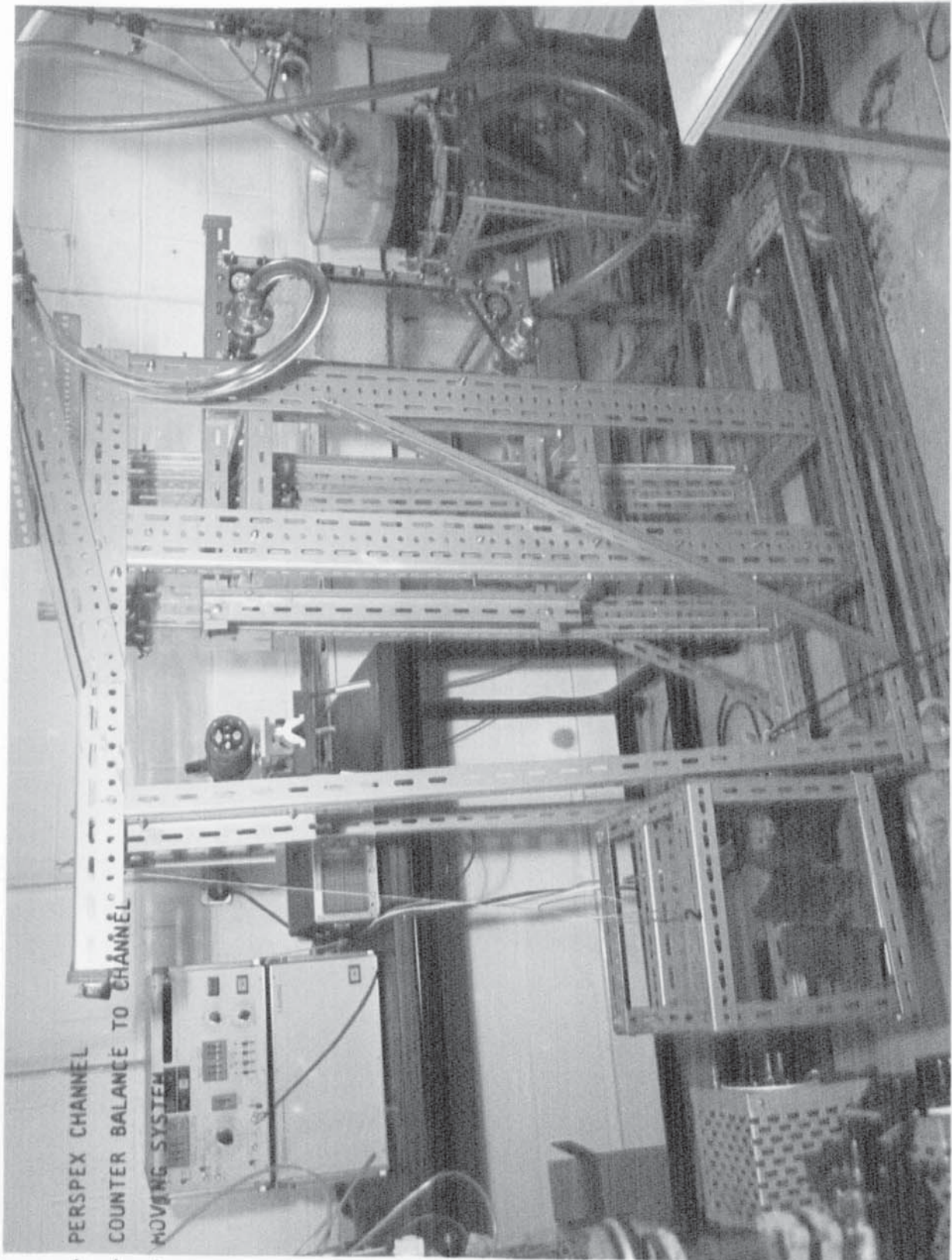
- 1 - PERSPEX CHANNEL
- 2 - COUNTER BALANCE TO CHANNEL
- 3 - MOVING SYSTEM

3

1

2

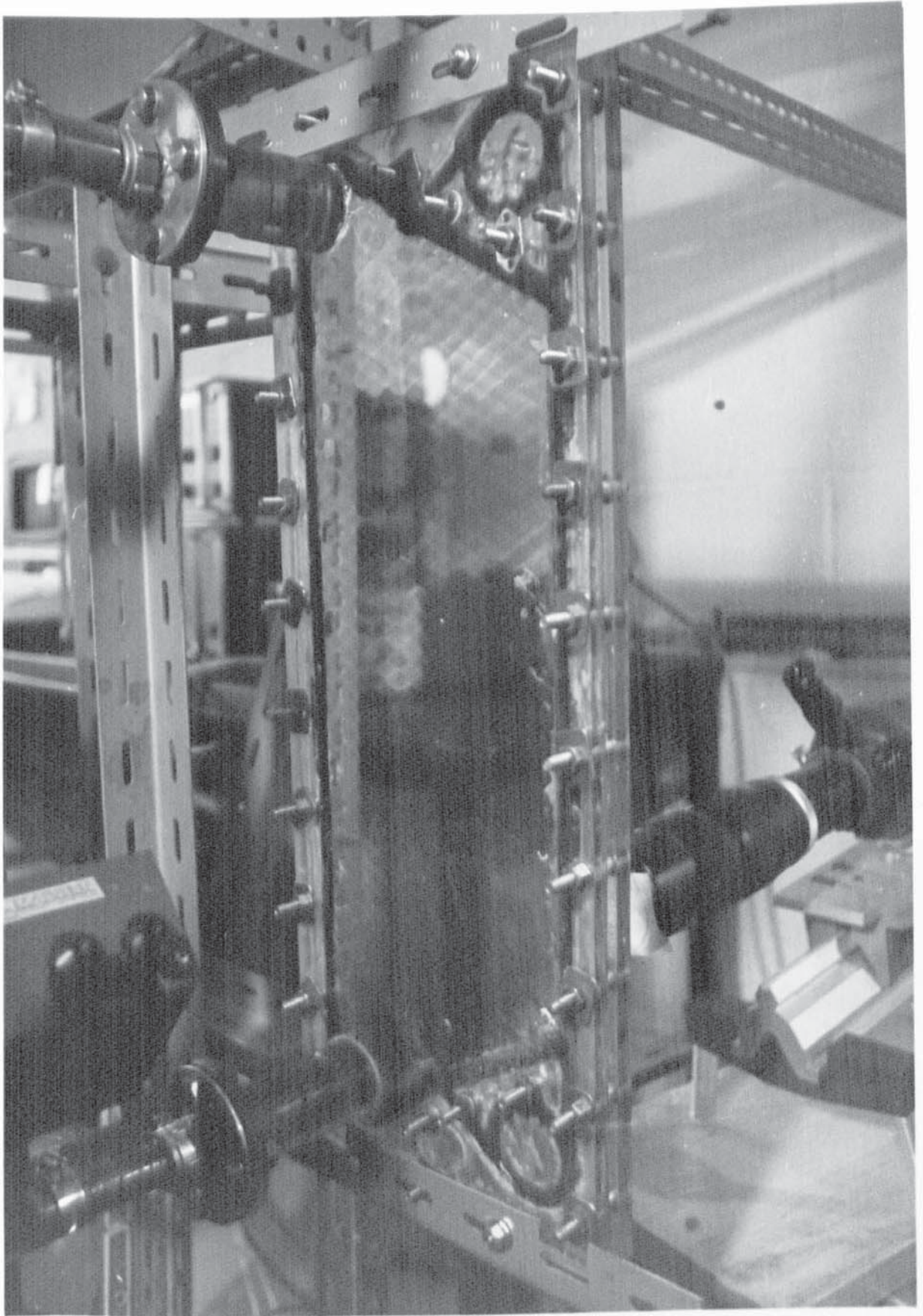




- 1 - PERSPEX CHANNEL
- 2 - COUNTER BALANCE TO CHANNEL
- 3 - MOVING SYSTEM

PLATE 4.5 - ASSEMBLY OF PERSPEX CHANNEL WITH THE EXPERIMENTAL RIG

PLATE 4.6 - PERSPEX CHANNEL OF SR1 PLATE HEAT EXCHANGER



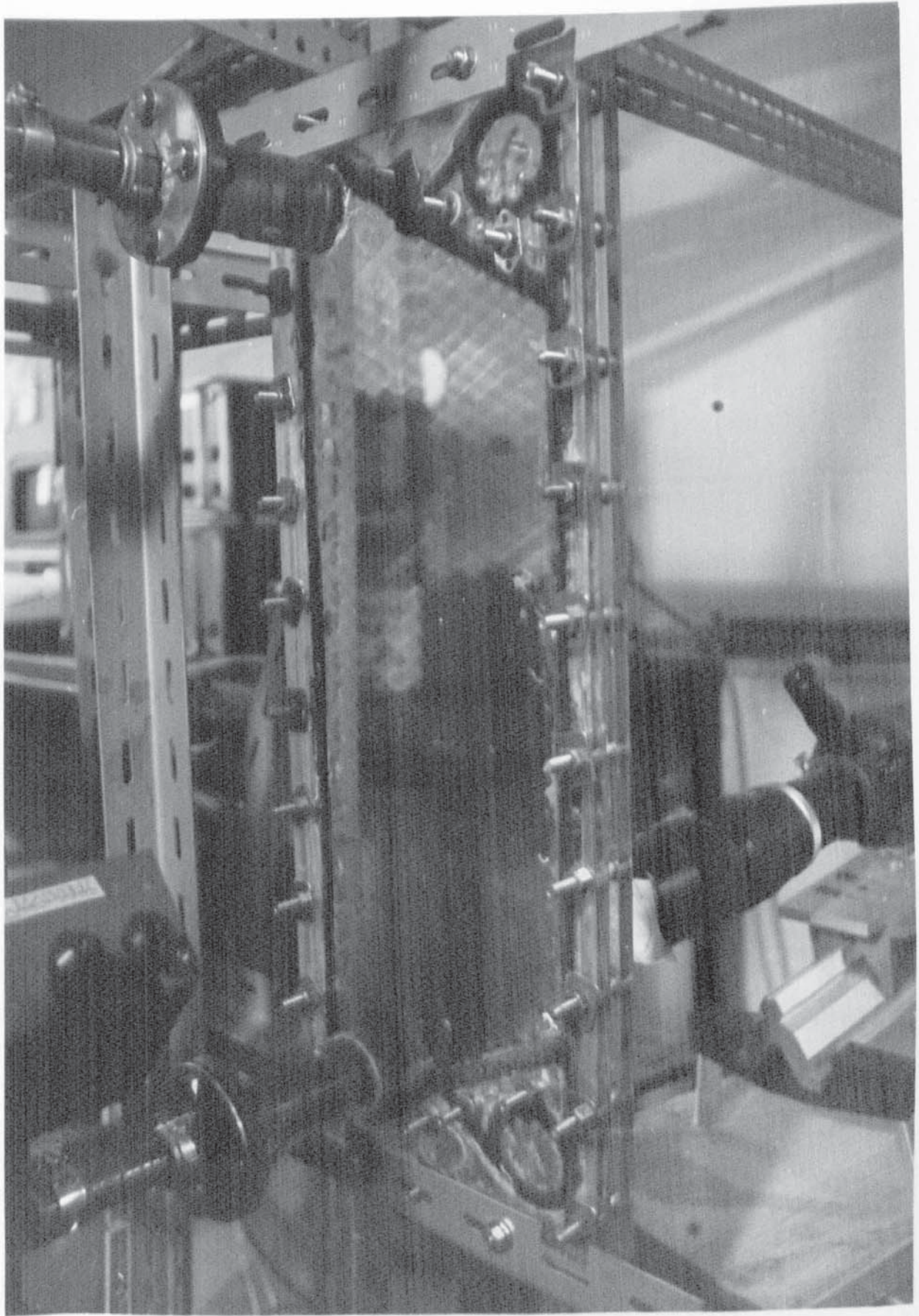


PLATE 4.6 - PERSPEX CHANNEL OF SR1 PLATE HEAT EXCHANGER

- 1 - LASER
- 2 - PERSPEX CHANNEL
- 3 - PHOTOMULTIPLIER TUBE
- 4 - EXTRA HIGH VOLTAGE
- 5 - PHOTON CORRELATOR
- 6 - VDU DATA PROCESSOR
- 7 - LINE PRINTER.

PLATE 4.7 - OPTICAL CONFIGURATION OF LDA SYSTEM FOR PERSPEX CHANNEL



1 - LASER

2 - PERSPEX CHANNEL

3 - PHOTOMULTIPLIER TUBE

4 - EXTRA HIGH VOLTAGE

5 - PHOTON CORRELATOR

6 - VDU DATA PROCESSOR

7 - LINE PRINTER



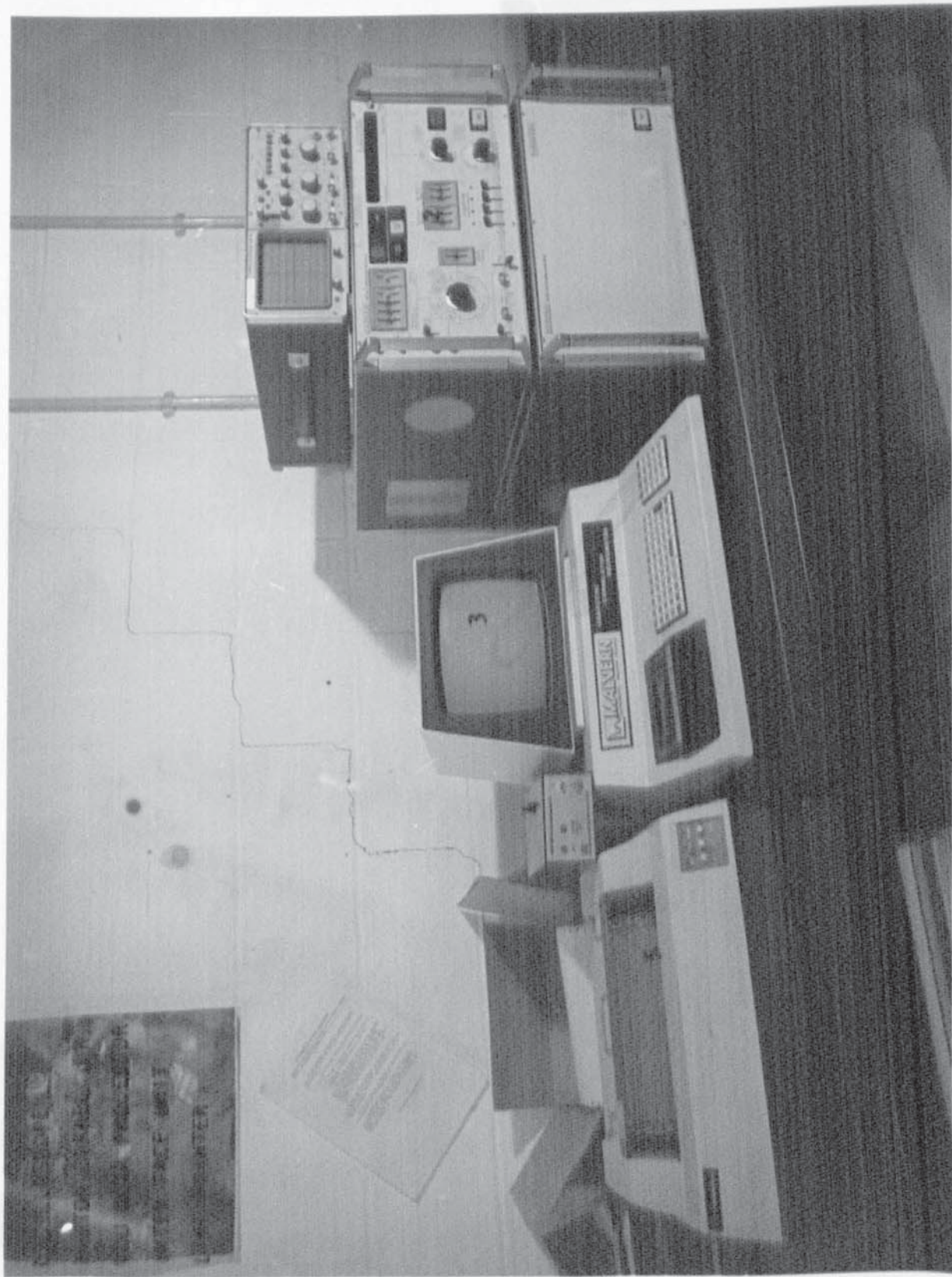
PLATE 4.7 - OPTICAL CONFIGURATION OF LDA SYSTEM FOR PERSPEX CHANNEL

- 1 - OSCILLOSCOPE
- 2 - PHOTON CORRELATOR
- 3 - VDU DATA PROCESSOR
- 4 - INTER FACE UNIT
- 5 - LINE PRINTER



PLATE 4.8 - SIGNAL PROCESSING AND OUTPUT UNITS



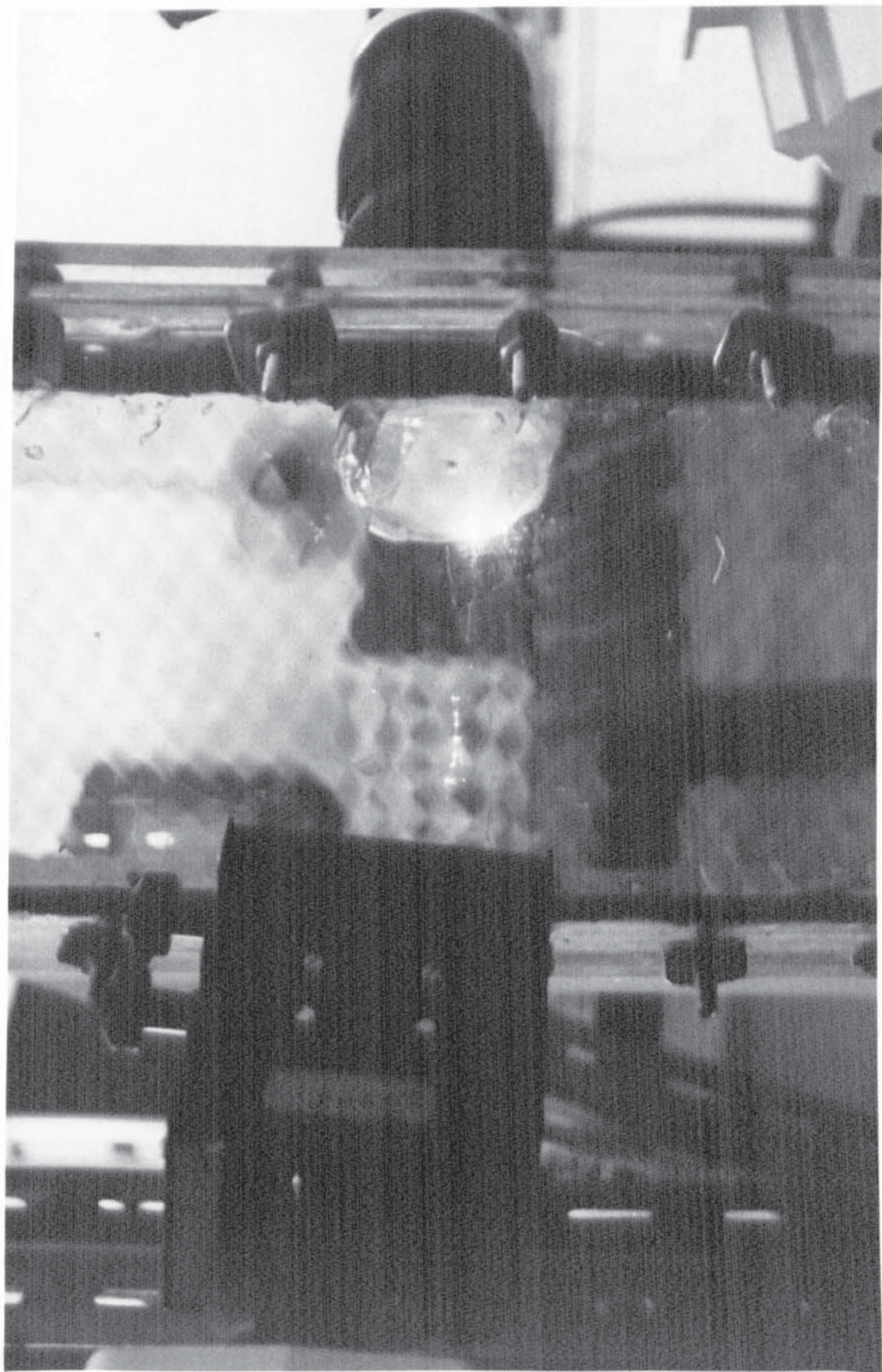


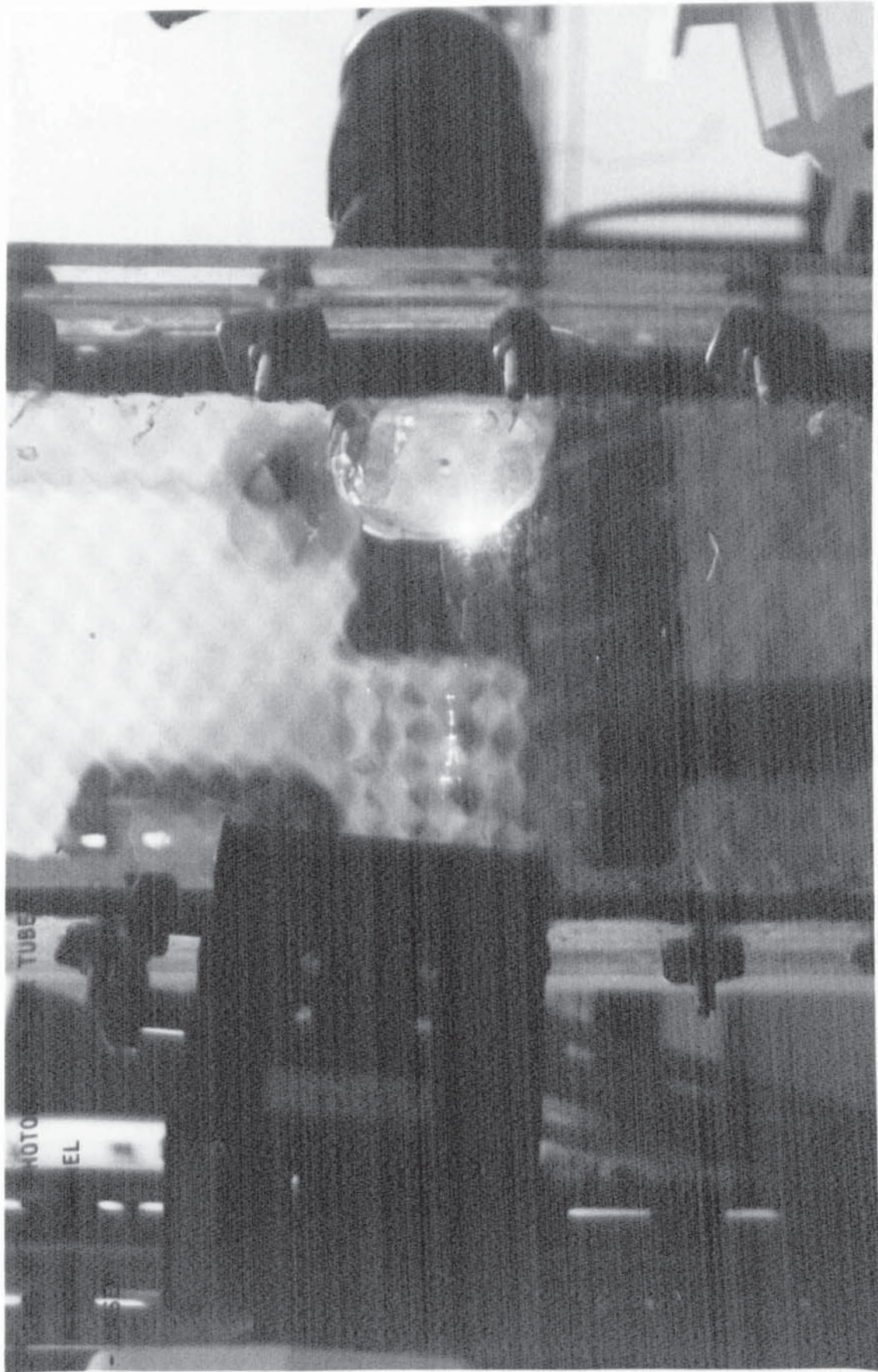
- 1 -
- 2 -
- 3 -
- 4 -
- 5 -

PLATE 4.8 - SIGNAL PROCESSING AND OUTPUT UNITS

- 1 - LENS OF THE PHOTOMULTIPLIER TUBE
- 2 - PERSPEX CHANNEL
- 3 - LASER

PLATE 4.9 - LASER BEAMS PASSING THROUGH THE CHANNEL





- 1
- 2
- 3 - ...

PLATE 4.9 - LASER BEAMS PASSING THROUGH THE CHANNEL

lined in Section 4.2.5.

The flow was not seeded since another analysis showed that there were sufficient scattering particles in the flow. Fringe spacing was measured as outlined in the earlier section 4.3.4.

Measurements were carried out for the Up-flow in vertical component because rotating the beam splitter showed that most of the flow was in an upward direction. Measurements were made in the three regions as outlined previously.

A series of experiments was carried out for Up-flow with different orientations of the beam splitter to identify local directions of the measured velocities.

Measurements were also carried out to examine the variation of velocity within individual cells, by moving the point of intersection of the laser beams across the cells. Results are given in Chapter 5 and discussed in Chapter 6.

4.4 DEVELOPMENT OF EXPERIMENTAL TECHNIQUE

4.4.1 INTRODUCTION

Several difficulties arose in applying Laser Anemometry in the present study. Those problems are discussed briefly with the development of the

technique, since commencement of the current research work. Some of the difficulties have already been discussed in section 4.3, but the following problems appear to be extremely trivial but took a great deal of time and effort to be solved. To prevent subsequent workers suffering the same difficulties, they are reported here. Although several references (11,13,20,21) also discuss these problems to some extent, they are reported here from the practical standpoint as they are encountered.

The current work followed the previous study (122), in which the author established the technique of LDA in a circular perspex tube and made preliminary attempts to investigate hydrodynamic characteristics in a perspex model of a three-dimensional Junior research size Plate-Heat Exchanger Channel.

The perspex tube was polished with perspex polish both inside and outside of the tube until the surface was very clear and smooth, thus allowing beams to pass through the thin walls of the tube without significant flare. No scattering particles were necessary because there were sufficient scattering centres in the tap water used as the working fluid. All the measurements were carried out in the forward scatter arrangement. There was no requirement of refractive index matched liquid since the walls were very thin, hence no significant refraction. There were few difficulties encountered, sensible results were obtained and much valuable practice in the basic

procedure of using LDA equipment.

4.4.2 SURFACE CONDITIONS

In the Junior perspex channel, flow was controlled from a constant head tank using water as the working fluid. The laser beams suffered refraction and reflection from all four surfaces, so that the photomultiplier became saturated and measurements could not be made. There was significant light diffusion at all four solid/fluid surfaces, scattering light in all directions. The amount of scattered light was greatly reduced after the lengthy procedure of polishing the surface using perspex polish. The polished surfaces did not reduce the flare sufficiently to enable measurements to be made but clearly showed there was internal scatter in the walls of the plate, presumably caused by changes in the perspex structure during ageing.

It also showed that smooth, well polished surfaces of the flow system was an extremely essential condition for measurements. This led to regular polishing of the SR1 plate channel, after every few weeks. It was found that wherever beam quality deteriorated in the channel, it was the appropriate time to clean and polish the plates. This deterioration could be seen visually by looking through the reflex viewer in the photomultiplier assembly. It was found that the

deterioration was largely due to particle settling on the surface of the channel.

4.4.3 SCATTERING PARTICLES

One of the most serious problems in the present study was the identification of particle size and type suitable to act as light scattering centres. It is helpful to inspect samples from the recycling vessel for particle size and concentration. It is considered good practice to ensure that particle size is smaller than the fringe spacing to obtain good signals. If many particles are larger than the fringe spacing then the fluid should be filtered, or the fringe spacing should be increased to accommodate particle size. In this work there was a good agreement in the particle size and the fringe spacing. Excessively large particles do give inaccurate measurements, and the impact of an occasional agglomerate or air bubble on the correlation curve was obvious on the oscilloscope display.

Following the various experiments using different particles described in section 4.3.2, it was concluded that suitable particles from the room exist in tap water and the oil mixture, either as atmospheric dust or as an integral component of the oils. Moving particles can be seen passing through the beam intersection region as little flashes of light in the reflex

viewer of photomultiplier. Such flashes are more apparent in the oil mixture than in water. It is helpful regularly to stir the oil mixture in the recycling vessel to provide uniformly distributed particles, rather than allow particles settling at the bottom of the recycling vessel.

4.4.4 ALIGNMENT AND SIGNAL PROCESSING

Although the standard procedure of alignment has been outlined in section 4.2.5, it will be repeated here in more detail, since it is the most important factor determining whether or not a velocity measurement could be made.

The qualitative appearance of correlation curve displayed on the oscilloscope was totally dependent on the accuracy of alignment. One of the continual problems was to ensure that the beams were crossing at the chosen point, so the procedure outlined in the operating manual (124) was initially followed rigorously. However, this was found to be unsatisfactory and it was decided that a more direct visual method would be developed. One of the beams was focussed on the pinhole as observed through the eyepiece of the photomultiplier assembly. The other beam was adjusted until it was also focussed on the pinhole, at which point the photomultiplier would be aligned on the cross-over point. This was also checked by using the reflex

eyepiece. This procedure was sometimes reversed by using the eyepiece first followed by viewing through the direct eyepiece.

Forward scatter was found to be a better arrangement when water was the working fluid even though flare was higher compared to the back scatter mode. The reduced flare was accompanied by a significant decrease in signal quality. When oil mixture was used, all the flare was removed and signal quality was found to be five times better in forward scatter compared to back scatter.

Sometimes, when the beams had been correctly aligned, a poor correlation curve of the type shown in Figure 4.7 was obtained. The operating manual suggests that such curves are caused by there being too few fringes in the intersection volume. One obvious method would be to adjust the fringe spacing and hence the number of fringes by moving the beams slightly. Alternatively, the photomultiplier may not be perfectly aligned on the cross-over point and it was found that a diminutive adjustment of the fine position controls of the photomultiplier tube would produce a better correlation curve.

In the optical forward arrangement, the PM tube always produced a better signal if it was placed 15-20° from the central optical axis.

Minor vibrations were a constant problem in affecting alignment, and therefore the value of the measured velocity. So, once the equipment was set up physical contact was kept to minimum.

CHAPTER 5

RESULTS

5. RESULTS

5.1 JUNIOR PARAFLOW SINGLE CELL

The results acquired for flow through a single cell of the Junior PHE's perspex channel using water, will be outlined for different experimental conditions. Experiments which showed any procedural errors were excluded as were those whose mass balance could not be obtained due to experimental errors.

5.1.1 SINGLE INPUT FLOWS

Table 5.1 shows the flow through tube "A" (see Figure 4.2) inlet only for different time intervals and the ratio of the outlet flows.

Similarly, Table 5.2 shows the results of flow through tube "B" inlet only.

5.1.2 SIMULTANEOUS INLETS AT SAME INITIAL PRESSURE

Table 5.3 shows the results of flow through a single cell, with the same initial levels of water in both tubes, together with the volume balance since the density is constant.

If the calculated flow through tubes is Q_T and Δh_A and Δh_B are the height changes in each tube of equal diameter.

TABLE 5.1 FLOW THROUGH TUBE "A" ONLY

Run No.	Volume Collected From Tube "A" Outlet (Cm ³)	Volume Collected From Tube "B" Outlet (Cm ³)	Time (S)	Ratio of outlet Volume, $\frac{\text{Tube "B" Volume}}{\text{Tube "A"}}$
1	10	40	4	4
2	5	37	3	7.4
3	7	40	3.8	5.71
4	7.5	42	4.5	5.6
5	12	46	4.2	3.83
6	9	36	3	4

TABLE 5.2 FLOW THROUGH TUBE "B" ONLY

Run No.	Volume Collected from Tube "A" Outlet (Cm ³)	Volume Collected From Tube "B" Outlet (Cm ³)	Time (S)	Ratio of outlet Volumes, $\frac{\text{Tube "B" Volume}}{\text{Tube "A"}}$
1	22	23.5	3	1.07
2	25	38	6	1.52
3	22	24	2	1.09
4	21	31	2	1.48
5	52	46	10	0.89
6	20.5	21.5	2	1.05

TABLE 5.3 FLOW THROUGH BOTH TUBES AT SAME INITIAL PRESSURE

Initial Inlet Levels (Cm ³)		Calculated Flow input From Tube "A" Q_{CA} (Cm ³)	Calculated Flow input from Tube "B" Q_{CB} (Cm ³)	Total flow calculated input for both Tubes Q_T (Cm ³)	Flow Measured at outlets		Total Flow Measured Q_M (Cm ³)
A	B				Q_{MA} (Cm ³)	Q_{MB} (Cm ³)	
93.25	93.25	6.95	14.07	21.02	5	16.5	21.5
70	70	17.19	30.22	47.41	22	26	48
71.9	71.9	8.05	30.21	38.26	18.5	21	39.5

TABLE 5.4 FLOW THROUGH BOTH TUBES AT DIFFERENT INITIAL INLET PRESSURES

Initial inlet levels (Cm)		Calculated Flow input From Tube "A" Q_{CA} (Cm ³)	Calculated Flow input From Tube "B" Q_{CB} (Cm ³)	Total flow calculated input for both Tubes (Cm ³) Q_T	Flow Measured at outlets		Total Flow Measured Q_M (Cm ³)
A	B				Q_{MA} (Cm ³)	Q_{MB} (Cm ³)	
45.7	50	15.25	17.48	32.73	13	21	34
55.2	58.3	4.28	19.48	23.76	10	11	22
83.6	72.5	17.91	30.36	48.27	19	25	44

$$\begin{aligned} \text{Then } Q_T &= (\Delta h_A + \Delta h_B) * A_t & (5.1) \\ &= Q_{CA} + Q_{CB} \end{aligned}$$

where A_t = Area of tube (Cm²)

Q_{CA} & Q_{CB} = Calculated flow input from tubes
"A" and "B" (Cm³)

Q_T = Total flow calculated input for both tubes (Cm³)

A_t was calculated to 0.7126 Cm²

No time interval was recorded, due to difficulties in the experimental procedure of operating valves and recording times. Therefore, volumes are quoted and these can be used effectively in place of mass balance since the density is constant.

5.1.3 VARIATION IN INLET PRESSURE

Table 5.4 shows the results of flow, with tubes, at different height levels of water, through the single cell.

In two of these results, tube "B" was at higher levels of water than tube "A", and in the other tube "A" was at higher level than tube "B".

5.1.4 DOUBLE INITIAL PRESSURE IN ONE INLET

The initial height level in one tube was twice that in the other tube. Because of experimental difficulties in that the tubes emptied very quickly, only a few measurements were successful and these are reported in Table 5.5.

In both runs, tube "A" contained higher water level, other runs where tube "B" had the higher water levels did not satisfy the mass balance were rejected.

TABLE 5.5 FLOW AFTER DOUBLING ONE INLET PRESSURE

Initial Inlet Levels (Cm)		Calculated Flow input from Tube "A" Q_{CA} (Cm ³)	Calculated Flow input from Tube "B" Q_{CB} (Cm ³)	Total Flow Calculated input for both Tubes Q_T (Cm ³)	Flow Measured at outlets		Total Flow Measured Q_M (Cm ³)
					Q_{MA} (Cm ³)	Q_{MB} (Cm ³)	
A	B						
60	30	15.18	12.32	27.5	11	14	25
50	25	10.97	12.97	23.94	12	10.5	22.5

5.1.5 NEW FLOW INTO ESTABLISHED FLOW

Table 5.6 shows the measurements of flow through a single cell when tube "B" was opened first to establish the flow and then tube "A" was opened after a short interval.

Table 5.7 shows the measurements of flow through a single cell when the procedure was reversed, with tube "A" being opened first. Only one run was successful, other runs were rejected because of disagreement in the mass balance.

TABLE 5.6 FLOW THROUGH TUBES WHERE TUBE "B" OPENED FIRST AND THEN TUBE "A"

Initial Inlet Levels (Cm)		Calculated Flow input from Tube "A" Q_{CA} (Cm ³)	Calculated Flow input from Tube "B" Q_{CB} (Cm ³)	Total Flow Calculated inputs for both tubes Q_T (Cm ³)	Flow measured at outlet		Total Flow Measured Q_M (Cm ³)
A	B				Q_{MA} (Cm ³)	Q_{MB} (Cm ³)	
77.5	99.5	15.25	51.64	74.89	48.5	25	73.5
52	139.5	18.88	62.57	81.45	51	30.5	81.5
26.6	48.3	9.69	24.44	34.13	21.5	14	35.5

TABLE 5.7 FLOW THROUGH TUBES WHERE TUBE "A" OPENED FIRST AND THEN TUBE "B"

Initial Inlet Levels (Cm)		Calculated Flow input from Tube "A" Q_{CA} (Cm ³)	Calculated Flow input from Tube "B" Q_{CB} (Cm ³)	Total Flow Calculated inputs for both tubes Q_T (Cm ³)	Flow measured at outlet		Total Flow Measured Q_M (Cm ³)
A	B				Q_{MA} (Cm ³)	Q_{MB} (Cm ³)	
33	41.5	5.34	11.76	17.10	10	7	17

5.2 VELOCITY MEASUREMENTS IN THE SR1 PERSPEX CHANNEL

Reynolds number was calculated using the standard dimensionless group given in Appendix A-3.0 and repeated here:

$$U = \frac{\text{Volumetric Flow Rate}}{\text{Area of Flow}} = \frac{Q}{b'W}$$

$$b' = D_e (\phi/2)$$

$$Re = \frac{\rho D_e U}{\mu}$$

where U = Average velocity of flow (m/s)

Q = Volumetric flow rate (m³/s)

b' = Mean plate gap (m)

W = Plate width available for flow (m)

Re = Reynolds number

ρ = Density of fluid (Kg/m³)

D_e = Equivalent diameter (m)

μ = Viscosity of fluid (kg/ms)

ϕ = Ratio of developed to projected area

Standard parameters provided by the manufacturers were used to calculate the Reynolds number and average velocity of flow. Some of these parameters are summarized in Table 5.8 with general information of the SR1 plate.

TABLE 5.8 PARAMETERS OF THE SRL PLATE

Parameters	Value
Developed/projected area	1.22
Plate flow width	0.171m
Equivalent diameter	$4.7498 \times 10^{-3} \text{m}$
Plate Pitch	$3.505 \times 10^{-3} \text{m}$
Plate thickness	$0.6096 \times 10^{-3} \text{m}$
Plate heat transfer area	0.08556 m ²
Developed mean plate Length	0.4975 m

The measurements which will be reported in following sections apply to oil as the working fluid, for different flow rates and operating conditions. Although the author did obtain some velocity measurements using water instead of oil, it was judged prudent not to include these as conclusive results, since they lacked repeatability owing to the severe experimental problems already outlined in section 4.3.2. The total number of individual measurements observed in the present research work is around 25000 using oil as the working fluid. In addition, some further 150000 attempts were made using water as the working fluid, but very few of these were successful.

5.1.2 LOW FLOW RATES

The velocity measurements were made for flow rates varying between Re of 0.0817 and 0.1616 using oil as the operating fluid. It was found difficult to present these results in any standard graphical method which would clearly indicate the velocity at a particular position in the channel without causing serious confusion. Therefore it was decided to propose a new method for clearly presenting these results.

The appropriate method based on the reproduction of the projected cell matrix of the channel onto two dimensional co-ordinates. Velocity values could then be printed at the appropriate position representing where the measurement was made.

A computer program was prepared (133) in collaboration with a postgraduate student following an M.Sc. course in which a computer project was an integral part. The program would reproduce the structure of the channel, that is peak to peak contact and the ridges of the corrugations similar to Figure 4.14. The program was written in Fortran 77 high level programming language on the HARRIS H500 computer facility available at the University of Aston. To display the structure of the channel, access was made to the software facility GINO, the graphical system available on the HARRIS computer.

This graphical display of the channel accommodated the most convenient method of showing the velocity measurements at appropriate locations. Therefore for each parameter in the graphical display a velocity measurement can be identified, providing immediate access to flow distribution in the channel.

During velocity measurements fringe spacing varied for different cell positions, but was always maintained to be greater than $10\mu\text{m}$ since most particles were of this size. Measurements were carried out in Up-flow and Down-flow in three zones of the channel; inlet, middle and outlet:

- (i) Inlet region - near where flow enters the channel
- (ii) Middle region - where velocity profile may be fully developed in the channel
- (iii) Outlet region - flow is collected and leaves the channel.

Although a turbulence level was also calculated for each velocity measurement by the "Malvern Program", this is not fully reported since it may only represent unstable flow at that point. Unstable flow may cause variations at a point arising from minor variations in flow at that point. It may not be of major significance and is therefore commented only in qualitative terms.

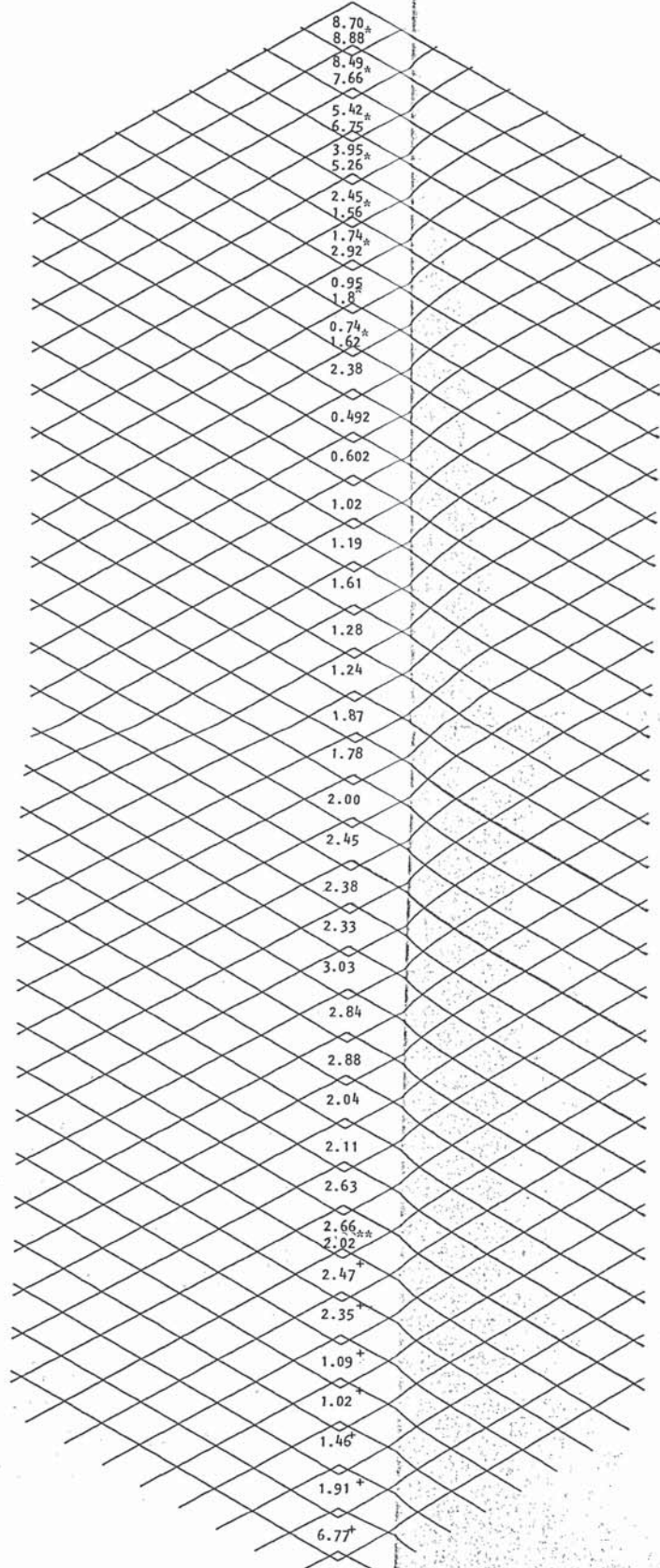
A preliminary set of measurements were made in the centreline of the channel to establish the technique. Figure 5.1 shows measurements in the Up-Flow direction for horizontal velocity component, at a Reynolds number of 0.1616 and average velocity of 0.3254×10^{-2} m/s. Each velocity measurement is an arithmetic average of thirty to fifty velocity observations. This average was needed because small fluctuations were observed in the rotameter float positions during the experiments. In some cells at the top section of the channel two measurements were made in each cell. One measurement is in the middle of the cell volume, while the other measurement is near the wall.

Part way through the sequence of experimental work, it was realised that the temperature was affecting measurements significantly, so the temperatures are also reported.

Turbulence ranges varied for each measurement in the cell. At the inlet region bottom section of Figure 5.1, in the same cell there was 0% turbulence and in the remaining cells turbulence range varied 7-13%.

This pattern was repeated until part way along the channel, that is until velocity at 3.03×10^{-2} m/s.

FIGURE 5.1



Velocity component measured - ← or →
 Point velocity - value shown X 10⁻² m/s
 Direction of overall flow - up flow
 Channel Reynolds number - 0.161
 Channel average velocity - 0.325 X 10⁻² m/s
 Channel oil temperature - 22° C

Note: + oil temperature: 20° C
 * measurements at the wall
 ** oil temperature: 16° C

FIGURE 5.1 - POINT VELOCITY MEASUREMENTS

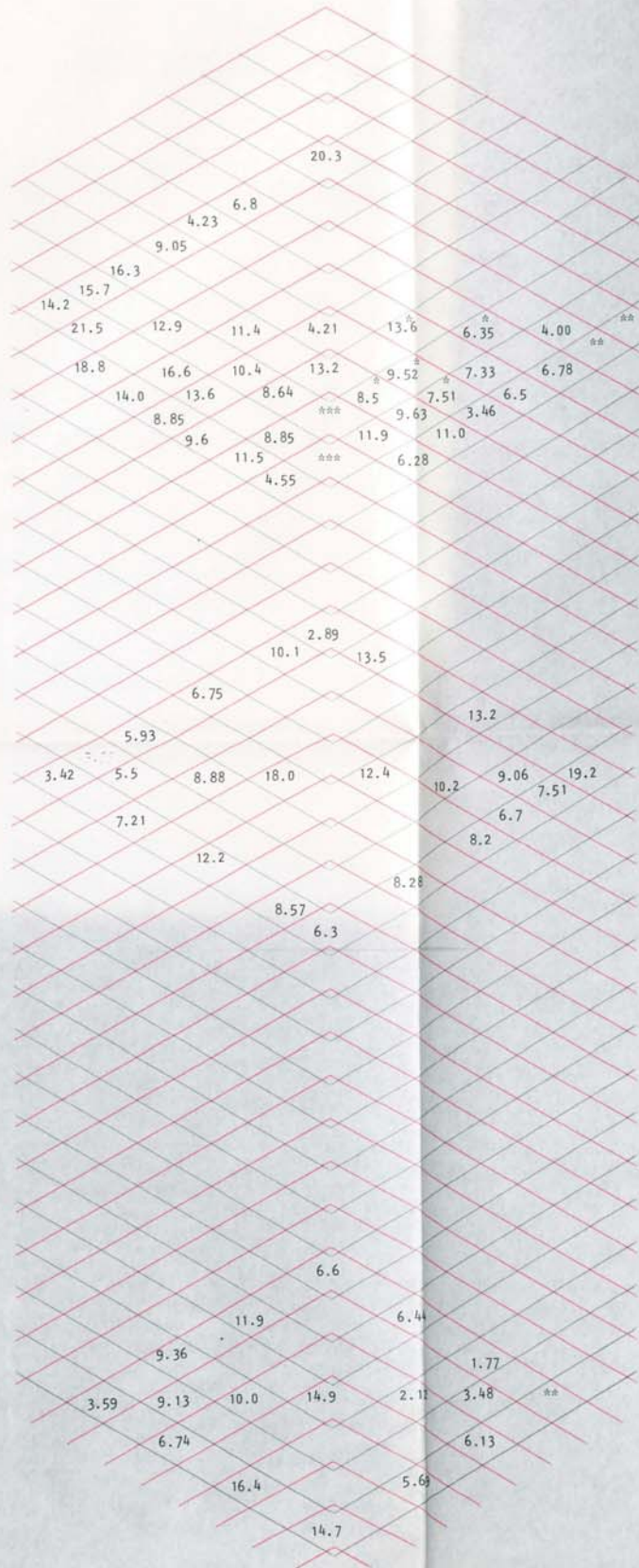
Then minimum turbulence was found to be in the range of 5-8% and a maximum of 18-21%.

Turbulence at the outlet region with two measurements in a cell showed changes. Turbulence at the centres of a cell volume was 0% but at the walls varied in the range 17-27%.

Figures 5.2 to 5.5 show the measurements in the three main sections for Reynolds numbers ranging from 0.0817 to 0.1616, in the Up-Flow direction. In each section various cells were selected as shown in the figures to form a view as to how the flow was behaving in the channel. In certain positions, especially near the ends of the channel there is no continuity of the selected pattern. The reason for this omission was the excessive flare from poor surfaces in some areas. Due to lack of time available and the long sample time needed for these measurements, the number of observations recorded were reduced. Each velocity measurement shown is an average of a minimum of five observations, and each measurement observed was at least in agreement with one other velocity measurement. These measurements were made in the middle of the cell volume, unless stated otherwise.

In the inlet section of flow there was very low turbulence generally 0% but this increased near the gasket on either side, at the edges of the channels to between 0%-10.5% while in the middle section,

FIGURE 5.2

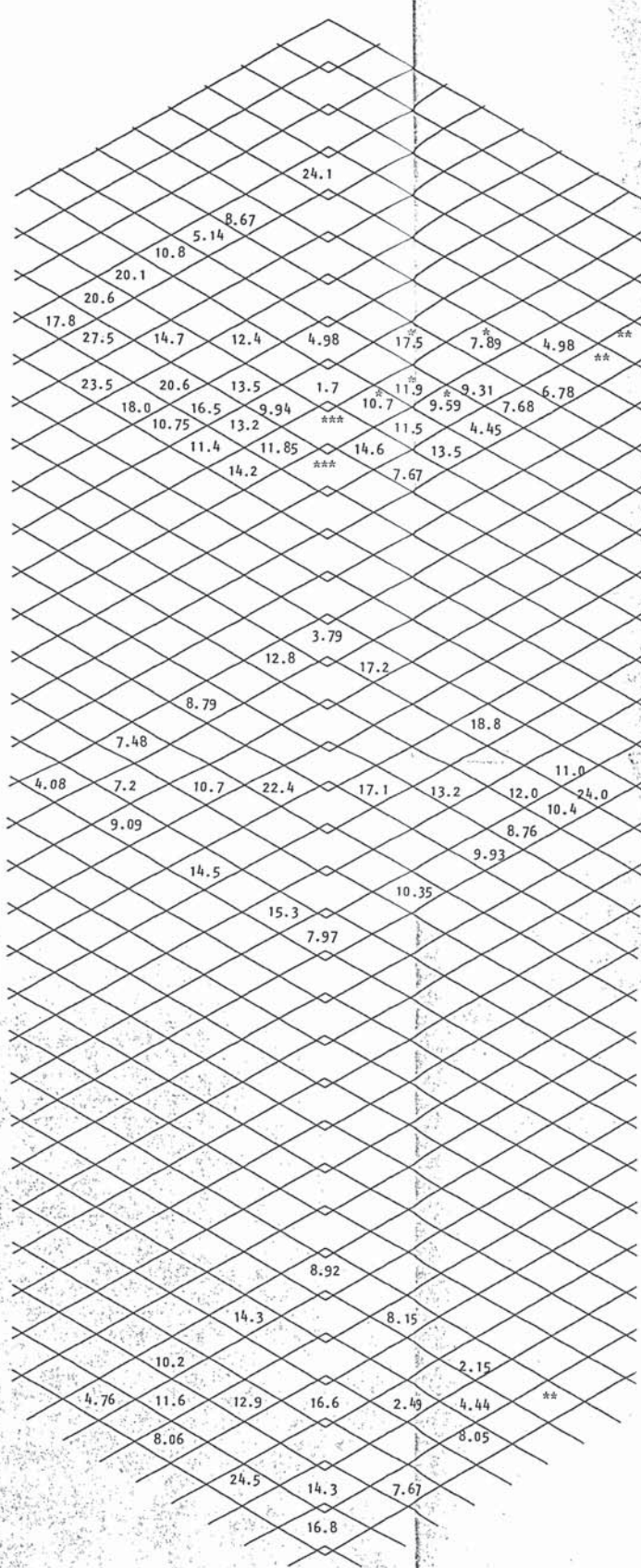


- Velocity component measured -
- Point velocity - value shown $\times 10^{-3}$ m/s
- Direction of overall flow - up flow
- Channel Reynolds number - 0.0817
- Channel average velocity - 1.6454×10^{-3} m/s
- Channel oil temperature - 22° C

Note: *measurements at the wall of channel
 ** no measurement because of excessive flare
 *** lack of flow in this component

FIGURE 5.2 - POINT VELOCITY MEASUREMENTS

FIGURE 5.3

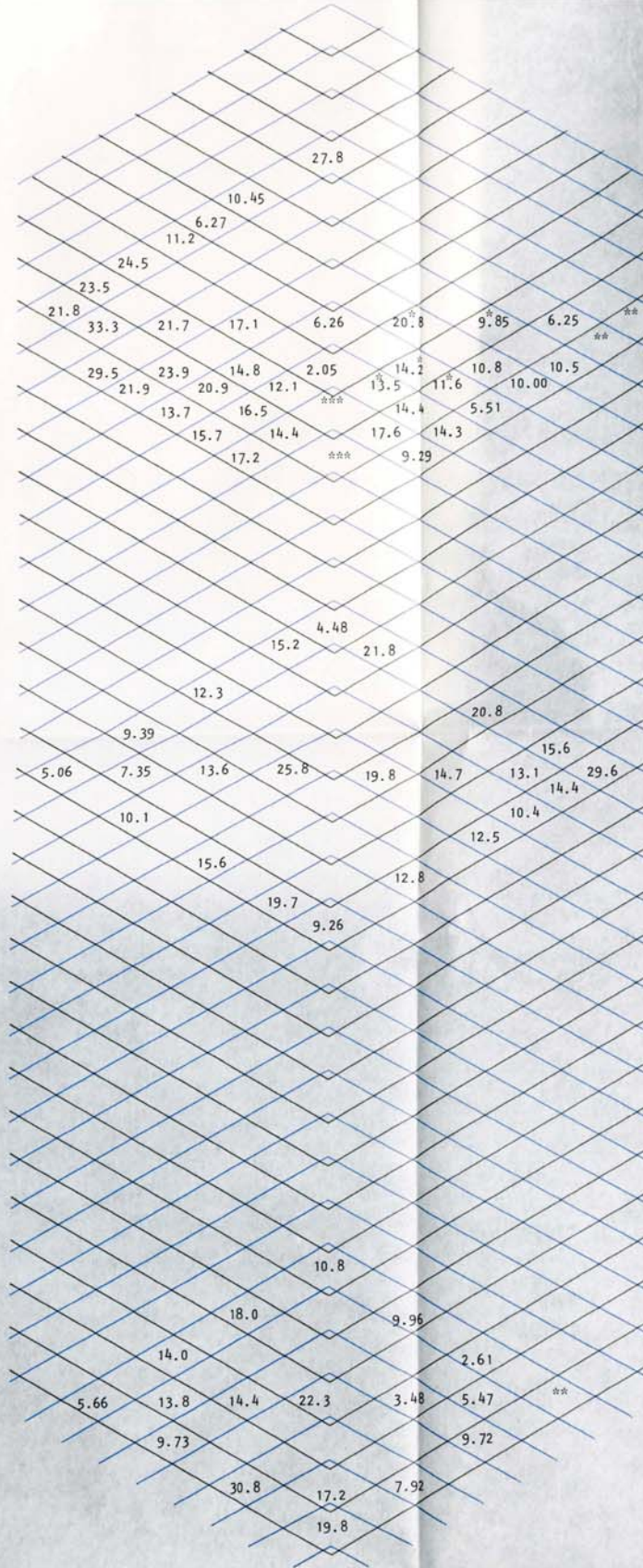


- Velocity component measured -
- Point velocity - value shown $\times 10^{-3}$ m/s
- Direction of overall flow - up flow
- Channel Reynolds number - 0.1028
- Channel average velocity - 2.07×10^{-3} m/s
- Channel oil temperature - 22° C

Note: *measurements at the wall of channel
 ** no measurement because of excessive flare
 *** lack of flow in this component

FIGURE 5.3 - POINT VELOCITY MEASUREMENTS

3

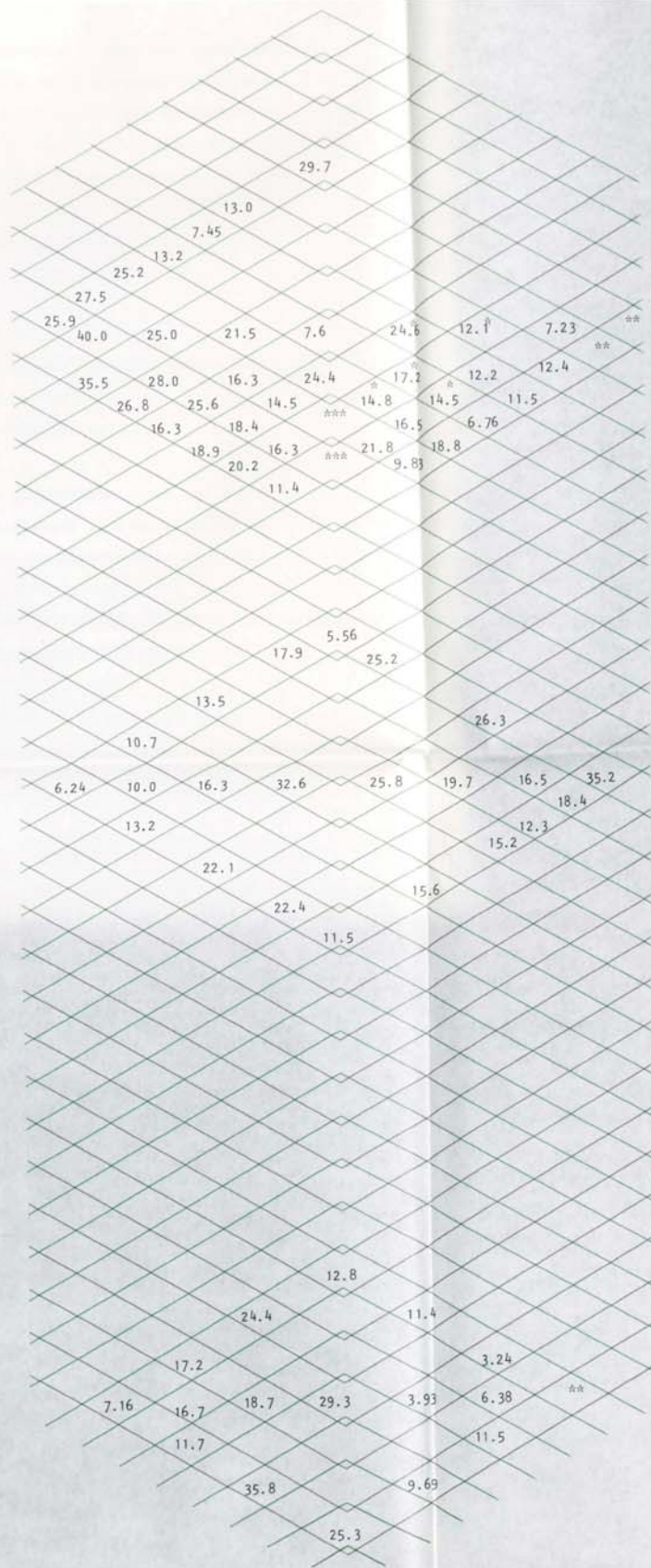


Note: *measurements at the wall of channel
 ** no measurement because of excessive flare
 *** lack of flow in this component

FIGURE 5.4 - POINT VELOCITY MEASUREMENTS

2

FIGURE 5.5



- Velocity component measured -
- Point velocity - value shown $\times 10^{-3}$ m/s
- Direction of overall flow - up flow
- Channel Reynolds number - 0.1616
- Channel average velocity - 3.254×10^{-3} m/s
- Channel oil temperature - 22° C

Note: *measurements at the wall of channel
 ** no measurement because of excessive flare
 *** lack of flow in this component

FIGURE 5.5 - POINT VELOCITY MEASUREMENTS

turbulence was even higher between 0%-12.5% at the edges of the channel and mostly 0% at the remaining points.

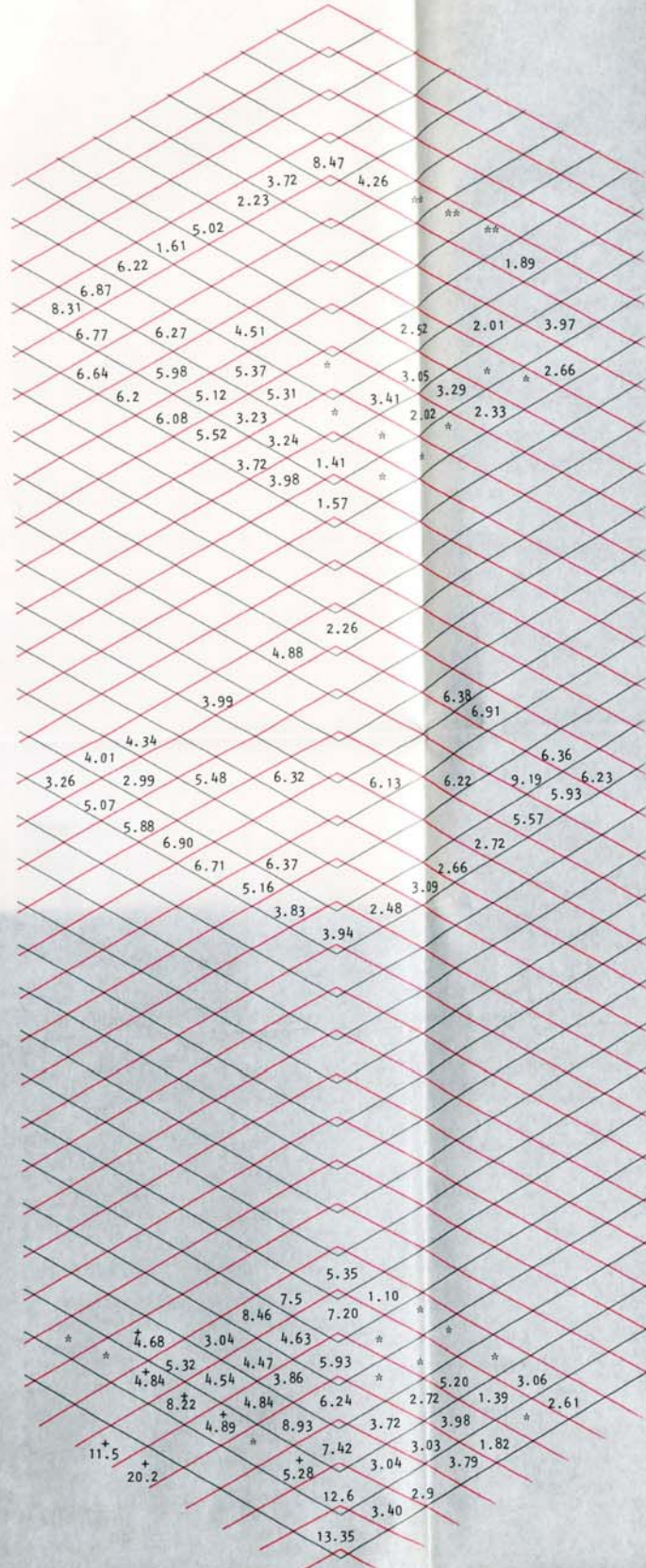
It was impossible to make any measurement in parts of the outlet section because no flow could be measured. Hence it was decided to examine this section in greater detail. In some cells, when it was difficult to make measurements in the centre of the cell volume, they were made wherever possible in the cell. The most suitable position in the cell was often found to be near the wall of the channel.

Turbulence in the outlet region was found greater near the gaskets in the range of 0-8% but mostly on the higher range side, but the turbulence in the rest of the section generally remained 0%.

During the experimental work, it was observed that there was variation in both velocity and turbulence from front to back on the centreline of a cell. This was not fully quantified but it was noted that the velocity varied by 40-100% of the centre point velocity, while the turbulence varied between 0 and 15%.

Figures 5.6 to 5.9 show velocity profiles in the channel in Down-Flow for Re , 0.0871 to 0.1616 using oil. In the three regions of inlet, middle and outlet, measurements were made in the pattern used previously. At some positions there were difficulties in making

FIGURE 5.6



- Velocity component measured -
- Point velocity - value shown $\times 10^{-3}$ m/s
- Direction of overall flow - down flow
- Channel Reynolds number - 0.0817
- Channel average velocity - 1.645×10^{-3} m/s
- Channel oil temperature - 22° C

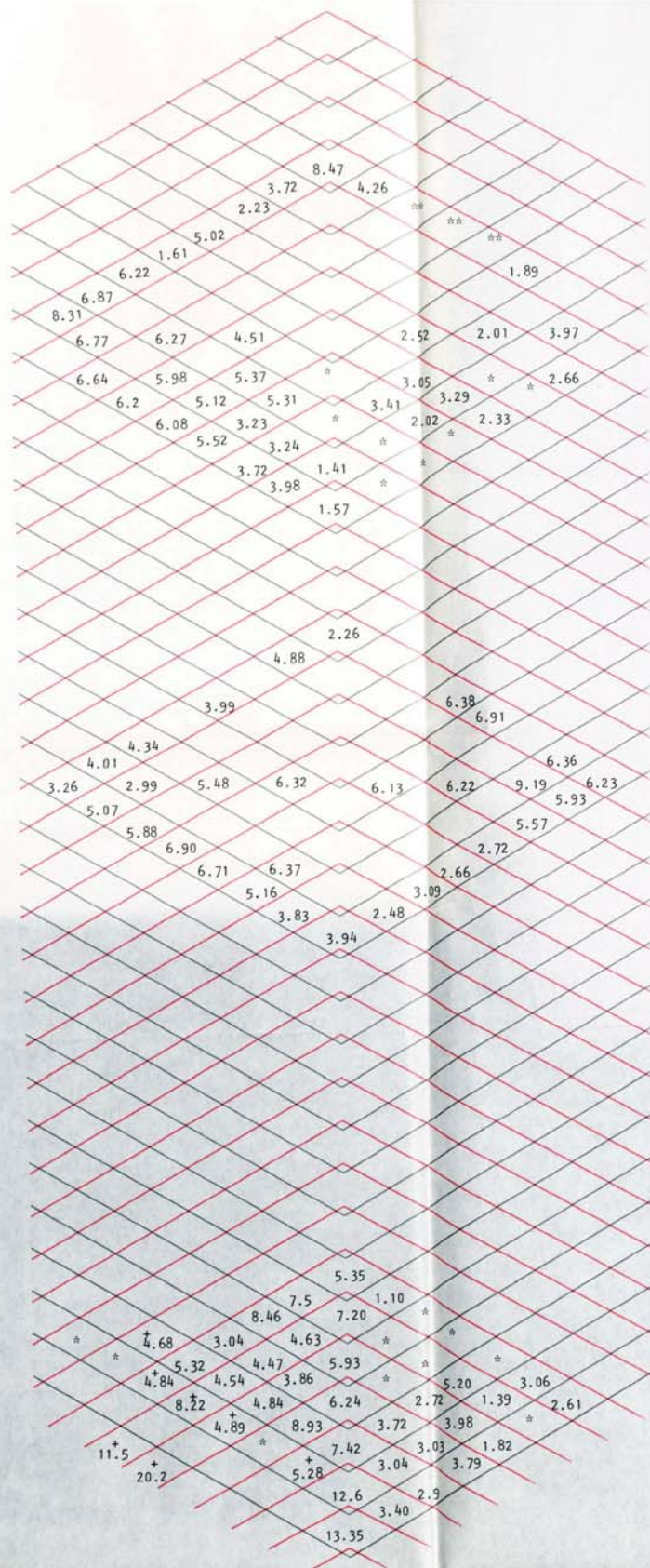
Note: * difficult to correlate, most flow in different direction
 ** difficult to correlate because of lack of flow
 + measurements near the wall of the channel

FIGURE 5.6 - POINT VELOCITY MEASUREMENTS

4



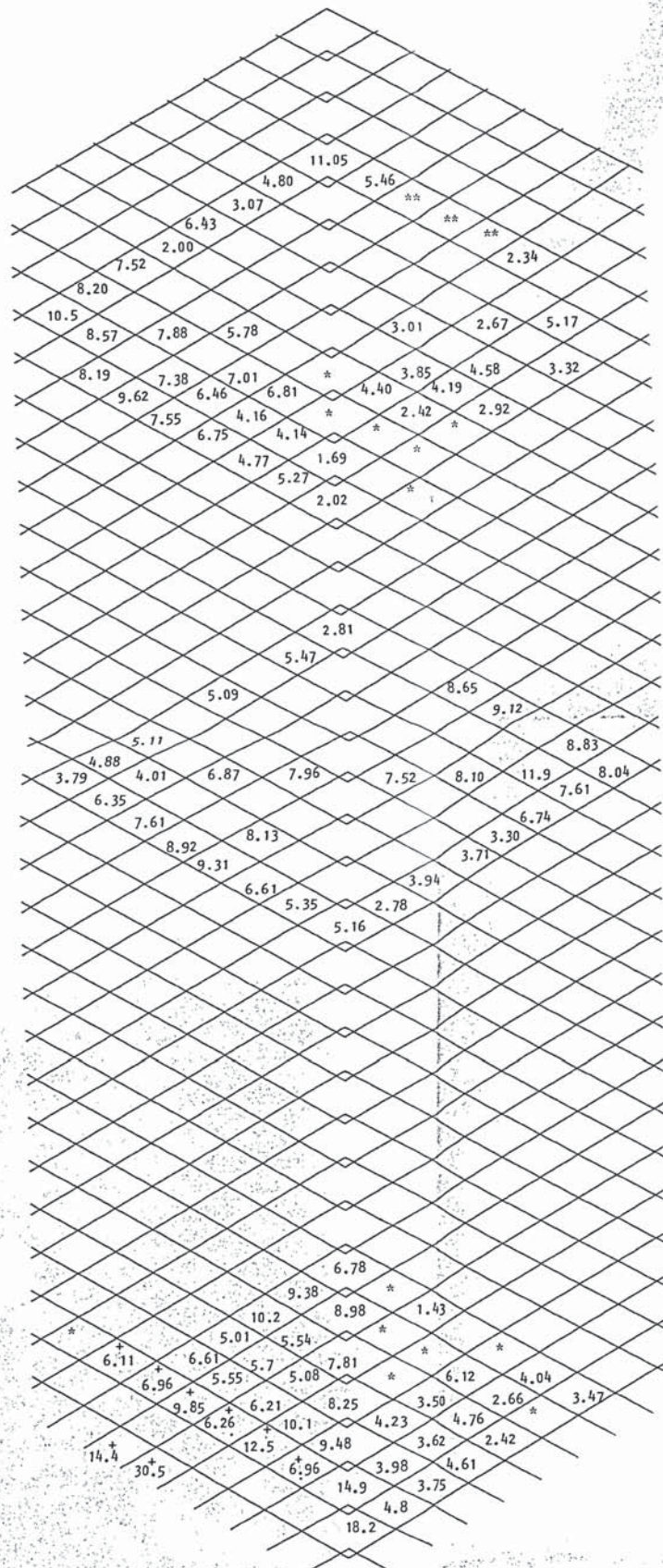
FIGURE 5.7



Velocity component measured - 60°
 Point velocity - value shows $\times 10^{-3}$ m/s
 Direction of overall flow - down flow
 Channel Reynolds number - 0.0817
 Channel average velocity - 1.645×10^{-3} m/s
 Channel oil temperature - 22° C

Note: * difficult to correlate, most flow in different direction
 ** difficult to correlate because of lack of flow
 + measurements near the wall of the channel

FIGURE 5.6 - POINT VELOCITY MEASUREMENTS



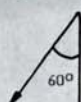
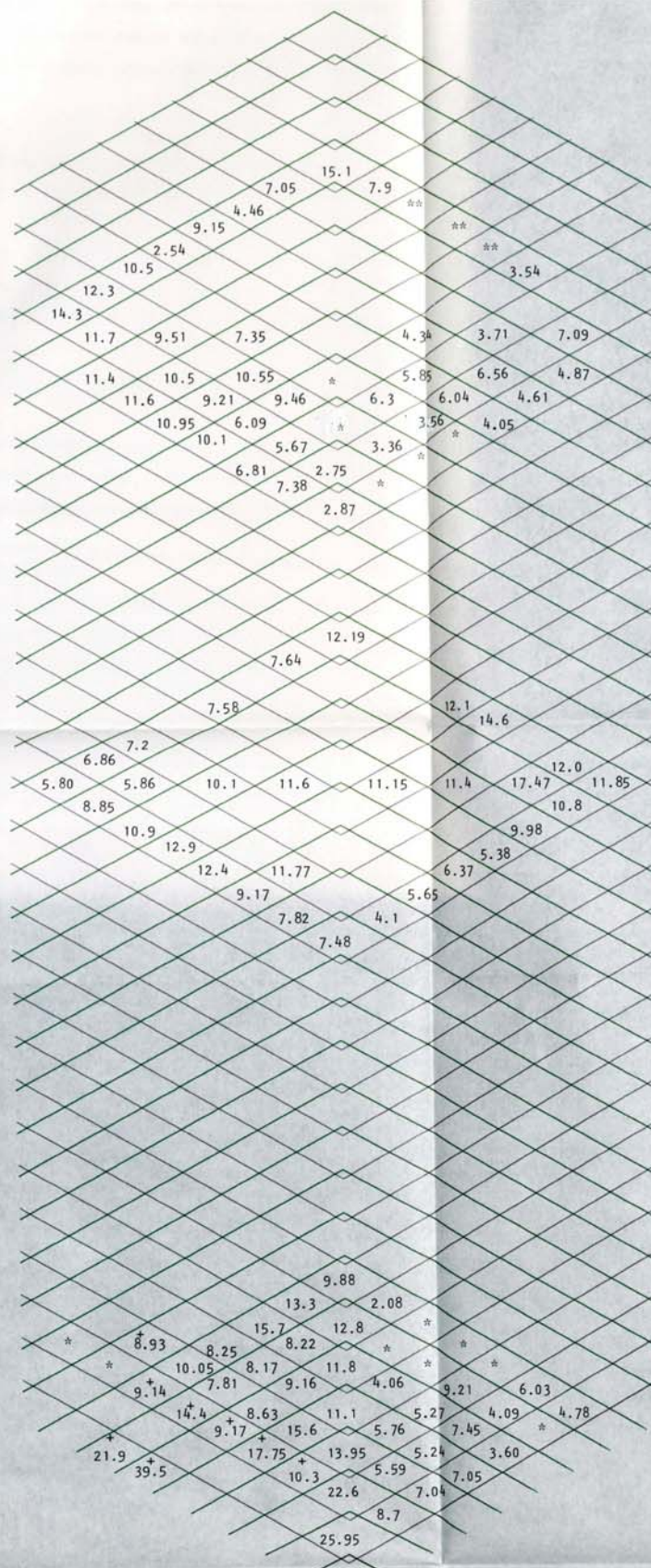
- Velocity component measured -
- Point velocity - value shown $\times 10^{-3}$ m/s
- Direction of overall flow - down flow
- Channel Reynolds number - 0.1028
- Channel average velocity - 2.07×10^{-3} m/s
- Channel oil temperature - 22° C

Note: * difficult to correlate, most flow in different direction
 ** difficult to correlate because of lack of flow
 + measurements near the wall of the channel

FIGURE 5.7 - POINT VELOCITY MEASUREMENTS

3

FIGURE 5.9



- Velocity component measured -
- Point velocity - value shown $\times 10^{-3}$ m/s
- Direction of overall flow - down flow
- Channel Reynolds number - 0.1616
- Channel average velocity - 3.254×10^{-3} m/s
- Channel oil temperature - 22° C

Note: * difficult to correlate, most flow in different direction
 ** difficult to correlate because of lack of flow
 + measurements near the wall of the channel

FIGURE 5.9 - POINT VELOCITY MEASUREMENTS

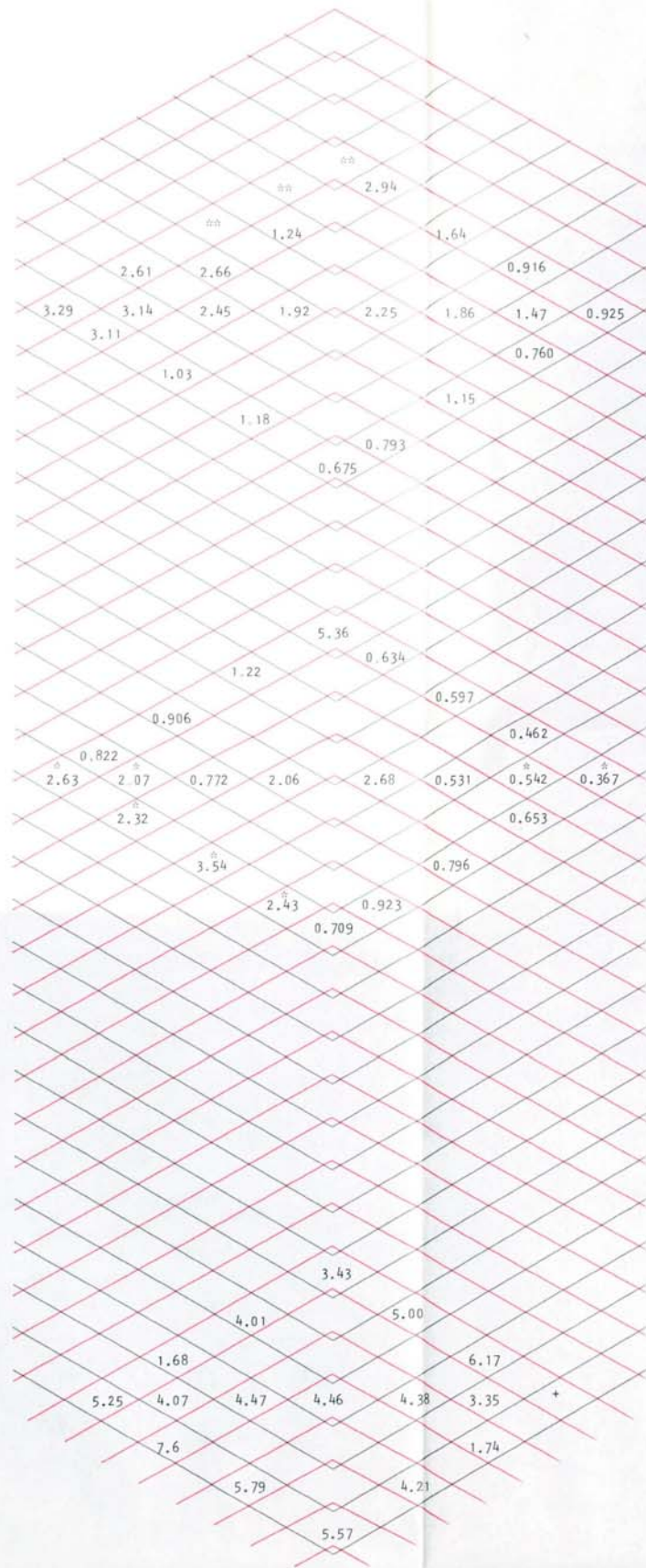
measurements and these are shown on the figures. Each velocity measurement shown is an average of a minimum of four observations, and at least one measurement was in agreement with one other velocity observation. The majority of the measurements were made in the centre of the cell volume unless stated in the velocity profile of the channel.

In the inlet region the overall turbulence was in the range 6-15%, but much higher at the edges of the channel in the range 10-22%, mostly in 18-22% range. Turbulence range on the righthand section of the channel was twice as high compared to the turbulence range on the lefthand side of the channel. In the middle region, the overall turbulence was in the range 8-15%, but much higher at the edges of the channel, in the range 15-23%.

In the outlet region, the overall turbulence in the channel varied from 6-22%, but a little higher at the edges of the channel in the range of 14-22%.

5.2.2 HIGH FLOW RATES

Figures 5.10 and 5.11 show velocity measurements for Reynolds numbers of 5.291 and 7.078 respectively for Up-Flow in the three main regions examined. The majority of measurements are made in the middle of the cell volume unless stated in the display of velocity profiles. Each velocity measurement is based on at least eight observations, and each measurement is in agreement with one other velocity measurement at the

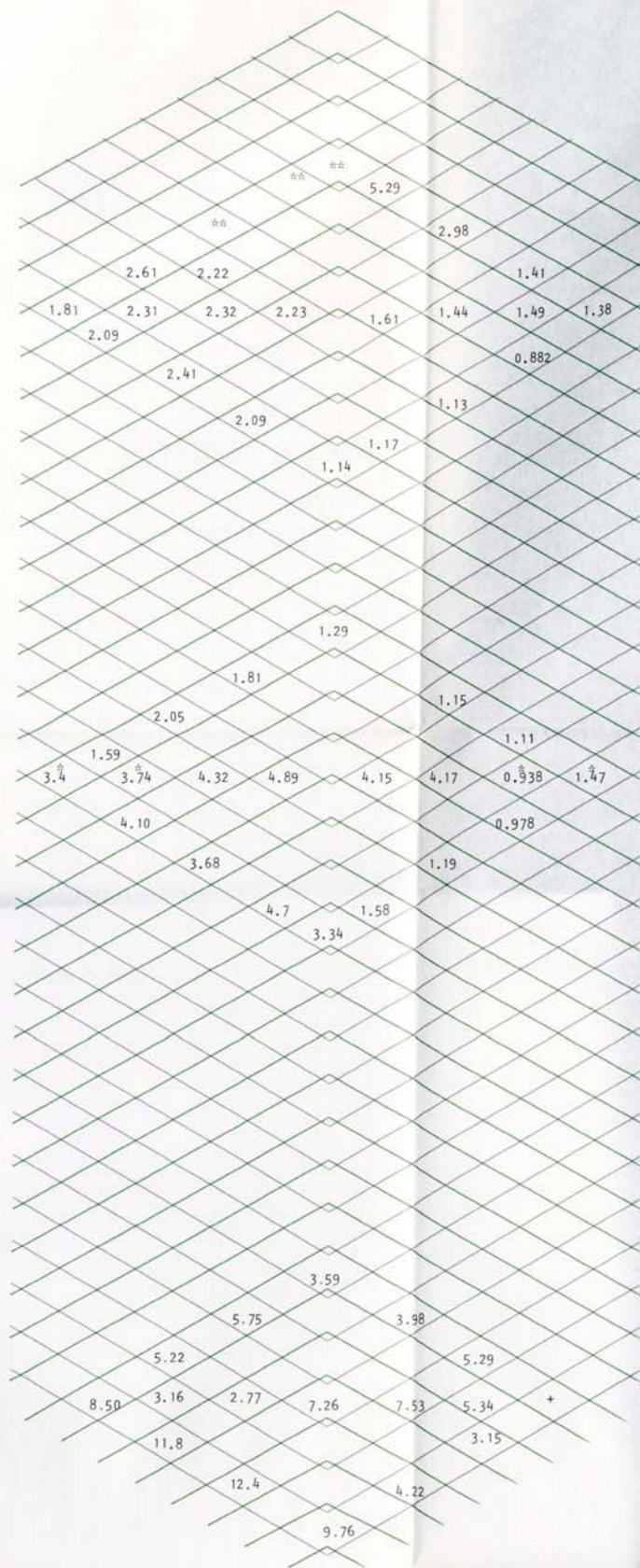


Velocity component measured - 
 Point velocity - value shown $\times 10^{-1}$ m/s
 Direction of overall flow - up flow
 Channel Reynolds number - 5.291
 Channel average velocity - 0.6772×10^{-1} m/s
 Channel oil temperature - 34° C

Note: * measurements near the wall of the channel
 ** outlet obstructed beam splitter
 + no measurement because of excessive flare

FIGURE 5.10 - POINT VELOCITY MEASUREMENTS

FIGURE 5.11



Velocity component measured - 
 Point velocity - value shown $\times 10^{-1}$ m/s
 Direction of overall flow - up flow
 Channel Reynolds number - 7.078
 Channel average velocity - 0.906×10^{-1} m/s
 Channel oil temperature - 34° C

Note: * measurements near the wall of the channel
 ** outlet obstructed beam splitter
 + no measurement because of excessive flare

FIGURE 5.11 - POINT VELOCITY MEASUREMENTS

same pattern.

Turbulence remained 0% for both flow rates across the channel but increased near the edge of the gasket, especially on the righthand side of the channel. Turbulence variation at these positions increased with the region, that is inlet region of 0%, middle region of 2-4% and in the outlet region 8-13%.

5.2.3 VELOCITY COMPONENTS

Figure 5.12 shows various velocity components in Up-Flow direction at a Reynolds number of 7.078. These measurements are made in each of the three sections, at a chosen position (as shown in Figure 5.12) and are made in the middle of the cell. Each measurement is an arithmetic average of ten velocity measurements.

Turbulence was 0% for nearly all the velocity components but varied for the component at 45° to the vertical. At the inlet, middle and outlet flow regime, turbulence varied in range of, 0-9.6%, 4-5% and 0-3% respectively.

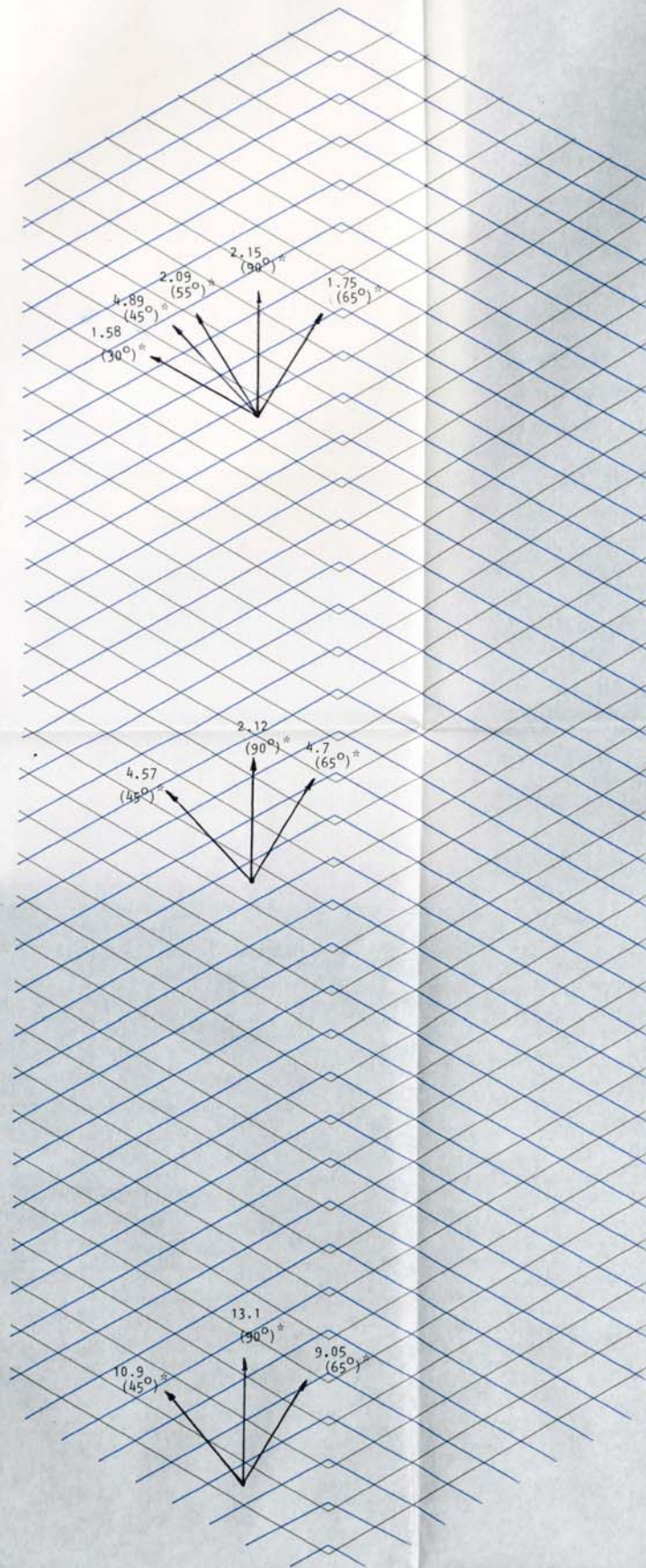
5.2.4 VARIATIONS ACROSS SELECTED SINGLE CELLS

Velocity measurements across selected single cells in the middle of the cell volume are shown in Figure 5.13, for Up-Flow at Reynolds number 7.078. In each measurement the vertical component was measured at three sections of the flow on both sides of the channel.

Each measurement was made in the middle of the cell volume and based on average of ten observations.

Turbulence was 0% for all the measurements in all the three sections of flow.

FIGURE 5.12

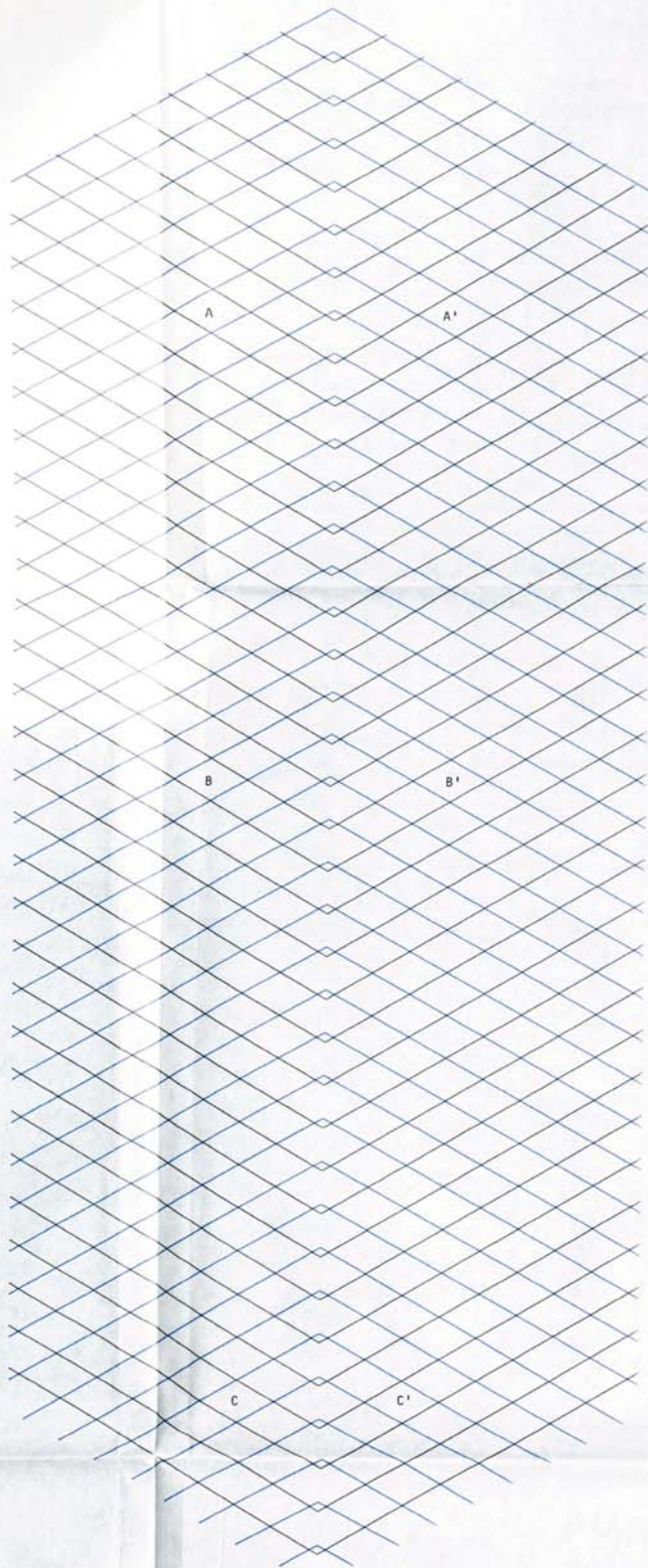
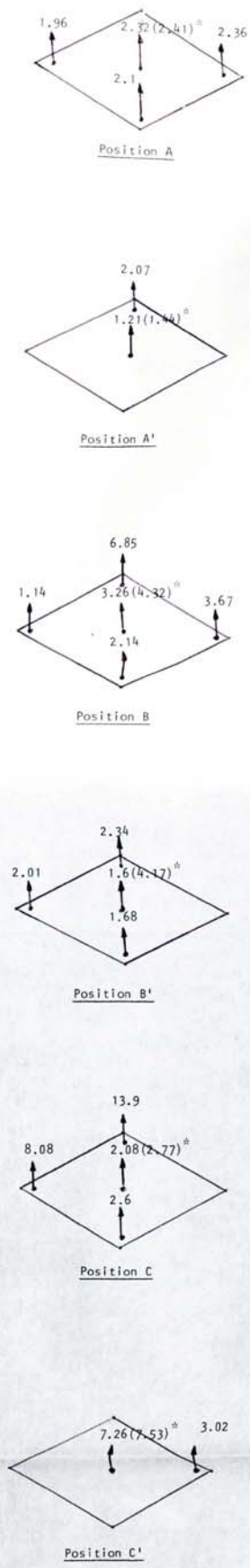


Point velocity	- value shown $\times 10^{-1}$ m/s
Direction of overall flow	- up flow
Channel Reynolds number	- 7.078
Channel average velocity	- 0.906×10^{-1} m/s
Channel oil temperature	- 34° C

Note: * the angle from the horizontal

FIGURE 5.12 - POINT VELOCITY MEASUREMENTS FOR SELECTED COMPONENTS

FIGURE 5.13



Velocity component measured \uparrow

Point velocity - value shown $\times 10^{-1}$ m/s

Direction of overall flow - up flow

Channel Reynolds number - 7.078

Channel average velocity - 0.906×10^{-1} m/s

Channel oil temperature - 34° C

Note: * value measured previously at that point
(see also Figure 5.11)

FIGURE 5.13 - POINT VELOCITY MEASUREMENTS
ACROSS SELECTED CELLS

CHAPTER 6

DISCUSSION ON FLOW DISTRIBUTION

6 DISCUSSION ON FLOW DISTRIBUTION

6.1 GENERAL

In this chapter, the analysis of results will be discussed, with some theoretical explanation in greater detail of the experimental problems encountered. Although some of these problems have already been mentioned in chapter four, their importance to the research project will now be treated in depth.

The discussion outlined is largely based on the present research work because no previous study has ever been reported on flow distribution in the junior PHE single cell or on velocity measurement at the micro-level. Hence no direct comparisons can be made with existing knowledge. General comparisons have been made with the qualitative study reported by Fattah (7) who used a dye injection technique in a Junior paraflow channel.

6.2 ANALYSIS OF JUNIOR PHE SECTION

6.2.1 FLOW SPLITTING AT CELL OUTLET

Tables 5.1 and 5.2 show the results of flow through single inlet tubes separately. Table 5.1 shows with flow in tube "A" the outlet ratios varied between 3.83 to 5.71 with a mean of 5.09, clearly showing that most of the flow, from tube "A" is collected at the opposite outlet. While Table 5.2 shows that for flow through tube "B" only, the outlet ratios varied between 0.89 to 1.52, with an average of 1.18, indicating an approx-

imately equal split of flow in the outlets. Therefore it is apparent that there is a difference of flow at the outlet dependent on which inlet tube is feeding the cell.

Ideally there should be an equal distribution of flow leaving the cell, with a ratio of flows at the outlets of 1. This is not the case for either of the inlets. Flow through tube "B" provides a better distribution than tube "A", hence indicating there is much greater resistance for flow from tube "A" to split equally compared to flow through tube "B". This greater resistance is generally reflected in other measurements shown in Tables 5.3 to 5.5 where flow at the outlet tube "B" was mostly higher than at outlet tube "A". In these measurements no initial Δ levels of tube were recorded because at that stage of experimental work it was not realised that height levels would affect flow distribution.

Values in Tables 5.3 to 5.5 are rearranged in the form of inlet and outlet measurements and split in flows in Figures 6.1 to 6.3. When considered in general terms they show that flow at inlet "A" appears at the outlet "B", while adding more flow from tube "B" inlet. This is the same distribution for tube "B" side showing the higher resistance for flow from side "A" to split up. Although Figure 6.3 shows that

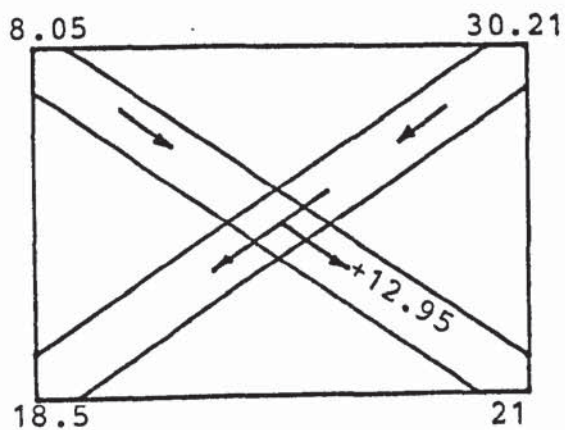
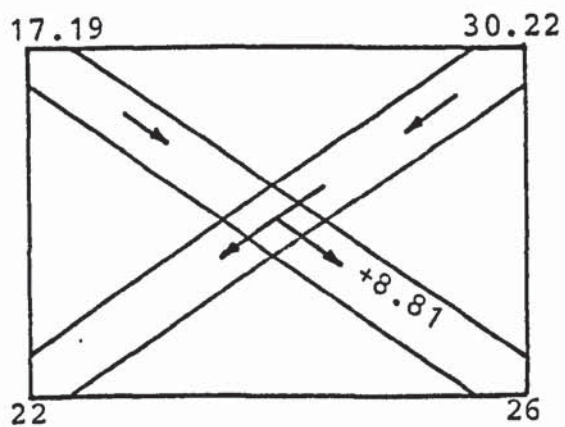
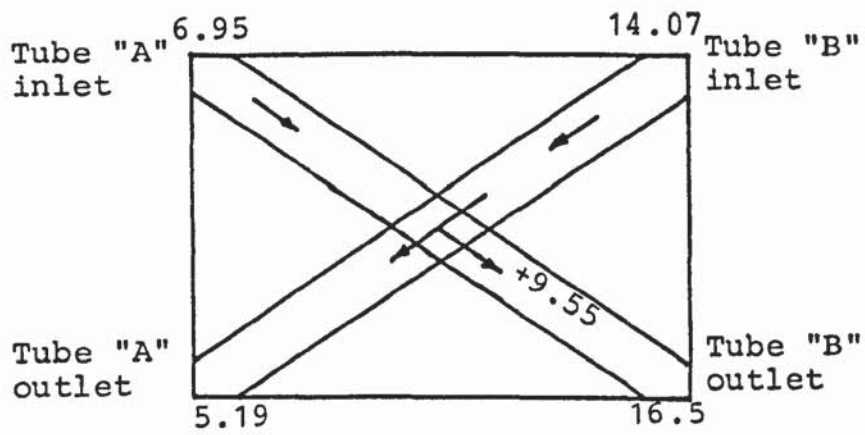


FIGURE 6.1 DISTRIBUTION PLOT FOR FLOW THROUGH BOTH TUBES AT THE SAME INITIAL PRESSURE

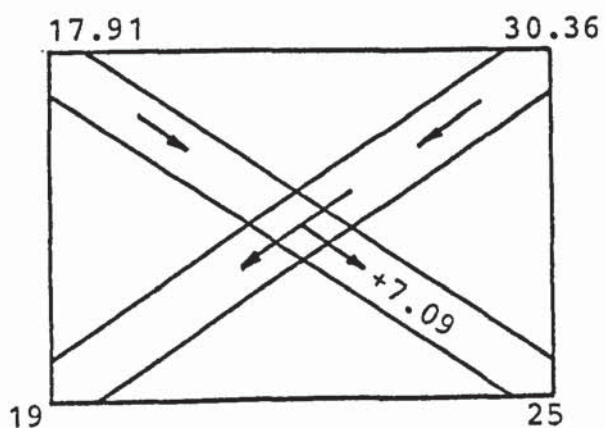
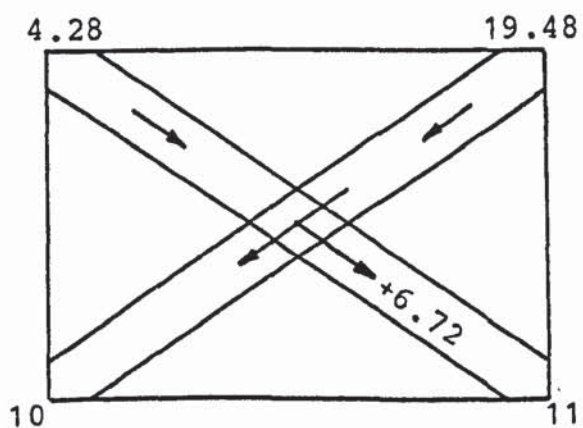
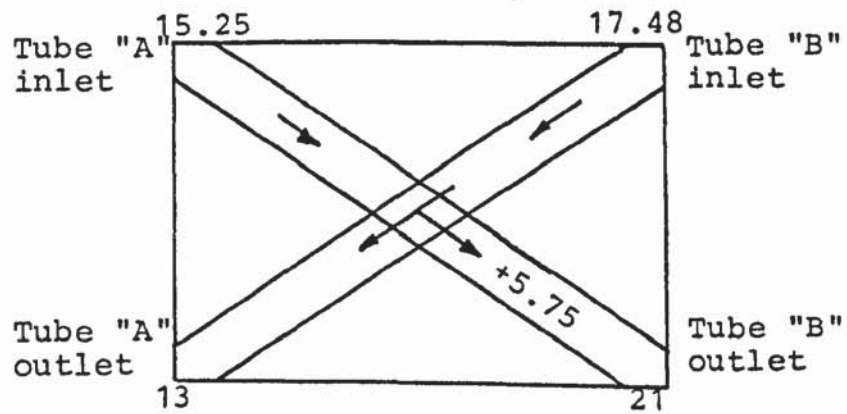


FIGURE 6.2 DISTRIBUTION PLOT FOR FLOW THROUGH BOTH TUBES
AT DIFFERENT INITIAL INLET PRESSURES

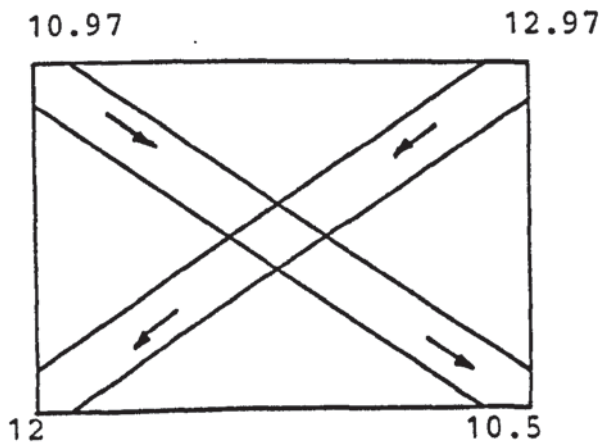
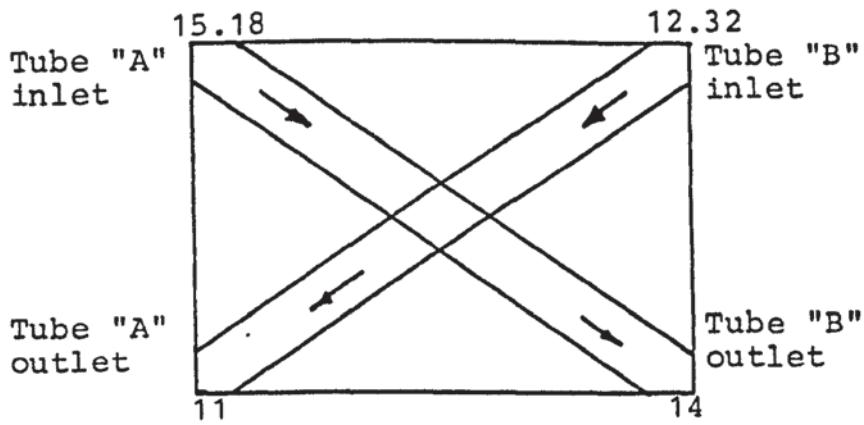


FIGURE 6.3 DISTRIBUTION PLOT FOR FLOW AFTER DOUBLING
ONE INLET PRESSURE

the total output was less than the total input, it nevertheless appears that the majority of the flow follows the course of the valley without any significant splitting. This shows that for doubling the pressure on one side of the channel caused the majority of flow to remain in appropriate valley.

Table 5.6 and 5.7 show that by opening taps at different intervals, the flow distribution is influenced when these results are shown, as in Figure 6.4. It is apparent under these conditions some of the flow from tube "B" inlet adds to the flow from tube "A" inlet, although the flow at outlet "A" was higher than at outlet "B". Again reinforcing the point made above that there is resistance of flow from tube "A" to split up while flow from tube "B" allows some split of flow.

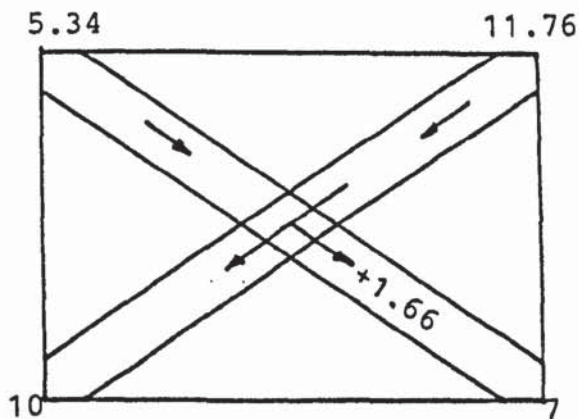
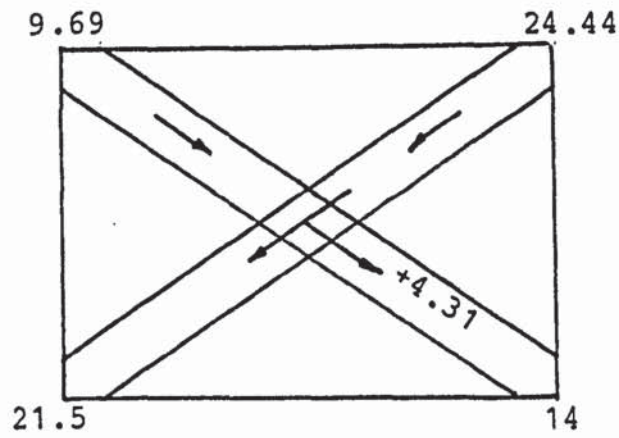
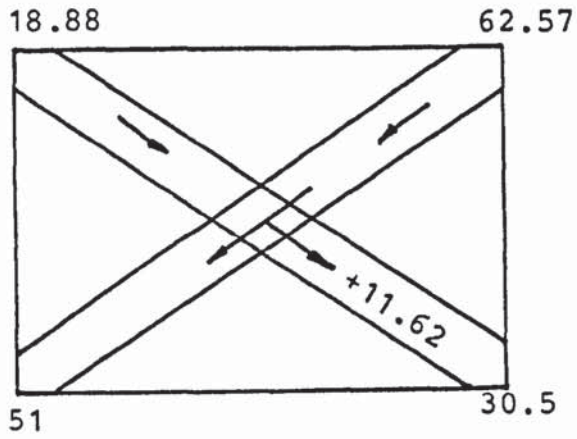
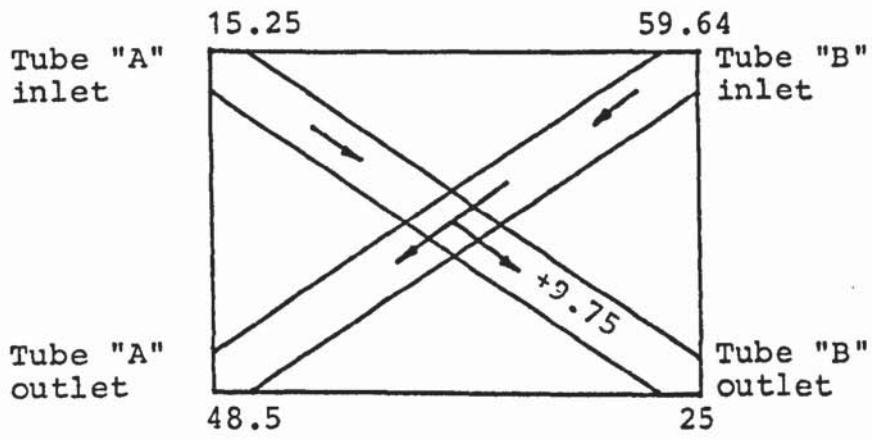


FIGURE 6.4 DISTRIBUTION PLOT FOR FLOW OPENED THROUGH TUBES
AT DIFFERENT INTERVALS

6.2.2 PERFORMANCE ANALYSIS

To analyse the performance of the single cell with different initial pressures of fluid, a criteria was developed. This criteria is based on the ratio of output of each tube to the total input. The development of this performance criteria is shown in Appendix A-4.0, with all the calculations for performances with changing pressures.

These performance criteria K_A and K_B are plotted against total flow rate input Q_T in Figure 6.5. The plot shows the ideal case where $K_A = K_B = 0.5$, and hence compares the difference between the measured and the ideal case. The performance criteria K_A and K_B do not necessarily add up to 1, due to slight discrepancy between the total input and total output flow. The causes of these discrepancies are outlined in section 6.2.3.

In Figure 6.5 the some performance criteria are not shown, but are given in Tables A-4.4 and A-4.5, because these runs were carried out largely to see if flow in one valley affected flow in the other valley, as discussed earlier. Although their performance criteria are calculated, the flow rates through the tubes were not for equal time intervals and therefore could not be used, to make any suitable comparison with other experimental results. Thus they were omitted from the plot.

FIGURE 6.5 PLOT SHOWING PERFORMANCE CRITERIA VS TOTAL FLOW

CALCULATED AT THE INPUTS FOR A SINGLE CELL

- Tube "A" Performance Criteria
- Tube "B" Performance Criteria
- △ △ Equal Pressure Levels
- ○ Different Pressure Levels
- × × Double Pressure Inlet in one tube.

K_A

PERFORMANCE CRITERIA BASED ON TUBE "A"

K_B

PERFORMANCE CRITERIA BASED ON TUBE "B"

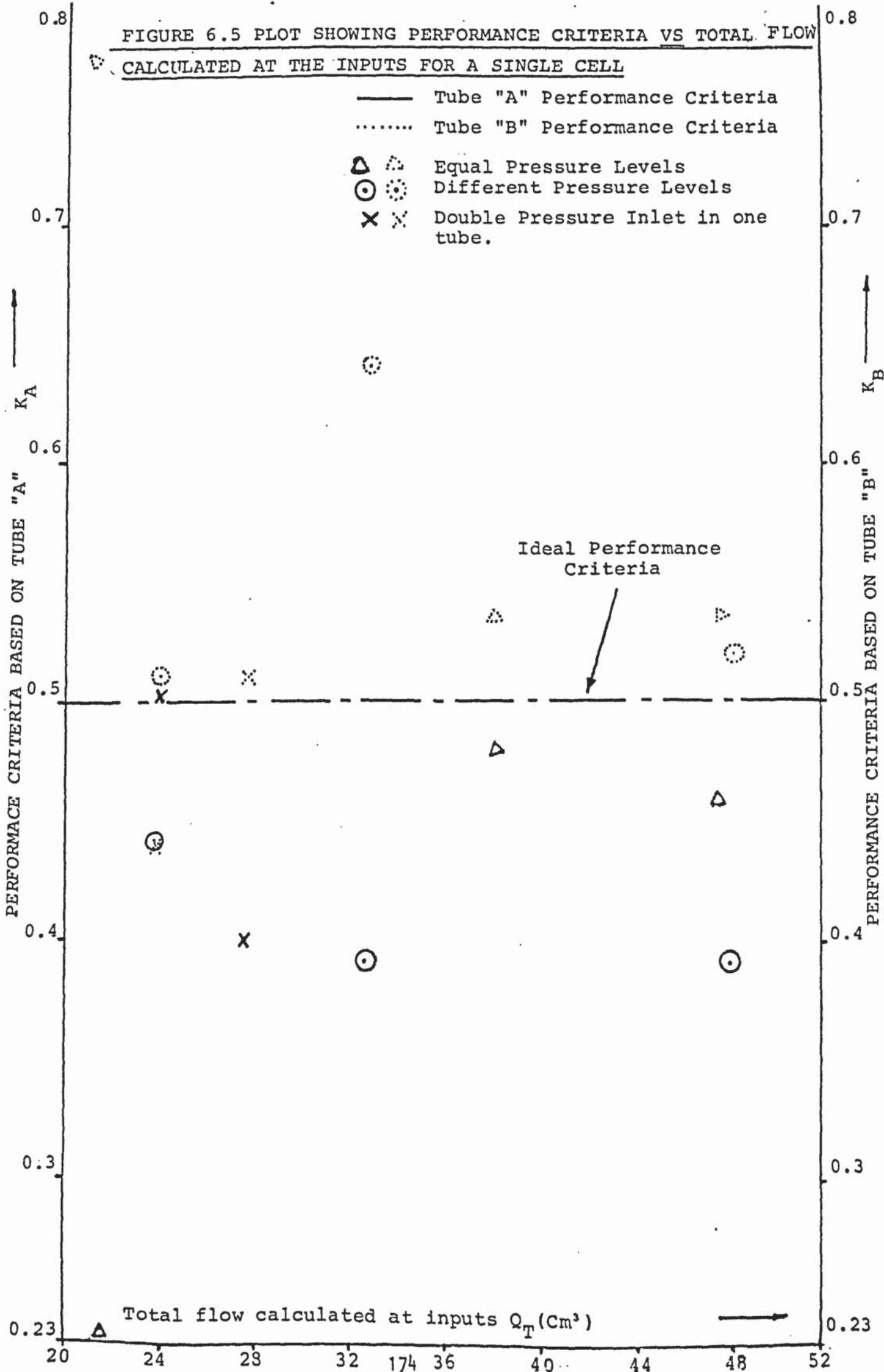
Ideal Performance Criteria

0.23

Total flow calculated at inputs Q_T (Cm³)

0.23

20 24 28 32 174 36 40 44 48 52



Examination of Figure 6.5 shows that different pressure gradient influences the performance criteria of the single cell. Different height levels of fluid are furthest away from ideal conditions especially for high flow rates.

The equal pressure performance criteria for two of the three sets of data are closest to ideality. For these two sets of data the maximum and minimum variation lies in the range of 9 - 3.3% within ideality, respectively. These are consistent results showing better distribution than for the overall data set. The third set of data points show maximum variation of 56% and minimum variation of 52% away from ideality; such high variations from ideality (the highest on all the results) suggesting experimental error, which may be accounted for due to the error associated with low flow rates.

When the inlet pressure levels are different, the low flow rate (23.76Cm³) maximum and minimum variation for ideality is 15.82% and 1.02% respectively. But there is greater variation for middle flow rate (32.73 cm³) variation is 20.56% and 28.32% for each data point in this set for high flow rate (48.27 Cm³) variation is 21.28% and 3.58% away from the ideality. There seems to be greater variation for higher flow rates. For lowest flow rate, the flow is better distributed from tube "A" inlet to tube "B" outlet.

When the pressure level is doubled in one inlet, the performance criteria shows for lower flow rate one data point achieves ideality with variation of 0.24%, while the other data point has variation of 12.28%. Also in the higher flow rate one data point achieves near to ideality, with variation of 1.82%, while the other data point has variation of 20%. In both flow rates ideality is achieved by flow through both tubes, although the tube "A" was on higher pressure for both runs. Therefore, showing distribution is not affected by higher water level in the particular tube. In fact doubling the height does not significantly affect the flow distribution.

6.2.3 PRACTICAL DIFFICULTIES IN MEASUREMENTS

During the experiments on small perspex sections of the Junior PHE, some practical problems were encountered, which are important to avoid when obtaining worthwhile results:

- (i) The section itself must be properly aligned, in order to make meaningful measurements. Since the channel section was not fixed to the wall, there was always the possibility of a slight inclination of the channel to the vertical. Although this was checked at regular intervals with a spirit level, on many occasions it was found to be slightly inclined. This can severely affect the measurements, because it favours flow on a particular side due to the gravitational effect.

- (ii) Timing was measured in only one particular experiment, because in other experiments it was impossible to operate taps as well as record time. Therefore personal judgement was relied upon for the timing. This may affect the flow rate because observing the water level to drop and operating the taps was on visual basis only. Error could be caused by both taps not closing at the same moment.
- (iii) Sometimes, air bubbles were trapped in the outlets, therefore affecting the amount of fluid collected and giving rise to discrepancy between the measured and the calculated flow. Such results had to be rejected.

The first factor (i) would influence the direction of the major flow, depending upon the inclination of the perspex section. There is a possibility that this may move for a short period, when taps are opened and rotate back again when taps were closed.

6.3 SR1 ANALYSIS USING WATER

In the experimental work using water, outlined in depth in section 4.3.2, the failure to obtain any satisfactory results requires further detailed explanation.

6.3.1 PROBLEMS OF ALIGNMENT

In the initial stages of the work, the major source of error was misalignment of the optical components especially without the lens, eventually placed in the laser beam. There was significant reflection and scatter at the inner surfaces of the channel and refraction at various interfaces: air/perspex, perspex/water, perspex/air. There was also significant internal reflection within the channel, exaggerated by the curved surfaces of the corrugations. Beam reflection is a common phenomena in most LDA studies and was expected. Refraction was also expected, but not to the extent that was actually encountered from the fact that the inner surfaces were profiled. This, and the scatter occurred at the surfaces resulted in major difficulties in obtaining and observing a cross-over point in the channel. Although some flare was reduced by placing a lens in the beam to focus the split beams more sharply at the cross-over point, this still remained a major problem throughout. Even with the lens the beams diverged due to the nature of the internal surfaces, as shown in Figure 6.6 (11). In the crossing region the beams are not plane parallel as they would be at the "waist" around a true focus. The effective angle between the beam varies across the intersection volume. The fringes sketched in are not parallel and if it was possible to obtain a signal (by reducing background light) then there could be an error in the calculated

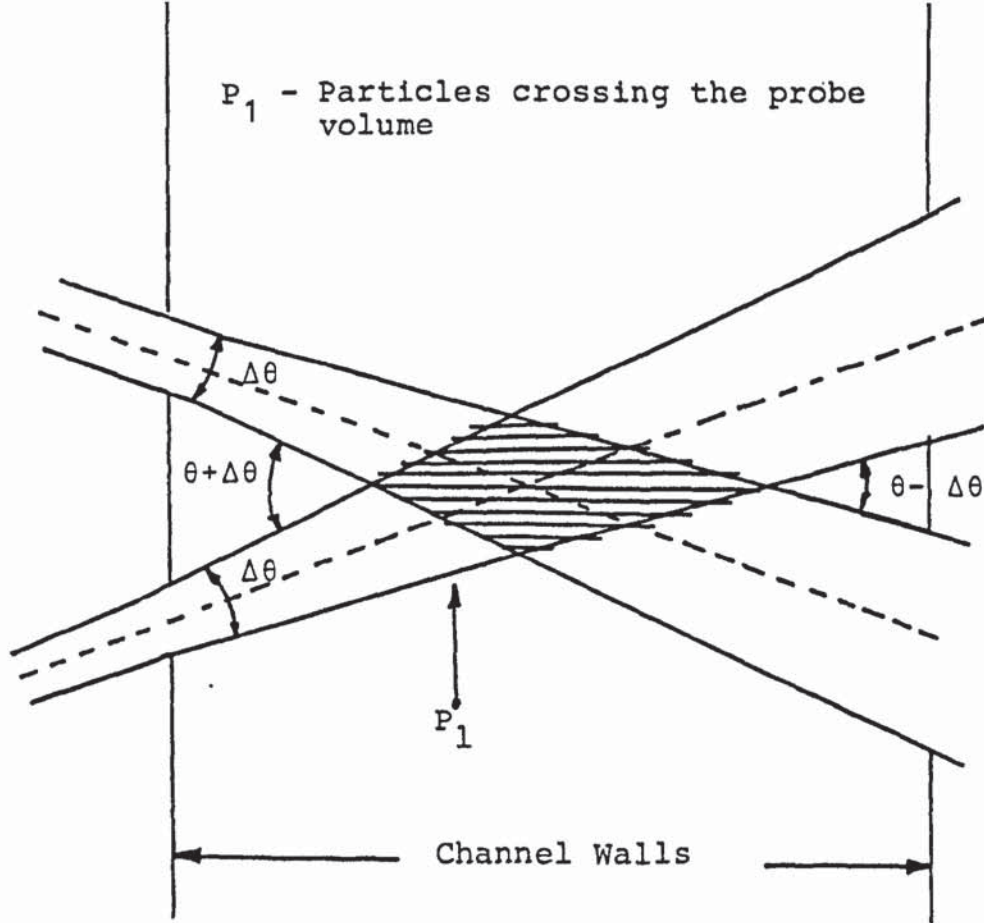


FIGURE 6.6 DIVERGENT BEAMS CROSSING IN THE CHANNEL

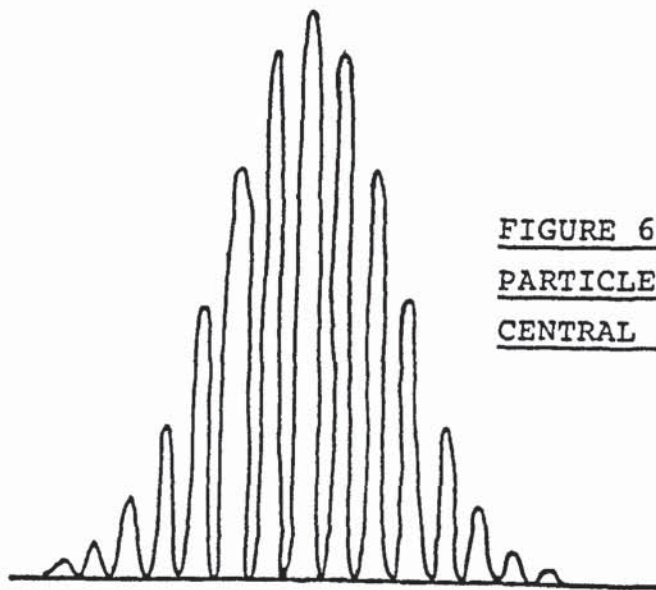


FIGURE 6.7 (a) SIGNAL FROM PARTICLES CROSSING IN THE CENTRAL REGION OF PROBE VOLUME

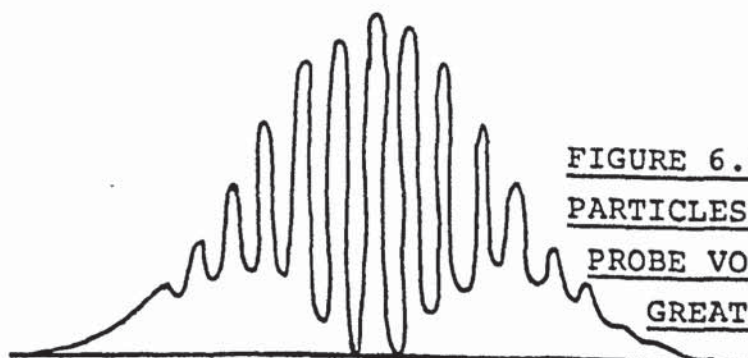


FIGURE 6.7 (b) SIGNAL FROM PARTICLES CROSSING IN THE PROBE VOLUME FOR PARTICLE SIZE GREATER THAN FRINGE SPACING

results. As illustrated, particles crossing the volume near the wall P_1 , on one side of the volume will give rise to a higher Doppler frequency than those with the same velocity crossing at the other end of the volume.

The crossing angle for the beams will also vary from $(\theta - \Delta\theta)$ to $(\theta + \Delta\theta)$ where θ is the nominal angle between beams, as shown depending on the convergence or divergence angle of each beam. Although these angles were small, there would be an error in the number of fringes in the intersection volume, and the fringe spacing is variable rather than constant. Under these conditions, accuracy and signal to noise ratio are affected hence there is real unreliability in any velocity measurements made.

Furthermore, reflection from the internal surfaces caused difficulty in identifying the cross-over region. Although the lens minimised this error it did not eliminate the problem. The stray light from reflections reaching the detector certainly affected any attempt to make accurate reliable velocity measurements.

6.3.2 LDA SIGNALS

Some of the factors which affected signal quality need to be briefly summarised. One of the important factors which needs considering is the particle size. Although large particle sizes generally increase the scattered light received by the detector, this does not necessarily improve the LDA signal, especially if the

diameter of particles becomes large compared with the fringe spacing. Large particles span light and dark bands of a fringe pattern and thus average out the variation of light intensity. The modulation of a signal from the passage of a particle is reduced. This is observed by the signals of particles crossing the region of intersection of light beams. Figure 6.7 shows different types of signal from particles crossing the intersection region.

Figure 6.7 (a) shows the ideal signal from a particle tracing a path through the centre of the fringe pattern formed by intersecting beams of equal intensity. The maximum depth of modulation possible corresponds to the high fringe contrast in the central region, provided the particle size is smaller than the fringe spacing.

The reduced modulation signal, Figure 6.7 (b) arises from two main reasons, either the particle size may be large compared to fringe spacing (mentioned above), or the intersecting beams are not of equal intensity.

A particle following a path off centre, e.g. P_2 in Figure 6.8, would produce intensity modulation signal of the type shown in figure 6.9.

One of the major problems was actually locating the position of the best intensity modulation signal. This was not necessarily in the middle of the cell volume,

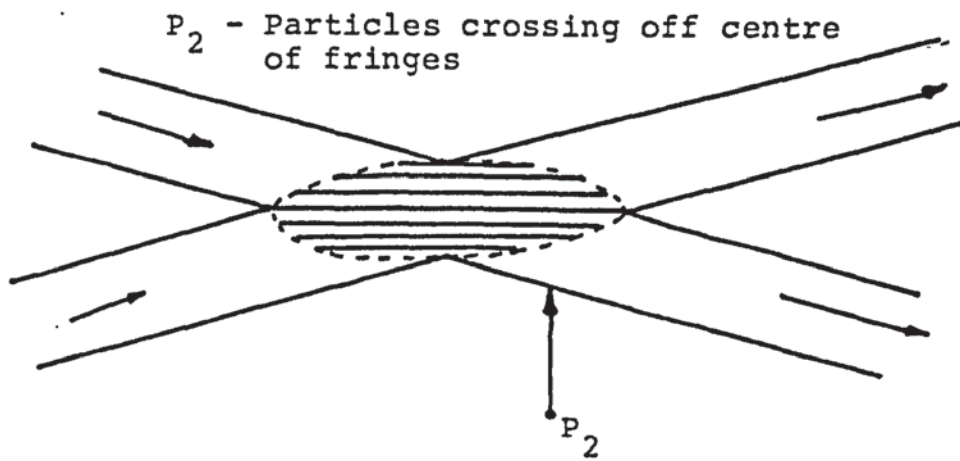


FIGURE 6.8 PARTICLES CROSSING PATH OFF CENTRE IN THE FRINGE PATTERN



FIGURE 6.9 SIGNAL OBTAINED FROM PARTICLES CROSSING OFF CENTRE OF FRINGE PATTERN

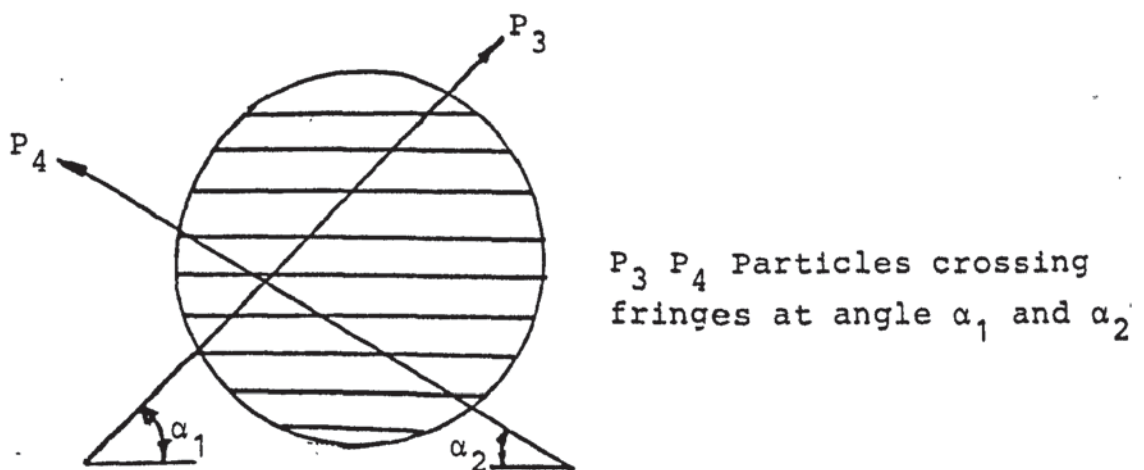


FIGURE 6.10 PATH OF PARTICLES CROSSING FRINGE PATTERN AT DIFFERENT ANGLES

so fine adjustments were made to the photomultiplier tube position to find the ideal signal. It appeared from visual observation that the failure to obtain ideal signals was largely due to particles not crossing the fringes perpendicularly but in various angular positions, e.g. P_3 , P_4 , as shown in Figure 6.10. Thus attempts were made to make measurements wherever possible in the volume, i.e. wherever the particles were crossing the fringe pattern perpendicularly, by fine adjustment to the photomultiplier tube position.

6.3.3. FAILURE IN REPEATABILITY

Attempts to reproduce some of the measurements made using water in the channel, were fruitless and some of the causes have been outlined earlier in sections 6.3.1 and 6.3.2 with the development of the experimental work in section 4.3.2. The main reason for abandoning water as the working fluid will be discussed in this section.

To explain the lack of repeatability of velocity measurement, the internal geometry has to be considered. When the beams were projected in the plane parallel to the axis of the corrugations, if they passed through the valley of the corrugation, they would refract, initially at the perspex wall and then the perspex/water medium, but both beams would refract equally and hence intersect in the channel, or more accurately in the cell volume, as shown in Figure 6.11. Thus the LDA requirements are

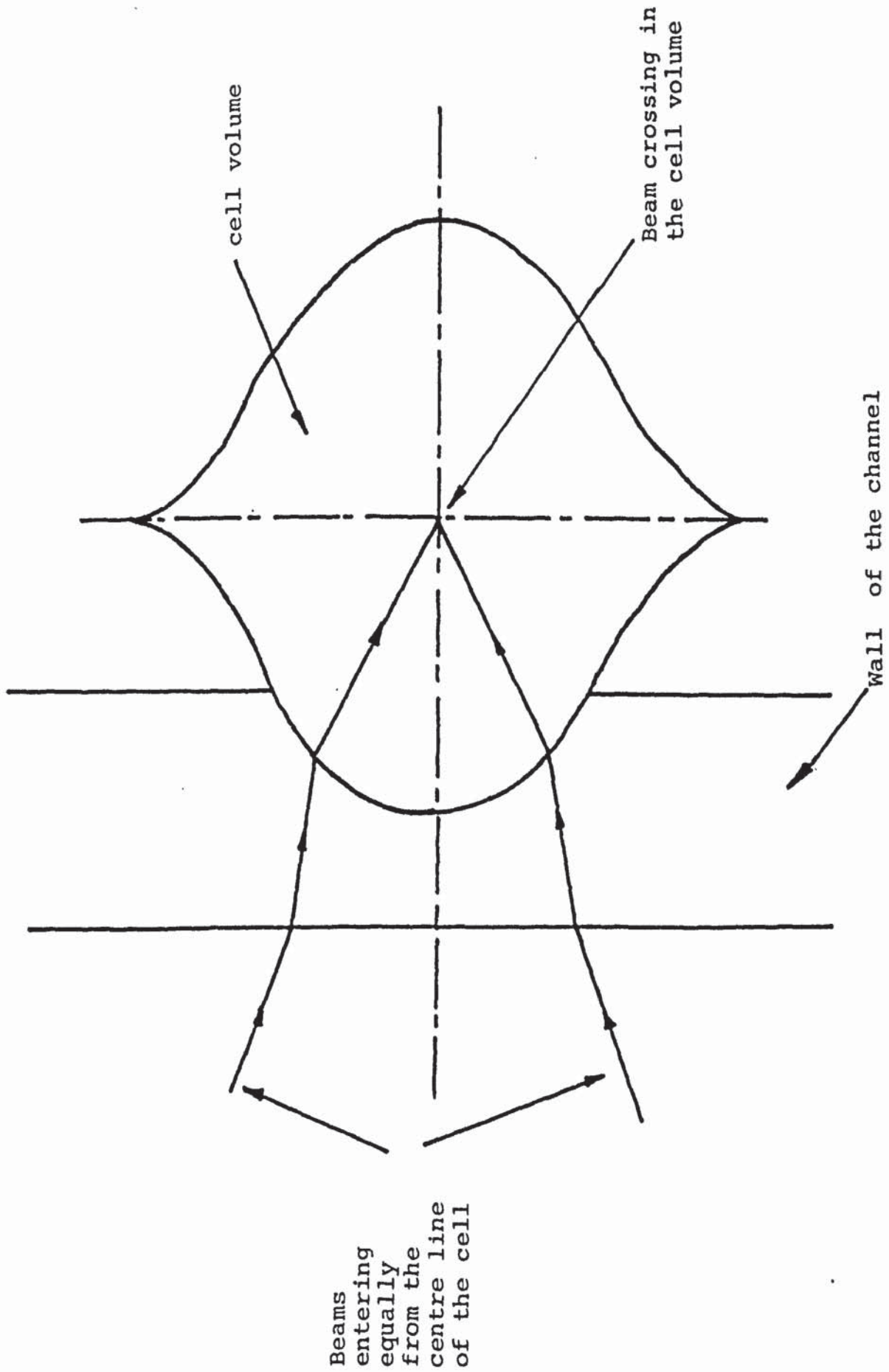


FIGURE 6.11 BEAMS INTERSECTING IN THE CELL VOLUME

satisfied and the signal can be analysed provided the other conditions, particle size, minimum flare and particles crossing fringes perpendicularly were satisfied.

This approach was successful in making measurements a number of times, but was not successful in making measurements at other positions (cells) in the channel. The main factors for this failure were thought to be either that the flow was very turbulent or the beams were not crossing in the correct manner in the channel. The former was rejected, since the flow was at a very low Reynolds number, and local disturbances were most likely to be sufficient to adversely affect the LDA technique. Therefore, the second factor remained for detailed examination.

Checks were made as mentioned in section 4.3.2 and following the procedure in the manual (124), to ensure that beams were crossing in the channel, satisfactory results were not obtained. Hence it was clear that the beams were not crossing correctly in the channel, even though they appeared to be intersecting one another. The behaviour of the beams in the working section of the channel was subjected to deeper analysis.

For intersection at a particular point, the beams should be projected in a plane parallel to the corrugation pattern and should enter the volume via the base of the valley. Refraction will occur at both perspex interfaces

where there is a change of medium, but the beams should intersect, if they have not been deflected. In practice the beams only partially intersected giving inadequate fringe pattern, even though visually they seemed to be intersecting properly. It was concluded that beams have a low probability of a correct intersection because of the following reasons:

- (i) It is extremely difficult to project beams accurately through the base of a valley since it is impossible to identify this visually. Therefore a trial and error method had to be relied upon to ensure the cross-over in the channel. If the beams do not cross the working volume exactly through the base of a valley, the refraction effect would deflect the beams slightly resulting in partial intersection at the best. Furthermore, the curved internal surfaces would affect the beams to some extent in a lens fashion. The beams would diverge or converge to different extent depending on the surface curvature at the point through which they pass, therefore affecting fringe spacing. Situations such as that depicted in Figure 6.12 would result, where the beams appear to be crossing in the channel.
- (ii) A closer examination of the arrangement of the beams splitter shows that one of the beams always remained fixed while the other beam moved to cross at the required position. When beams are

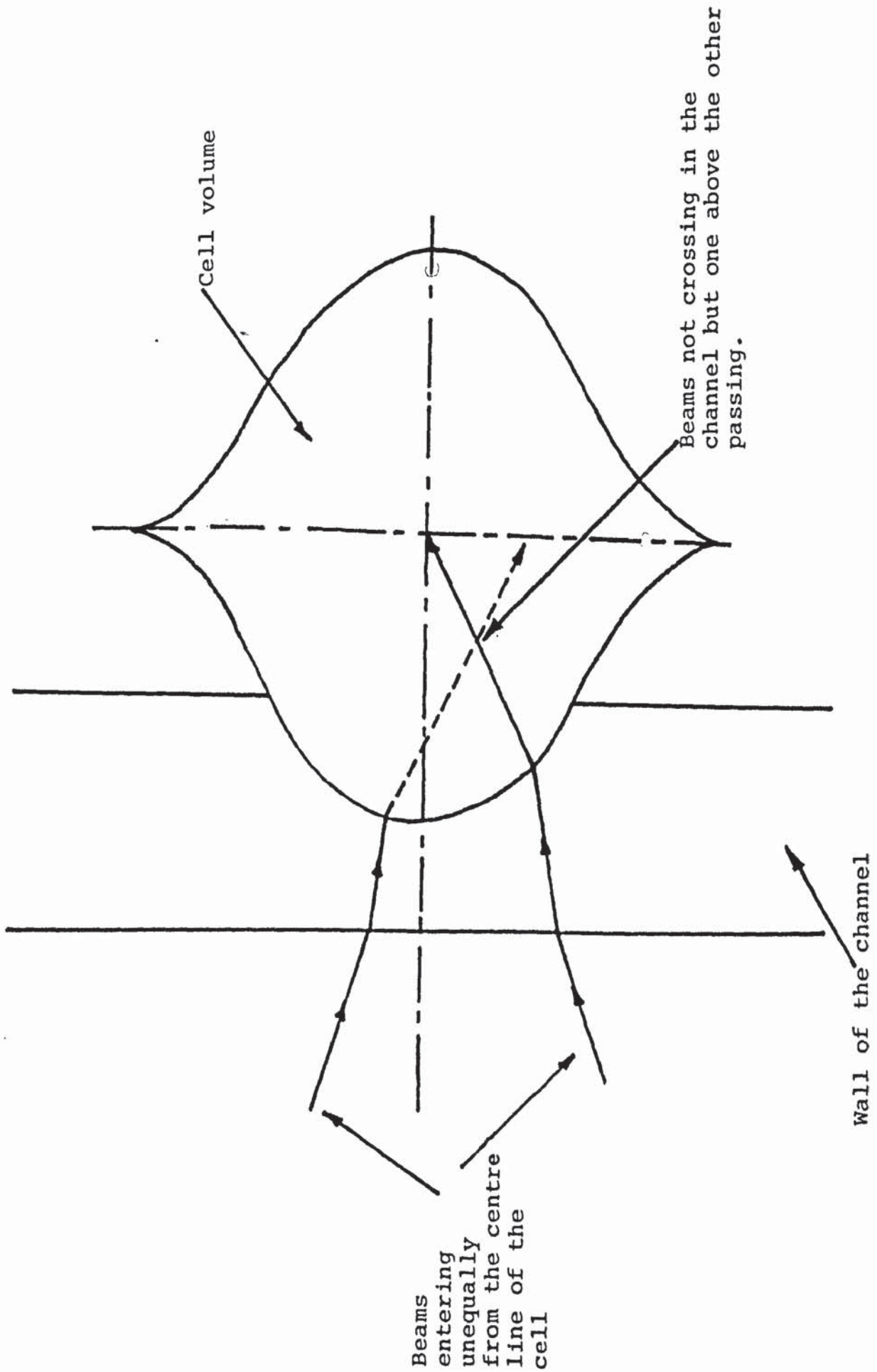


FIGURE 6.12 BEAMS NOT INTERSECTING IN THE CELL VOLUME

projected at the channel, one of them could enter the channel at a different angle to the other beams and hence refract at different angles in the plate walls and then in the water. Thus they may or may not meet in the channel depending on the amount of refraction for each beam. The possibility of beams crossing in the channel could be very much reduced by this type of beam splitter.

By chance, after extensive trial and error experimentation, some velocity measurements were made, but it was totally impossible to repeat these results. In fact, it was found that a slight movement in the equipment of as little as 0.1mm completely destroyed any chances of repeating results, even after spending a great deal of time. This highlighted the extreme sensitivity of the equipment to positioning and alignment.

The first problem (i) can be overcome by delicate time consuming trial and error procedure, but the latter would be the most difficult of all to solve. Accurate repeatable results measurements would only be possible if the beams could be projected into the cells at identical positions for each cell. This was found to be impossible. The author feels those results obtained were possibly due to beams only partially intersecting one another, and sufficient to produce a signal but are therefore most unlikely to be either accurate measurements or repeatable. Thus water was abandoned as a working fluid and a refractive index matched liquid was considered to be the only way that the problem of beam deflection caused by surface curvature could

be eliminated.

6.4 VELOCITY MEASUREMENTS ANALYSIS OF LOW FLOW RATES

In this section, the analysis of measurements at low flow rates would be discussed for both Up-flow and Down-Flow. An attempt will be made to relate the present work with any previous study available from those reviewed in Chapter 3.

6.4.1 HORIZONTAL COMPONENT IN UP-FLOW

Figure 5.1 shows point velocity measurement on the centre line of the channel, for the horizontal component of the flow. The velocity component could be in either direction as shown, depending on the actual flow direction at the chosen point. The particles can cross the vertical fringes in any direction, (see also section 6.7) although the overall flow is in the upward direction. The LDA system used could not compute the direction, this could be obtained by visual inspection using the reflex viewer.

The cells on the centre line of the channel are larger than the other cells because of the geometry of the plates where the chevrons meet. The average velocity was computed at 0.3254×10^{-2} m/s at 22°C and it was assumed that this value was not adversely affected by small changes in temperature. In some cells two measurements are shown, this is because during the experimental work, an interesting variation of velocity was noted in the cell volume, and a large difference in turbulence values was found across the cell volume. This will be discussed further in this section.

Initial observation of the velocity measurement show that each single value except one is higher than the channel average velocity. Although it has been normally accepted by design engineers of PHE's that local velocities are about four times the average velocity (116) the present measurements show that the maximum local velocity can be 27 times the average velocity.

When the flow just enters the channel, the fluid elements or particles, flow in a continuous stream and therefore provide a high velocity of 6.77×10^{-2} m/s, nearly 21 times higher than the average velocity. But these elements begin to spread in the channel and undergo continued changes of velocity while moving higher up the channel. The channel can be conveniently divided into five sections and can be discussed as follows:

- (i) The channel section having velocities of 1.91 to 1.09×10^{-2} m/s have a minimum and maximum value of 3.13 and 5.8 times greater than the average velocity, respectively. These changes of velocities depended on fluid elements distributing into the channel immediately after leaving the inlet port,
- (ii) In the channel section of velocities shown from 2.35 to 2.00×10^{-2} m/s the range of minimum and maximum increased between 6.27 and 9.31 times greater than the average velocity. This can be explained by packages of fluid elements coming together in this section, which were distributed after entering the inlet in section (i) region.

- (iii) In velocity section of 1.78 to 1.02×10^{-2} m/s, the range was found to be decreased 3.13 to 5.47 times that of average velocity. It appears that there is a more even distribution of flow once again in this section, and therefore a drop in the velocity range.
- (iv) The section of 0.602 to 0.238×10^{-2} m/s have some velocities less than the average velocity, unexpectedly, there is a decrease in range of 0.73 to 1.85 times greater than average velocity. This greater decrease can be explained by the possibility that the flow is more evenly distributed.
- (v) The remaining section has velocities in the middle of the cell, as well as near the wall, it was difficult to estimate the distance between the wall and the intersection point near the wall.

For the centre of the cell, the velocity range varied between 4.98 and 27.28 times greater than the average velocity. There was an increase in the velocity while moving up towards the outlet of the channel. Such increases can be explained because the flow is ready to leave the outlet and packages of fluid elements are continuing to cross the beams fringes at a much greater velocity.

For the measurement near the wall of a cell, the velocity range varied between 2.27 and 26.74 times greater than the average velocity. There was an increase in velocity and an interesting feature noted was the large increase of computed turbulence at the wall, whereas the centre of the cell volume mostly registered 0% turbulence.

The variations of turbulence in the channel can be caused by the following factors:

- (i) The overall flow is laminar but, as distribution occurs in the channel, small fluid elements can follow many directions, thus giving rise to unsteady flow and a general increase in turbulence over the plate channel.
- (ii) This increase of turbulence is smaller in the top section of the channel at the centre of the cell. Here flow is ready to leave and the fluid elements or particles combine together to cross the scattering volume, perpendicular to the fringes, hence registering 0% turbulence.
- (iii) The increase of turbulence near the wall, in the top section of the channel, arises from the change in flow distribution of fluid elements approaching the channel outlet. At the wall, a high flow rate of fluid exists along the valley of the corrugations, in a position where it crosses the beam interference fringes at an angle sufficient to provide a good signal. The degree of turbulence registered depends on the angle of the particles crossing the intersection volume (as shown in Figure 6.10) and variation in the velocity of these particles crossing. Since the cell geometry is three dimensional and adjacent cells are interconnected by flow paths, only one direction of flow could be considered during a particular measurement because of the complicated nature of flow. It was established that the particles were crossing

the fringe region at an angle suitable for producing a suitable signal. The long and tedious methods of fine adjustments of the PM tube discussed in Chapter 4 validated this conclusion.

Inspection of the overall channel measurements in Figure 5.1 shows that the changes in range of velocities or the maximum and minimum variation of velocities discussed earlier arise from changes in flow direction at certain points. Comparison with the dye visualisation experiments reported by Fattah (7) for very low Reynolds numbers using glycerol as a viscous liquid, similar trends in the patterns of flow can then be observed. Fattah observed for 65.45% aqueous glycerol solution in the Junior PHE perspex channel upwards flow, that the flow sequence started with flow travelling "straight" up the channel followed by minor splits, with the dye filament shifting from the left side to the right side of the channel in a broad sinusoidal wave. Similar trends can be detected in the velocity measurement results in regions where there are increases and decreases in values.

Initially the flow enters the channel and moves immediately straight upwards until the point is reached where the velocity is 1.09×10^{-2} m/s. The majority of the flow then tries to follow a sinusoidal wave by shifting towards the right hand side of the channel, (as shown by higher velocity measurements). This flow reaches the right side of the channel where by decrease in velocity, in range of 1.87 to 0.238×10^{-2} m/s, and then all the flow

returns from the right to leave at the outlet on the left. This shift is shown by sudden increases to very high velocities in the top section of the channel.

Therefore the flow pattern appears to be following that encountered in Fattah's dye injection experiments, even though there are differences in fluids used, and in the size of channel employed. General comparisons are still justified since the overall complex geometry of the channels involved is very similar.

6.4.2 ANGULAR COMPONENT IN UP-FLOW

The angular component of the measurements was parallel to the corrugations in the channel, i.e. 60° to the vertical, as shown in Figures 5.2 to 5.5. This component was chosen for the main reason that it proved easier to correlate the flow in this direction and more regular measurements could be made, while in other directions it was rather difficult to correlate the flow. This supported the original belief that the majority of the flow was in this direction.

There are some measurements missing from the grid of cells chosen for investigation. Although a line of note is added to the bottom of each figure it is essential to comment upon these before proceeding with the analysis of velocity measurements.

The main purpose of choosing a diamond grid structure was that an overall view of the flow pattern could be

obtained across the channel without examining each individual cell. Where it proved appropriate, more cells within the grid were examined to clarify the overall picture.

In the top region, on the right side of the channel, some measurements were made at the wall of the cell, since it was impossible to correlate flow in the centre of these cells. Experiments showed that the flow was very small indeed in the middle of the cell volume and was barely detectable. The only convenient position in the cell, where reliable measurements could be made, was near the wall, where the majority of the flow was presumably parallel to the corrugations. Visual observation of the beam intersection volume using the reflex viewer on the PM tube confirmed that there was virtually no flow through the middle of these cells.

Furthermore, in this region, it was extremely difficult to correlate flow in some positions because of lack of flow in this component. Presumably flow must be in some other component and this is confirmed when values for the horizontal component values at $Re = 0.1616$ are examined in Figure 5.1. The horizontal component values are 0.492 and 0.602×10^{-2} m/s, showing that the flow in this cell is no longer parallel to chevron pattern. The change of direction in different positions will be discussed later.

One other position where it was impossible to make measurements is shown because excessive flare from a very poor surface prevented identification of the centre of the

cell. Further polishing did not improve the surface so no measurement could be made. Generally it was difficult to make measurements at the edge of the channel, since perspex quality has deteriorated either during manufacture or through internal stresses arising from clamping the plates together. Further polishing had no noticeable affect on improving laser beam or signal quality.

Examination of the point velocity measurements for four different flow rates (Reynolds number from 0.0817 to 0.1616) show very similar velocity profiles; Figures 5.2 to 5.5. Every velocity measurement is higher than the average velocity in the channel.

In the inlet region, when flow leaves the distributor, there is an unequal distribution of flow. For $Re = 0.0817$ the ratio of maximum to minimum measured velocities is 4.568 with similar values for increasing Reynolds number: 5.147, 5.442 and 5. This uneven distribution could largely arise from the physical design of the distributor unless the velocity is higher in a different direction at the point in question. However, the initial experiments clearly showed that the velocity was at a maximum in the 60° component. Dye injection by Fattah (7) had showed that as soon as dye was injected, it favoured entrance to one particular corrugation via the distributor. Fattah did not comment on this initial flow behaviour. Perhaps it was not obvious in the photographic technique used, but becomes more clear when values are quantified in the current work.

The values across the channel, from left to right for all four flow rates show an increase of velocity to the centre line of the channel, then a large drop and then an increase. This latter increase is attributed to the flow returning from the edges of the channel, as also observed across the middle and the outlet region of the channel. The maximum to minimum velocity ratios on the left side across the channels are 4.14, 3.487, 3.44 and 4.081 for increasing flow rates, showing a slight variation in velocity change between the four flow rates. The reason for the initial increase in velocity when moving from left to right could be that the majority of the flow entering the channel is curving towards the left side of the channel. This is also shown by the increase in velocity along the corrugations on the left side of the channel, e.g. for $Re=0.1616$ (Figure 5.5) the velocities 7.16 to 24.4×10^{-3} m/s. On the right hand side there is also an increase in velocities along the corrugations, e.g. for $Re=0.1616$ (Figure 5.5) the velocities 3.24 to 12.8×10^{-3} m/s. The velocities on the left side of the channel are higher than those on the right side. This indicates that the attributed majority of flow favours the ports side of the channel.

The middle region shows similar characteristics in measurements across the channel, from left to right there is an increase, followed by a decrease, but not as severe as the inlet region, and finally an

increase at the edge of the channel. This latter increase is the return of flow from the edges of the channel. The ratio of maximum to minimum velocity measurements across the channel on the left side of the channel are 5.263, 5.49, 5.11 and 5.224 for increasing Reynolds numbers. This high ratio is unexpected and difficult to explain since it was anticipated that flow would be fully established in the middle region and that point velocities would be very similar. Perfect distribution of flow would result in an ideal ratio of 1.0 at comparable points across the channel.

The measurements parallel to the corrugations on the left hand side of the channel show an increase in velocity from left to right, e.g. for $Re=0.1616$ velocity varies from 6.24 to 17.9×10^{-3} m/s. Also the velocities on the right side are much higher than the velocities on the left side of the channel. This is the opposite case to the inlet region. Therefore, the cause of these high velocities is attributed to the flow move curving from the right back towards the middle and some towards the left shown by high velocity 17.9×10^{-3} m/s for $Re=0.1616$ or 10.1×10^{-3} m/s for $Re=0.0817$ (see Figures 5.5 and 5.2). It appears that most of the flow, which was curving towards the left of the channel at the inlet has come towards the right side in the middle region similar to patterns Fattah obtained.

At the outlet region, the chosen measurement grid was incomplete on the right side of the channel in Figures 5.2 to 5.5. This was because it became impossible to make any measurement in the centre of cell volume since the fluid was flowing in the valleys and thus starving the centre of flow. Therefore measurements could only be made near the wall of the cell (as indicated). To compensate for the loss of these measurements in the channel, other positions across the channel were chosen for examination.

At the outlet region just before the fluid is collected and ready to leave, the velocity measurements parallel to the corrugations show variation across the distribution. Towards the edge of the channel, near the gasket on the left side, the velocities are in the same range (e.g. for $Re=0.1616$, 25.9, 27.5, 25.2 $\times 10^{-3}$ m/s and for $Re=0.0817$, 14.2, 15.7, 16.3 $\times 10^{-3}$ m/s) and then further along the corrugations there is a reduction in velocities by half compared to the previous three values.

The measurements across the channel generally show a decrease from left to the centre of the channel, and then an increase followed by a decrease of velocities. The changes in velocities across the top part of the channel appear to be different from the other two regions, but it should be remembered that the measurements on the right side cannot really be compared with the others since they were not measured in the

centre of the cell volume. The ratio of maximum to minimum velocities across the channel on the left side for $Re=0.0817$ (velocity range 21.5 to 4.21×10^{-3}) is 5.107 and for higher flow rates the ratios are 5.522 , 5.319 and 5.263 in increasing order. These ratios are very similar to the middle region showing there is little overall change in velocity profile between these regions.

It is clear from inspection of Figures 5.2 to 5.5 that the velocities are higher on the left side of the channel than on the right side. This is as expected because the flow leaves from this side of the channel and fluid has to be collected in this region. It appears that the flow which left the middle region from the right side of the channel (mentioned earlier) approaches the left side of the channel in this region. This would also explain to some extent the starvation of fluid on the right side of channel.

Examining the flow measurements in Figures 5.2 to 5.5 clearly highlights one of the main features of the velocities in that they are much higher than the average velocity used traditionally in the past for this type of channel. The ratios of maximum local velocity to the average velocity were found to be 12.34 , 11.84 , 11.83 and 11.00 for increasing Reynolds numbers, although previously it has been reported (116) that true velocities due to corrugation were about four times that of the average velocity.

Analysis of velocity measurements of the type reported usually employs some form of statistical technique to show any degree of variation within the measurements. Therefore, the standard deviation has been calculated for chosen sets of data taken across the channel for each of the three region.

The calculation procedure for standard deviation is summarised in Appendix A-5.0 and the results are summarised in tabular form in Tables A-5.1 to 5.4 for Up-flow.

These tables show a consistent and interesting effect that the standard deviation is increasing for all flow rates from the inlet to the outlet region. This indicates a significant increase in spread of velocities while moving up the channel.

At this stage, another comparison can be made between Figures 5.1 and 5.5 for the velocities on the centre line of the channel. The comparison of velocity components in two directions can be made at certain common cells.

In Figure 5.1 the value near the inlet shows a measurement of 6.77×10^{-3} m/s in the horizontal component, while the 60° component is 25.3×10^{-3} m/s in Figure 5.5, therefore showing that more of the flow is in horizontal component. At the next common cell

the velocities are reversed, the component parallel to the corrugation is nearly three times that of the horizontal component. Then again in the next common cell the velocity in the horizontal component is 2.47×10^{-3} m/s but is 12.8×10^{-3} /s in the 60° component. These higher values of the horizontal component are maintained in the two common cells of the middle region of Figure 5.5, where the horizontal component is still about twice the 60° component.

The next two cells in Figure 5.5 (shown by * * *) contain no measurement because of lack of flow in this direction. It was suspected that the flow may be in another direction and this is confirmed in Figure 5.1 where values of 0.602 and 0.492×10^{-3} m/s in the horizontal component were found.

The cell with a velocity of 24.4×10^{-3} m/s in figure 5.5 has a higher 60° component of flow than its counterpart in Figure 5.1 which shows a horizontal component of 0.238×10^{-2} m/s. This is reversed in the next cell where the velocity in the horizontal component becomes twice that of the 60° component. Furthermore, the common cells containing the highest velocity in both flow rates show the horizontal component (5.26×10^{-2} m/s) in Figure 5.1 to be 1.8 times larger than the 60° component (29.7×10^{-3} m/s) in Figure 5.5.

These common cells certainly show that in the very initial and final cells the horizontal component

is the most dominant for flow in the middle of the channel. This was not found to be the case when measurements were made at other cells, there the majority of the flow was found flowing parallel to the chevron pattern. It is also evident that the horizontal component is also more dominant than the 60° one of the remaining cells in the middle of the channel.

Turbulence in the centre of the channel was mostly computed as 0% for all three regions but was higher at edges of the channel, i.e. near the gasket. In the inlet, middle and outlet regions, the ranges varied 0-10.5%, 0-12.5% and 0-8% respectively. There is no significant difference in these turbulences, but the higher values may be caused by the gasket which would obstruct fluid elements and disturb the flow pattern. Random variations in velocity and flow directions would affect the computed value of turbulence.

Inspection of the overall flow distribution for Up-flow at low flow rates, indicates that the flow is following a sinusoidal wave path, i.e. most of the flow is shifting from the left (at the inlet) to the right (in the middle region) and back to the left (at the outlet region) of the channel. This supports the findings reported previously by Fattah (7).

Furthermore, the now quantified values in each cell show that there is mal-distribution during Up-flow in the channel when only part of the channel is being used.

6.4.3 DOWN FLOW

Figures 5.6 to 5.9 show point velocity measurements parallel to the corrugations of the channel, i.e. at 60° to the vertical direction. This component was chosen for the reason outlined in the previous section.

The number of cells investigated was increased to examine the distribution in more depth. Velocity values are not shown in some cells of the grid structure chosen for examination, as indicated in the brief notes added at the bottom of each figure, for the following reasons:

- (i) At the inlet region, on the right side of the channel, it was found to be difficult to make acceptable measurements because there was lack of flow. This was confirmed visually through the reflex eye-piece on the PM tube where very few particles would cross the intersection volume.

It should be noted that successful measurements could be made during Down-Flow in those positions where reliable values could not be obtained in Up-Flow, see Figure 5.2.

- (ii) In the outlet region, the measurement is incomplete due to the fact that the outlet flange connection physically obstructed the beam splitter from aligning in this region. Similarly

it was impossible to make measurements at the inlet, at the immediate start of the distribution zone, because of obstruction by the inlet flange connection.

(iii) In the middle region of the channel, there are a few cells which do not show any velocity measurements, because the joints of cellulose acetate used to identify the position of individual cells, affected the quality of the beams.

At the outlet region, some measurements are shown at the wall of the cells rather than in the centre. This is because it was difficult to correlate the flow in the 60° component and it appeared that the majority of flow was in a different direction. Nevertheless, measurements were made wherever possible, and in this case the only suitable position found was near the wall of a cell.

Examination of the point velocity measurements in Figures 5.6 to 5.9 at four different flow rates with Re in the range 0.0817 to 0.1616 shows similar flow behaviour. All these measurements except one show higher values than the average velocity of flow. Close observation shows that these velocities are much nearer the average than their counterpart cells for Up-Flow.

At the inlet region, where the flow has just entered point velocities parallel to the corrugation are widely varied. Although the flow has already passed through the distribution zone, it is interesting to make the comparison of the maximum to minimum velocity values at 5.261, 5.525, 5.111 and 5.944 for increasing flow rates. These are similar values to those calculated in Up-Flow, confirming that poor distribution occurs in the initial stage. Furthermore, the flow appears to prefer a particular corrugation as observed previously in the Up-Flow.

In the inlet region, the values across the channel from left to right for all flow rates generally show a decrease of velocity to the right, except at the edges of the channel where an increase occurs caused by the return of flow at the end of the corrugations. The rates of maximum to minimum velocity ratio across the channel for the set 6.77 to 3.97×10^{-3} m/s of $Re = 0.0817$) was 3.368. Similarly for other Reynolds numbers the ratio was 3.21, 3.35 and 3.154 for increasing flow rates respectively. These ratios are slightly lower than for the inlet region of Up-Flow. The decrease in velocity across the channel can be explained by the sinusoidal wave effect taking place: the flow enters the channel initially on the left side of channel, some is distributed to the right but the majority remain on the left side until it turns towards the right further along the channel.

In the middle region, the velocities across the channel are higher; the ratios of maximum and minimum velocities are 3.074, 3.14, 3.3 and 3.012 for Figures 5.6 to 5.9 respectively. There is a slight decrease from the ratios at the inlet region but a ratio of 1 would be expected as an ideal case for a perfectly distributed profile. This shows that velocity profile is not perfectly developed...

The measurement on the right side of channel in this region, parallel to the corrugations, e.g. for $Re=0.1616$ values of 12.1, 14.6×10^{-3} etc., show that the majority of the flow is on this side but turns to the left within the measurement grid chosen as it progresses down the channel. The turn towards the left is confirmed by the high velocities parallel to the corrugations compared with the same level on the right hand side e.g. from 8.85 to 7.82×10^{-3} m/s. This trend is evident for all the other flow rates in this region.

In the outlet region, the velocities on the left side are higher than the right side as would be expected. Flow is combining in this area prior to leaving the channel. There is no set pattern for velocities across the channel but the ratios of maximum to minimum velocity are calculated to be 5.914, 3.703, 3.505 and 3.521 for increasing flow rates. For example, in the cells where the velocities are 14.4 to 4.78×10^{-3} m/s (see Figure 5.6 at $Re=0.1616$), these ratios are higher

than in the middle region, as opposed to the situation in Up-Flow, where the ratios in the middle and outlet region were nearly the same.

It is apparent that the majority of the flow has been collected from the left side of the middle region, to the left of the outlet region. Unlike Up-Flow there was no 'starvation' area in the outlet region, but there was such an area in the inlet region on the right side of the channel.

Examining the overall picture of flow measurements in Figures 5.6 to 5.9, the main feature is that cell velocities (except in one cell) are higher than the average velocity of flow. The ratios of maximum local velocity to the average velocity in a cell were found to be 8.116, 8.792, 7.873 and 7.975 for increasing Reynolds numbers. Although these are higher than traditionally expected (116), they are considerably reduced (by 34.23%, 25.74%, 33.45% and 27.32%) compared to the Up-Flow situation.

A statistical analysis of the three main regions, inlet, middle and outlet, using standard deviation is shown in Tables A-5.5 to 5.8 for Down-Flow. The calculation procedure was as outlined in Appendix A-5.1.

The measurements chosen for the three regions were taken across the channel for the purposes of calculating

the standard deviation. In the inlet region the chosen points were those on the highest position, e.g. for $Re = 0.0817$, the set 6.77 to 3.97×10^{-3} m/s. In the middle region, there is only one set of measurements across the channel, and in the outlet region, the measurements chosen were in those cells shown in Figure 5.6 where the velocities vary from 8.22 to 2.61×10^{-3} m/s.

Tables A-5.5 to 5.8 show that the standard deviation is increasing from the inlet to the outlet region. This is repeated for all the Reynolds numbers in the range examined. This shows that there is a significant increase in the spread of velocities when moving from one region to the next. These standard deviations are less than those calculated for Up-Flow: thus indicating that the variation of velocities across the channel is less in Down-Flow.

Turbulence was found to be higher at the edge of the channel than in the centre area, similar to Up-Flow, but the values are much higher compared to Up-Flow. In the inlet region the turbulence on the right side was twice that of the left side, a possible explanation for this is that since most of the flow is on the left side as shown by high velocities, the flow pattern is more fully developed (indicated by low turbulence). This is not the case on the opposite side of the channel, where the flow may be in different directions and could be unsteady at a point. Consequently calculated turbulence values would be high.

Turbulence in the middle and outlet regions were similar in value. Also as expected, the turbulences near the gasket are higher than in the centre of the channel. The increase at the edges of the channel has already been explained in the previous section on Up-Flow, but the higher values of turbulence in the centre of the channel need explanation. The possible and plausible explanation which can be put forward is that the flow is less fully developed compared to Up-Flow in the same regions.

Examining the overall flow distribution for Down-Flow for low flow rates, it is evident that the flow is following the sinusoidal wave path, i.e. most of the flow is shifting from the left (at the inlet) to the right, then back to the left (in the middle region), remaining on this side until leaving at the outlet. This behaviour of flow had been depicted by Fattah for $Re = 7$ using water, and, although the fluids and Re are different, laminar flow exists in both cases with strong similarities in the results.

The velocity measurements and turbulence calculations show that there is a difference between Up and Down-Flow, which could not be detected by Fattah. He found no difference in his study on the heat transfer section, but velocity measurements shown indicate difference in behaviour.

Finally, the velocity measurements show that there is mal-distribution during Down-Flow in the channel.

6.5 VELOCITY MEASUREMENTS ANALYSIS OF HIGH FLOW RATES

Velocity measurements were made at the higher Reynolds number, only in the Up-Flow mode of operation at $Re = 5.291$ and 7.078 .

6.5.1 REYNOLDS NUMBER 5.291

Figure 5.10 shows point values for the vertical component of velocity. This component was chosen because adjusting the beam splitter showed that the maximum flow was in this direction. The number of cells examined was reduced compared to experiments at the lower flow rates.

Nearly all the measurements were made in the centre of the cell volume but there were a few exceptions where measurements were made near the wall of the channel. In these positions it was difficult to correlate the centre flow, even after fine adjustments to the PM tube. It is suspected that the majority of the flow was in a different direction in these cells. Examination of the results shown in Figure 5.10 indicates that in the inlet region where the flow just enters the channel, the distribution is very good since the maximum to minimum velocity ratio is 1.448. This is three times less than found in the Up-Flow situation for low flow rates (see section 6.4.2). The values across the channel show variation, but the maximum to minimum velocity ratio is 1.567. This is nearly half that was found in low flow rate, of the inlet region. The flow is therefore more evenly distributed across the channel.

In the middle region, the velocities are lower compared to the inlet region, unlike the case during low flow rates. The maximum and minimum velocity ratio is increased to 7.302 across the channel. Although the ideal ratio would be 1 in this region because velocity profile should be developed, this is not the case. It was considered that the reduced velocity in the direction could be accounted for by an increase in velocity in other directions and this will be confirmed in section 6.7. It appears that a more uniform profile is established for this component than is the case during any of the previous flow rates. This distribution is well established until reaching the position where the velocity in the cell is 2.68×10^{-1} m/s, after this point there is a five fold velocity decrease across the full width of the channel. The last two measurements given are taken near the cell wall since the centre velocity had been reduced in the vertical component and the only reliable measurements that could be made was near the wall.

In the outlet region, the velocities increase compared to the middle region, with higher values at the left side of the channel compared to the right. This is expected since this is the region nearest to the outlet. The ratio of maximum to minimum velocity is 3.557, showing a velocity distribution well away from the ideal ratio of 1. The velocity measurements near the gasket edge of the channel, on the right side show areas where the velocity is reduced significantly.

Examination of the overall picture of flow measurements causes an interesting feature to emerge in that some velocities are less than the average velocity. Velocities as low as 45% of the average are observed, totally unlike velocity measurements discussed earlier. Even so, the maximum ratio of local to average velocity is found to be 11.22, which is very similar to Up-Flow ratios at low flow rates. It is difficult to explain clearly how such low velocities might exist without detailed additional investigations. It could be mainly due to preference the fluid elements take a particular path leading to maldistribution or it could be that there is a much higher velocity component in a different direction. The low velocities are more obvious near the right side at the edge of the channel. The flow in these cells is returning from the edge and flowing along the corrugation of the channel. Previous measurements were found to be relatively higher, see Figures 5.2 to 5.5. at the low flow rates, but for this vertical component they are low. Since the amount of flow passing along the channel is constant, then changes in velocities in one direction must mean that velocity components in another direction would also change to compensate.

Results of the standard deviation calculation across the channel for the three regions are summarised in Table A-5.8. These show that in the inlet region, there is a much higher variation in velocities than at low flow rates, but not for the middle and outlet regions.

These standard deviations are different from previous Up-Flow measurements where these are increasing as flow progresses up the channel.

Turbulence in the channel was computed at 0%. This may be due to fluid elements being much more "cohesive" in this region but spreading in different components as indicated by the changes in velocity when moving through the channel. Turbulence was high at the edges of the channel as expected (similar to low flow rates) showing unsteady flow.

From Figure 5.10 it is clear that there are regions where velocities are lower than the average velocity, which undoubtedly shows that there is some mal-distribution of flow. The velocity profile is not perfectly developed across the width of the channel as expected in the middle region. It appears that the majority of the flow remains on the port side of the plate.

6.5.2 REYNOLDS NUMBER 7.078

Examination of the results, in the inlet region, where the flow just enters, shows reasonable distribution with a maximum to minimum velocity ratio of 1.459. This ratio is only 0.745% higher than that calculated for Reynolds number 5.291. Nevertheless, it is still only one third that calculated for Up-Flow at low flow rates (see section 6.4.2). The velocities across the channel show variation, with the maximum to minimum velocity ratio being 3.069. This ratio is high because of one rather

low measurement at 2.77×10^{-1} m/s.

In the middle region, the velocities are lower than at the inlet in contrast to the low flow rates. The maximum and minimum velocity ratio is increased to 5.213 across the channel: but this ratio may be misleading because only two velocity measurements (at the edge of the channel on the right side) were low compared to the rest of the measurements. Such a decrease in velocity can be accounted for by an increase in other components of velocities (see also section 6.7).

In this region, the velocity profile is more uniform at the flow rate until the point is reached where the velocity is 4.17×10^{-1} m/s, beyond which the velocity drops significantly.

In the outlet region, the velocities decrease compared to the middle region. This behaviour is different from that at a Reynolds number of 5.291 and can be explained by increases in different components of velocity, since the flow across the width of plate for both middle and outlet region is equal. The velocities are higher on the left side compared to the right side of the channel. This is expected because the majority of the flow combines together in this area, ready to leave via the outlet port. The ratio of maximum to minimum velocity ratio is 1.681 across the channel, showing better distribution compared to the other regions.

Inspection of the overall picture of flow measurements shows that all but one of the velocities are higher than average. It is, of course, possible that there may be more cells which have velocities less than the average velocity. The ratio of maximum and average velocity is 13.68, which is 18% higher than the ratio in the previous section.

Standard deviations for each of the regions across the channel are shown in Table A-5.10. These standard deviations show that in the inlet region there is the highest variation of velocities, less variation in the middle region and even less variation (nearly one sixth of the inlet region) in the outlet region. These standard deviation trends are different compared to the lower Reynolds number of 5.291, with an interesting exception in the middle regions, where the standard deviations are nearly equal. This certainly shows that velocity patterns are very similar.

Turbulence values at this flow rate were similar to those observed at Re of 5.291. High turbulences were observed near the gasket while in the centre of the channel turbulence remained at 0% for all three regions. The increase of turbulence at the edges of the channel can be explained by variations of velocities and their components in these areas.

Figure 5.11 shows clearly mal-distribution exists in the channel, according to the measured velocities.

These velocity measurements strongly indicate that the velocity distribution is not ideal across the width of the channel as would have been expected in the middle region. It is apparent that once the flow has entered the channel, the majority of the flow tends to favour one side of the channel.

6.6 RELATING VELOCITY MEASUREMENTS AND PERFORMANCE CRITERIA

The analysis of the studies of flow through a single cell in the Junior PHE and the measured point velocities in the SR1 channel, would be incomplete unless a useful inter-relationship can be identified. Therefore a simple technique is developed of relating the two different measurements as a first step towards formulating a method of predicting flow distribution through this type of three-dimensional heat exchanger channel.

It is an acknowledged fact that the physical geometry of the SR1 plate is highly complex with valleys and peaks of the chevron corrugations crossing one another at an angle. Frequent point-to-point contact of the peaks occurs at the boundary of each cell resulting in a complex flow pattern through the interconnected grid of cells. The simplest description of flow through a chosen cell is that the fluid can approach from two directions, pass through the cell and leave in two directions (corresponding to the valleys in corrugations). The method that flow divides when leaving the cell, will have a profound effect on the flow distribution.

The analysis in section 6.2.2 and Figure 6.5 for the performance criteria of the Junior PHE cell showed that the ideal split in flow would be 0.5, but in practice, it was actually dependent on the pressure driving force of the fluid entering the cell. Originally, it was assumed that at some point along the length of the channel the flow was fully developed and ideal in the sense of the same flow rate of fluid passing through each cell. Although experiments on the SR1 channel proved this to be impossible, it was taken as the starting point for preparing a method of predicting distribution.

For example, consider the situation where there are five cells across the channel and the flow approaching these cells is perfectly distributed. Then let the flow in each cell split 60% towards the right and 40% towards the left. The flow distribution can then be computed as shown in Figure 6.13, as it progresses from row to row of the cells. Because of the geometry of the plates, alternate rows contain four cells so the flow towards the gasket must be redirected. The cells are staggered relative to the preceding row.

It is clear in Figure 6.13 how the flow pattern changes for the hypothetical set of circumstances chosen for this particular example and can be considered as a simple example of how mal-distribution occurs. It is equally clear that any flow network could be examined in similar fashion by a suitable computing technique.

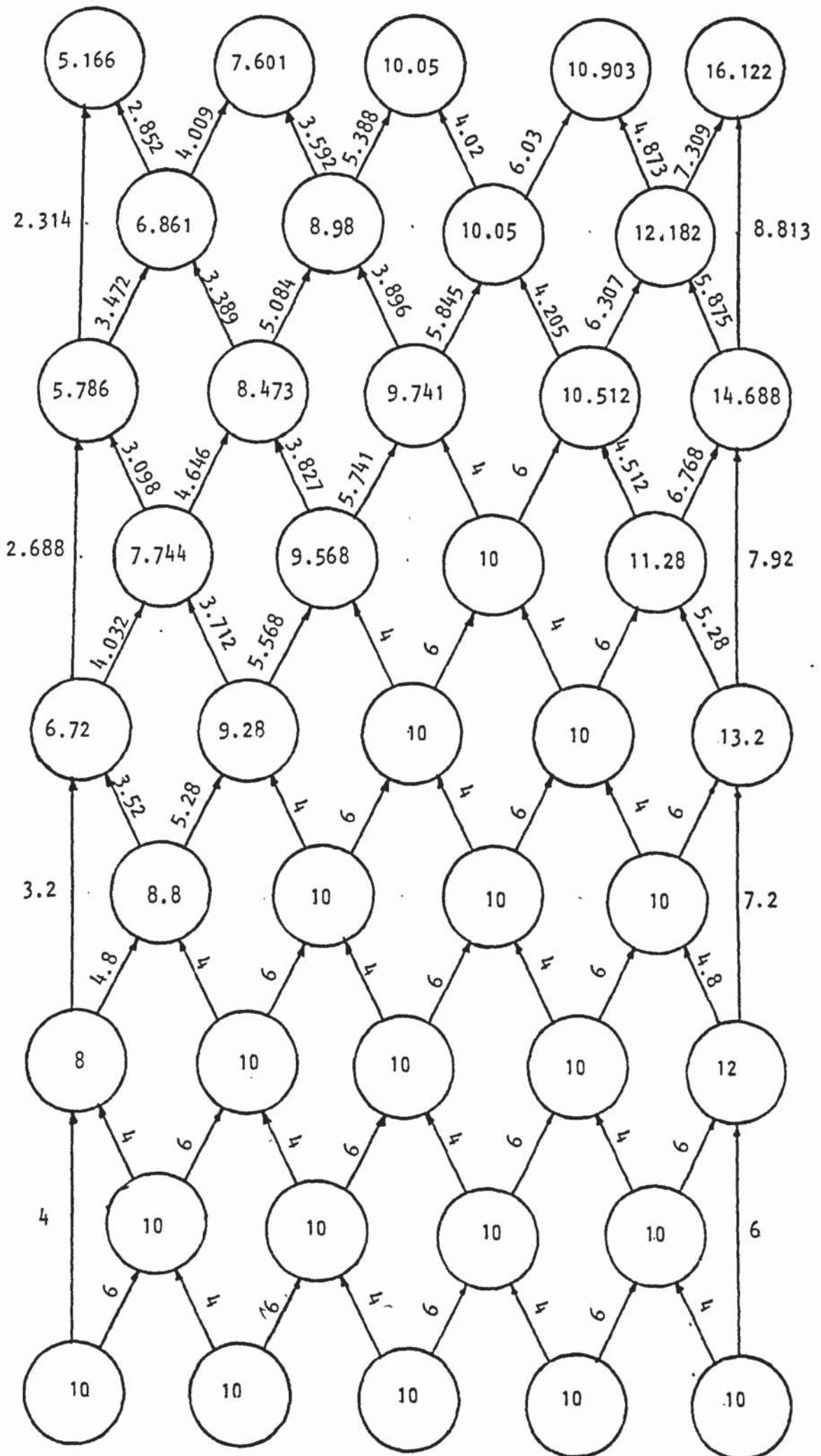


FIGURE 6.13 A SIMPLE DEVELOPMENT OF MAL-DISTRIBUTION IN CELLS

Further developments would be needed to evaluate the real situation starting from the channel inlet distributor.

6.7 ANALYSIS OF VELOCITY COMPONENT MEASUREMENTS

Measurement of different velocity components was initiated after the investigation of high flow rates at Re 5.291 and 7.078, since large reductions in velocity were observed when moving up the channel. Since the flow rate across the width of a channel is steady then the reduction of velocities in the vertical component may be explained by a corresponding increase in another component. Alternatively the experimental measurements could be seriously in error. Therefore a series of experiments was carried out to determine the cause of the observed pattern.

Three cells in the three regions were chosen for detailed examination at the positions shown in Figure 5.12. The vertical component for the inlet and outlet regions can be compared with corresponding results in Figure 5.11, because the chosen cells are common to both experiments. The velocities in these cells show that in the inlet and outlet region the velocities are only 5.343% and 2.791%, respectively higher than the earlier measurements; thus indicating that the results are repeatable with good agreement at a given point under the same flow conditions.

Examination of these results in more detail for the inlet region shows that the dominant

component is the vertical one with lower values of the other components. The velocity components at 45° to the horizontal, is lower by 16.79% and the other remaining component at 65° to the horizontal, is reduced by 30.92%

In the middle region, there is no single dominant component, indicating that the flow distribution is slightly more uniform. The velocity components at 45° and 65° to the horizontal are about 2.2 times higher than the vertical component.

In the outlet region, more velocity components were measured than in the other regions, since it was desirable to examine this cell in greater depth because of the variations in velocities observed in Figures 5.10 and 5.11. There is no doubt in Figure 5.12 that there is a significant variation in velocities among the components. The dominant velocity component is at 45° to the horizontal towards the left side and is 2.3 times greater than the vertical component. The dominant component arises from the fact that the flow is ready to leave at the outlet port. Since the port is positioned above and to the left of the cell, then most of the flow would follow the sort of path observed. It appears that the fluid elements prefer to follow 45° component at the particular point under the flow conditions in existence at the time.

Relative to the vertical component in that cell, the smallest velocity measured was 26.5% lower while

the highest was 2.3 times larger.

Examination of the overall flow component measurements shows clearly that large variations occur depending on the direction and the chosen position. The flow is more uniformly distributed in the middle region and remains so until near the outlet. The measurements clearly indicate the effect of component direction on the magnitude of the measured result.

6.8 VELOCITY MEASUREMENT ANALYSIS ACROSS SELECTED CELLS

The variations of velocities across chosen cells on both sides of the channel in the three regions are shown in Figure 5.13, for the vertical component. It was difficult to assess the exact position of measurement because of the complex geometry of the cells and the desire to determine velocities near to the point-to-point contacts bounding each cell. In some cells measurements are missing because most of the flow in the centre of the cell volume was in another direction, hence it was difficult to correlate in the vertical component. Some velocity measurements shown were measured previously and taken from Figure 5.11.

In the inlet region, the measurements in cell C' shows velocity in the cell centre to be 2.404 times the velocity at the edge of the cell; while in cell C, the velocities at the top and bottom of the cell are 6.683 and 1.25 times the centre velocity. The velocity on the horizontal axis at the edge of the cell is 3.885 times the centre velocity.

In the middle region, the measurements in cell B are generally higher than in cell B'. At the top of the cells, the velocity in B is 1.4 times the centre velocity of 3.26×10^{-1} m/s while in B' the corresponding velocity is 2.1 times the centre velocity which is only 1.6×10^{-1} m/s. The velocity in the horizontal axis at the edge of the cell B' is 1.203 times the centre velocity, while in cell B, the velocity across the cell, on one side is reduced by a factor of 2.86 the centre velocity and 1.126 times the velocity on the other side. The velocity at the bottom of cell B' is nearly equal to the centre, but in the cell B the velocity at the bottom is 34.35% lower compared to the centre velocity.

At the outlet region, in cell A', velocity at the top of the cell is 1.711 times the velocity in the centre whereas cell A contains a reasonably uniform velocity profile.

It is clear from Figure 5.13 that there are large variations of velocities across the cells in the horizontal and vertical directions. Velocities at the top of the cells are higher than measurements in other positions, due to flow coming together from all round the cell prior to moving to the next cell. In some positions, it was impossible to make measurements probably because the majority of the flow was in a different direction to that measured.

CHAPTER 7

CONCLUSIONS

7 CONCLUSIONS

7.1 JUNIOR PHE SINGLE CELL

The study of a single cell of the Junior PHE section provided the following conclusions:

- (i) The flow through individual inlet tubes show different distribution at the outlet from a cell. Better distribution is achieved using tube "B", where the outlet split is nearly equal as shown in Table 5.1. The distribution using tube "A" is divided into the average ratio of 5:1 at the outlet as shown in Table 5.2

Flow through both tubes simultaneously indicated (Figures 6.1, 6.2 and 6.4) consistently some of the flow from tube "B" inlet adds to the flow from tube "A" inlet.

Therefore there is more resistance on the tube "A" side, for flow to split up compared to flow through tube "B" inlet.

- (ii) The performance of a single cell showed that the pressure levels influence the flow distribution. The tested distribution, approaching ideality, was achieved when there was equal pressure in both inlet tubes.

7.2 SR1 VELOCITY MEASUREMENTS

The study on SR1 plate channel provided the following conclusions:

- (i) Laser Doppler Anemometry can be successfully applied to the study of the hydrodynamic characteristics in a PHE channel. This technique is especially successful when a refractive-index matched liquid, e.g. a mixture of cod-liver oil and tung oil is used as the working fluid. Although measurements are possible using water, repeatability and reliability of these measurements is not possible for two reasons. Firstly, laser beam flare at the solid-fluid boundaries was a major problem, causing saturation of the photomultiplier tube, and, secondly, the great difficulty encountered when attempting to ensure that the laser beams intersected properly in the cell volume, due to the complex internal geometry of the channel. Although the former could be partially solved, the latter is impossible to overcome consistently to produce reliable results.

- (ii) The surface quality is a prime factor influencing the LDA signal quality. Regular polishing of the perspex surfaces using perspex polish is an absolute necessity for good signals to be obtained.

- (iii) Significant differences exist between Up-Flow and Down-Flow contrary to the previous opinions held by Fattah (7) who found no difference between the two types of flow. Evidence of these differences is shown in point velocity measurements in Figures 5.2 to 5.5 and Figures 5.6 to 5.9 for Up-Flow and Down-Flow respectively, and in the calculated values of standard deviation shown in Tables A-5.1 to A-5.4 and Tables A-5.5 to A-5.8.
- (iv) At low flow rates, $Re < 1$ the majority of the flow is parallel to the channel corrugations, in both Up and Down Flow, with the major velocity component at 60° to the vertical. At higher flow rates, $Re = 5.291$ and 7.078 the maximum velocity was observed in the vertical component, with further confirmation in Figure 5.12 for the inlet region. However, at higher Reynolds number, the components with maximum flow varied with the region in the channel under consideration.
- (v) At low flow rates with $Re < 1$, in Up-Flow, the flow followed a sinusoidal wave path, with most of the flow shifting from the left (at the inlet) to the right (in the middle region) and back to the left (at the outlet region) of the channel. This path was very similar to the one observed by Fattah (7) for 65.5% aqueous glycerol using dye injection technique.

In the Down Flow for $Re < 1$, most of the flow shifted from the left (at the inlet) to the right but then some came back to the left (in the middle region) remaining on this side and leaving at the outlet, giving a more uniform distribution. This flow path was similar to the one depicted by Fattah for a somewhat higher Re of 7 using water in Down-Flow.

At high flow rate, Reynolds number 5.291 and 7.078, the overall distribution shows that most of the flow remained in one half of the channel, the velocity profile does not uniformly develop across the channel in the middle region, contrary to expectation.

- (vi) At low flow rates, the fluid leaving the inlet distributor was not evenly spread, ratios of maximum to minimum point velocities varied between 4.568 and 5.442 in the Up-Flow mode. This ratio was even higher in Down-Flow: varying between 5.261 to 5.944 for the varying Reynolds numbers examined.

At high flow rates there was more even distribution in this region during Up-Flow. The velocity ratio was lower at 1.448 and 1.459 for Reynolds number 5.291 and 7.078 respectively.

- (vii) At low flow rates, local velocities measured in the cells were higher than the overall average velocity for Up and Down Flow. In Up-Flow, the

ratios of local velocity in a cell to the average velocity were found to be 12.34, 11.84, 11.83, and 11.00 for Reynolds numbers 0.087, 0.1028, 0.1293 and 0.1616 while for Down-Flow these ratios were lower by 34.23%, 25.74%, 33.45% and 27.32% respectively for increasing Reynolds numbers. Measurements during Up-Flow for the horizontal component of flow in cells on the vertical centre line of the channel produced a maximum ratio of 27 times the average velocity.

However, at high flow rates of Reynolds number 5.291, some velocities were found to be lower than average velocity, even though the maximum ratio of local velocity to average velocity was 11.22, similar in value to low flow rates. For $Re=7.078$, velocities were higher than the average velocity and the ratio of maximum velocity and average velocity was 13.69, 18% higher than the ratio for $Re=5.291$.

(viii) Measurements taken across the channel for low flow in the Up-Flow direction showed a range of maximum to minimum velocity ratios in the inlet region somewhat different to the middle and outlet regions as shown by calculations in sections 6.4.2. The extremes of variations between the latter two regions were 2.96% and 0.041% (for $Re = 0.0817$ and $Re=0.1293$) respectively. In the Down-Flow, there

was a decrease in the maximum and minimum velocity ratio across the channel, between the inlet and middle region. The extremes in the changes were 8.729% and 0.492% for $Re=0.0817$ and $Re=0.1293$. The ratio range increased between the middle and outlet regions; for $Re=0.0817$, the increase was a factor of 2, but for other flows was between the extremes of 15.2% and 5.8% for $Re=0.1028$ and $Re=0.1293$ as shown by ratio calculation in section 6.4.3.

At high flow rates with Reynolds numbers 5.291 and 7.078, measurements in Up-Flow showed that the range of maximum to minimum velocity ratios in the inlet region was nearly half that observed for low flow rates. However, there is an increase in the range between the middle and inlet regions of 4.66 times and 1.70 for Reynolds numbers 5.291 and 7.078 respectively. Moving from the middle region to the outlet region resulted in a decrease in maximum and minimum velocity ratio ranges across the channel 51.29% and 67.75% for increasing Reynolds numbers.

- (ix) Maldistribution was identified across the channel width. A criteria of performance for individual cells is proposed as a step towards an understanding of mal-distribution.

(x) The velocities measured are dependent on directions as shown by Figures 5.1 and 5.5 for $Re=0.1616$ on the horizontal and 60° components. Velocities with direction in the various regions of the channel are shown in Figure 5.12. For each region, the dominant components are:

- (i) Inlet - Vertical component
- (ii) Middle - no dominant component
- (iii) Outlet - 45° to the horizontal component

for $Re=7.078$, for overall Up-Flow direction as analysed in section 6.7.

(xi) There is a variation of velocity across individual cells, dependent on position in the channel as shown in Figure 5.13. Velocities are generally higher at the top (outlet) of the cell, e.g. in the inlet region, the velocity at the top of a cell was 6.683 times the velocity in the centre of the cell. In the middle section, this ratio decreased to 1.4 but increased slightly to 1.711 in the outlet region. In the inlet and middle regions the velocity is generally lower in the centre of the cell, compared to measurements at the edges of the cell. But in the outlet region, velocities at the edges of the cell diminish by about 9.5% at least, compared to the centre value. The velocities across the cell's horizontal axis can be as high as 3.885 times the centre velocity (as analysed in section 6.8).

Furthermore there is variation of velocity across the cell from back to front, i.e. in the third dimension of the channel, as shown in the top region of Figure 5.1.

Finally, the velocity measurements made are certainly repeatable as the comparison measurements (in brackets measured previously) shown in Figure 5.13.

CHAPTER 8

RECOMMENDATIONS FOR FURTHER WORK

8 RECOMMENDATIONS FOR FURTHER WORK

The implications of the present research work on design methods for PHE are examined by directions that future work of this type should take. The overall objectives of this project would be two fold: firstly to define completely the flow patterns established in this type of channel during laminar flow and examine ways of controlling the flow patterns; and secondly to generate mathematical models for the velocity and shear stress profiles at any position for given conditions, so that the heat transfer coefficient could be estimated locally using the heat and momentum transfer analogies. The following recommendations for further work are prepared:

8.1 SINGLE CELL

- (i) Any perspex section of a single cell should be fixed more rigidly than was the case with the rig used in the current work to establish the viability of the technique. Movement of the cell section should be avoided while a test is in progress.

- (ii) A small injection of the dye could be introduced into one of the inlet tubes with the apparatus arranged so that continuous, controlled flow could be achieved. The split of flow could then be analysed by measuring dye concentration in each outlet, and hence the performance criteria would be calculated and compared with the present work.

- (iii) The tube inlets and outlets could be inclined at the same angle as the corrugations, to approximate more closely to the actual fluid path approach to a cell. The work could be repeated, with dye injections if possible into one of the tubes and observing the division of flow as outlined above.

- (iv) The feasibility of experimenting with a single cell constructed from stainless steel should be considered. Any change in performance could then be attributed to the change in surface in contact with the fluid.

8.2 LASER DOPPLER MEASUREMENTS

The extension of research work using Laser Anemometry can be developed as follows:

- (i) Examination in greater detail of all cells in the PHE channel:
 - (a) Measure velocities at a large number of points within a cell to establish the full, three-dimensional velocity profile within the cell. Hence the shear stress profile can be estimated. It is expected that a frequency shifting device would be essential to ensure directional discrimination when investigating points between the front and back surface of the cell. In the present set-up the LDA equipment, a suitable device would be Electro-optic phase

Modulator available from Malvern Instruments at about £2000. This modulator can be attached to or in front of the beam splitter to provide minimum adjustments once the LDA equipment is arranged.

- (b) Modifications should be made to the moving system of the perspex channel in order that positioning and alignment can be simplified. A sophisticated optical x-y-z table would be necessary so that fine adjustments within each cell can be made with the maximum adjustment.
- (ii) Higher flow rates should be investigated in both the quasi-turbulent and turbulent regions. A frequency shift device would then be essential to determine vectors, and difficulties will be encountered in obtaining suitable flow rates of a refractive index matched liquid.
- (iii) The effect of heat transfer on velocity distribution should be studied with a modified rig incorporating a channel pack. A perspex plate could be used on the cold fluid side to allow visual observation. The hot side could be a channel containing hot liquid, condensing vapour or a specially fabricated, electrically heated plate to provide a constant heat flux.
- (iv) A considerable amount of information on the flow at a point can be obtained if more than one

velocity component is measured simultaneously. It is possible to measure two components of velocity in the same probe volume by forming two superimposed set of fringes. These can be obtained from an argon ion laser, which, when operating in "all-line" mode would provide both blue and green fringes (11). Two detectors would be required to observe the intersection volume and two correlators to analyse each set of signals. The addition of frequency shift would result in a very useful research tool.

8.3 GENERAL DEVELOPMENT

Further development can be carried out in two main sectors of computation:

- (a) A mathematical description of the channel could be prepared in a matrix element from where each matrix element represents one cell. The effect on distribution of various values of the ratios of flows leaving a cell can then be examined. The predicted velocity profile could be compared with the measured velocity profile.
- (b) The computer program developed (133) to show point velocities measurements in the channel can be extended to represent point velocities in a better form. This would be done by replacing the value by an arrow, where the length of the arrow represents the velocity and the direction of the arrow shows the direction of the component

measured.

- (c) These two programs can also be linked together where measurements predicted from (a) can be plotted on the channel representation in (b).

APPENDIX A - 1.0

A-1.0 GENERAL DESCRIPTION OF THE COMPUTER SYSTEM
AND PROGRAM FOR ANEMOMETRY

As indicated earlier in Section 2.5, a computer system was used in conjunction with the LDA equipment. This will be discussed in sections relevant to this project.

A-1.1 BACKGROUND

A computer system known as the 6022 Malvern data processor was used. It is an integrated desk-top computer designed to give the Malvern correlator K7023 and its Anemometry system an on-line sample to answer capability. The programs are written in high-level BASIC, and can be loaded from tape using an integral cassette unit.

For a detailed operation of the data processor and description of the system see reference (30).

A-1.2 DESCRIPTION OF APPLICATION PROGRAM FOR LASER
ANEMOMETRY

The program used in this study was entitled 'Malvern application program', which was provided by Malvern Instruments on a cassette tape.

The tape contains two sections; the first called the 7023ML Loader and the second the application program. The cassette is placed into the cassette unit, the "SHIFT" key held down and press and release the RUN/STOP key, finally releasing "SHIFT", causing the first

section to be played in, taking about 30 seconds to load. This is then followed by an automatic link load of the following section. About 6-8 minutes are required to load this programme. Once this is complete, the algorithm is ready to be used. A general structure of the program is shown in Figure A-1.1.

A dialogue starts with the data processor, when several parameter values are requested, as listed in Table A-1.1.

Most parameters are self-explanatory but some require further explanation and are outlined below. The brackets show current value automatically assigned by the program.

- (1) The Laser wavelength 6328°A , was marked on the Laser.
- (2) Beam Radius had to be calculated, because a lens was used to sharpen the beams as recommended by Abiss et al. (24), see also Appendix A-20.
- (3) The Laser beam radius was 550 microns (available from the Laser manual(123)).The focal length of the lens was measured to be 14.4cm.
- (4) Fringe spacing was calculated by providing values of beam separation and distance to beam crossing, (both of these were measured for each individual experiment).

Parameter	Value
Is a printer attached (= NO)	Yes
Printers IEEE-488 Address (=4)	
Laser Wavelength - A° (=6328)	
Beam Radius - microns (=250)	
Enter Value, or "C" to calculate	C
Laser beam radius - microns (= 700)	550
Lens focal length - Cm (= 10)	
1 - 100 Cm valid range	14.4
Beam radius - microns =	52.737119
Fringe spacing - microns (= 15.82)	
Enter Value, or "C" to calculate	C
Beam Separation - mm (= 20)	
Distance to beam crossing - Cm (= 50)	
Fringe spacing =	
Is frequency shift used (Yes/NO)	No

TABLE A-1.1 - Questions requested by the Program

- (5) The special frequency shift accounts for fringe movement relative to the particle, but this option was not used in the current work.

Once the data for the experimental conditions are completed, then the programme provides the following choices as shown in Figure A-1.1:

- (i) change in experimental parameters
- (ii) enter Auto-sequence program
- (iii) execution of experimental program
- (iv) enter the error list

The Auto-sequence program provides selection of four different displays on the oscilloscope of the K7023, these options are:

- (a) static display
- (b) static display with pause
- (c) dynamic display
- (d) dynamic display with pause.

The user can choose any one of these display options to observe the correlation function when making measurements.

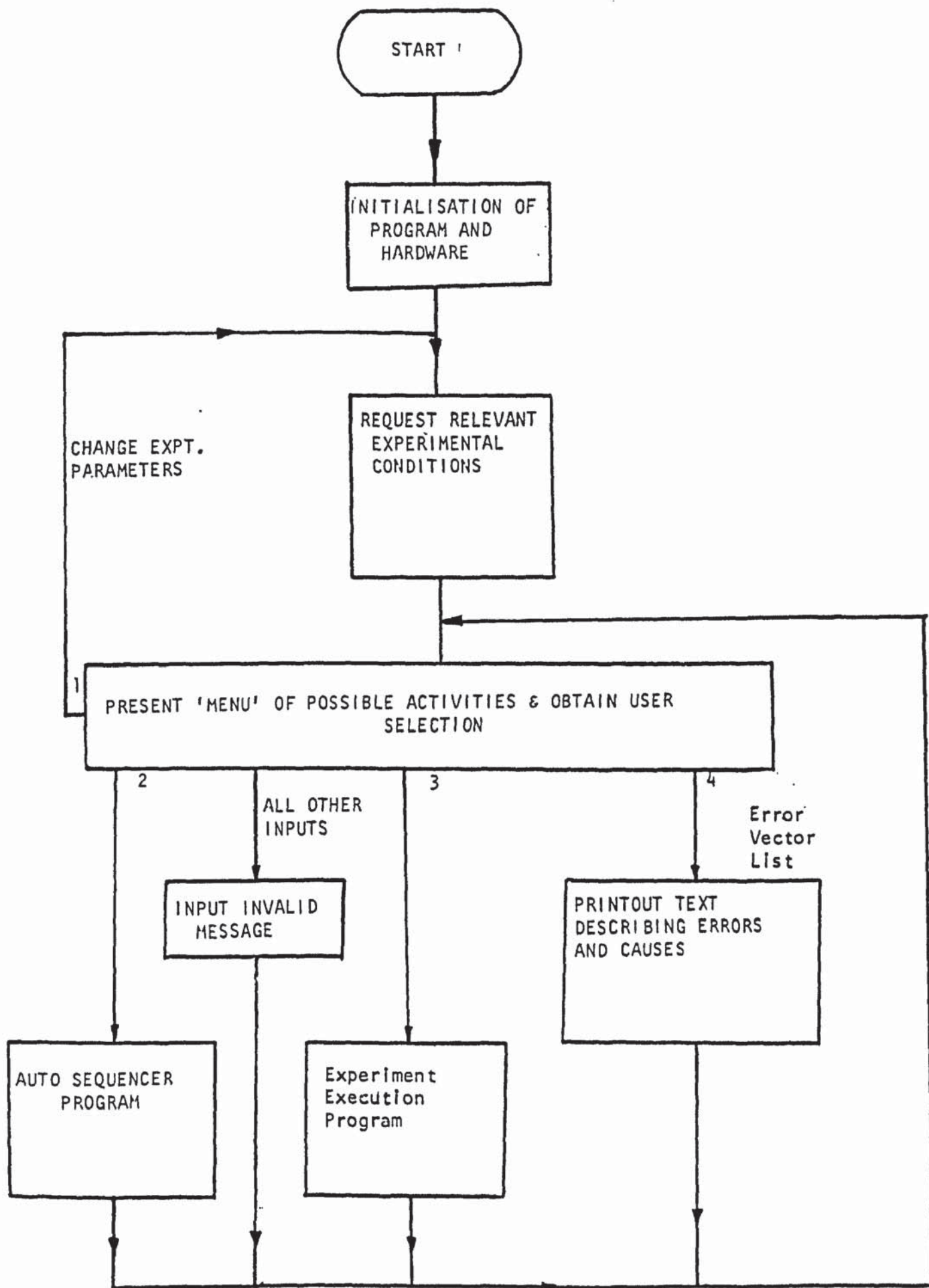


FIGURE A-1.1. GENERAL STRUCTURE OF MALVERN APPLICATION PROGRAM

The execution program follows the block structure as shown in Figure A-1.2. The first block holds a dialogue with the user which requests the correlator frontpanel information, e.g. sample time, and reminds the user of the parameter values used. Then the program provides a choice of single shot or continuous run operation; single shot being one experiment only and the result calculated, while the continuous selection will cause a sequence of experiments to be performed with a full set of results displayed.

When these run options are completed the processor displays a page summary of the current values of the experimental and correlator parameters as a header to any result generated. The program allows the user to run the programme, or change parameters or abort the program completely as shown in Figure A-1.2.

The Malvern application program provides a further facility where some of the information can be directed to a line printer.

In order to preserve the result, a line printer Newbury 8300S was attached to the data processor with an interface IEEE-488 connector.

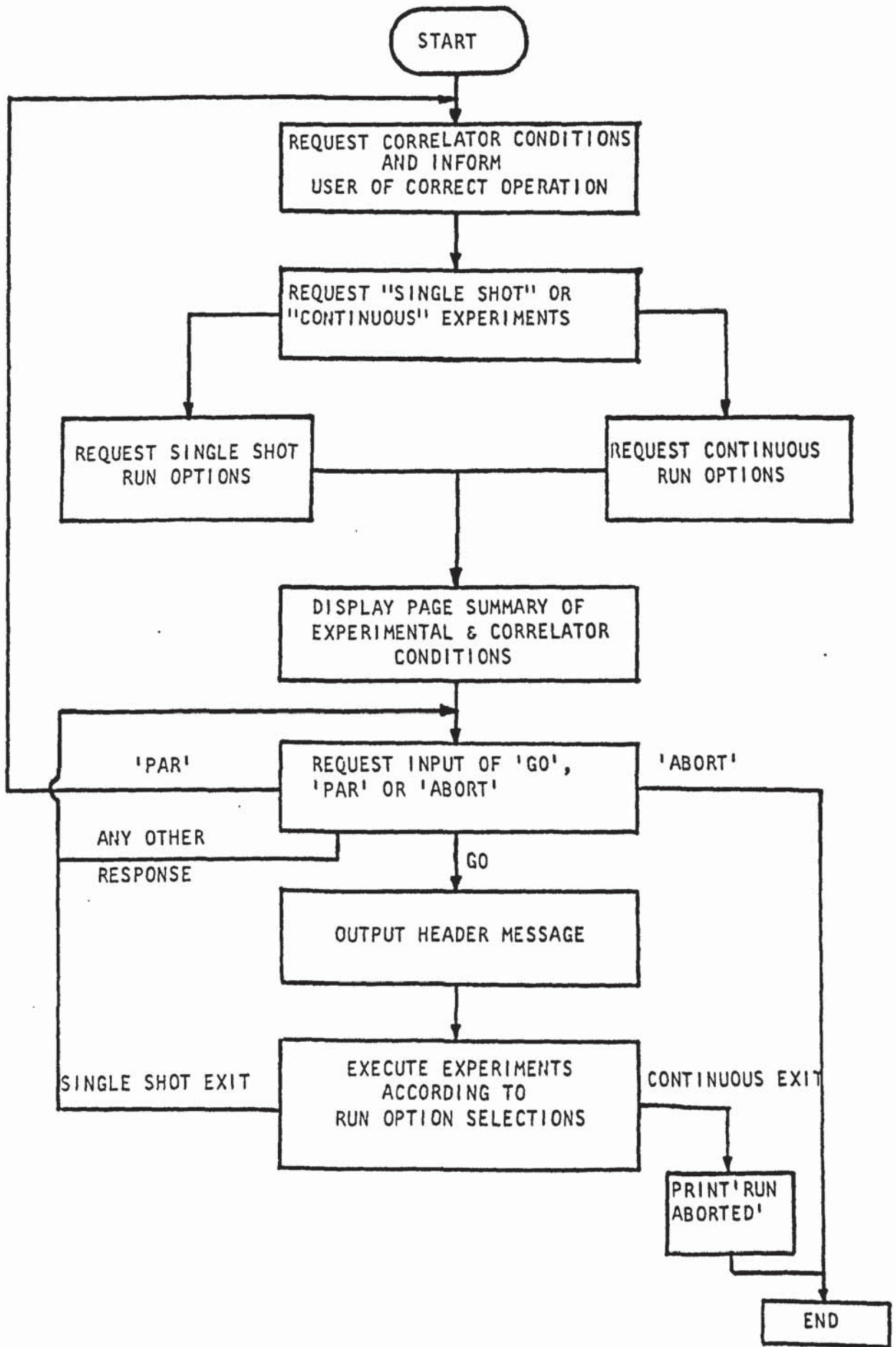


FIGURE A-1.2. STRUCTURE OF EXPERIMENTAL EXECUTION PROGRAM

APPENDIX A - 2.0

A-2.0 CALCULATION OF BEAM RADIUS AT FOCUS

To calculate the velocity of flow using the "Malvern Program" it was necessary to provide a value for the beam radius at the crossover point. Although the beam radius of the laser light leaving the laser is 0.5mm, this can be changed by using a suitable lens and has to be calculated at the point where the beams intersect.

The operating manual (29) provides a formula to calculate the beam radius r_f at focus:

$$r_f = \frac{4\lambda F}{\pi r}$$

where F = focal length of the lens

λ = wavelength of laser light

r = beam radius of the laser.

This was checked in the "Malvern Program" but a different formula was listed:

$$r_f = \frac{\lambda F}{\pi r}$$

To clarify this inconsistency, a few text books were consulted, and a variation in formulas was found.

For example Rudd (22) and Drain (11) agree with the equation in the program, but Durst et al. (13) provide a different formulae

$$r_f = \frac{5}{4} \frac{\lambda F}{\pi r}$$

Greated and Durrani recommend (20) $r_f = \frac{\lambda F}{2\pi r}$ and

Adrain (33) provides $r_f = \frac{2\lambda F}{\pi r}$

It was difficult to decide which equation was the most accurate, since they differ by a factor of up to 4. The operating manual pointed out this was an approximate expression and it has only marginal impact on the calculation of velocity. Therefore it was decided to use the existing equation, in the "Malvern Program" particularly since this was the most common expression appearing in the text books (11,13).

The calculation for the beam radius as focus is shown below, for He-Ne laser Wavelength $\lambda = 632.8\mu\text{m}$, beam radius $r = 0.5\text{mm}$, and focal length of lens $F = 14.4\text{ Cm}$;

Using equation $r_f = \frac{\lambda F}{\pi r}$

$$\text{Substituting data } r_f = \frac{632.8 \times 10^{-6} \times 14.4 \times 10^{-2}}{3.142 \times 0.5 \times 10^{-3}}$$

$$\therefore r_f = 52.731129 \times 10^{-6} \text{m.}$$

This value was calculated by the program and used in further calculation as mentioned previously in Appendix A-1.1.

APPENDIX A - 3.0

A-3.0 CALCULATIONS OF REYNOLDS NUMBER

A-3.1 PARAMETERS OF SR1 PLATE

The formula for the calculations of Reynolds number were adopted as standardised by Fattah (7).

The parameter listed below are provided by APV Ltd., for SR1 plate:

$$\phi = \frac{\text{Developed Heat Transfer Area}}{\text{Projected Heat Transfer Area}} = 1.22$$

The equivalent diameter (D_e) = $4.7498 \times 10^{-3} \text{ m}$

Plate width (W) = 0.171m

$$\begin{aligned} \therefore \text{Plate gap (b')} &= D_e \left(\frac{\phi}{2} \right) = 4.7498 \times 10^{-3} \times \frac{1.22}{2} \\ &= 2.89 \times 10^{-3} \text{ m} \end{aligned}$$

A-3.2 CALCULATION OF REYNOLDS NUMBER USING WATER

The maximum flow rate was at tube reading 100 on the flowrator as shown in calibration Figure 4.12. Then the maximum Reynolds number would be:

$$\begin{aligned} \text{Mass flow rate (G)} &= 710 \times 10^{-3} \text{ kg/min} \\ &= \frac{710}{60} \times 10^{-3} \text{ kg/s} \end{aligned}$$

$$\text{Volumetric flowrate (Q)} = \frac{G}{\rho} = \frac{710}{60} \times \frac{10^{-2}}{10^3} = 11.833 \times 10^{-4} \text{ m}^3/\text{s}$$

Hence

$$\begin{aligned} \text{Average Velocity } u &= \frac{Q}{b \cdot w} = \frac{11.833 \times 10^{-6}}{2.89 \times 10^{-3} \times 0.171} \\ &= 23.944 \times 10^{-3} \text{ m/s} \end{aligned}$$

∴ Reynolds number (Re)

$$\begin{aligned} &= \frac{\rho D u}{\mu} = \frac{10^3 \times 4.7498 \times 10^{-3} \times 23.944 \times 10^{-3}}{10^{-3}} \\ &= 113.73 \end{aligned}$$

Similarly following the calculation as above for tube reading 10 provided Re = 4.54, average velocity = 0.9558×10^{-3} m/s.

Following above calculations at a tube reading 15 Re = 10, average velocity = 2.105×10^{-3} m/s.

Therefore laminar flow exists on the flowrator until scale reading 15.

A-3.3 CALCULATION OF REYNOLDS NUMBER USING OIL

The maximum flow rate was at tube reading .00 on the flowrator as shown in calibration curve in Figure 4.13. Then the maximum Re can be calculated at oil temperature 20°C.

$$\begin{aligned} \text{Mass flow rate (G)} &= 89.98 \times 10^{-3} \text{ kg/min} \\ &= 1.4997 \times 10^{-3} \text{ m/s} \end{aligned}$$

Then

∴ Volumetric flow rate (Q)

$$= \frac{G}{\rho} = \frac{1.4997}{0.9295} \times \frac{10^{-3}}{10^3} = 1.6134 \times 10^{-6} \text{ m}^3/\text{s}$$

Average velocity (U)

$$= \frac{Q}{b'w} = \frac{1.6134 \times 10^{-6}}{2.89 \times 10^{-3} \times 0.171} = 3.265 \times 10^{-3} \text{ m/s}$$

∴ Reynolds number (Re)

$$= \frac{\rho DeU}{\mu} = \frac{0.9295 \times 10^3 \times 4.7498 \times 10^{-3} \times 3.265 \times 10^{-3}}{0.0927}$$

∴ Re = 0.1555

When operating temperature was increased to 22°C, the calibration in Figure 4.13 was not affected significantly, so it was decided to maintain this calibration but calculate the new Reynolds number because of slight changes in the physical properties.

The new physical properties were at 22°C.

$$\rho = 931.98 \text{ kg/m}^3$$

$$\mu = 0.08986 \text{ Kg/ms}$$

and using the above calculation procedure range of average Reynolds number and velocity were calculated for the flowrator used as shown in Table below:

TABLE A-3.1 REYNOLDS NUMBER RANGE FOR LOW FLOW RATE MEASURED

Flowrator Scale Reading	Reynolds Number (Re)	Average Velocity U (m/s) x 10 ⁻³
100	0.1616	3.254
90	0.1293	2.604
80	0.1028	2.07
70	0.0817	1.645

Therefore the range available on the flowrator is in the laminar flow regime.

A-3.4 CALCULATION FOR HIGHER REYNOLDS NUMBER USING OIL

It was extremely difficult to measure the effluent leaving the channel at higher flow rates, although still remaining in the laminar flow regime, that is ($Re < 10$). Therefore a procedure was developed to estimate the Reynolds number.

Since the maximum flowrate was measured for water and oil for earlier calibrations (see section 4.3.2 and 4.3.4) using the same flowrator and the float, this provides the ratio of water and oil flow rates. Hence this ratio can be used to estimate the flow rate of oil in the larger modified equipment described in section 4.3.5 when compared with manufacturer's calibration curve for water.

ROTAMETER : FISCHER & PORTER ½FP-17G-10

FLOAT : ½GUSVT-410

Maximum water flow rate = 710×10^{-3} kg/min.

Maximum oil flow rate = 89.98×10^{-3} kg/min.

$$\therefore \text{Ratio of water : oil} = \frac{710 \times 10^{-3}}{89.98 \times 10^{-3}} = 7.891$$

So there is a reduction in flowrate of oil by 7.891 times.

ROTAMETER : METRIC SIZE TUBE SIZE 47F

FLOAT : STAINLESS STEEL S SIZE 47

Using the larger modified equipment the flow rate of oil at tube reading 3 can be estimated. The manufacturer's calibration curve shown in Figure A-3.1, provides the water flow rate at this position 19.8 kg/min, then the amount of oil leaving the same equipment would be:

$$\text{Oil Mass flow rate (G)} = \frac{19.8}{7.891} = 2.509 \text{ kg/min}$$

To calculate the Reynolds number for this flow rate, one assumption has to be made. That is there is not a significant difference in flow rates at different temperatures of fluids.

Then at operating temperature of oil of 34°C, the new physical properties were required. Density, was measured to be 933.98 kg/m³ but viscosity changed which was calculated from equation 4.1

$$\rho = 933.98 \text{ kg/m}^3$$

$$\mu = 0.05678 \text{ kg/ms}$$

FLOAT: STAINLESS STEEL S SIZE 47
ROTAMETER: METRIC SIZE TUBE SIZE 4.7F

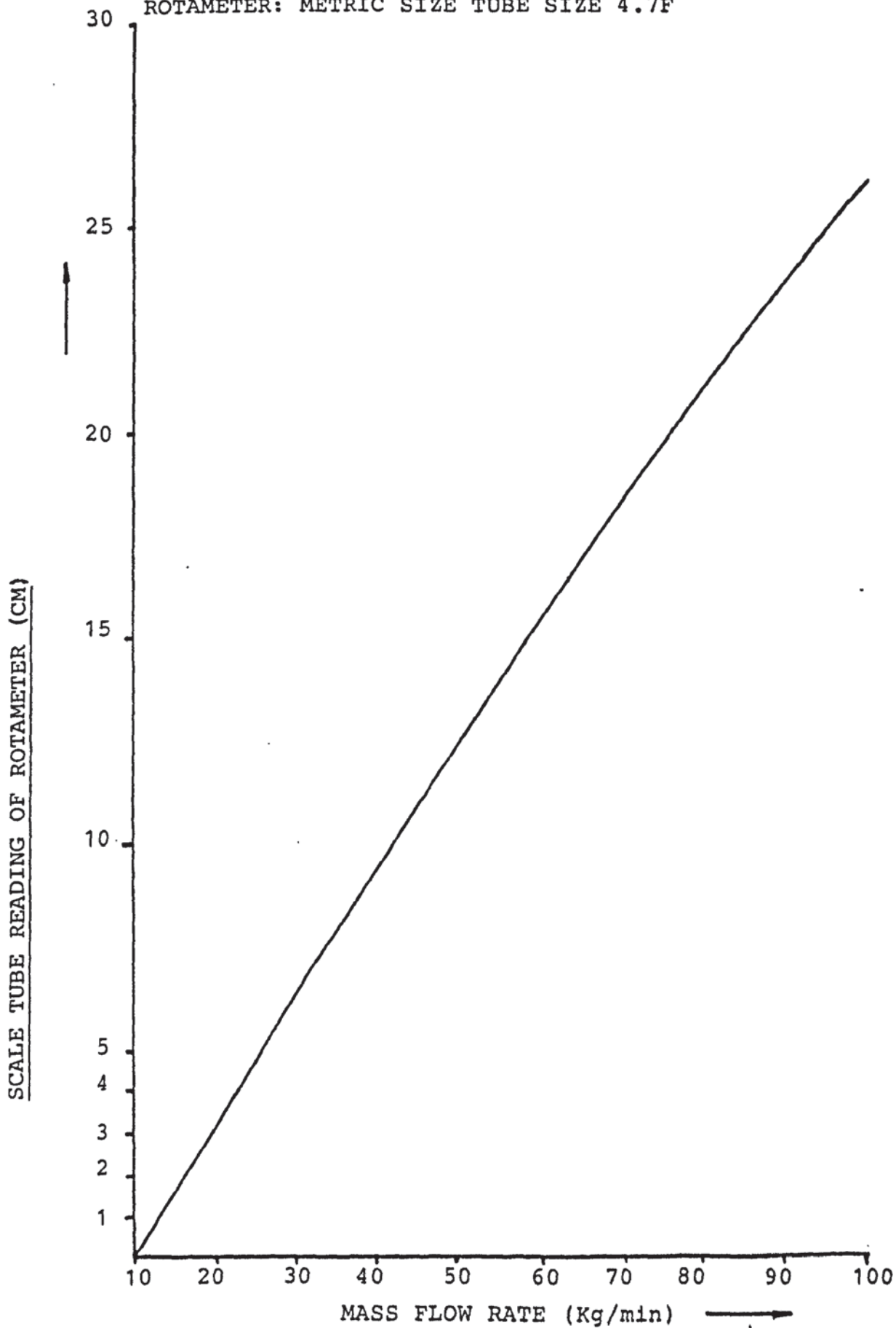


FIGURE A-3.1 CALIBRATION CHART FOR WATER

Then following the calculation procedure in A-3.2, $Re = 7.078$ and average velocity = 9.0598×10^{-2} m/s.

For the flow to remain in laminar regime, that is $Re < 10$ the float should remain below tube reading 6.

Table A-3.2 summarises the Reynolds number and average velocity for particular positions on the scale reading of the flowrator where measurements were made in the laminar regime.

TABLE A-3.2 REYNOLDS NUMBER RANGE OF HIGH FLOW RATE

MEASURED

Flowrator Scale Reading	Reynolds Number (Re)	Average Velocity U (m/s) $\times 10^{-1}$
3	7.078	0.906
1.5	5.291	0.6772

APPENDIX A-4.0

APPENDIX A-4.0 CALCULATION FOR PERFORMANCE OF SINGLE CELL FOR THE JUNIOR PHE SECTION

The basic method to quantify the performance of a single cell would be by relating output and input flows for various operating conditions. A basic relationship is shown below for a single experimental run.

Let

Total calculated flow for input tubes A and B

$$= Q_T = Q_{CA} + Q_{CB}$$

Flow measured at Tube "A" outlet = Q_{MA}

and Flow measured at Tube "B" outlet = Q_{MB}

Then the performance of cell based on individual tubes, K_A and K_B , is given by $\frac{\text{Flow outlet of a tube}}{\text{Total flow input}}$

$$\text{for Tube A } K_A = \frac{Q_{MA}}{Q_T}$$

$$\text{and Tube B } K_B = \frac{Q_{MB}}{Q_T}$$

Using the performance criteria, K_A and K_B , calculations were carried out for the tabular results of 5.3 to 5.7 and shown in Tables A-4.1 to A-4.5.

In these tables the performance criteria K_A and K_B do not always satisfy the condition $K_A + K_B = 1$ in some cases this is simply due to slight variation between the total input and total output of flow to the single cell. For these runs $K_A + K_B > 1$, maximum variation was 2%, and for $K_A + K_B < 1$, maximum variation was 10%.

If K_A and K_B had the value of 0.5, then the flow situation would be ideal, i.e. the input to a cell, from whatever direction, would be equally divided into the two outlets. The further the actual values are away from 0.5 the less ideal is the flow split in one cell. Then the hydrodynamic behaviour is biased in one direction with consequent impact on flow patterns and heat transfer .

TABLE A-4.1 PERFORMANCE OF SINGLE CELL FOR BOTH TUBES
AT SAME INITIAL PRESSURE

Run No.	Flow Measured at outlets		Total Calculated input flow Q_T (Cm ³)	Performance criteria of single cell based on	
	Q_{MA} (Cm ³)	Q_{MB} (Cm ³)		Tube "A" K_A	Tube "B" K_B
1	5	16.5	21.02	0.2378	0.7849
2	22	26	47.41	0.464	0.5484
3	18.5	21	38.26	0.4835	0.5488

TABLE A-4.2 PERFORMANCE OF SINGLE CELL FOR BOTH TUBES
AT DIFFERENT INLET INITIAL PRESSURES

Run No.	Flow Measured at outlets		Total Calculated input flow Q_T (Cm ³)	Performance criteria of single cell based on	
	Q_{MA} (Cm ³)	Q_{MB} (Cm ³)		Tube "A" K_A	Tube "B" K_B
1	13	21	32.73	0.3972	0.6416
2	10	11	23.76	0.4209	0.5051
3	19	25	48.27	0.3936	0.5179

TABLE A-4.3 PERFORMANCE OF SINGLE CELL FOR DOUBLE ONE INLET PRESSURE

Run No.	Flow Measured at outlets		Total Calculated input flow Q_T (Cm ³)	Performance criteria of single cell based on	
	Q_{MA} (Cm ³)	Q_{MB} (Cm ³)		Tube "A" K_A	Tube "B" K_B
1	11	14	27.5	0.4	0.5091
2	12	10.5	23.94	0.5012	0.4386

TABLE A-4.4 PERFORMANCE OF SINGLE CELL FOR TUBE "B" OPENED FIRST AND THEN TUBE "A"

Run No.	Flow Measured at outlets		Total Calculated input flow Q_T (Cm ³)	Performance criteria of single cell based on	
	Q_{MA} (Cm ³)	Q_{MB} (Cm ³)		Tube "A" K_A	Tube "B" K_B
1	48.5	25	74.89	0.6476	0.3338
2	51	30.5	81.45	0.6262	0.3745
3	21.5	14	34.13	0.6299	0.4102

TABLE A-4.5 PERFORMANCE OF SINGLE CELL FOR TUBE "A" OPENED FIRST AND THEN TUBE "B"

Run No.	Flow Measured at outlets		Total Calculated input flow Q_T (Cm ³)	Performance criteria of single cell based on	
	Q_{MA} (Cm ³)	Q_{MB} (Cm ³)		Tube "A" K_A	Tube "B" K_B
1	10	7	17.10	0.5848	0.494

APPENDIX A-5.0

APPENDIX A-5.0 CALCULATION OF STANDARD DEVIATIONS

A-5.1 LOW FLOW RATE: UP-FLOW

To calculate standard deviations across the channel for Reynolds number 0.0817 Figure 5.2, cells were chosen with the following velocity ranges:

Inlet - 3.59 to 3.48 x 10⁻³ m/s

Middle - 3.42 to 19.2 x 10⁻³ m/s

Outlet - 21.5 to 4.00 x 10⁻³ m/s

Standard deviation σ is calculated by the equation (134)

$$\sigma = \left[\frac{\left\{ \left(\sum_{i=1}^n x_i^2 \right) - n' \bar{x}^2 \right\}}{n' - 1} \right]^{\frac{1}{2}} \quad (\text{A-5.1})$$

where x_i = ratio of velocity measured to average velocity of flow for sample i

\bar{x} = mean average of velocities across the channel*

n' = number of samples under investigation for this analysis.

The calculations were carried out using the standard deviation equation and these are summarised in tabular form below:

* Dimensionless velocities in the form of the ratio measured to average velocity, V/U were used.

TABLE A-5.1 STANDARD DEVIATIONS FOR UP-FLOW

RE = 0.0817

REGION	$\sum_{i=1}^n x_i^2$	n'	\bar{x}	\bar{x}^2	σ
INLET	160.7	6	4.379	19.17	3.021
MIDDLE	435.7	8	6.585	43.36	3.563
OUTLET	376.16	7	6.423	41.25	3.815

The same calculations were carried out for higher flow rates, i.e. increasing Reynolds numbers. The cells chosen for analysis were the same as those examined in the above flow rate. These calculations for increasing Re (refer to Figures 5.3 to 5.5) are tabulated below.

TABLE A-5.2 STANDARD DEVIATIONS FOR UP-FLOW

RE = 0.1028

REGION	$\sum_{i=1}^n x_i^2$	n'	\bar{x}	\bar{x}^2	σ
INLET	145.9	6	4.25	18.06	2.739
MIDDLE	436.7	8	6.68	44.66	3.369
OUTLET	360.2	7	6.21	38.56	3.88

TABLE A-5.3 STANDARD DEVIATIONS FOR UP-FLOW

RE = 0.1293

REGION	$\sum_{i=1}^n x_i^2$	n'	\bar{x}	\bar{x}^2	σ
INLET	143.0	6	4.17	17.39	2.78
MIDDLE	385.9	8	6.193	38.44	3.35
OUTLET	365.7	7	6.32	39.94	3.78

TABLE A-5.4 STANDARD DEVIATIONS FOR UP-FLOW

RE = 0.1616

REGION	$\sum_{i=1}^n x_i^2$	n'	\bar{x}	\bar{x}^2	σ
INLET	150.5	6	4.209	17.71	2.98
MIDDLE	380.8	8	6.235	38.87	9.98
OUTLET	335.1	7	6.057	36.68	3.614

A-5.2 LOW FLOW RATE : DOWN-FLOW

The procedure for calculating standard deviation was that outlined earlier, but the cells chosen were different once in the outlet region, i.e. those cells where the velocities were 8.22 to 2.61×10^{-3} for Re of 0.0817 .

The calculation of deviations are summarised in tabular form for increasing Reynolds numbers.

TABLE A-5.5 STANDARD DEVIATIONS OF DOWN-FLOW

RE = 0.0817

REGION	$\sum_{i=1}^n x_i^2$	n'	\bar{x}	\bar{x}^2	σ
INLET	48.64	6	2.639	6.966	1.17
MIDDLE	106.8	8	3.482	12.12	1.186
OUTLET	53.98	6	2.636	6.948	1.568

TABLE A-5.6 STANDARD DEVIATIONS OF DOWN-FLOW

RE = 0.1028

REGION	$\sum_{i=1}^n x_i^2$	n'	\bar{x}	$\overline{x^2}$	σ
INLET	49.44	6	2.66	7.076	1.18
MIDDLE	109.6	8	3.513	12.34	1.546
OUTLET	55.24	6	2.73	7.453	2.105

TABLE A-5.7 STANDARD DEVIATIONS OF DOWN-FLOW RE = 0.1293

REGION	$\sum_{i=1}^n x_i^2$	n'	\bar{x}	$\overline{x^2}$	σ
INLET	44.66	6	2.52	6.35	1.145
MIDDLE	101.1	8	3.42	11.7	1.038
OUTLET	47.77	6	2.554	6.523	1.314

TABLE A-5.8 STANDARD DEVIATIONS OF DOWN-FLOW RE = 0.1616

REGION	$\sum_{i=1}^n x_i^2$	n'	\bar{x}	\bar{x}^2	σ
INLET	34.39	6	2.238	5.009	0.931
MIDDLE	94.85	8	3.27	10.69	1.153
OUTLET	44.61	6	2.47	6.101	1.26

A-5.3 HIGH FLOW RATE : UP-FLOW

The procedure for calculating standard deviation was followed using equation A-5.1. The cells chosen were those across the channel in the three regions in Figures 5.10 and 5.11.

The calculations are summarised in tabular form for increasing Reynolds number.

TABLE A-5.9 STANDARD DEVIATIONS FOR UP-FLOW RE = 5.291

REGION	$\sum_{i=1}^n x_i^2$	n'	\bar{x}	\bar{x}^2	σ
INLET	248.0	6	6.369	4.056	0.9638
MIDDLE	52.19	8	2.15	4.623	1.47
OUTLET	91.37	8	3.194	10.20	1.18

TABLE A-5.10 STANDARD DEVIATIONS FOR UP-FLOW RE = 7.078

REGION	$\sum_{i=1}^n x_i^2$	n'	\bar{x}	\bar{x}^2	σ
INLET	277.6	6	6.363	40.49	2.632
MIDDLE	138.8	8	3.735	13.95	1.569
OUTLET	33.82	8	2.014	4.056	0.4425

REFERENCES

REFERENCES

1. Yeh, Y, and Cummins, H.Z.
Localised Fluid Flow Measurements with an He-Ne laser spectrometer, Applied Physics Letters, Vol. 4, 1964, pp. 176-178.
2. Fuller, R.
Plate Heat Exchangers in Sea Water Cooling Systems - Cooling Sea Water, Int. Mech. Eng. Proceeding 1979, pp. 29-37.
3. Bond, M.P.
Plate Heat Exchangers for Effective Heat Transfer, The Chemical Engineer, April 1981, pp.162-167.
4. Cross, P.H.
The use of Plate Heat Exchangers for Energy Economy, The Chemical Engineer, March 1982, pp.87-90.
5. Chislom, D.
Developments in Heat Exchanger Technology - 1 Applied Science Publishers, Ltd., 1980.
6. Patten, T.
N.E.L. Report No. 482, East Kilbride, Glasgow, National Engineering Laboratory, 1-6, 1971.
7. Fattah, A.F.M.A.
Hydrodynamic Characteristics of a Plate Heat Exchanger Channel, PhD. Thesis 1975. University of Aston.
8. Ito, A. and Masubuchi, M.
Experimental Frequency Analysis of Plate Heat Exchanger Systems, Technology reports, Osaka University, Vo. 27, March 1977, No. 1337-1363 pp. 261-269.
9. Callaghan, 'O' P.W.
Energy for Industry, Pergamon Press, 1979.
10. Price, A.F. and Fattah, A-F.M-A.
Hydrodynamic Characteristics of a Plate Heat Exchanger Channel, Trans. I.Chem.Eng., Vol.56, 1978, pp217-228.
11. Drain, L.E.
The Laser Doppler Technique, Wiley, 1980.
12. Foreman, J.W. Jr. George, E.W. and Lewis, R.D.
Measurement of Localised Flow Velocities in Gases with a Laser Doppler Flowmeter, Appl. Phys. Lett. Vol. 7, 1965, pp.77-78.
13. Durst, F., Melling, A., and Whitelaw, J.H.
Principles and Practice of Laser Doppler Anemometry Academic Press, London, 1976.

14. Durst, F., and Whitelaw, J.H.
Proceedings of the Royal Society A 324, 1971,
pp 157-81.
15. Von Stein, H.D., and Pfeifer, H.J.
J.Metrologia Vol. 5, 1969, pp.59-61.
16. Mazumder, M.K. and Wankum , D.L.
IEEE Journal of Quantum Electronics QE5, 1969,
pp.316-318.
17. Penny, C.M.
Differential Doppler Velocity Measurement,
Applied Physics Letters, Vol. 16, 1970, pp,167-169.
18. Brayton, D.B. and Goethert, W.H.
A new Dual-scatter Laser Doppler Shift Velocity
measuring technique, ISA Trans. Vol. 10, 1971,
pp. 1943-1949.
19. Lading, L.
Differential Doppler heterodyning technique,
Applied Optics, Vol. 10, 1971, pp. 1943-1949.
20. Durrani, T.S. and Greated, C.A.
Laser Systems in Flow Measurements, Plenum Press,
New York, 1977.
21. Watrasiewicz, B.M. and Rudd, M.J.
Laser Doppler Measurements, Butterworths, London,
1976.
22. Rudd, M.
A new Theoretical Model for the Laser Doppler meter,
J.Physics E, Vol. 2, 1969, pp,55-58.
23. Smart, A.E.
Special problems of Laser Anemometry in Difficult
Applications, Laser Optical Measurement for Aero
Engine Research and Development, AGARD - LS-90,
1977, pp, 6.1 - 6.18.
24. Abiss, J.B., Chubb, T.W. and Pike, E.R.
Optics and Laser Technology, Vol.6, 1974, pp.249-261.
25. Pike, E.R.
Photon correlation velocimetry, Photon Correlation
Spectrometry and Velocimetry, eds. Cummins, H.Z.
and Pike E.R., Plenum Press, New York, 1977,
pp, 246-343.
26. Pike, E.R.,
Book review in, Electronics and Power, Vol.24,
October 1978, p. 767.
27. Abiss. J.B.
Photon Correlation Velocimetry in Aerodynamics,
Photon Correlation Spectroscopy and Velocimetry;
Cummins, H.Z., and Pike, E.R., eds., Plenum Press,
New York, 1977, pp. 386-424.

28. Cummins, H.Z., and Pike, E.R.
Photon Correlation Spectroscopy and Velocimetry,
Plenum Press, New York, 1977
29. Malvern Instruments Manual:
The Fringes Mode Velocity and Turbulence
Algorithm.
30. Malvern Instruments Manual:
Malvern Computing Data Processor MDP7023V.
31. Klewe, R.C.
Proceedings of the Conference on Photon Correlation
Techniques in Fluid Mechanics, Cambridge, 1977.
32. Buchare, P.
Proceedings of LDA symposium, Copenhagen, 1975.
33. Adrain, R.J. and Fingerson, L.M.
Laser Velocimetry Theory Application and
Techniques, Course held at TSI Laboratories,
May 1980.
34. Ware, B.R.
Laser Doppler Velocimetry,
International Laboratory, Vol.11, No. 3, April 1981,
pp. 14-24.
35. Meyers, J.F.
Application of Laser Velocity to large scale and
specialised Aerodynamic Tests, TSI Quarterly,
Vol. 5, No. 4, Nov.-Dec., 1979, pp. 5-12.
36. Weinert, T.W.
Velocity Measurements at the High Speed Wind
Tunnel TV 15° using a Laser Doppler Anemometer,
DISA No. 26, February 1981, pp.7-10.
37. Boutier, A., Lefevre, J., Perouze, C., and
Papainirnik, O.
Operational two-dimensional Laser Velocimetry
for various wind-tunnel measurements, Third
International Workshop on Laser Velocimetry and
Particle Sizing, held at Purdue University,
eds., Thompson, H.D., and Stevenson, W.H.,
July 1979, pp. 15-24.
38. Crosswy, F.L., Brayton, D.B., and Barnett, D.O.
Design and Evaluation of a Laser Doppler
Velocimeter for the AEDC-PWT 4-ft Transonic
Tunnel, Third International Workshop on Laser
Velocimetry and Particle Sizing, held at
Purdue University, eds., Thompson, H.D., and
Stevenson, W.H., July 1979, pp. 463-472.
39. Morse, A.P., Whitelaw, J.H. and Yiamenskis, M.
Turbulent Flow Measurements by Laser Doppler
Anemometry in Motored Piston-cylinder Assemblies,
Trans. of ASME, Journal of Fluid Engineering,
Vol. 101, June 1979, pp. 208-216.

40. Ramos, J.I., Gary, A., and Sirignano, W.A.
Study of Turbulence in Motored Flow-stroke
Internal Combustion Engine, AIAA Journal, Vol.19,
No. 5, May 1981, pp. 595-600.
41. Matsuoka, S., Nagakura, K., Kawai, T. and
Kamimoto, T.
Application of Laser Doppler Anemometry to a
Motored Diesel Engine, SAE Paper 800965,
Tokyo Institute of Technol. Japan,
Sep.11 1980, pp.53-64.
42. Witze, P.O.
Application of Laser Velocimetry to a Motored
Internal Combustion Engine, Third International
Workshop on Laser Velocimetry and Particle
Sizing, held at Purdue University, eds.,
Thompson, H.D., and Stevenson, W.H., July 1979,
pp.239-250.
43. Rask, R.B.
Velocity Measurements inside the cylinder of a
Motored Internal Combustion Engine, Third
International Workshop on Laser Velocimetry
and Particle Sizing held at Purdue University,
eds. Thompson, H.D., and Stevenson, W.H.,
July 1979, pp.251-260.
44. Yeoman, M.L. and Taylor, A.
Velocity Measurements in the Manifold of an
Internal Combustion Engine, Third International
Workshop on Laser Velocimetry and Particle Sizing,
held at Purdue University, eds. Thompson H.D.,
and Stevenson, W.H., July 1979, pp. 261-266.
45. Dyer, T.M., and Witze, P.O.
Laser Velocimetry Measurements in a Constant
Volume Internal Combustion Engine Simulator,
Third International Workshop on Laser Velocimetry
and Particle Sizing, held at Purdue University,
eds., Thompson, H.D., and Stevenson, W.H.,
July 1979, pp. 267-270.
46. Ross, J.N.
Studies of an Electrostatic Precipitator using
Laser Doppler Anemometry, Optica Acta, Vol.27,
No. 1, 1980, pp. 19-23.
47. Danielsson, L., and Lundgren, S.
Measurements of Velocity Distribution and
Profile of Rotating Annular Jets, Physica Scripta,
Vol. 19, 1979, pp. 383-387.
48. Habib, M.A., and Whitelaw, J.H.
Velocity Characteristics of Confined Coaxial
Jets with and without Swirl, Trans. of ASME,
Journal of Fluid Engineering, Vol. 102,
March 1980, pp. 47-53.

49. Adrain, R.S., Alder, R.L., Klewe, R.C., Richards, P.H., Smith, G.D., and Wright, D.G. Preliminary studies using Photo Correlation Velocimetry in Turbomachinery and Combustion Systems, *Physica Scripta*, Vol.19, 1979, pp. 441-446.
50. Power, J.A., Straziser, A.J., and Seasholtz, R.G. Efficient Laser Anemometer for Intra-Rotor flow mapping in Turbomachinery, *Trans. of ASME, Journal of Engineering for Power*, Vol.103, April 1981, pp.424-429.
51. Allos, T.I., and Elder, R.L. Measurement of flow velocity in the Vaneless diffuser of a high speed centrifugal compressor using a Laser Doppler Anemometer, *Optica Acta*, Vol.27, No. 1, 1980, pp.110-126.
52. Miles, J. The Application of Laser Anemometry to the Measurement of Air flow through a cascade of Turbine Blades, *Optica Acta*, Vol.27, No. 1, 1980, pp.67-81
53. Dunker, R.J., and Hungenberg, H.G. Transonic Axial Compressor using Laser Anemometry, and Unsteady Pressure Measurements, *AIAA Journal*, Vol. 18, No. 8, August 1980, pp.973-979.
54. Wisler, D.C., and Mossey, P.W. Practical Application of LV Systems to Aero Engine Research and Development, *Laser Optical Measurement Methods for Aero Engine Research and Development*, AGARD-LS-90, 1977, pp.5.1 - 5.17.
55. Schodl, R. A Laser-Two-Focus (L2F) Velocimeter for Automatic Flow Vector Measurements in the Rotating Components of Turbomachines, *Transactions of the ASME, Journal of Fluids Engineering*, Vol.102, December 1980, pp. 412-419.
57. Sullivan, J.P. LDV Measurements on Propellers, *Third International Workshop on Laser Velocimetry and Particle Sizing*, held at Purdue University, eds., Thompson, H.D., and Stevenson, W.H., July 1979, pp.531-536.
58. Kawase, Y., Tedjojuwono, K., and Asakura T. Application of Laser Doppler Velocity Measurement of charged dust particles in light electric field, *OPTIK*, Vol.56, No. 3, 1980, pp.283-292.
59. Tedjojuwono, K., Kawase, Y, and Asakura, T. Application of Laser Doppler Velocimeter to Velocity Measurement of charged dust particles in high electric field, *OPTIK*, Vol.59, No. 1, 1981 pp. 49-62.

60. Tedjojuwono, K., Kawase, Y., and Asakura, T.
Studies of the Dynamic behaviour of charged dust particles in high electric fields using Laser Doppler Anemometry, Optics and Laser Technology, August 1981, pp. 187-192.
61. Owen, F.K.
Measurements in Combustion Systems, Third International Workshop on Laser Velocimetry and Particle Sizing, held at Purdue University, eds. Thompson, H.D., and Stevenson, W.H., July 1979, pp. 123-135.
62. Moreau, P., and Labbe, J.
Laser Velocimetry in a high velocity combustion flow, Third International Workshop on Laser Velocimetry and Particle Sizing, held at Purdue University, eds., Thompson, H.D., and Stevenson, W.H., July 1979, pp. 136-146.
63. Smith, G.D., and Giel, T.V.
Two Component Laser Velocimeter Measurements in Dump Combustion Flowfield, Third International Workshop on Laser Velocimetry and Particle Sizing, held at Purdue University, eds., Thompson H.D., and Stevenson, W.H., July 1979, pp. 147-157.
64. Driscoll, J.F., and Pelaccio, D.G.
Laser Velocimetry Measurements in a Gas Turbine Research Combustor, Third International Workshop on Laser Velocimetry and Particle Sizing, held at Purdue University, eds., Thompson, H.D., and Stevenson, W.H., July, 1979, pp. 158-165.
65. Santoro, R.J., Fernandez-Pello, A.C., Dryer, F.L. and Glassman, I.
Third International Workshop on Laser Velocimetry and Particle Sizing, held at Purdue University, eds., Thompson, H.D., and Stevenson, W.H., July, 1979, pp. 166-170.
66. Santoro, R.J., Fernandez-Pello, A.C., Dryer, F.L., and Glassman, I.
Application of a two-component LDV to the Measurement of flows induced by flames propagating over condensed fuels, Applied Optics, Vol. 17, No. 23, 1 December 1978, pp. 3843-3849.
67. Kugler, H.P.
Recent Results in Rocket Exhaust Anemometry. Physica Scripta, Vol. 19, 1979, pp. 447-452.
68. Grabek, E., Mierzwinski, S., Popiotek, Z., and Patasz, J.
Application of the Laser Doppler Anemometer to Industrial Problems, DISA, No. 25, February 1980, pp. 30-34.

69. Fuiji, S., Eguchi, K., and Gomi, M.
Swirling Jets with and without Combustion,
AIAA Journal, Vol. 19, No. 11, September 1981,
pp. 1438-1442.
70. Caveny, L.H., Collins, K.L., and Cheng, S.W.
Direct Measurements of Acoustic Admittance using
Laser Doppler Velocimetry, AIAA Journal, Vol 19, No. 7,
July 1981, pp 913-917.
71. Cenker, A.A.
Laser Doppler Velocimeter Measurements on Supersonic
Mixing Nozzles that Employ Gas-Taps, AIAA Journal,
Vol. 20, No. 3, March 1982, pp.383-389.
72. Wang, C.P. Bernard, J.M. and Lee, R.H.
Feasibility of Velocity Field Measurement in a
Fluidized bed with a Laser Anemometer, Third
International Workshop on Laser Velocimetry and
Particle sizing, held at Purdue University,
eds., Thompson, H.D. and Stevenson, W.H., July 1979,
pp. 455-462.
73. Laudan, J.
Wake Field Measurements on a ship model with an
LDA system, DISA, No. 26, February 1981, pp 23-26.
74. Bonner, R., and Nossal, R.
Model for Laser Doppler Measurements of Blood Flow
in Tissue, Applied Optics, Vol.20, No.12, 15 June 1981,
pp.2097-2107.
75. Eiju, T., Matsuda, K., Ohtsubo, J. Hanma, K., and
Shimizu, K.
A Frequency shifting of LDV for Blood Velocity
Measurement by a moving wedged glass, Applied
Optics, Vol. 20, No.22, 15 November 1981,
pp.3833-3837.
76. Riva, C.E., Timberlake, G.T. and Fake, G.T.
Laser Doppler Technique for Measurement of eye
Movement, Applied Optics, vol. 18, No. 14, 15 July
1979, pp 2486-2490.
77. Mazumder, M.K., Wanchoo, S., McLeod, P.C., Ballard, G.S.,
Mozumdar, S., and Caraballo, N.
Skin Friction Drag Measurements by LDV, Applied Optics,
Vol. 20, No. 16, 15 August 1981, pp.2832-2837.
78. Escudier, M.P., Bornstein, J., and Zehnder, N.
Observations and LDA Measurements of Confined
Turbulent Vortex Flow, J.Fluid Mech., Vol.98,
Part 1, 1980, pp. 49-63.
79. Modarress, D., and Johnson, D.A.
Investigation of Turbulent Boundary-Layer Separation
using Laser Velocimetry, AIAA Journal, Vol.17, No.7,
July 1979, pp.747-752.

80. Orloff, K.L. and Olson, L.E.
High-Resolution LDA Measurement of Reynolds stress
in Boundary Layers and Wakes, AIAA Journal, Vol.20,
No. 5, May 1982, pp. 624-631
81. Deshpande, M.D., and Giddens, D.P.
Turbulence Measurements in a Constricted tube,
J. Fluid Mech., Vol.97, Part 1, 1980, pp. 65-89.
82. Durst, F., Keck, T., and Kleine, R.
Turbulence Quantities and Reynolds Stress in pipe flow
of Polymer Solutions measured by Two-channel Laser-
Doppler Anemometry, Private Communication, available
from University of Karlsruhe, West Germany.
83. Lu, C.C.
Measurements of Turbulent Flow Velocity for Sudden
Expansion Cylindrical Tube using Laser-Doppler
Velocimeter (LDV), AIChE Journal, Vol. 26, No. 2,
March 1980, pp.303-305.
84. Chedron, W., Durst, F., and Whitelaw, J.H.
Asymmetric Flows and instabilities in symmetric
ducts with sudden expansions, J.Fluid Mech., Vol. 84,
Part 1, 1978, pp. 13-31.
85. Yao, S.C., and Pfund, P.A.
Fluid flow and heat transfer over tube or rod bundles
Symposium: New York, ASME, 1979, Presented at the
Winter Annual Meeting of the American Society of
Mechanical Engineers, New York, December 2-7, 1979.
86. Owen, J.M. and Pincombe, J.R.
Velocity Measurements inside a Rotating Cylindrical
Cavity with a radial outflow of Fluid, J.Fluid Mech.
Vol. 99, Part 1, 1980, pp.111-127.
87. Faher, J.H. and Leibovich, S.
An Experimental Map of the Internal Structure of a
Vortex Breakdown, J.Fluid Mech., Vol.86, Part 2,
1978, pp 313-335.
88. Oba, R., Ikohagi, T., and Yasu, S.
Supercavitating Cavity Observations by means of Laser
Velocimeter, Transactions of the ASME, Journal of
Fluids Engineering, Vol. 102, December 1980,
pp.443-440.
89. Van de Sande, E., Sloof, R., and Hiemstra, W.
Turbulent Velocity Profiles in a Straight Circular
Pipe at Higher Temperatures, Trans. I.Chem.E., Vol.59,
1981, pp. 283-285.
90. Smart, A.E. and Mayo, W.T.
Applications of Laser Anemometry to High Reynolds
Number Flows, Physica Scripta, Vol. 19, 1979, pp.426-440.
91. Van de Sande, E., Belde, A.P., Hamer, B.J.G. Hiemstra, W.
Velocity Profiles in an Accelerating Pipe Flow
started from Rest, Proceedings of the Third Inter-
national Conference on Pressure Surges, held at
University of Kent. Vol.1, March 1980, pp.1-14.

92. Lau, J.C., Whiffen, M.C., Fisher, M.J. and Smith, D.M.
A Note on Turbulence Measurements with a Laser Velocimeter, J.Fluid Mech., Vol. 102, 1981, pp. 353-366.
93. Corti, M., Martinelli, M. and Parmigiani, F.
A Laser Doppler Velocimeter for Pulsatile Water Flow Measurements in Resonant Hydraulic Circuits, Optics and Laser Technology, June 1980, pp. 155-157.
94. Kramer, H., and Meissner, J.
Application of the Laser Doppler Velocimetry to Polymer Melt Flow Studies, International Congress on Rheology, 8th, Sept. 1-5, 1980, Eds., Astarita, G., Marrucci, G., and Nicolais, L. Plenum Press, New York, 1980, Vol.2, pp. 463-468.
95. Du-Toit, C.G., and Sleat, J.F.A.
Velocity Measurement Close to Rippled Beds in Oscillatory Flow, J.Fluid Mech., Vol. 112, 1981, pp. 71-96.
96. Bertelsen, A.
Measurement of Secondary Flows by a Frequency Tracking Laser Doppler Anemometer, DISA, No. 27, January 1982, pp. 23-26.
97. Ivanov, V.P., Babenko, V.V., Blokhin, V.A., Kozlov, L.F. and Korobov, V.I.
Velocity Field in a Flow-Turbulence Hydrodynamic Facility, using a Laser-Doppler Technique, Journals of Engineering Physics, Vol. 37, No.5., 1979, pp. 1293-1298.
98. Lesinski, J., Mizera-Lesinska, B., and Boulos, M.I.,
Laser Doppler Anemometry Measurements in Gas-Solid Flows, AIChE Journal, Vol. 27, No.3, May 1981, pp. 358-364.
99. Stümke, A., and Umhauer, H.,
Local Particle Velocity Distributions in Two-Phase Flows Measured by Laser-Doppler Velocimetry, Proceedings of the Dynamic Flow Conference, Marseille, September 1978, pp.345-372.
100. Durst, F.,
Studies of Particle Motion by Laser Doppler Techniques, Proceedings of the Dynamic Flow Conference, Marseille, September, 1978, pp.345-372.
101. Martin, W.W., and Abdelmessih, A.H.,
Characteristics of Laser-Doppler Signals from bubbles Int., J. Multiphase Flow, Vol. 7, 1981, pp.439-460.
102. Farmer, W.M.
Measurement of Particle Size and Concentrations using LDV Techniques, Proceedings of the Dynamic Flow Conference, Marseille, September 1978, pp. 373-396.

103. Jensen, A.C., and Lading, L.
The Optimum Code in Sign-Particle Velocity Estimation with a Laser Anemometer, RISO National Laboratory Report, R413, 1980, pp.1-21.
104. Larsen, P.S. Engelund, F., Sumer, B.M. and Lading L.
Techniques of Sizing and Tracking of Particles : A report on EuroMech 120, J.Fluid Mech., Vol.99. Part 3, 1980, pp.641-653.
105. Wilson, J.C., and Liu, B.Y.H.
Aerodynamic Particle Size Measurement by Laser-Doppler Velocimetry, J.Aerosol Science, Vol.11, 1980, pp.139-150.
106. Negus, C.R., and Drain, L.E.
The Visibility Method of Droplet Sizing, presented at, Heat Transfer and Fluid Flow Service Research Symposium, Oxford, 22-23, September 1980, pp.1-6.
107. Bachalo, W.D.
Method for Measuring the Size and Velocity of Spheres by Dual-beam light scatter Interferometry, Applied Optics, Vol. 19, No. 3, 1 February, 1980, pp. 363-370.
108. Fingerson, L.M.
Relating Light Scattering Theory to Actual Laser Velocimeter Systems, TSI Quarterly, Vol. 6, No. 4, 1980, pp.3-7.
109. Fontaine, J., and Lannoy, F.
Experimental Determination of Flow Model in a Plate Heat Exchanger, Revue Generale de Thermique, Vol.14, No. 164-165, Aug.-Sept. 1975, pp. 573-579.
110. Roig, S.M. Vitali, A.A., Rodriguez, E.O. and Rao, M.A.
Residence Time Distribution in the Holding Section of a Plate Heat Exchanger, Food Science Technology, Vol. 9, Pt.4, 1977, pp. 255-256.
111. Okada, K., Ono, M., Tomimura, T., Okuma, T., Kono, H., and Ohtani, S.
Temperature Distribution of Fluid in Plate Type Heat Exchanger, Kogaku Kogaku, Vol. 34, 1970, pp. 93-95.
112. Marriott , J.,
Performance of an Alfaflex Plate Heat Exchanger, Chemical Engineering Progress, Vol. 73, No. 2, 1977, pp.73-78.

113. Cooper, A., Sutor, J.W., and Usher, J.D.
Cooling Water Fouling in Plate Heat Exchangers,
Proceedings 6th International Heat Transfer
Conference, Vol. 4, 1978, pp. 403-406.
114. Leginky, V.M., Babenko, Y.A., and Dikiy, V.A.
Heat Transfer - Soviet Research, Vol. 11, No. 2,
March-April 1979, pp. 143-150.
115. Cross, P.H.
The Use of Plate Heat Exchangers for Energy
Economy, The Chemical Engineer, March 1982,
pp. 87-90.
116. Auth, W.J. and Loiacono, J.
Plate and Spiral Heat Exchangers, Proceedings of
1976 Fall Lecture Series of New Jersey, Practical
Aspects of Heat Transfer, American Institute of
Chemical Engineers, New York, 1978, pp. 108-138.
117. Johansson, H.
Plate Heat Exchangers for the Power Industries
Heat Exchanger Reliability, Proceedings of a
Seminar, held in Toronto, Canada, 1st May 1980,
pp. 129-146.
118. Parrott, D.L.
Design and Use of Plate Heat Exchangers in
Industry, Int. Mtg. Ind., Heat Exchangers and
Heat Recovery, held at Liege, Belgium, 14-16
November, 1979, Paper No. A1, pp. 1-18.
119. Okada, K., and Ohno, M.
Practical Designing Method of the Plate Heat
Exchanger, Kogaku, Sochi, Vol. 20, No. 6, 1978,
pp. 11-19.
120. Raju, K.S.N., and Chand, J.
Consider the Plate Heat Exchanger, Chemical
Engineering, August 1980, pp. 133-144.
121. Rosenhow, W.M.
Why Laminar Flow Heat Exchangers Can Perform
Poorly, Proceedings of Nato Advanced Study
Institute on Heat Exchangers, Thermal-Hydraulic
Fundamentals and Design, ed., Sadik Kaka C.,
Istanbul Turkey, August 4-15, 1980.
122. Kumar, A.
Measurement of Laminar Velocity Profiles in a
Tube and a Plate Heat Exchanger Channel using
Laser-Doppler Anemometer Technique, M.Sc. Thesis,
University of Aston, 1980.
123. Malvern Instruments Manual:
Model 124B Helium-Neon Laser and Adjustable Beam
Splitter and Polarisation Unit Type RF 307 Manuals.
124. Malvern Instruments Manual:
K7023 Correlator Handbook.

125. Jenkins, W.
Malvern Instruments, Malvern Worcs., England.
Private Communication, 1981.
126. Chu, W.P. and Robinson, D.B.
Scattering from a moving Spherical Particle by
two crossed coherent plane waves, Applied Optics,
Vol. 16, No. 3, March 1977, pp. 619-626.
127. Cole, J. B. and Swords, M.D.
Laser Doppler Anemometry Measurements in an
Engine, Applied Optics, Vol. 18, No. 10,
15th May 1979, pp. 1539-1545.
128. Prockter, C.E. and Conway, A.
Kempe's Engineers Year Book for 1969, 74th Edition,
Morgan-Grampian (Publishers) Ltd., Volume one,
1969, p83.
129. Deast, R.C.
CRC Handbook of Physics and Chemistry, 53 edition,
Published by Chemical Rubber Co., Cleveland, 1972-1973.
130. Kleine, R.
Private Communication, Tables provided at a course
held at University of Karlsruhe in 1980.
131. Day, D.K.
A Safe Pyre "Vanishing Solution", Physics Teacher,
Vol. 15, Oct. 1977, p 438.
132. Kirk and Othmer
Encyclopedia of Chemical Technology, 2nd Edition,
Published by John Wiley & Son Inc . 1966
Vol. 9, 1966, pp. 803-809
133. Zafar, I.A.
Flow Distribution in a Plate Heat Exchanger Channel,
M.Sc. Computer Project Report,
University of Aston in Birmingham,
Department of Chemical Engineering, March 1982.
134. Chatfield, C.
Statistics for Technology, Published by Chapman and
Hall Ltd., 1970.